An analytical study of reinforced concrete beam-column joint behavior under seismic loading

Nilanjan Mitra

A dissertation submitted in partial fulfillment
of the requirements for the degree of

Doctor of Philosophy

University of Washington

2007

Program Authorized to Offer Degree: Department of Civil & Environmental Engineering

University of Washington
Graduate School

This is to certify that I have examined this copy of a doctoral dissertation by

Nilanjan Mitra

and have found that it is complete and satisfactory in all respects,
and that any and all revisions required by the final
examining committee have been made.

Chair of the Supervisory Committee:

_____
Laura N. Lowes

Reading Committee:

_____
Laura N. Lowes

_____
Dawn Lehman

_____
Gregory R. Miller

_____
Peter Mackenzie-Helnwein

Date: _____

University of Washington

Abstract

An analytical study of reinforced concrete beam-column joint behavior under seismic loading

Nilanjan Mitra

Chair of the Supervisory Committee:
Assistant Professor Laura N. Lowes
Department of Civil & Environmental Engineering

Recently, researchers have sought to develop performance-based design methods that enable the design of a structure to achieve specific performance objectives, typically in excess of 'life-safety', under a given level of earthquake loading. Accomplishing performance-based design requires accurate prediction of component load and deformation demands, and typically nonlinear analysis is employed to determine these demands. The research presented here focuses on developing a series of analysis and design tools to support the performance-based design of one particular structural component: reinforced-concrete beam-column joints.

This particular component is chosen for investigation because, despite the fact that laboratory and post-earthquake reconnaissance suggest that joint stiffness and strength loss can have a significant impact on structural response, the inelastic response of these components is rarely considered in analysis or design.

Data from previous experimental investigations of joints, spanning a wide range of geometric, material and design parameters, were assembled. Using these data, a series of models were developed and applied to advance understanding of the seismic behavior, simulation and design of reinforced concrete beam-column joints. These include a 1) discrete choice probabilistic failure initiation model, 2) continuum model for joints, 3) strut-and-tie models for joint and 4) a component-based super-element model for the joint region.

TABLE OF CONTENTS

LIST OF FIGURES

LIST OF TABLES

ACKNOWLEDGMENTS

I would like to express my sincere thanks and gratitude to my advisor, Dr. Laura N. Lowes for her invaluable advice, patience, guidance, exceptional support and encouragement throughout the course of my graduate study and the research work. I have learnt a lot from her since I joined University of Washington in 2001. I would also like to thank her, for her continued financial support as a graduate student through 5 years of my graduate study in University of Washington. Perhaps it would be less to say that I am indebted to her in many ways.

Graduate study for 5 years is like a roller-coaster which goes through ups and downs. It would have been really hard for me if I did not have Dr. Peter Mackenzie-Helnwein, Dr. Pedro Arduino, Dr, Greg Miller and Dr. John Fergusson by my side and listen to me when I needed them the most. I would like to take this opportunity to express my sincere appreciation and gratitude towards Prof. Peter Mackenzie, Prof. Pedro Arduino, Prof. Greg Miller and Prof. John Fergusson. Thank you very much for your time out of your busy schedule to be available for discussions, suggestions and chats.

I would like to thank Prof. Dawn Lehman and Prof. John Stanton for developing in me the appreciation for experimental work. Before I joined University of Washington, I only had experience in analytical methods. Working with them all through these years, I have learnt that experimental and analytical work go hand in hand, one is incomplete without the other. I believe this realization would be fruitful for my academic carrier in the future.

Thanks are also due to my PhD committee graduate student representative, Prof. Keith Holsapple, my reading committee members and also the staff in University of Washington, namely Lorna Latal, Renate Staub, Arla Webb, Dr. Serhad Atakturk. These people have helped me in several ways. Thank you very much for all your help.

I would also like to take this opportunity to thank my wife Dr. Sudeshna Mitra and

my parents Dr. Bharati Mitra and Mr. Karunamoy Mitra for their continued support and encouragement. Without their mental support and inspiration it would have been almost impossible to complete this degree. Thank you very much for being there when my spirits were down and also kindling in me the attitude of never to give up but to continue. I would also like to thank my uncle Mr. Kalyan Kumar Das in this regard.

Last but not the least, my heartfelt thanks and appreciation goes to my colleagues and friends who were there available always for discussion, chat or a beer or movie after work. Out of many friends in University of Washington, I would like to thank in particular Dr. Kathryn Petek, Dr. Tyler Ranf, Dr. Mike Berry, Dr. Alex Lindbad, Mr. Jaewon Jung, Dr. Jung Yoo, Mr. Debashis Mondal, Mr. Tyler Sprague. Thank you all very much for your company, help and cooperation which made my stay in Seattle a memorable and a treasured experience.

Chapter 1

INTRODUCTION

1.1 Motivation for the study

Current building codes for the design of structures under earthquake loading are intended to prevent structural collapse and ensure the life-safety of the occupants. However, in recent years, new design philosophies have been introduced: namely *Performance-Based Seismic Design* (PBSD). The primary objective of PBSD is to enable the design of structures to achieve specific performance objectives, including those beyond 'life-safety'. Accomplishing *Performance-Based Seismic Design* requires 1) the ability to accurately predict the demands, which may be defined by loads, or deformations or both on various components that develop under various levels of earthquake loading and 2) to design components to achieve specific performance objectives under these earthquake induced demands.

Previous research indicates that PBSD of joints requires consideration of the inelastic response of the beam-column joints in determining demands on the frame components. For example, post-earthquake reconnaissance suggests that joint failure may result in structural failure (EERI 1994). Additionally, experimental investigation indicates that strength and stiffness loss in a structure in seismic loading can be attributed to the loss of strength and stiffness of the joint region, with detailing typical of modern as well as pre-1970's construction. However, to date, relatively few studies have addressed the development of tools to support PBSD of joints. Thus, detailed investigation of the joint response is essential to develop tools which would enable the design and analysis of joints subjected to seismic loading.

1.2 Scope of work

The objective of this research is to use the results of previous experimental investigations of joints to improve the understanding of the joint behavior, develop response models for use in PBSD of reinforced-concrete frames and develop tools to support PBSD of individual joints. To meet the research objective, data from a series of previous experimental investigations of joints were assembled. These experimental investigations span a wide range of design, material and geometric parameters. The experimental data set provides the basis for the development, calibration and validation of design and analytical models for reinforced concrete beam-column joints, that are presented in this thesis. In assembling the data set, only tests of two-dimensional building joint sub-assemblages without slabs, beam eccentricity or out-of-plane beams for which response is determined by beam flexural yielding and/or joint failure were considered. Additionally, only joints with a "typical" test setup, subjected to pseudo-static cyclic loading were included in the data set. Finally, if sufficient information about joint geometry, material properties and response were not provided in the literature data for the test, the experimental test was not included in the data set. The data set includes data for joints with design parameters typical of modern (post 1967) as well as older construction.

Using these data, a series of models were developed for reinforced concrete beam-column joints. These include a 1) statistical model, 2) continuum finite element model, 3) component-based super-element model, and 4) strut-and-tie model. A brief description of the models along with the contribution of these modeling efforts in advancing PBSD of joints is described in the following subsections.

1.2.1 Statistical model

The primary objective for many experimental investigations is to identify the parameters that determine failure in the connection region. In this study, to determine the relative influence of various design parameters in determining if a joint will fail and also to provide a method for determining the probability of a particular joint failing, a discrete choice probabilistic model is developed. The assembled set of experimental data was used to

calibrate the model.

1.2.2 Continuum finite element model

Given a set of parameters that determine if a joint will exhibit strength deterioration or ductile response, continuum finite element modeling was explored as a means of establishing the mechanism by which these parameters affect response. A commercial finite element analysis code, DIANA 9.1, was used to accomplish the analysis. To evaluate the software and determine the impact of concrete, steel and bond zone constitutive model parameters in analytical results, a series of benchmark tests were performed. Following this a set of analysis was performed for reinforced-concrete beam-column joints to explore continuum finite element method as a means of improving understanding of joint behavior and thereby providing a basis for development of simplified response and design models for PBSD. However, the results of analysis of joint sub-assemblage indicated that continuum finite element analysis using DIANA 9.1 could not provide additional insight into joint behavior.

1.2.3 Component-based model

PBSD requires accurate prediction of component load and deformation demands under earthquake loading. Since beam-column joints may exhibit significant stiffness and strength loss under earthquake loading, models are required to simulate the inelastic response to enable accurate simulation of frame response. In this thesis, a two-dimensional component-based joint super-element was developed using data from the experimental data set. The model represents an extension and generalization of the model developed previously by Lowes and Altoontash (2003). Unlike the previous model, this model developed here is 1) appropriate for use with joints with a wide range of design parameters and 2) results in a robust numerical formulation.

1.2.4 Strut-and-Tie models

Strut-and-tie models are used widely by engineers for dimensioning of members and detailing of reinforcement steel, in particular for members with distributed stress field. ACI 318-05

Appendix A, AASHTO, EuroCode-2, National Building Code of Canada 2005 and the New Zealand Building Code provides recommendations for use of the strut-and-tie methodology to design structural components. However, these building codes are not intended for seismic design. Additionally, these requirements are prescriptive in nature and do not provide clear links between design requirements and response mechanisms, as such; they are not easily extended to support performance-based design. ACI Committee 445 has currently initiated an investigation of the application of strut-and-tie methods to design structural components for seismic loading. Thereby, in this thesis, investigation was carried out for strut-and-tie modeling of reinforced concrete beam-column joints subjected to seismic loading. Experimental data from the assembled data set were used as a basis for this study.

Simple and higher resolution strut-and-tie models were developed for most of the joints in the data set. Some correlations were observed between strut-and-tie design parameters (e.g. strut stress) and joint performance measures (e.g. brittle failure vs. ductile response). Conservative recommendations for design of joints using strut-and-tie models were proposed since the recommendations as provided by ACI 318-05 were found to be inadequate.

1.2.5 Contribution of modeling efforts in advancing PBSD of joints

Amongst the four methodologies of varying refinement and complexity that were used to better understand the inelastic behavioral mechanism within the joint region, each had its own place in design/assessment process. The probabilistic model is simple to use and provides a first-hand estimate of failure initiation within the joint region. Even though, these provide very accurate results but these do not give us a better knowledge as regards to the inelastic behavioral mechanism within the joint region. The complex continuum analysis of joints provides us with a detailed description of the inelastic behavioral mechanisms governing joint behavior but cannot be used in PBSD due to huge computational overhead required as regards to analysis time and numerical convergence problems. But these models provides us with the basis for various assumptions in the simplified design models such as the strut-and-tie method as well as the analytical component-based models. The simplified models (strut-and-tie models) require the introduction of assumptions,

as such they tend to be less accurate and over-conservative, but can be used to provide guidelines for making the assumptions that are based on design. Even though these simplified models provide a first hand rough estimate about design, but these cannot be used to generate load-deformation response envelopes, which is essential within the context of PBSD. For load-deformation response analysis we can rely on the use of component-based super-element model of joints, which has been found to give results within reasonable accuracy. Component-based super-element models provides us with a computationally robust analytical methodology for modeling of joints and can also be utilized in frame analysis of structures. This methodology is able to distinguish between the different failure mechanisms and is thereby recommended as the analytical method for PBSD of joints. This modeling methodology provides the right balance in between complexity, computational time and the inelastic behavioral details along with load-deformation response analysis of joints.

1.3 Outline of chapters

The research outlined above is presented in the next five chapters (Chapters 2 to 6).

Chapter 2 provides a background of the behavior of joints subjected to earthquake loading and presents the experimental data set. The impact of various design parameters on joint performance is investigated qualitatively and also through the development of a discrete choice probabilistic model.

Chapter 3 describes the nonlinear continuum finite element modeling that was done using DIANA 9.1. Benchmark analyses were done to evaluate the constitutive models available in DIANA 9.1 and the simulation results were discussed. Finally, analyses of two reinforced-concrete beam-column joints from the experimental data set are presented and the results of these analyses are discussed.

Chapter 4 presents a component-based joint element developed for use in modeling of two-dimensional frames subjected to earthquake loading. The super-element formulation and hysteretic models for the components that make up the super-element are presented. Finally, the model is validated through comparison of simulated and observed response parameters.

Chapter 5 presents the results of an investigation to extend the strut-and-tie modeling

methods for design of reinforced concrete beam-column joints subjected to seismic action. Recommendations were proposed for strut, node and bond capacities for conservative design of joints in seismic region. No clear distinctive correlation could be obtained in between the different demand and performance measures with respect to different type of failure mechanism in the joint region.

Chapter 6 summarizes the research effort and presents conclusion along with future research directions.

Chapter 2

EXPERIMENTAL DATA SET AND STATISTICAL MODEL FOR JOINTS

2.1 Introduction

The chapter is intended to provide an understanding of the seismic behavior of joints and serve as a basis for the model development efforts presented in subsequent chapters. First, the behavior of joints subjected to seismic loading as understood and observed in previous studies are presented. Second, a data set is assembled from previous experimental investigations of reinforced concrete beam-column joint sub-assemblages subjected to reversed cyclic loading. These experimental tests include joints with a wide range of material, geometric, and design parameters. Third, the impact of various design parameters on joint response are investigated qualitatively and finally a statistical model is developed that predicts whether a joint with a specific set of design parameters will exhibit brittle or ductile response. A model application of this proposed probabilistic model is also shown in this chapter.

2.2 Behavior of joints subjected to seismic loading

In a 2D building frame subjected to earthquake loading, beams and columns experience flexure and shear loading. Figure 2.1(a) shows the forces that could be expected to develop in a 2D frame subjected to earthquake and gravity loading. In modern frames subjected to moderate and severe earthquake loading, it is expected that the beams will develop flexural strength at the joint while columns will develop moments that approach the yield moment. In older frames, shear failure of beams and columns or flexural yielding of columns may preclude beams achieving yielding flexural strength. Figure 2.1(b) shows the expected loads and resultants at the perimeter of the joint region.

The load distribution, shown in Figure 2.1, can result in severe loading of the joint. The moment reversal in the beams and columns results in large shear forces within the joint.

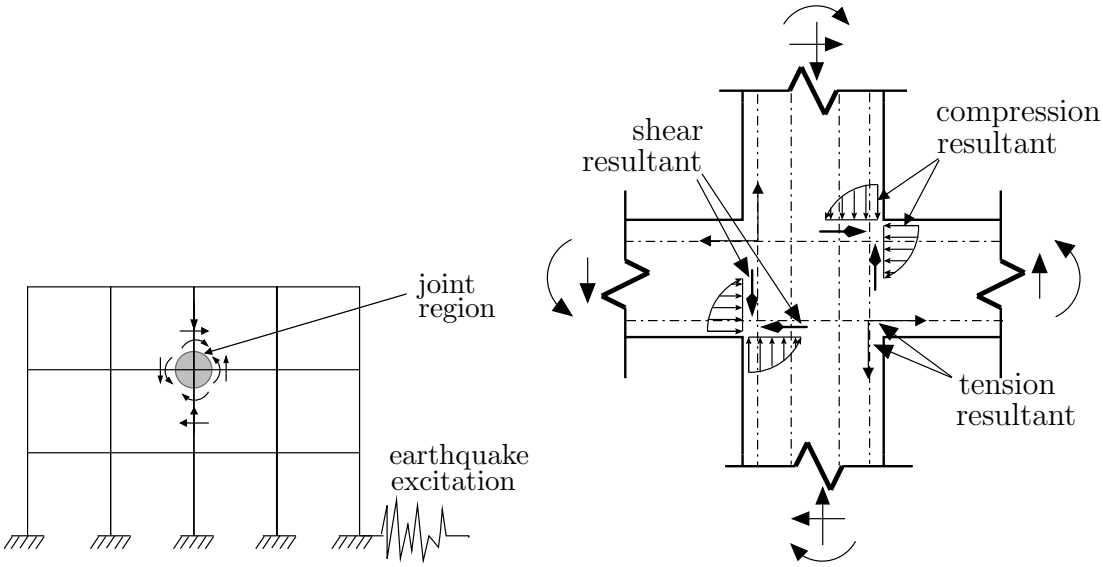

(a) Building frame with joint region (b) Detailed view of joint region

Figure 2.1: Seismic loading in a building frame beam-column joint region

Additionally, the stress reversals in the beam, and to some extent column, longitudinal steel may require high bond stresses within the joint. Figure 2.2 shows the two mechanisms for load transfer within the joint, as were proposed in the seminal paper by Paulay et al. (1978). In the first mechanism, referred to as the strut mechanism (shown in Figure 2.2(a)) joint shear is transferred via a single concrete compression strut. The transverse steel in the joint is assumed to increase the deformation capacity of the strut. The second mechanism, the truss mechanism (shown in Figure 2.2(b)), assumes a uniform bond stress distribution along beam and column reinforcements. In this mechanism, the shear stress within the joint is transferred via a series of concrete compressive struts and steel tension ties.

In evaluating the tension and compression resultants at the perimeter of the joint (as shown in Figure 2.1(b)), it is assumed that the forces are obtained by dividing the moments with the tension-compression lever arm. For sake of simplicity, this lever arm distance is assumed to be constant and thereby we obtain joint shear stress to be proportional to the story shear at all times. Shiohara (2001) strongly criticized this above concept of constant lever arm distance and showed that along with the change in bond stress of the beam longitudinal reinforcing bars, this lever arm distance changes and has significant implication

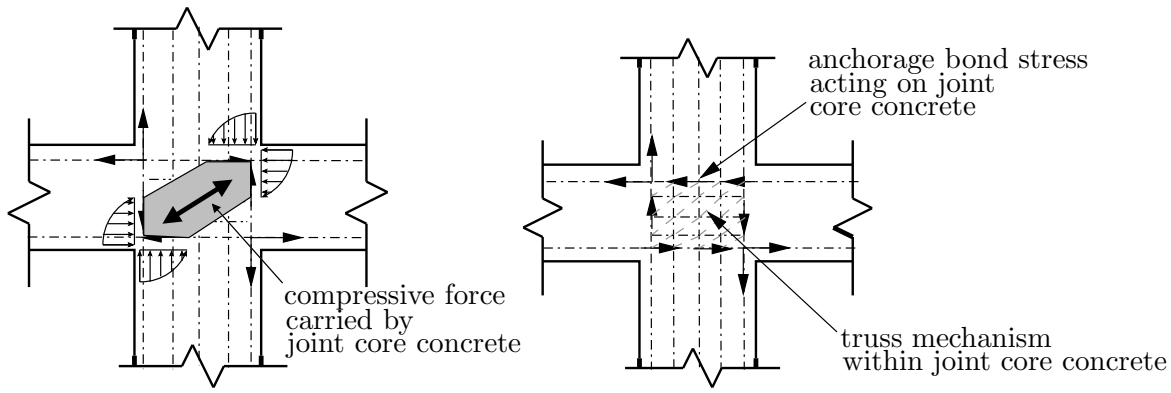

(a) Compressive force within the joint (b) Anchorage forces within the joint

Figure 2.2: Internal forces within the joint

on the joint shear stress. Moreover, the widely accepted assumption of joint shear stress being proportional to the story shear is not a valid assumption. Even though the model of load-transfer within the joint by Shiohara (2001) shows more promise and represents the actual behavior with more accuracy, the numerical modeling of this phenomenon would be computationally intensive and also challenging. An approximate attempt has been made to include this phenomenon in the numerical model in chapter 4.

Even though researchers are yet to come to a consensus as how to evaluate the tension and compression forces at the joint perimeter, but it is widely accepted that there are two primary inelastic mechanisms which are responsible for failure of the joint. These two inelastic mechanisms are: 1) anchorage of beam longitudinal bars in the joint thereby resulting in bar-slip and 2) joint shear failure. It is also assumed that bond stress does not decrease prior to yielding of the bars. The coupling action between these two mechanisms is still an open area of research and was pointed out Shiohara in his research.

Thereby, joint failure can occur prior to as well as after the yielding of the beam-longitudinal bars. If the failure occurs prior to the beam reinforcement steel yielding, then it is referred to as *brittle mechanism*, else if the joint failure occurs after yielding of beam reinforcement steel, then it is referred to as a *ductile mechanism* of failure.

2.3 Experimental data set

The results of previous experimental tests of joints were reviewed to assemble a data set for use in investigating the seismic behavior of joints and developing, evaluating and validating joint models. An experimental data set including 110 building sub-assemblage tests from 20 investigations conducted around the world during the last 40 years was assembled. The data set is restricted to include only two-dimensional interior building joint sub-assemblages without slabs, beam eccentricity or out-of-plane beams for which response is determined by beam flexural yielding and/or joint failure. Thus, joints in which response is determined by column yielding, column splice failure, and beam shear failure have not been included in the data set. All of the joints in the data set have deformed longitudinal reinforcing steel in the beams and columns. Only joint tests for which sufficient geometry, material, and response data were provided in the literature were included in the data set. Geometric, material and design parameter data for all of the specimen in the data set are provided in Appendix A in tables A.1, A.2, A.3 and A.5. All joint sub-assemblages had approximately the same configuration and all were tested using a similar joint test set up. The data set includes joints with design parameters typical of modern (post-1967) as well as older construction. Seismic design provisions for joints were introduced in the *Uniform Building Code* in 1967 and in the *American Concrete Institute (ACI)* building code in 1971; thus a distinction has been made in between pre-and post-1967 specimen. Mosier (2000) also concluded that most buildings designed prior to 1967 and some designed between 1967 and 1979 had detailing that could be expected to result in non-ductile response under earthquake loading.

2.3.1 Test programs included in the data set

Experimental investigations by research groups were reviewed for this study. Of these, 110 tests by 20 different research groups were found to meet the criteria listed above for inclusion in the data set. All of the 20 test programs are discussed below; studies and individual tests that were not included in the data set are identified.

Durrani and Wight (1982)

The experimental test program (DW in table 2.1) consisted of six full-size interior beam-column sub-assemblages. Three specimen were not considered in the data set since these specimen had slabs or transverse beams. The experimental test program concluded that lower joint shear stress demand and greater hoop steel in the joint prevents the joint failure due to a shear mechanism in the joint core.

Otani, Kobayashi and Aoyama (1984)

The experimental test program (OKA in table 2.1) consisted of twelve half-scale interior beam-column sub-assemblages. Six of the specimens were not included in the data set since these specimen had transverse beams. The researchers concluded that number of column middle reinforcement does not play a significant role in determination of joint response. Moreover, the shear failure behavior of the joint could be improved by increasing the amount of joint hoop steel and reducing the joint shear stress demand.

Meinheit and Jirsa (1977)

The experimental test program (MJ in table 2.1) consisted of fourteen full-scale sub-assemblage specimen. Seven specimen were not included in the data set because these specimen either had eccentric lateral beams or lateral load was applied to excite the weak axis bending of the columns. The experimental study concluded 1) that interior column bars provide minimal lateral confinement of the joint and increase in the joint shear strength, 2) column axial load influences the magnitude of shear cracking stress and also the inclination of the shear cracks in the beam-column joint; but not the shear strength of the joint, 3) shear strength is not a linear function of the volume of joint hoop reinforcement.

Walker, Alire, Lehman and Stanton (2001-2003)

The experimental test program (PEER in table 2.1) consisted of twelve half-scale sub-assemblages with no transverse joint reinforcement. These specimen were considered to be representative of joints constructed before 1967. This study evaluated the impact of shear

stress and load history on joint performance. Five of the twelve specimens tested were included in the data set. Specimens with non-standard reversed cyclic loading were not included in the data set because no other joints with non-standard loading were found in the literature and it was thought that modeling these might skew the results of the study. The research concluded that joints maintain strength and adequate stiffness when drift demand is less than 1.5% and shear stress is less than $10\sqrt{f_c}\ psi$ where f_c represents the compressive strength of concrete.

Park and Ruitong (1988)

The experimental test program (PR in table 2.1) consisted of four interior beam-column sub-assemblages. All the four specimen were included in the data set. The researchers concluded that for low axial load ratio, column interior bars are required to transmit the shear force through the joint. Researchers also recommended a limit on the diameter of longitudinal bars passing through the joint for interior beam-column joints of ductile frames when plastic hinges form in the beams adjacent to the column faces. This limit was intended to reduce the bond stress demand in the joint.

Noguchi and Kashiwazaki (1992)

The experimental test program (NK in table 2.1) consisted of six interior beam-column sub-assemblages. Only five specimen were included in the data set. One specimen was excluded because it was subjected to monotonic, rather than cyclic loading. The researchers concluded 1) that maximum joint shear strength did not increase significantly with an increase in concrete compressive strength, 2) the effect of confinement provided by joint lateral reinforcement became significant only at large deformation levels, specifically drift angles in excess of 1/50 rad.

Oka and Shiohara (1992)

The experimental test program (OS in table 2.1) consisted of eleven one-quarter scale interior beam-column sub-assemblages. Two specimens were not considered in the data set because

of the presence of slabs. The researchers concluded that 1) joint shear capacity increased with an increase in concrete compressive strength but that the relationship was not linear, and 2) joint shear capacity increased with an increase in the percentage of longitudinal reinforcement in the beams.

Kitayama, Otani and Aoyama (1987)

The experimental test program (KOA in table 2.1) consisted of six interior beam-column sub-assemblages. Two of these specimen were not used in the current study because the material properties and response data were not provided for these specimens. The researchers recommended restrictions on beam bar diameter through the joint, joint shear stress demand, minimum lateral reinforcement in the joint region. The experimental test program also concluded that column axial load ratio smaller than 0.3 does not exhibit beneficial effect on the bond resistance along the beam reinforcement within the joint region and that smaller than 0.5 does not influence the joint shear strength.

Park and Milburn (1983)

The experimental test program (PM in table 2.1) consisted of two interior beam-column sub-assemblages. All the specimen were included in the data set. The researchers concluded that relocating the beam plastic hinges away from the face of the joint resulted in better joint behavior.

Endoh, Kamura, Otani and Aoyama (1991)

The experimental test program (EKOA in table 2.1) consisted of four interior beam-column sub-assemblages. All the four specimen were included in the data set. The researchers concluded that 1) the strength loss in the post peak regime of the load-deformation response was more significant for light-weight concrete than normal strength concrete and 2) joint shear strengths of light weight concrete were smaller than normal strength concrete due to reduced compressive strength of light weight concrete.

Higashi and Ohwada (1969)

The experimental test program (HO in table 2.1) consisted of 17 one-third scale interior beam-column sub-assemblages. Four specimen were excluded from the data set because they included transverse beams; six additional specimen were excluded because they exhibited column yielding prior to beam yielding. The results of the study included identification of joint shear demand as an important parameter in determining if a joint will exhibit brittle failure under earthquake loading.

Beckingsale (1980)

The experimental test program (B in table 2.1) consisted of two interior beam-column sub-assemblages. Both the specimen were included in the data set. The researcher observed that the specimen with low column axial load exhibited failure due to bar-slip while the specimen with a higher column axial load did not. The researcher also concluded that the experimental data showed that the two joint load-transfer mechanisms proposed by Paulay et al. (1978) did indeed develop.

Attaalla and Agbabian (2004)

The experimental test program (AA in table 2.1) consisted of four interior beam-column sub-assemblages. Three out of the four specimen were included in the data set; one specimen was excluded because steel fibers were used instead of steel bars to confine the joint core. The researchers concluded that joint shear strength, expressed as a function of the square root of the concrete compressive strength is an inappropriate measure of shear demand for joints with high strength concrete.

Birss, Park and Paulay (1978)

The experimental test program (BPP in table 2.1) consisted of two interior beam-column sub-assemblages subjected to cyclic loading. Both the specimen were included in the data set. The researchers concluded that the mechanism of joint load transfer proposed by Paulay et al. (1978) are satisfactory for design. The results of the study also indicate relocating

beam hinges away from the column face result in the beam-column joint region to remain within the elastic regime.

Teraoka, Kanoh, Hayashi and Sasaki (1997)

The experimental test program (TKHS in table 2.1) consisted of 14 half-scale interior beam-column sub-assemblages. All of fourteen specimen were included in the data set. The results of this study included a method for predicting the ductility, performance, and hysteretic behavior of joints.

Hayashi, Teraoka, Mollick and Kanoh (1994)

The experimental test program (HTMK in table 2.1) consisted of 11 half-scale interior beam-column sub-assemblages. All eleven specimen were included in the data set. The result of this study included a model relating bond strength with bar slip for beam longitudinal reinforcing steel. The results of this study also show that both beam bar bond and joint shear stress demand plays a role in joint failure under earthquake loading.

Teraoka, Kanoh, Tanaka and Hayashi (1994)

The experimental test program (TKTH in table 2.1) consisted of seven half-scale interior beam-column sub-assemblages. Six of seven specimen were included in the data set; one specimen was excluded as steel plates were used to provide confining reinforcement within the joint region. The researchers concluded in being able to predict the ultimate shear strength of the joint panel as well as the shear panel envelope using a proposed empirical equation.

Zaid (2001)

The experimental test program (Z in table 2.1) consists of four half-scale interior beam-column sub-assemblages. Three out of four specimen were considered in the data set. One specimen was excluded because of an a-typical joint reinforcing detail (in which the beam longitudinal bars were bent in the joint region along the joint diagonal) developed on basis of

Shiohara (2001) model. Experimental results confirmed the conclusions of Shiohara (2001) in that the lever arm distance between the tension and compression forces at the perimeter of the joint does indeed change along with loading of the joint and thereby joint shear stress cannot be assumed to be proportional to the story shear.

Joh, Goto and Shibata (1992)

The experimental test program (JGS in table 2.1) consisted of 13 half-scale interior beam-column sub-assemblages. Only six were included in the data set; three tests were excluded because they were designed so that beam yielding would occur away from the beam-column interface; four tests were excluded because they were eccentric beam-column joint connections. The researchers concluded that 1) a large volume of transverse joint reinforcement may reduce the slip of beam bars in the joint and enhance joint stiffness after cracking, 2) similar volume of stirrup reinforcement in the beam end does not significantly reduce the stiffness degradation resulting from beam bar bond deterioration within the joint; 3) bond deterioration of beam bars within the joint may be prevented by relocating the beam plastic hinge, but sliding shear deformation may occur at the plastic hinge.

Fujii and Morita (1992)

The experimental test program (FM in table 2.1) consisted of four interior beam-column sub-assemblages. All four specimen were included in the data set. The researchers concluded 1) column axial load ratio had no impact on the shear strength of joints, 2) an increase in the joint transverse reinforcement ratio increased the joint shear capacity, 3) once joint shear strain reaches 0.5%, degradation of shear rigidity was accelerated under subsequent load reversals.

Other experimental investigation not included in the data set

There were also several sets of internal reinforced concrete beam-column experimental test programs which were were not included in the data set since they did not meet one of the criteria as described in the beginning of this section. Those include Hanson and Connor

(1967), Leon (1990), Hakuto et al. (2000), Blakeley et al. (1975), Soleimani et al. (1979), Pessiki et al. (1990).

Table 2.1: Parameter variation in the experimental test programs

Specimen	f_c	Beam long. reinf.			Column int.	Jnt. hoop steel			p
		b_dia	b_no	b_yld	bars (c_int)	j_dia	j_no	j_yld	
DW	√		√				√		√
OKA	√		√	√	√		√		√
MJ	√				√	√	√	√	√
PEER	√	√	√	√	√				
PR	√	√	√	√		√		√	√
NK	√		√		√				
OS	√	√	√	√			√	√	√
KOA		√	√	√	√	√	√	√	
PM	√	√	√	√			√		
EKOA	√	√	√	√	√		√	√	√
HO	√			√					√
B	√		√						
AA	√						√		√
BPP	√					√		√	√
TKHS	√	√	√	√		√		√	
HTMK	√	√	√	√		√		√	√
TKTH	√	√		√					√
Z		√	√	√					
JGS	√			√	√	√	√	√	√
FM				√			√		√

Parameters which control joint response

From these experimental investigations, several parameters were identified by researchers which control joint response. These parameters have been identified as:

- concrete compressive strength (f_c)
- beam longitudinal reinforcement bar diameter (b_dia), number (b_no) and yield strength (b_yld)
- number of column interior longitudinal reinforcement bars (c_int)
- joint hoop reinforcement diameter (j_dia), number (j_no), and yield strength (j_yld)

- column axial load normalized with column sectional area and concrete compressive strength (p)

The variation of above parameters that were considered in each of these set of experimental tests are shown in table 2.1.

2.3.2 Joint design parameters

The results of these previous experimental studies as well as previous analytical studies suggest a number of joint design parameters that could be expected to determine joint performance under earthquake loading. These parameters are described in the following paragraph and table A.5 lists detailed values of these parameters for each joint in the data set. Table 2.2 provides summary statistics for the parameters in the data set.

The joint design parameters are:

1. Measured concrete compressive strength, f_c.
2. Observed maximum joint shear strength as per recommendations of ACI-ASCE Committee 352 (2002):

$$\tau_{\max\_ACI} = \frac{1}{h_c b_j}\left(T_{bL} + C_{bR} - V_c\right) = \frac{1}{h_c b_j}\left(\frac{M_L + M_R}{j h_b} - V_c\right) \tag{2.1}$$

   where h_c is the height of the column section, b_j is the maximum out-of-plane dimension of the beam or column, T_{bL} and C_{bR} are, respectively the tension and compression resultants at the beam-joint interface on the left and right of the joint at the maximum column load, M_L and M_R are, respectively, the moments at the beam-joint interface on the left and right side of the joint when maximum column lateral load V_c is applied at the column free end, and jh_b is the distance between the tension and compression resultants in the beam at the beam-joint interface where h_b is the height of the beam and the ratio j is taken as 0.85 per ACI-ASCE Committee 352.
3. Observed maximum joint shear strength defined per our study:

$$\tau_{\max} = \frac{1}{h_c b_j}\left(\frac{M_L + M_R}{h_b} - V_c\right) \tag{2.2}$$

where h_c, b_j, M_L, M_R, h_b and V_c are as defined above. This definition of joint stress uses the entire joint volume with the result that horizontal and vertical stresses are equal. This definition was the development for the current study for use with the joint component model presented in chapter 4 as it results in consistent definition of joint stress-strain within the element formulation. Additionally this definition of maximum joint shear strength was considered since the previous definition is dependent upon jh_b and it has been observed that j, ratio of the beam height which determines the distance in between the tension and compression resultants, varies with the lateral load applied to the system.

4. Nominal joint shear stress, τ_{nom}, defined per Eq. 2.2 with moments and shear force corresponding to beams carrying nominal flexural strength (ACI 318-05) at the perimeter of the joint. This parameter normalized by the square root of the concrete compressive strength is used to develop the statistical joint response model (Section 2.5).
5. Maximum beam bar anchorage length, ξ, expressed in terms of beam bar-diameter (d_b). Here it is assumed that the width of the anchorage length is equal to the joint width. Thus, this parameter is typically the width of the joint divided by the minimum beam longitudinal reinforcing bar diameter.
6. Bond index, μ, equal to the normalized maximum beam-bar bond stress in the joint, assuming the reinforcing bar yields, in tension and compression, on opposite sides of the joint:

$$\mu = \frac{f_y d_b}{2h_c\sqrt{f_c}} \tag{2.3}$$

where f_y is the actual yield strength of the beam reinforcement (nominal values were used where data were not provided), d_b is the beam bar diameter, and h_c, f_c are as defined previously.

7. Joint transverse steel ratio, ρ_j, equal to the ratio of the area of the transverse steel in one hoop layer within the joint region (A_t) to the product of the vertical spacing of the hoop steel in the joint region (s_t), and maximum out of plane dimension of the beam or column (b_j).

$$\rho_j = \frac{A_t}{s_t b_j} \tag{2.4}$$

8. The ratio of total joint transverse steel capacity to joint shear force demand, ϕ :

$$\phi = \frac{A_{st} f_{yt}}{\tau_{\max} h_c b_j} \tag{2.5}$$

where A_{st} is the total area of joint transverse reinforcement passing through a plane normal to the beam axis, f_{yt} is the yield strength of the joint hoop steel (nominal values were used where data were not provided), and $\tau_{\max}$, h_c and b_j are as defined previously.

9. The ratio of total joint transverse steel capacity to the joint shear force at nominal strength, ϕ_{nom}, which is defined identical to Eq. 2.5 with $\tau_{\max}$ replaced by τ_{nom}.

10. The ratio of total internal column longitudinal steel capacity to joint shear force at nominal strength:

$$\varphi_c = \frac{n_{int\_c} A_{s\_col} f_{y\_c}}{\tau_{nom} h_b b_j} \tag{2.6}$$

where n_{int_c} is the total number of interior bars in the column section, which is assumed to play a role in resisting shear in the joint core, A_{s_col} refers to the cross-sectional area of a single column reinforcing steel, f_{y_c} refers to the yield stress of column longitudinal bar, and τ_{nom}, h_b, b_j are as defined previously.

11. Column axial load ratio, p:

$$p = \frac{P}{A_g f_c} \tag{2.7}$$

where P is the column axial load, A_g is the the gross cross-sectional area of the column, and f_c is as defined previously.

12. Joint aspect ratio, ι, defined as the ratio of the height of the beam section, h_b, to the height of the column section, h_c.

$$\iota = \frac{h_b}{h_c} \tag{2.8}$$

13. The ratio of yield strength of top longitudinal bars to that of the bottom longitudinal bars, ϖ, defined as

$$\varpi = \frac{(n \cdot f_y \cdot A_s)_{bt}}{(n \cdot f_y \cdot A_s)_{bb}} \tag{2.9}$$

where the subscript $(.)_{bt}$ refers to the top longitudinal beam bars and subscript $(.)_{bb}$

Table 2.2: Summary statistics for the experimental data set of 110 specimens

parameter	minimum	maximum	mean	C.O.V.
f_c (MPa)	21	118	51	0.49
$\tau_{\max\_ACI}$ (MPa)	2.03	18.29	7.09	0.53
$\tau_{\max}$ (MPa)	1.60	14.87	5.78	0.53
τ_{nom} (MPa)	1.52	18.57	6.13	0.58
$\tau_{\max\_ACI}/\sqrt{f_c}$ $(\sqrt{MPa})$	0.26	1.51	0.78	0.36
$\tau_{\max}/\sqrt{f_c}$ $(\sqrt{MPa})$	0.19	2.29	0.80	0.52
$\tau_{nom}/\sqrt{f_c}$ $(\sqrt{MPa})$	0.23	2.32	0.86	0.49
ξ d_b	$15.71d_b$	$31.48d_b$	$21.83d_b$	0.15
μ $(\sqrt{MPa})$	0.92	4.28	1.92	0.40
ρ_j	0.000	3.801	0.700	0.811
ϕ	0.00	2.70	0.62	0.90
ϕ_{nom}	0.00	2.76	0.63	1.04
φ_c	0.00	3.00	0.79	0.57
p	0.02	0.48	0.14	0.62
ι	1.00	1.50	1.08	0.13
ϖ	0.99	2.50	1.25	0.32

refers to the bottom longitudinal beam bars, n refers to the number of longitudinal beam bars, f_y refers to the yield stress of the bars, A_s refers to the cross-sectional area of the longitudinal bars.

2.3.3 Factors that determine joint response

Data obtained from experimental testing typically include the load and deformation response history, a description of damage progression, which may or may not be supported by measurements such as crack width or extent of spalling. In order to compare the experimentally observed with the simulated response in a quantifiable manner, a number of joint response parameters were computed. These included

1. *Maximum strength*: the maximum lateral load resisted by the sub-assemblage.
2. *Drift at maximum lateral load*: the ratio of lateral displacement of the top of the column to the total height of the sub-assemblage, at the point of maximum load.
3. *Drift at last cycle*: the ratio of the lateral displacement of the top of the column to the total height of the sub-assemblage, at the last load cycle.

4. *Drift capacity*: the ratio of the lateral displacement of the top of the column to the total height of the sub-assemblage, at failure. Failure is assumed to occur if there is decrease in strength of more than 20% from the maximum strength during cycles to displacement demands in excess of that associated with maximum strength.
5. *Strength loss at last cycle*: the loss of strength from the maximum during last load cycle.
6. *Strength loss at drift capacity*: the loss of strength from the maximum at the load cycle corresponding to the drift capacity.
7. *Initial stiffness*: the stiffness of the load-deformation response of the specimen in linear elastic range.
8. *Post-yield stiffness*: the tangent stiffness to the load-displacement history of the specimen after computed yield to the maximum strength. Here, yield is defined as first yield of the reinforcing steel based on loading in excess of that required to develop the computed yield moment. Stiffness were not computed for joints that exhibit softening prior to yield. Many factors such as the behavior within the joint core and flexural stiffness of beams and columns contribute to this parameter.
9. *Unloading stiffness at maximum strength*: stiffness at unloading from the maximum strength load cycle. This is a measure of stiffness deterioration of the specimen associated with inelastic response within the joint core when the global system reaches maximum strength.
10. *Pinching ratio*: the ratio of the strength at zero drift to the strength at maximum strength.
11. *Joint failure mechanism*: Each joint in the experimental data set is assumed to exhibit one of the three response mechanisms: joint failure prior to beam yielding (JF), beam flexural yielding followed by joint failure (BYJF), beam yielding with no joint failure (BY). A failure is assumed to occur if the sub-assemblage strength developed during the first cycle to a displacement demand exceeding the historic maximum displacement demand is less than 80% of the maximum strength. Beam yielding occurs if the sub-assemblage strength is greater than that required to yield beam longitudinal

reinforcement, on one side of the joint.

12. *Joint failure initiation mechanism*: Each joint was assumed to exhibit either a "brittle" failure mechanism in which the joint core failed in shear prior to flexural yielding of the beams, or a "ductile" failure mechanism in which the flexural yield strength of the beams were developed prior to failure.

These joint response parameters are discussed in greater detail in chapters 4 and 5.

2.4 Relationship between joint design and response parameters

To provide a basis for development of response models and design methodologies, the relationships between various design and response parameters were investigated.

Durrani and Wight (1982), Joh et al. (1991), Oka and Shiohara (1992) suggests that with an increase in shear stress demand, τ_{nom}, there would be an increase in trend for joint failure prior to beam yielding. Similarly, Durrani and Wight (1982), Fujii and Morita (1991), Oka and Shiohara (1992) suggests that with an increase in amount of transverse steel within the joint, ϕ_{nom}, one would expect a decreasing trend for joint failure prior to beam yielding since transverse steel resists the shear mechanism within a structure. Even though these trends were observed in clusters from plots in Figure 2.3 but no definitive direct and clear trend could be observed between a single demand parameter and the type of joint failure mechanism or the drift capacity of the joint. It should be noted in here that only 79 out of 110 specimens in the data set are being shown in plots Figures 2.3(a), 2.3(b) and 2.3(c) since complete load deformation response plots could be obtained for only 79 specimens out of 110 specimen in the literature so as to distinguish between BYJF and BY specimen. Figure 2.4 represents the effect of joint demand parameters on the a joint response parameter: the drift capacity. Only around 40 specimen are shown in Figures 2.4(a), 2.4(b) and 2.4(c) since drift capacity could only be obtained for specimen which exhibited more than 20% reduction in strength from maximum at the last drift cycle, which was typically more than 4% drift.

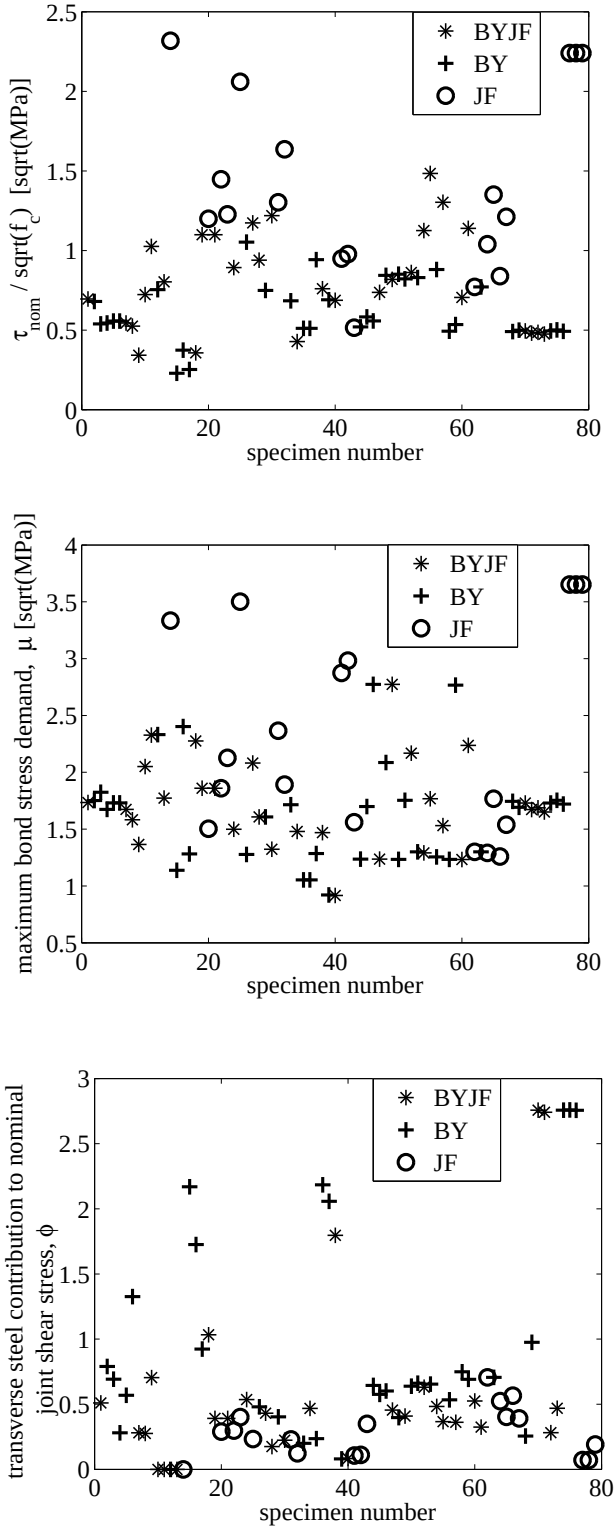

Figure 2.3: Effect of joint demand parameters on failure mechanism in joints

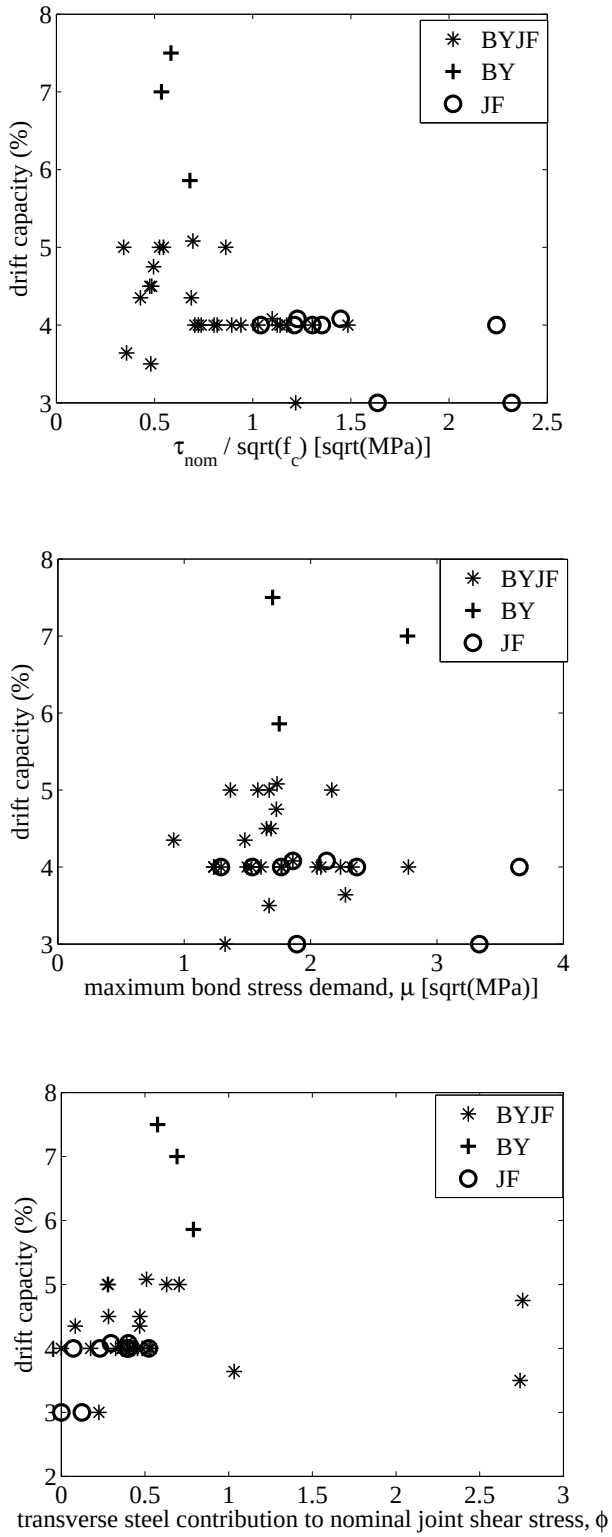

Figure 2.4: Effect of different joint demand parameters on drift capacity in joints

2.5 Probabilistic failure initiation model for interior building joints

The above study of joint design and response parameters indicates that a number of design parameters are required to determine a response parameter. To quantify the impact of individual design parameters on the failure initiation mechanism (joint failure prior or after beam yielding) a statistical model was developed.

In developing the statistical model, it should be noted that the failure initiation mechanisms are qualitative in nature whereas the parameters that are assumed to determine this qualitative response are quantitative in nature. A review of the literature indicates that previous research have not addressed the development of a probabilistic model which relates the qualitative nature of failure with quantitative design parameters. The closest study was by Zhu et al. (2006) in which a statistical model was developed to determine the failure mode for reinforced concrete columns. However, in this study, while discrete numbers were assigned to each of the column failure modes, a linear regression model was used to predict failure modes as a function of design parameters; thus, the ordered qualitative nature of the discrete dependent variables was ignored and were treated as continuous quantitative variables. As a result, the discrete qualitative nature of the failure modes could not be properly captured in such a modeling framework. Thereby, in order to associate the qualitative nature of failure modes with different quantitative variable, a discrete choice model should be utilized (Ben-Akiva and Lerman 1985, Greene 2000, Hayashi 2000, Wooldridge 2002, Washington et al. 2003).

Discrete choice models are used commonly in situations where the dependent variable represents several discrete choices or states. The application areas of discrete choice models are primarily transportation engineering, economics, and social and health sciences. For example, a discrete-choice modeling approach can be used in transportation engineering to model the decision an individual makes regarding his/her transportation mode from work to home. The individual can choose any one of the transportation modes which are auto, public transport or walking. These three different choices are assigned with different numbers such as 1, 2 or 3 which are just three discrete values and do not have any meaning attached to these values. Moreover, it should be noted that these numbers are purely

discrete, and intermediate values, for example a value 2.5, does not mean anything (Ben-Akiva and Lerman 1985). In such models, the choice of a travel mode 1, 2 or 3 is generally considered to be correlated with individuals' socio-economic and personal attributes. Given an individuals' set of socio-economic factors and personal attributes, an individual tries to maximize his/her utility from these different discrete choices. This concept originates from utility theory and is the basic building block of discrete-choice modeling (Anderson et al. 1992). Thus, a discrete choice model is used to calculate the probability of occurrence of each of the available choices, given the assumption that the individual seeks to maximize utility.

If there are two possible choices, the discrete choice model simplifies to a binary discrete-choice model. A statistical model of two choices in which the distribution of the error term (difference between an observed and a predicted value) follows Gumbel distribution is referred to as the *binary logit model*. A detailed description of this model can be found in Ben-Akiva and Lerman (1985), Greene (2000), Hayashi (2000), Wooldridge (2002), Washington et al. (2003).

2.5.1 Proposed binomial logit model for the study

The dependent variable y is dichotomous and consists of two possible choices/states: beam yielding prior to joint failure represented as choice 0 and joint failure prior to beam yielding represented as choice 1. A binomial logit model is used to determine the probability of occurrence of each of these choices. The binomial logit model is described in brief in the following paragraph. For a better and more elaborate description of the model is the reader is referred to Ben-Akiva and Lerman (1985), Greene (2000), Hayashi (2000), Wooldridge (2002), Washington et al. (2003).

Consider the occurrence of two events, $y = 0, 1$, such that the summation of the probabilities of their occurrence, $\mathbb{P}_{y=0}$, $\mathbb{P}_{y=1}$, is unity:

$$\mathbb{P}_{y=1} + \mathbb{P}_{y=0} = 1 \tag{2.10}$$

According to Ben-Akiva and Lerman (1985) and other references listed above, the logistic

regression of the above equation can be expressed as:

$$\log[\frac{\mathbb{P}_{y=1}}{\mathbb{P}_{y=0}}] = \sum_{k=0}^{K} \beta_k x_k \tag{2.11}$$

where β represents the vector of coefficients for the vector of covariates x. For the current study, the covariates x are the joint design parameters; while, the coefficients β represents the influence of these design parameters to determine the probability of failure initiation mechanism within the joint. The number of entities in the vector is represented by $k = 0 \cdots K$. From Eqs. 2.10 and 2.11 and according to Ben-Akiva and Lerman (1985) and other references listed above, it follows that

$$\mathbb{P}_{y=1} = \frac{exp[\sum_{k=0}^{K} \beta_k x_k]}{1 + exp[\sum_{k=0}^{K} \beta_k x_k]} \tag{2.12}$$

$$\mathbb{P}_{y=0} = \frac{1}{1 + exp[\sum_{k=0}^{K} \beta_k x_k]} \tag{2.13}$$

This modeling framework wad adopted to develop a probabilistic failure initiation model for reinforced concrete beam-column joints.

2.5.2 Model input and output

The assembled set of 110 experimental data (table A.5) was used to calibrate the binomial logit model and the software package, *LIMDEP 8.0*, was used for the statistical analysis. Initially, a combination of all relevant non-correlated design parameters, listed in table A.5, were used to calibrate the model. The coefficients for the parameters were readily estimated using standard maximum likelihood method. The parameters in which there was a coefficient of correlation of more than 0.6 were eliminated to finally obtain the variable list used in the final development of the probabilistic model. Re-running the analysis a number of times and reviewing the results indicated that the variables which had maximum impact in the response mechanism were $\tau_{nom}/\sqrt{fc}$, μ, ϕ, p, ϖ. The meaning of each of these symbols have

Table 2.3: Binomial logit model estimation results

variable	β	t-statistic	p-value
constant	-0.66		
$\tau_{nom}/\sqrt{f_c}/0.86$	1.63	1.86	0.062
$\mu/1.92$	3.91	3.44	0.006
$\phi_{nom}/0.63$	-1.40	-1.88	0.060
$p/0.14$	-1.64	-2.59	0.0095
$\varpi/1.25$	-3.04	-2.24	0.025

been described in section 2.3.2. The relationship of these covariates or independent variables with the dependent variable of failure initiation in joint being either due to beam yielding or joint shear is shown in Figure 2.5. These independent variables were divided by their mean values so as to obtain a comparable range between the independent variables. Table 2.3 lists the coefficients or β values, t-statistic and p-values for each of these independent variables divided by their respective mean values. The β values represent the coefficients of the independent variables or covariates divided by their respective mean values. The *t-statistic* determines the statistical significance of each of the β values and is determined by whether we can reject the null hypothesis $H_o : \beta = 0$ for each β value. The *p-values* gives a measure of confidence interval of a particular covariate. The p-value represents the smallest level of significance α that leads to the rejection of the null hypothesis. If the p-value is more than or equal to α, then the null hypothesis is rejected. In this investigation the value of α is assumed to be 0.10. The p-value and t-statistic are interrelated, the smaller the value of p, the larger is the value of t-statistic and larger is the rejection of the null hypothesis. For a detailed description of these terms the reader is advised to refer Ben-Akiva and Lerman (1985), Hayashi (2000), Wooldridge (2002), Washington et al. (2003).

The t-statistic and p-value of each of the statistical model coefficients are listed in table 2.3 followed by a detailed description of the parameters and their relative influence on determination of the joint failure initiation mechanism. The constant term represent the value of the intercept of the expression in Eq. 2.11.

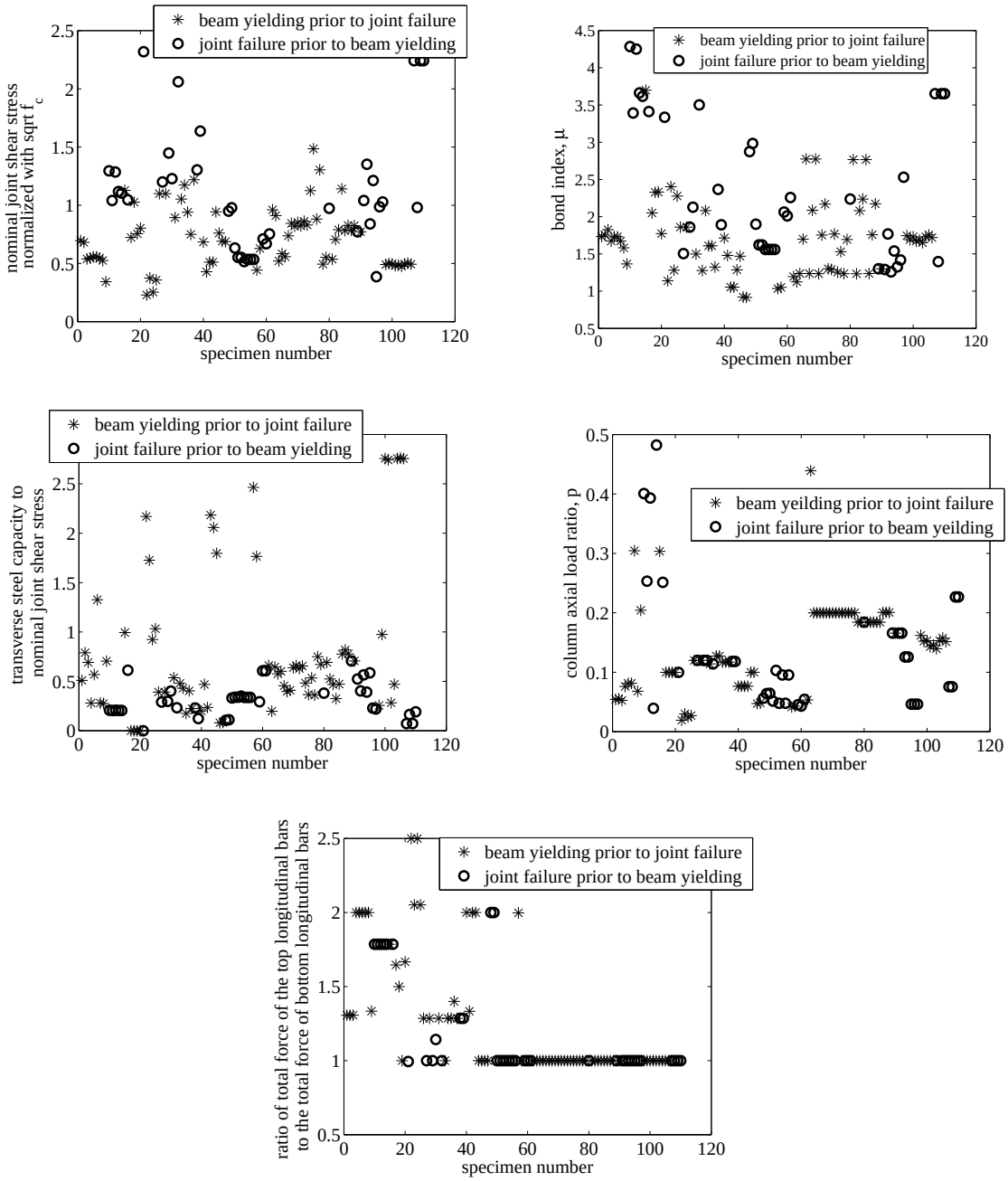

Figure 2.5: Effect of different parameters on failure initiation mechanism within the connection region

Influence of nominal joint shear strength

The data in table 2.3 show that an increase in nominal joint shear strength normalized by the square root of concrete compressive strength of concrete, $\tau_{nom}/\sqrt{f_c}$, (or joint shear stress demand at beam yielding) results in an increase in the probability of joint shear failure prior to beam yielding. This could be expected, since if the section is modified such that the shear demand at beam yielding is increased, then the propensity of the specimen failure initiation by joint shear prior to beam yielding is also increased. Previous research (Durrani and Wight 1982, Joh et al. 1991, Oka and Shiohara 1992) also supports this result that a higher joint shear stress demand results in an increased probability of brittle failure. This independent variable was also observed to be very significant with a p-value of 0.062 indicating that the value of the coefficient obtained for the variable is 94% accurate.

Influence of bond index

A higher value of μ is associated with a higher bond stress demand, at yielding of reinforcing steel, which could be expected to result in increased damage and increased likelihood of joint failure prior to beam yielding. Previous research (Oka and Shiohara 1992, Pantazopoulou and Bonacci 1994) also supports the above result as obtained from the statistical model. This independent variable was also observed to be very significant with a p-value of 0.006 indicating that the value of the coefficient obtained for the variable is more than 99% accurate.

Influence of transverse steel capacity to joint shear force demand

The independent variable ϕ_{nom} exhibits a negative correlation with the probability of joint shear failure prior to beam yielding, as expected (Durrani and Wight 1982, Fujii and Morita 1991, Oka and Shiohara 1992). This implies that increasing ϕ_{nom} (i.e. increasing the area or the yield strength of joint hoops) decreases the likelihood of a joint failure prior to beam yielding. It should also be noted in here that an upper limit to the amount of joint reinforcement was identified by Kurose (1987), beyond which the overall resistance of the beam-column joint assemblies is not improved. This independent variable was observed to

be significant with a p-value of 0.06 indicating that the value of the coefficient obtained for the variable is 94% accurate.

Influence of axial load ratio

There is no consensus within the research community as to the impact of axial load on the seismic response of joints. It has been argued that axial load improves the shear resistance of the beam-column joints by confining the joint core (Kitayama et al. 1987) or by equilibrating part of an inclined compressive strut that forms in the joint as a result of joint shear action (Paulay et al. 1978, Paulay 1989). However, it has also been concluded that column axial load affects the deformation but not the joint strength (Meinheit and Jirsa 1977, Kurose 1987, Fujii and Morita 1991, Bonacci and Pantazopoulou 1993). The statistical model indicates that an increase in column axial load ratio, p, decreases the likelihood of joint failure prior to beam yielding decreases. This can probably be justified by principles of mechanics in which if a specimen is subjected to higher column axial load, which means a higher value of p, the probability of shear failure decreases since the axial load will increase friction and thereby would tend to reduce the shearing action. The p-value for this independent variable was observed as 0.0095, suggesting that the coefficient is 99% accurate.

Influence of the ratio of the capacity of top to bottom longitudinal reinforcing bars

The independent variable ϖ defines the ratio of beam top to bottom reinforcement yield strength. If ϖ is unity, the beam has the same reinforcement top and bottom and both top and bottom reinforcement yield simultaneously if the sub-assemblage is subjected to reversed-cyclic load. If $\varpi \neq 1$ then reinforcement at top and bottom will yield at different times. Thereby the specimen cannot fully trace back to elastic state in a reversed cyclic loading. This unequal force thereby results in an increased probability of beam yielding prior to joint failure (Ichinose 1987) and hence the negative coefficient of this variable can be explained. Results show a higher value of ϖ decreases the probability of the initiation mechanism of joint failure prior to beam yielding. The p-value for this independent variable was observed as 0.025, suggesting that the coefficient is 97% accurate.

Model evaluation

Eq. 2.12 with the β values as shown in table 2.3 were used to calculate the probability for choice $y = 1$ or the failure initiation mode of joint shear prior to beam yielding. Figure 2.6 represents the results obtained from statistical analysis for choice $y = 1$. The specimen which exhibited beam yielding prior to joint failure, represented by choice $y = 0$, are plotted as circles whereas the specimen which exhibited joint failure prior to beam yielding, represented by choice $y = 1$, are plotted as squares. Each square or circle represents a single specimen test. Ideally for the event $y = 0$, the circular symbols should be near to zero whereas for event $y = 1$, the square symbols should be near to unity in Figure 2.6, which is also what is being observed from the plot. To assess the accuracy of the model, if a threshold value for predicting event $y = 1$ is taken as 0.5, then 65 out of 72 specimen could be predicted correctly with our approach for event marked by $y = 0$ and 25 out of 38 specimen could be predicted correctly for event marked by $y = 1$. Overall probability of prediction was also considerably good with a pseudo R-squared value of 0.45. Pseudo R-squared is a measure of goodness of fit for binary discrete choice models. McFadden (1974) suggests the measure $(1 - L_{ur})/L_o$, where L_{ur} is the log-likelihood function for the estimated model and L_o is the log-likelihood function for the model with only one intercept. Conceptually, pseudo R-squared values used in logistic regression are similar to R-squared values used in linear regression, the difference being that R-squared values are estimated using ordinary least-square estimate whereas pseudo R-squared values are estimated using maximum likelihood estimate. For detailed discussion of pseudo R-squared values the reader is referenced to Wooldridge (2002).

The statistical model developed here defines the probability that a joint with specific values of $\tau_{nom}/\sqrt{f_c}$, μ, ϕ_{nom}, p, ϖ will exhibit either joint failure prior to or after beam yielding. The above independent variables were identified as the most important variables determining failure initiation within joints.

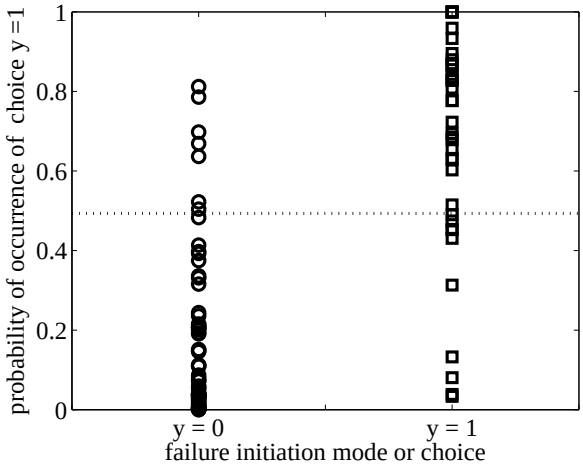

Figure 2.6: Failure initiation probability occurrence

2.6 Model application

In order to test the model with a sample outside the data set in chapter 2, sample data for a specimen from *Proposed Benchmark Problem for Blind Analysis: Tests for Validation of Mathematical Models on R/C Beam-column Joints* by Shiohara and Kusuhara (2006) was taken. The data set along with the results of the modeling efforts would be published in ACI special publication report following ACI convention in Atlanta in April 2007. In the following paragraphs, the geometric and material properties of sample A1 in the report are described which is followed by the results of the statistical analysis to determine the type of failure initiation of the model.

The geometric properties of sample A1 consists of the length of the columns from the base to the free end as 1470 mm, distance between the beam supports as 2700 mm. The cross sectional dimensions of the column is 300 by 300 mm and the beam is 300 by 300 mm. 8 bars of diameter 12.7 mm were used both in the top and bottom of the beam. 3 sets of transverse steel of diameter 6 mm and of square orientation (number of hoop legs = 2) were used for reinforcement in the joint region. The concrete compressive strength of the sample is 28.3 MPa. The yield strength of the reinforcing bars is 456.4 MPa. The yield strength of the transverse steel in the joint is 325.6 MPa. The axial load applied to the specimen is 216 kN. From experimental observations it was observed that the maximum

lateral load of the specimen is 126.6 kN. The lateral load corresponding to the point when the beam steel yields was obtained from the moment curvature analysis of the beam section as 147.35 kN. Since this load is larger than the experimental maximum load, the specimen exhibits a shear type of failure prior to beam yielding. Similar observations were made from the experimental study which concluded that the specimen exhibited a joint shear type of failure. Thereby, using the empirical equation for determination of probability of the specimen exhibiting joint shear failure prior to beam yielding, as expressed in Eq. 2.11 with coefficient values listed in table 2.3, the objective would be to determine the probability of occurrence of the event.

The demand parameters, or independent parameters for the statistical model, for the sample are evaluated. The value of $\tau_{nom}/\sqrt{f_c}$ is obtained as 1.15; μ as 1.82; ϕ_{nom} as 0.11; p as 0.08 and ϖ as 1. The ratio of these independent parameters or covariates with their respective mean values are considered and along with the coefficients from table 2.3 were used in Eq. 2.11 to obtain a probability value of joint shear failure initiation prior to beam yielding as 0.91.

2.7 Conclusions

An experimental data set for interior building beam-column joint tests was assembled. This data set includes 110 joints from 20 different experimental investigations with a wide range of design parameters that exhibit a wide range of performance in the laboratory.

These data were used to investigate the impact of various design parameters on joint response parameters. Plots of response variables versus design parameters indicate a specific trend could not be observed just by varying a single design parameter, but instead a combination of several design parameters influenced the behavior of a single response parameter.

The experimental data-set was then finally used to develop a probabilistic failure initiation model based on logistic regression. The model determines the probability of a joint with specific value of design parameters $\tau_{nom}/\sqrt{f_c}$, μ, ϕ_{nom}, p, ϖ to exhibit a joint failure prior to beam yielding. This model also identifies the upward or downward trend of the probability of joint failure prior to beam yielding with the variation of design parameters

that influence failure initiation within joints.

The model requires less computational overhead and can be utilized as a first hand estimate of the type of joint failure initiation mechanism (ductile/brittle) within the structure. This study would help an engineer in new or retrofit construction since it identifies the trends for the parameters which are of importance in determining the failure initiation mechanism for a joint specimen. A model application of using this proposed model is shown in section 2.6. Even though this study would provide a basic estimate of failure initiation within a specimen but it does not provide an engineer with a detailed load-deformation response analysis of the joint region subjected to seismic loading. Thereby, analytical methods are investigated in the following chapters to determine the load-deformation response of the specimen subjected to seismic loading.

Chapter 3
CONTINUUM MODELING OF JOINTS

3.1 Introduction

Research presented in chapter 2 identified the design parameters that determine seismic performance of joints, but it fails to provide an insight into why these design parameters affect joint response. To improve understanding of the joint response mechanisms that determine behavior and finally to develop a mechanistic model, a nonlinear continuum modeling strategy was investigated.

This chapter first presents a review of previous research that applied nonlinear continuum finite element modeling to investigate the behavior of beam-column joints. Second, the scope of the current modeling effort, which was determined in part by the results of previous studies, is presented. Third, the concrete, steel and bond-zone constitutive models employed in the continuum model are presented. Fourth, the results of a series of a validation analysis are presented, which include comparison of simulated and observed response histories for a series of plain and reinforced concrete specimens. Fifth, the results of a series of analysis of two joint specimen from the experimental data set are presented and evaluated to yield conclusions about the viability of continuum modeling for investigating joint behavior.

3.2 Review of research efforts to simulate the response of interior RCBC joints

The response of joints under seismic loading is determined by multiple, complex material phenomena including cracking of concrete, crushing of confined and unconfined concrete, closing of concrete cracks under load-reversal, shearing across concrete crack surfaces, yielding of reinforcing steel and damage to bond-zone concrete. Accurate simulation of joint response requires accurate simulation of all these phenomena. Given the complexity of the simulation effort, relatively few research studies have applied continuum modeling to interior building beam-column joints; these studies include Will et al. (1972), Noguchi (1981),

Pantazopoulou and Bonacci (1994).

One of the first studies was by Will et al. (1972) in which 2D continuum finite element analysis was performed to understand the pre-peak response mechanism of an external beam column joint subjected to monotonic loading. Four-node plane stress elements were used for both concrete and steel bars. Concrete was modeled as a linearly elastic material both in tension and compression. Cracks were initiated normal to the maximum principal stress direction and upon cracking the modulus of elasticity, normal to the crack direction, was set to zero, implying brittle fracture. Bond slip was simulated using link elements with a linear bond stress-slip relation The reinforcing steel was simulated using 2 node truss elements with elastic stress-strain relationships.

Noguchi (1981) analyzed the nonlinear behavior of planar joints using 3 node (linear strain) triangular elements both to model concrete and longitudinal steel. The representation of longitudinal steel using 3 node triangular elements enabled simulation of dowel action. Stirrups and ties were modeled using truss elements. Uniaxial response of concrete was modeled using the constitutive model by Darwin and Pecknold (1977). Cracking of concrete was modeled by in the context of discrete crack approach using crack-link springs. These springs were placed along the potential cracking directions predetermined from experimental test results. Upon crack initiation along a particular grid line, the initial large stiffness of these springs were set to zero. Bond slip between steel and concrete was modeled using bond-link springs whose stiffness were determined from bond stress-slip relations by Darwin and Pecknold (1977). The influence of bond characteristics of the beam bars on the tie-strain within the joint was judged as insignificant. However, the bond deterioration caused the local compression failure of concrete near the joint. Post-peak compressive stress softening behavior of concrete was suggested to be incorporated in the analytical model to avoid over-estimation of beam yield strengths.

Pantazopoulou and Bonacci (1994) performed 2d continuum analysis of joint sub-assemblages to investigate the influence of different design parameters on joint behavior. Plain concrete was modeled using four-node plane stress elements; two-node nonlinear truss elements were used to model the reinforcing steel in beams, columns and joint. Inelastic concrete behavior was defined based on modified compressive field test for concrete (Vecchio and Collins 1986)

under two dimensional state of stress. A trilinear hardening material model was considered to represent the reinforcement bars. Bond between concrete and reinforcement was modeled using a contact element (Atrach 1992). The researchers concluded that 1) the joint transverse steel serves to confine the joint core concrete and contributes to the shear resisting mechanism, 2) participation of the joint core concrete to the mechanism of shear resistance decreases with the increase in the volume of joint transverse steel, and 3) joint performance deteriorates rapidly after yielding of joint hoops.

3.3 Scope of the modeling effort

For the current study, the objective of the continuum modeling effort is to improve the understanding of nonlinear response mechanisms that determine the seismic behavior of RC joints. However, the need for accurate simulation of response must be balanced against the computational effort of the analysis. The following paragraphs discuss the chosen scope of the continuum modeling effort so as to achieve a balance between accurate simulation of response mechanisms and computational effort.

3.3.1 Two-dimensional simulation

Observations of experimental tests and the results of post-earthquake reconnaissance show that the beam-column joints accumulate damage, exhibit stiffness loss and potentially exhibit strength loss that may result in structural failure. Even though a 3D frame is the most typical structural system, two-dimensional representation and simulation of joints in a building structure is being considered in the research since 2D joints represents the worst-case scenario. The out-of-plane members, if present, improve system response by providing increased confinement in the joint region. Previous research by van Mier (1984) concludes that a relatively small confining pressure (5 to 10 percent of one of the in-plane stresses) results in a significant increase in strength of concrete in the plane of primary loading.

It is known from previous research that a moderate earthquake excitation in a building structure is predominantly resisted by frame members, whereas severe excitation may result in activation of inelastic response mechanisms in the joint region. Since the loading in the beam-column joint is primarily from frame action, which for typical structural analysis is

considered to be two-dimensional, it is reasonable to consider a 2D representation of the joint region. It is assumed that under severe loading conditions, dilation or expansion of concrete which is controlled by transverse hoops is negligible in comparison to the longitudinal and in-plane applied loading, thereby a plane stress generalization of the problem is reasonable.

3.3.2 Pseudo-static loading

Experimental observations show that strain rate affects the tensile strength, compressive strength, fracture energy of concrete (Hughes and Gregory 1972; 1978, Ross et al. 1995; 1996, Yon et al. 1992). However, in relatively low strain rates developed under earthquake loading, the effect of strain rates on the material properties of concrete are insignificant (Lowes 1999). Moreover in seismic loading, the period of time during which strain rates approach the peak values may be so limited that it is unnecessary to consider the effect of load rate in the constitutive model for concrete.

3.3.3 Software used

A commercial nonlinear finite element software package, DIANA 9.1, was used for the finite-element modeling and simulation effort. DIANA 9.1 has all the necessary element formulations and nonlinear constitutive models required for continuum modeling of joints. A plane stress quadrilateral element was used to represent concrete, a truss element to represent longitudinal steel reinforcement, and an interface element to represent the bond action in between steel and concrete. The constitutive models used for each of these elements and their response to different type of loading has been provided in subsequent sections in this chapter.

3.4 Constitutive models for simulation of reinforced concrete structures

The response of a reinforced concrete structure is characterized by the response of it's constituent materials: concrete, steel and bond elements. Since, loading in a beam-column connection results primarily from the flexural action in the beams and columns, the constitutive model selected to represent concrete should represent well the behavior of concrete under

uniaxial and biaxial tension and compression. The reinforcements are subjected to uniaxial forces and the effect of dowel action has been neglected in the analysis of beam-column joints subjected to seismic loading. Thereby, the constitutive model for reinforcements should be able to capture the uniaxial response of tension and compression. The tangential response of the bond elements connecting the reinforcement bar with the concrete should also be modeled when selecting a constitutive model for the bond element. The radial response of the bond element need not be considered in our analysis, since radial bond response usually results in splitting failure and this type of failure mechanism is not typically observed in case of a beam-column joint. The behavior and constitutive models used for concrete, steel and bond elements are discussed in the following sections.

3.4.1 Compressive response of plain concrete

Plain concrete is a composite comprising mortar, which may include voids, microcracks and aggregates. The response of plain concrete under compressive loading is determined by the nucleation and propagation of microcracks which occurs primarily in the mortar and the interface between mortar and aggregate (van Mier 1984, Vonk 1992, Mehta and Monteiro 1993, Kotsovos and Pavlovic 1995).

Despite the fact that concrete is a composite, for modeling of RC structures, concrete is typically modeled as a homogenous material to facilitate the analysis process by reducing the computational demand of the analysis. Moreover, very few data exist for simulation of the response of mortar, and aggregate-mortar interface zones. At uniaxial compression stress levels less than approximately 30% of the concrete compressive strength, concrete behaves as a linear elastic material as the pre-existing microcracks are stable and do not propagate. As the stress level increases up to the maximum strength, these microcracks starts to grow and the formation of combined mortar and interface-zone cracks can be observed. This phenomenon is observed in laboratory compression tests of concrete cylinders and also nonlinearly in the gross load-deformation response history. After the maximum compressive strength is reached, the microcracks localize in narrow bands and coalesce to form macro-cracks that result in the strength loss.

Theory of plasticity which includes the definition of a yield surface, flow rule, and hardening/softening rule was used to represent the behavior of concrete in compression.

Plasticity based models for modeling compressive response in concrete

Plasticity theory has been used by many researchers to represent the response of concrete in compression with good results (Resende and Martin 1984, Simo and Ju 1987, Frantziskonis and Desai 1987, Mazars and Pijaudier-Cabot 1989, Pramono and Willam 1989, Lubliner et al. 1989, Yazdani and Schreyer 1990, Cervera and Oliver 1995, de Vree et al. 1995, Lee and Fenves 1998, Lowes 1999). Typically, plasticity model is defined by a yield surface, flow rule, and hardening/softening rule. The yield/failure surface is the surface that bounds the elastic domain. The hardening/softening rule defines the evolution of the yield/failure surface. The flow rules define the evolution of a set of internal variables that uniquely define the material state.

Assuming a homogenous, isotropic material, the general form of the yield surface for concrete can be represented as (Chen and Han 1988)

$$f(I_1, J_2, J_3) = 0 \tag{3.1}$$

where I_1 is the first invariant of the stress tensor and J_2 and J_3 are respectively the second and third invariant of the deviatoric stress tensor. These invariant of the stress tensor are expressed in principle plane (with σ_1, σ_2 and σ_3 as principal stresses) as follows

$$\begin{aligned}
I_1 &= \sigma_1 + \sigma_2 + \sigma_3 \\
J_2 &= \frac{1}{6}\left[(\sigma_1 - \sigma_2)^2 + (\sigma_2 - \sigma_3)^2 + (\sigma_3 - \sigma_1)^2\right] \\
J_3 &= \frac{1}{27}\left[(\sigma_1 - \sigma_2)^2(\sigma_1 - 2\sigma_3 + \sigma_2) + (\sigma_2 - \sigma_3)^2(\sigma_2 - 2\sigma_1 + \sigma_3) + (\sigma_3 - \sigma_1)^2(\sigma_1 - 2\sigma_2 + \sigma_3)\right]
\end{aligned}$$

A variety of yield/failure surface have been proposed for concrete. Chen (1982) provides a detailed discussion and classifies these, by the number of material constants appearing in the expression, as one-parameter through five-parameter models. A brief review of these follows:

- *One-parameter model:* These models include the von Mises and Tresca failure criterions. These are pressure independent surfaces and are typically not used for modeling concrete compressive response. However, these are sometimes used to define the tensile behavior of concrete.
- *Two-parameter model:* Drucker-Prager and Mohr-Coulomb are the simplest pressure-dependent failure surfaces and are widely used to model concrete compressive response. In these models, the octahedral shear stress τ_{oct} depends linearly on the octahedral normal stress σ_{oct}. Moreover the Drucker-Prager surface suffers from another shortcoming: independence of the angle of similarity, or lode angle, θ. Thereby these models cannot be applied for describing failure of concrete in high triaxial compression range (Chen and Han 1988). However these models do reasonably well in a two-dimensional range.
- *Three-parameter model:* Bresler and Pister (1958) proposed a generalized Drucker-Prager surface that assumes a parabolic dependence of τ_{oct} on σ_{oct}.
- *Four-parameter model:* Ottosen (1977) proposed a four-parameter model. Simplifying the relationship proposed by Ottosen, Hsieh et al. (1982) proposed another four-parameter model. Both the models exhibit a parabolic $\tau_{oct} - \sigma_{oct}$ relationship and lode angle or θ-dependence and are valid for a wide range of stress combinations.
- *Five-parameter model:* Willam and Warnke (1975) proposed a highly refined and smooth five parameter model which can be utilized for a wide range of stress combinations. This model also exhibit a parabolic $\tau_{oct} - \sigma_{oct}$ relationship and lode angle or θ-dependence.

For the current study, the Drucker-Prager model is used. The improvement of the higher parameter models over the Drucker-Prager model is primarily to include a parabolic dependence of τ_{oct} on σ_{oct}. The parabolic dependence is important for simulation of response under loading to large hydrostatic pressure levels. For the current application, in which concrete is subjected to only moderate hydrostatic pressure loading, the Drucker-Prager model is adequate for defining the yield surface of concrete.

Beyond definition of the yield surface, definition of a plasticity-based constitutive model

requires also specification of the plastic flow rule. The flow rule defines the orientation of the plastic strain. Two options exist: associative flow in which the orientation of the plastic strain is normal to the yield surface and non-associative flow in which the orientation of the plastic strain is not normal to the yield surface. Typically, to obtain improved numerical stability and due to lack of precise data for model calibration, associative flow is assumed (Lubliner et al. 1989). The primary drawback of this approach is overestimation of plastic dilation (Chen and Han 1988) at compressive loading, which can be a significant problem for cases of high hydrostatic pressure. For the present problem, this could be expected to result in over-estimation of the confining effect of transverse steel on concrete strength.

Evolution of the plastic yield surface i.e., the hardening/softening rule, is the final component of a plasticity-based model. For the current study, a hardening function is calibrated such that the concrete response under uniaxial compression matches the empirical curve proposed by Popovics (1973).

The Drucker-Prager yield surface, associative flow rule, strain-hardening rules, that are used for modeling of concrete behavior, are provided in details in the DIANA 9.1 manual on material modeling. The nonlinear relationship between the internal state variable, κ, and cohesion, c, in the Drucker-Prager expression was calibrated based on the following approach:

- Concrete is assumed to be linear elastic until the compressive stress equals 30% of the maximum compressive strength.
- Strain hardening assumption is being used, thereby the internal state variable, κ, is defined as a function of the rate of plastic strain $\underline{\underline{\dot{\varepsilon}^p}}$.
- Popovics (1973) relation was utilized to determine the uniaxial stress-strain response of the material.
- For any strain value above that associated with 30% of the maximum compressive strength of concrete, the plastic strain is obtained by subtracting out the elastic strain from the total strain. In an uniaxial case, the elastic strain is represented as $\varepsilon^e = \sigma/E_c$ where E_c is the modulus of elasticity of concrete.

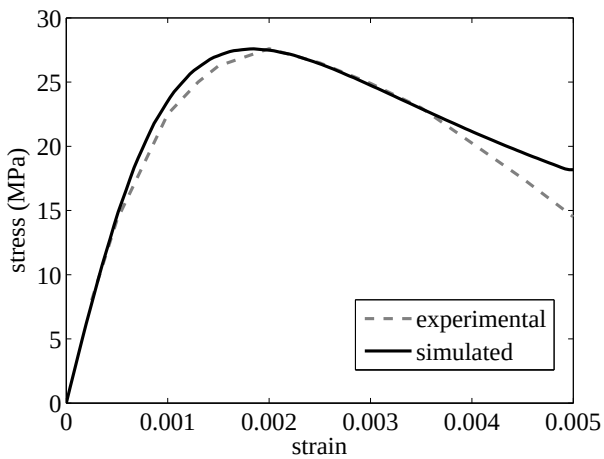

Figure 3.1: Simulation of unconfined uniaxial compression test by Karsan and Jirsa (1969)

- The cohesion parameter, c, corresponding to the previously calculated κ, is computed using the equation for the yield surface for uniaxial case.

For normal strength concrete, the ratio between the uniaxial compressive strength and the equal biaxial compressive strength is approximately 1.16 (Kupfer and Gerstle 1973) which results in a friction angle $\phi \approx 10°$ (DIANA 9.1 manual on materials). Utilizing the above process, we obtain a good correlation between simulated and observed compressive stress strain response for a 25.4 mm square concrete specimen block with unconfined compressive strength of 27.6 MPa, and initial stiffness of 31.7 GPa. (Karsan and Jirsa 1969). Figure 3.1 shows the comparison in between the observed and the simulated stress-strain response.

3.4.2 Modeling concrete crack response

Tensile loading of concrete results in the development of discrete cracks. When a concrete specimen is loaded in tension, up to approximately 90% of it's maximum tensile strength, it behaves as a linearly elastic material. At loads beyond 90% of the tensile strength, micro-cracks form and rapidly coalesce to form macro-cracks perpendicular to the principal stress direction. These micro-cracks widen resulting in strength and stiffness deterioration. The energy released per unit area of the crack surface is referred to as the fracture energy density,

or simply the fracture energy, which is considered to be a material parameter.

It should be realized that a crack (a macro-crack) represents a displacement discontinuity. Cracks have been modeled discretely by researchers (Ngo and Scordelis 1967), but this process requires a-priori knowledge of the orientation and the location of the crack. Thereby, within the context of continuum finite elements, it is a standard practice to model this displacement discontinuity in a smeared manner over a certain region with reduced strength and stiffness (Rashid 1968). Thus cracking is simulated using a fictitious constitutive model that avoids the need for change in geometry and remeshing. Within this smeared concept, in which fictitious constitutive models are used to represent crack, there are four different ways to model cracks: 1) using empirical formulaes obtained from shear panel tests of reinforced concrete panels (Vecchio and Collins 1986), 2) phenomenological approach of using fixed, rotating and multiple rotating cracks (de Borst and Nauta 1986), 3) use of damage plasticity relationships (Lubliner et al. 1989), and 4) microplane models (Bažant 1984). A comprehensive review of the behavior of all these different smeared crack models (with the exception of the first one) is provided in Rots and Blaauwendraad (1989), de Borst (2002). Apart from introducing cracks through fictitious changes in the constitutive models, cracks can also be introduced by local enrichment of stress and/or displacement and/or strain relationships of the element formulation in finite element analysis. These methods include the 1) Cosserat continua (de Borst 1991), 2) Higher order gradient (Voyiadjis and Dorgan 2001) and 3) Embedded discontinuity methods (Jirásek 2000). A comprehensive review of the Cosserat and the Higher order gradient methods are provided in de Borst (2002), whereas a review of different methods under the embedded discontinuity methods are provided in Jirásek (2000). A more detailed and complete literature review of all these different methods of modeling cracks are presented in Appendix C. For our application, discontinuous strain multi-directional fixed crack (de Borst and Nauta 1986) was considered because of its' availability in the commercial software program DIANA 9.1.

Within the context of smeared formulation of cracks in concrete, once the concrete reaches it's tensile strength it does not behave in a brittle manner but exhibits a tensile softening response. The post-peak tensile stress-strain relationship has been approximated

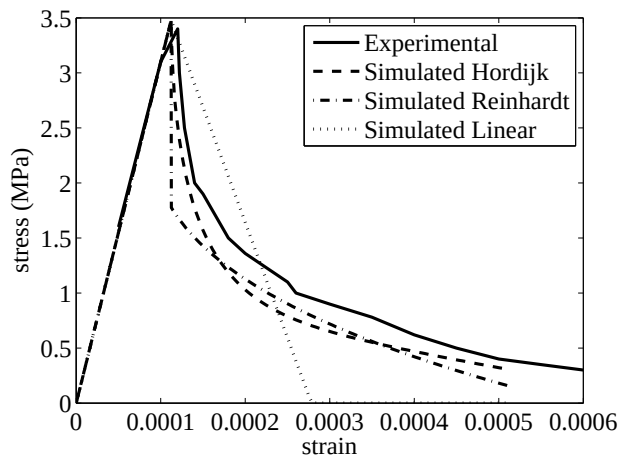

Figure 3.2: Simulation of uniaxial tensile test by Gopalratnam and Shah (1985)

by different functions ranging from linear, exponential curve by Reinhardt (1984),

$$\sigma_{cr} = \begin{cases} f_t \left(1 - \frac{\varepsilon_{cr}}{\varepsilon_{cr}^{ult}}\right)^{0.31} & if \;\; 0 < \varepsilon_{cr} < \varepsilon_{cr}^{ult} \\ 0 & otherwise \end{cases} \tag{3.2}$$

cubic exponential curve by Hordijk (1991).

$$\sigma_{cr} = \begin{cases} f_t \left(\left(1 + \left(3\frac{\varepsilon_{cr}}{\varepsilon_{cr}^{ult}}\right)^3\right) \exp\left(-6.93\frac{\varepsilon_{cr}}{\varepsilon_{cr}^{ult}}\right) - \frac{\varepsilon_{cr}}{\varepsilon_{cr}^{ult}}\left(1 + 3^3\right)\exp\left(-6.93\right)\right) & if \;\; 0 < \varepsilon_{cr} < \varepsilon_{cr}^{ult} \\ 0 & otherwise \end{cases} \tag{3.3}$$

where σ_{cr} refers to cracked concrete stress, ε_{cr} refers to cracked concrete strain, f_t as the tensile strength in concrete, ε_{cr}^{ult} as the ultimate concrete cracked strain after which there is zero stress. Figure 3.2 shows that the cubic exponential curve by Hordijk (1991) performs better in simulating the experimentally observed response of Gopalratnam and Shah (1985) tension block loaded uniaxially. The experimental concrete tension block has dimensions of 305 by 76 by 19 mm with an initial stiffness of 33.5 GPa, tensile strength of 3.62 MPa and fracture energy of 56 N/m.

The modeling of crack initiation and propagation is one of the most important aspects for failure analysis of concrete structures. Even though the primary source of formation

of cracks in concrete is tensile loading, since concrete as a material is weak in tension, but in a two-dimensional force field both tension and compression contributes to formation of cracks. The mechanism of crack formation and propagation in concrete structures is significantly different from cracking exhibited by other materials, such as metal or glass, in that it is not a sudden onset of new free surfaces, but a continuous forming and connecting of microcracks (Mehta and Monteiro 1993). There exists a huge literature on modeling of cracks in quasi-brittle materials such as concrete. As discussed in the previous paragraph, that even though comprehensive reviews have been proposed by several researchers (Rots and Blaauwendraad 1989, Jirásek 2000, de Borst 2002) of one or more categories of crack formulation, a full complete comprehensive review of all different modeling strategies of cracks is yet to be done. A complete comprehensive review of different methods of modeling of cracks have been presented in Appendix C.

In this thesis, a smeared methodology using a decomposed-strain multi-directional fixed crack model (de Borst and Nauta 1986) was used to represent cracks in concrete because of it's simplicity and it's ability to be used with plasticity models. The model is based on decomposition of the total strain increment at a gauss-quadrature point into a concrete and a crack-strain increment. This decomposition permits the combination of the phenomenon of crack formation with other non-linear phenomena such as plasticity to represent the behavior of concrete in compression. As the name suggests, multiple cracks are allowed to form at a gauss quadrature point. A crack is said to originate once the cracking criterion is satisfied (i.e. user specified threshold angle is exceeded and also the maximum tensile strength is exceeded). The threshold angle refers to the angle from the plane of the first crack to a plane where the next crack can originate. Thereby, if the threshold angle is provided as 180° then this model reduces down to a single fixed crack model, whereas theoretically if the threshold angle is made equal to 0° and the effect of other open cracks at the gauss-quadrature points are erased then it represents a rotating-crack model (refer Gupta and Akbar (1984), Crisfield and Wills (1989)). Details about this model can be found in de Borst and Nauta (1986) and also in the DIANA 9.1 manual on material modeling.

3.4.3 Modeling of reinforcements

For the current study, reinforcing steel is assumed to act as a truss element and carry load only along its axis. Plasticity-based models are used to model reinforcing steel. In this thesis, von Mises plasticity is used to characterize the constitutive behavior of reinforcing steel. For simplicity reasons, the material is considered to be perfectly plastic and Bauschinger effect is not considered.

3.4.4 Modeling of bond between reinforcement and concrete

Bond refers to the transfer of stress between reinforcing steel and concrete; bond develops through the combined action of chemical adhesion, friction, and mechanical interaction response between the lugs of the reinforcing steel and bond-zone concrete. Bond is necessary for composite action in RC structures and is critical to the behavior of RC structures (Paulay et al. 1978). The results of a number of studies indicate that 1) chemical adhesion is lost early and is negligible for deformed reinforcement, 2) friction controls response for well confined bond-zones near failure when large slip between concrete and steel has resulted in crushing of all the concrete between the lugs and reinforcing steel, 3) friction and mechanical interaction determine response for most bond-zones at intermediate slip levels (Lutz and Gergeley 1967), 4) mechanical interaction results in radial and splitting type of failure. The mechanics of bond can be found in classic papers of Rehm (1957), Lutz and Gergeley (1967). Bond is manifested by two different mechanisms: flexural bending in which multiple cracks form perpendicular to the bars; anchorage in which cracks form parallel and perpendicular to the bar axis eventually developing into conical surfaces and bar stress varies from a maximum at one "free end" to zero stress at the other end.

Experimental bond tests typically result in data characterizing average bond stress versus slip, where slip is the displacement of the reinforcing bar relative to the surrounding concrete in the direction of the bar axis. Bond material models are typically fit to these data (Viwathanatepa et al. 1979, Eligehausen et al. 1983, Morita and Kaku 1984, Shima et al. 1987, Gambarova et al. 1989a, Malvar 1991). Apart from these, there also exists more fundamental bond models that represent the behavioral mechanism of bond. Even then

experimental results are required for calibration of these models. An extensive review of experiments and analytical investigations on bond can be found in Cox (1994). From a theoretical perspective, bond can be modeled at several scales: 1) Rib/Lug scale models (Hungspreug 1981, Reinhardt et al. 1984, Ožbolt and Eligehausen 1992, Yao 1992, Wang 1993), 2) Bar scale models and 3) Member scale models (Feenstra 1993, Vecchio and Collins 1986, Hsu 1988). In this thesis one dimensional "bar-scale models" have been considered since these models are most commonly used.

In a bar-scale model, reinforcing bar and concrete is treated as a continuum, and the mechanical interaction of the ribs are homogenized and modeled as interface phenomena. Most of the existing models on bond are at this level since this level characterizes the local bond behavior within a global framework of finite element methods. Springs, interface elements or contact elements can be utilized in this modeling strategy to represent the bond action in between steel and concrete. This modeling strategy can be subdivided into two different types:

- *One dimensional models* in which only the normal stress slip relation in between the concrete and bar was modeled. Experimental studies are an essential basis of these models and these have also been extended to cyclic bond behaviors. Examples in this category include Morita and Kaku (1973), Dörr (1978), Viwathanatepa et al. (1979), Tassios (1979), Shipman and Gerstle (1979), Eligehausen et al. (1983), Filippou (1986), Yankelevsky et al. (1992), and many others.
- *Two dimensional models* incorporates both the normal stress and radial dilation into the formulation. Prominent contributions in this category are by de Groot et al. (1981), Morita and Fujii (1985), Mehlhorn and Keuser (1985), Mainz et al. (1992), Cox (1994).

In this thesis, the reinforcements are connected to the concrete region through interface elements whose material relationship has been calibrated to match the uniaxial bond-slip model proposed by Eligehausen et al. (1983).

3.5 Benchmark simulation studies

To improve understanding of the finite element simulation of the response of concrete structures, a number of simulation of experimental tests were conducted using DIANA 9.1. These include the simulation of concrete, fracture-energy tests, bond pull-out tests, a bond flexural crack formation test and flexural tests of reinforced concrete beams. For each of these simulation studies, a prototype model was developed and then modified to evaluate the impact of different constitutive models and parameters on predicted response. Details of the comparison between simulation and experimental data are presented below.

3.5.1 Simulation of concrete tensile response - three-point bend test

Simulation of the behavior of concrete in tension is critical to modeling the behavior of joint sub-assemblages. To obtain a better understanding of the application of DIANA 9.1 for simulation of concrete response to tensile loading, simulated and observed load-displacement histories, and crack patterns for a series of "three-point test" of plain concrete beams were compared. Specifically, results were used to identify the way in which various model parameters affect predicted response, and ultimately identify a preferred approach to model concrete subjected to tensile loading.

Typically, experimental three-point bend tests on a notched beam (Hillerborg et al. 1976, Hillerborg 1985, Malvar and Warren 1988, Malvar and Fourney 1990, Kozul and Darwin 1997, Martin et al. 2006) are carried out to determine the fracture energy of a specimen[1]. The fracture energy is a measure of the toughness of a material, and is defined as the energy absorbed in creating a unit area of the fracture surface. Fracture energy of concrete is a property which is inherent with tensile loading of a specimen. Since the compressive strength of concrete is 5 to 10 times the tensile strength, energy absorption due to plastic compressive response is not expected to occur in these tests and all energy dissipation is assumed to occur through concrete fracture (Hillerborg 1985).

Simulation of the experimental test specimen by Malvar and Warren (1988), Martin

[1] Apart from three-point bend tests there are also other methods to determine fracture-energy and thereby behavior of concrete in tension, namely Jenq and Shah (1985), Bažant and Pfeiffer (1987).

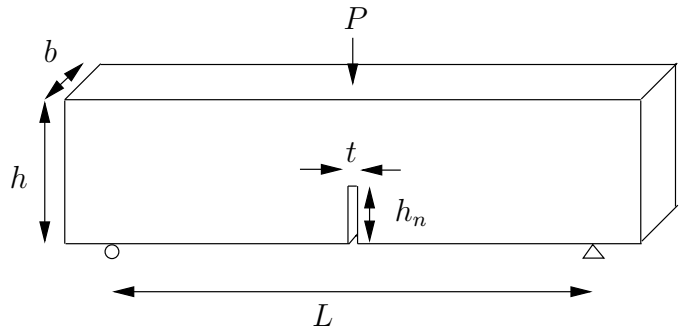

Figure 3.3: Simulation of concrete tensile response: 3 point bend test

et al. (2006) were used for the benchmark study on tensile behavior of concrete. Figure 3.3 shows a prototype specimen. Tables 3.1 and 3.3 provide the specimen geometry details and tables 3.2 and 3.4 provide the specimen material specifications.

The prototype model, shown in Figure 3.3, has length between the supports represented by L, height of the specimen as h, out of plane depth of the specimen b, notch width t, height of the notch from the beam base at the middle length of the beam h_n. A monotonically increasing load P is applied at the top of a simply supported specimen. The material properties required for simulation are concrete tensile strength f_t, fracture energy G_f, shear retention value β, poison's ratio ν, modulus of elasticity for concrete E_c. The prototype model had the following characteristics:

- Concrete model with phenomenological multi-directional smeared cracks (de Borst and Nauta 1986) and Hordijk model (Hordijk 1991) for tension softening.
- A crack is induced if the normal stress in a plane exceeds the value of tensile strength of concrete, f_t. Origination of other crack planes are based on results if the both the tensile strength and the threshold angle is exceeded.
- A threshold angle of 60° was chosen since a large number of cracks would defeat the purpose of a robust solution and would generate unnecessary convergence problems.
- The crack band width was taken as the element dimension perpendicular to the direction of loading, under the assumption that only one major crack in the specimen contributes to failure by cracking.
- Eight-node quadrilateral elements with 2 by 2 gauss quadrature integration scheme

Table 3.1: Malver-Warren geometry

L	h	b	t	h_n
394 mm	102 mm	102 mm	10 mm	51 mm

Table 3.2: Malver-Warren material

f_t	E_c	ν	G_f	β
3.1 MPa	21.7 GPa	0.18	73 N/m	0.01

Table 3.3: UW specimen geometry

L	h	b	t	h_n
18 in	6 in	3 in	0.25 in	3 in

were used to represent the concrete region.

- According to RILEM specifications controlled loading is to be applied on the top surface of the specimen to produce a specific rate of crack width opening. Since such load-control is not possible for typical finite element solution algorithms, loading in the finite element is introduced by monotonically increasing vertical displacement (in the negative direction) at the point of load application.

The modeling parameters that were varied in the prototype model were the fineness of the mesh, threshold angle for subsequent crack formation θ, shear retention value β, type of post-peak softening curve, fracture energy parameter G_f, tensile strength of concrete f_t, modulus of elasticity of concrete E, crack models, element types and gauss quadrature rules for different elements.

Malvar and Warren (1988) test

The dimension and material properties of the prototype specimen are provided in tables 3.1 and 3.2. Good correlation could be observed between the observed and simulated load-deformation response of the specimen (Figure 3.4).

Martin et al. (2006) test

The model material and geometric parameters are shown in tables 3.3 and 3.4.

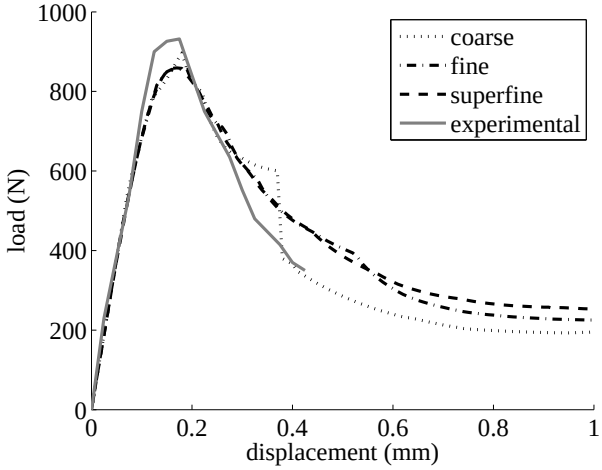

Figure 3.4: Simulation of 3 point beam-bending fracture energy test by Malvar and Warren (1988)

Table 3.4: UW specimen material

f_t	E_c	ν	G_f	β
526.5 psi	5530 ksi	0.2	0.8 lb/in	0.001

Figure 3.5(a) shows a good correlation between the simulated and experimental load-deformation fracture energy response. It is to be noted that there is significant difference between the three experimental strength predictions. The reason for this is primarily due to errors in testing procedure and measurement of beam deflection that are discussed in detail in Martin et al. (2006). Figure 3.5(b) shows the crack patterns at different displacement steps as observed in the simulation study which closely matches the crack patterns observed in the laboratory. For purpose of clarity, the figure only shows the zoomed region above the notch where the crack forms.

Impact of mesh refinement

The mesh size was varied in the specimen test by Martin et al. (2006) and since the fine and the superfine meshes provide essentially the same response in Figure 3.6, it confirms that the solution is not exhibiting mesh-sensitivity but is converging towards an exact solution as the deformation field is more accurately represented by more elements. The size of the mesh in the coarse mesh specimen was 0.125 by 0.25 mm, in the fine mesh specimen was

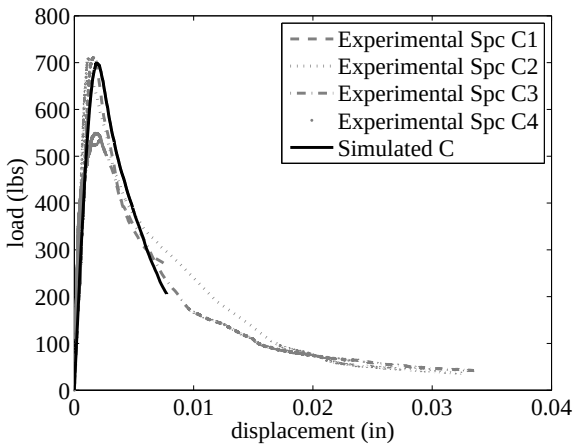

(a) Simulation of experimental investigation at UW

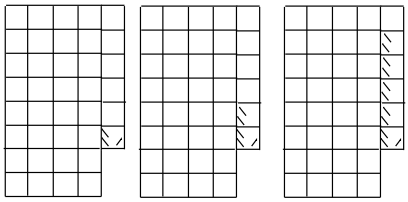

(b) Progression of cracks while using Q8 2*2 element

Figure 3.5: Simulation of fracture energy test at University of Washington

0.125 by 0.1875 mm and in super-fine mesh specimen was 0.125 by 0.125 mm. A total of 847 eight-node quadrilateral elements were used for the concrete region in simulation of the specimen for coarse mesh size, 1129 for fine mesh size and 1693 for super-fine mesh size. The figure also confirms a good correlation between the elastic simulated and observed initial stiffness of the specimen.

Impact of concrete post-peak softening curve

The behavior of concrete in tension is not purely brittle but instead, characterized by moderately rapid strength loss (de Borst and Nauta 1986, Feenstra and de Borst 1995). A number of different post-peak curve for concrete in tension have been proposed by different researchers such as an exponential decay curve (Cornelissen et al. 1986) expressed in Eq. 3.2, cubic exponential decay curve Hordijk (1991) expressed in Eq. 3.3. These different post-peak softening curves were used in the simulation of the sample. Figure 3.7 identifies that the Hordijk curve, which has been used in the prototype model, gives a better correlation with experimental data.

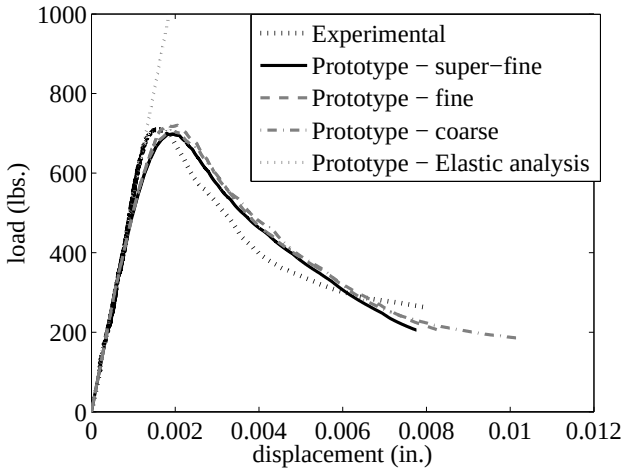

Figure 3.6: Simulation for mesh-sensitivity

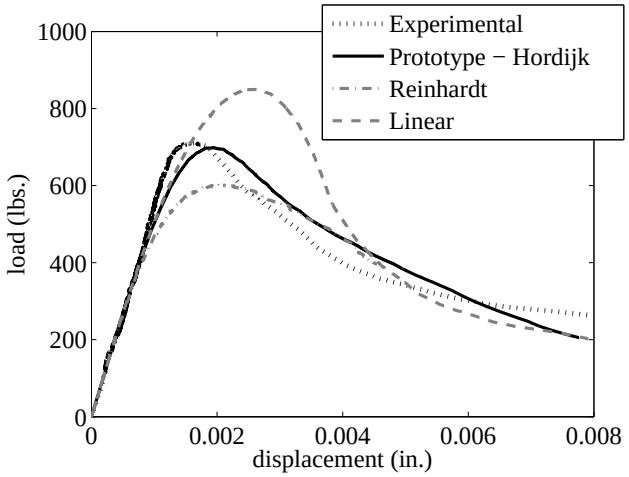

Figure 3.7: Simulation with different tension softening curves

Impact of concrete cracking model

A smeared crack model was used in this study because of its simplicity. However, the smeared crack model can be implemented in a number of different ways. The prototype model in the thesis uses a decomposed strain multi-directional fixed crack model developed by de Borst and Nauta (1986) (refereed to as the *prototype DSMFC model*). The prototype model was compared with other smeared crack models namely total strain smeared fixed crack developed by Rots and Blaauwendraad (1989) (referred to as *TSSFC*) and total strain smeared coaxial rotating crack model developed by Crisfield and Wills (1989) (referred to as *TSCRC*). The shear retention parameter β for the fixed crack models was taken as 0.001. Figure 3.8 shows the response behavior of each of these models. It was observed from Figure 3.8 that co-axial rotating crack model performs better than fixed crack models in the post peak regime since there is a release of energy associated with the rotation of the primary crack (Rots and Blaauwendraad 1989). Co-axial rotating smeared cracks also exhibit some drawbacks associated with numerical convergence (Crisfield and Wills 1989, Jirásek 2000) and thereby decomposed strain multi-directional fixed crack model (de Borst and Nauta 1986) was considered as the prototype model for further analysis since the response from these models are better than that obtained from single fixed crack models due to partial release of energy with development of new cracks in different orientations and exhibits lesser convergence problems in comparison to co-axial rotating crack models. Moreover, these decomposed strain multi-directional fixed cracks can be combined with different plasticity models to represent behavior of concrete in compression.

Impact of shear retention factor

Figure 3.9 shows the effect of shear retention factor, β, on the global load-deformation response. At its most basic level, β relates to shear stiffness of cracked concrete. The shear retention factor, β, causes the principal stress in the cracked integration point to rotate upon further loading (Cope et al. 1980). Shear retention in combination with tensile softening (i.e. residual tensile strength at small crack widths), may result in the principal tensile stress to easily exceed the tensile strength in a direction other than the normal to the crack.

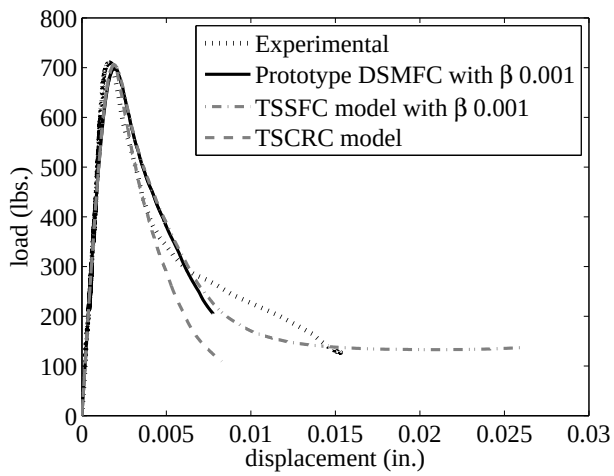

Figure 3.8: Simulation with different crack models

This explains the stiffening in the post-peak response when β is increased from 0.001 to 0.05 in the total strain single fixed crack ('TSSFC') model. If the shear retention factor, β, is near to 0, then this phenomenon of stress-locking does not occur (Figure 3.9).

Impact of crack threshold angle

Figure 3.10 shows the effect of threshold angle, θ, for subsequent crack formation. In a multiple fixed crack model the angle between the normal to the crack and the direction of the principle tensile stress must exceed the threshold angle for another crack surface to form. As the threshold angle, θ, becomes close to $0°$, a multi-directional fixed crack model exhibits response similar to a rotating crack model. Rots and Blaauwendraad (1989), Jirásek (2000) explains that with more number of cracks, there would be more energy dissipation and thereby would result in less stiffened load-deformation response. On the other hand, more cracks would result in more numerical convergence problems (Crisfield and Wills 1989). In order to strike a balance, a threshold angle of $60°$ has been chosen for the prototype model.

Impact of element types and integration rules

It was also observed that the use of different elements and integration rules varied the load-deformation response of the specimen. Simulation with a 8-node quadrilateral with a 2 by

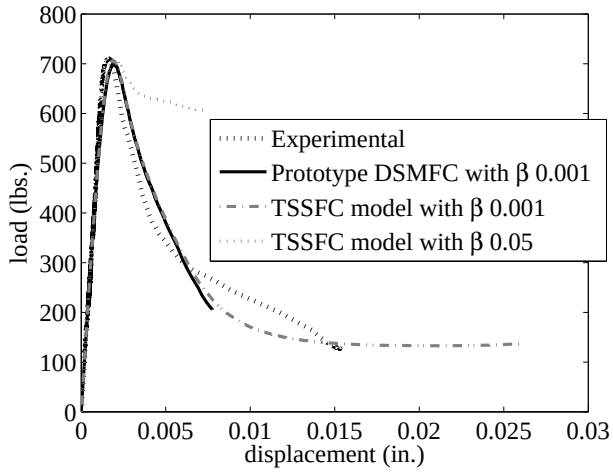

Figure 3.9: Different crack models with different β values

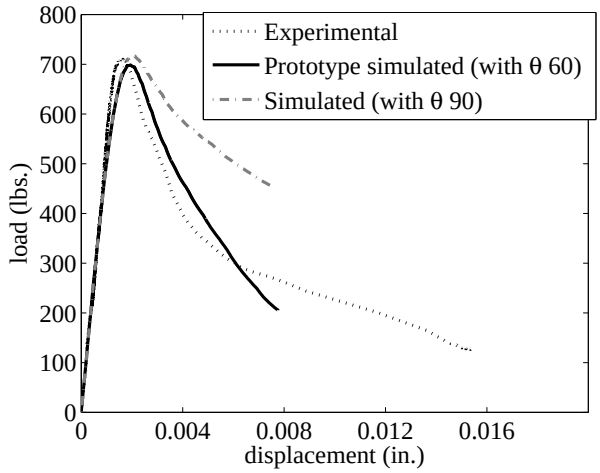

Figure 3.10: Variation of threshold angle for subsequent crack formation, θ

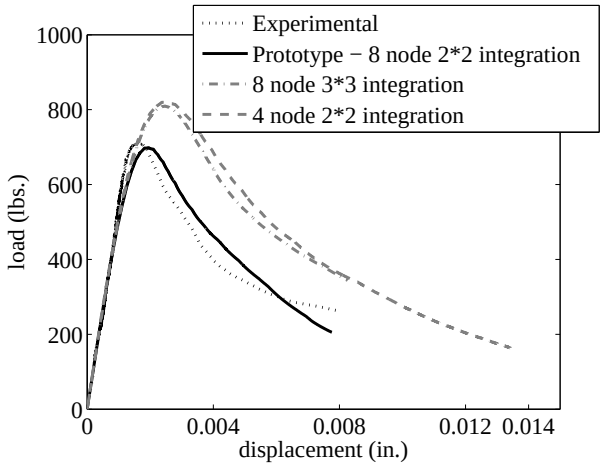

(a) Variation with element type chosen

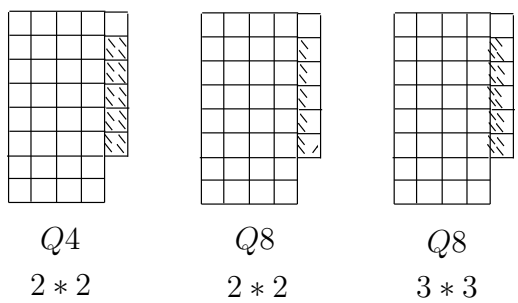

(b) Crack formation in the notched region

Figure 3.11: Fracture energy test simulation with different element types

2 gauss quadrature integration scheme produced the best correlation with the experimental data in comparison to simulations by using a 4-node quadrilateral with a 2 by 2 integration rule or a 8-node quadrilateral with a 3 by 3 integration rule (Figure 3.11(a)). Ideally only one set of crack should develop in the notched region, which is observed in Q8 (2*2) in Figure 3.11(b) and thereby the use of characteristic length or crack band width, h, equal to the width of the element perpendicular to the crack is justified. But in other element types and integration rules two sets of cracks are observed and thereby the characteristic length used in these cases should be changed from that of the width of the element perpendicular to the crack (which was used in the simulation) to half it's value in order to obtain good correlation with the observed response.

Impact of material model parameters

A parametric study was conducted to determine the effect of material model parameters (e.g. modulus of elasticity, fracture energy and tensile strength) on the global response. All the parameters were varied by 10% higher and lower of the actual value provided by the experimental investigation. Analyses of specimen $C3$ in Martin et al. (2006) were done in which the fracture energy parameter, G_f, (Figure 3.12(a)); tensile strength of concrete, f_t, (Figure 3.12(b)); modulus of elasticity of concrete, E_c, (Figure 3.12(c)) were varied by approximately 10% of the measured value. These parameter variations were considered to represent the potential experimental error in measured values. It was observed that an approximate 10% variations in the material parameter obtained from experiments resulted in less than 10% variations in the simulated response.

Preferred model parameters

The results of the simulation study suggest that the preferred concrete model employs Drucker-Prager model for concrete in compression, decomposed strain multi-directional fixed crack model for concrete in tension, Hordijk model for tension softening in concrete and a threshold angle of 60° for new crack formation.

3.5.2 Bond tests

Bond response is a critical component in modeling of RC structures. Modeling bond behavior between concrete and reinforcing steel requires modeling in directions parallel and perpendicular to the bar. An elastic model is used to represent the bond response perpendicular to the direction of the bar. The response in the direction parallel to the bar is calibrated based on an empirical model by Eligehausen. Based on experimental data of Eligehausen et al. (1983) the maximum bond stress is taken as 2.46 times square root of the maximum compressive strength of concrete (in MPa), whereas the residual strength is taken as 0.9 times the square root of maximum compressive strength of concrete (in MPa). The slip levels are also defined based upon experimental data provided by Eligehausen. The slip at maximum stress is defined by a plateau from 1 to 3 mm and the residual strength is

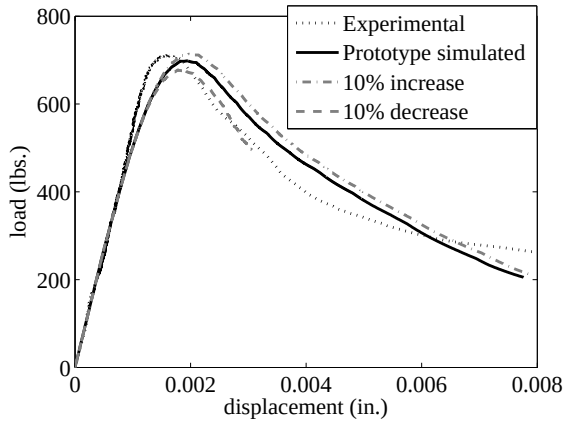

(a) Variation of fracture energy parameter, G_f

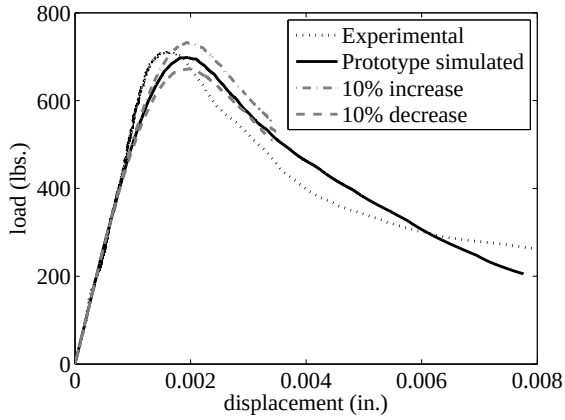

(b) Variation of tensile strength of concrete, f_t

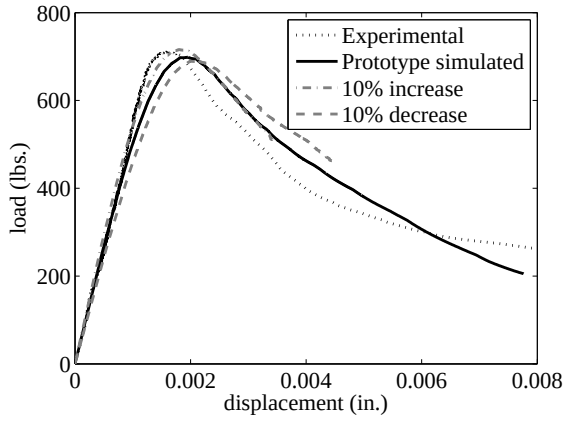

(c) Variation of modulus of elasticity of concrete, E_c

Figure 3.12: Material parameter variation of the UW simulations

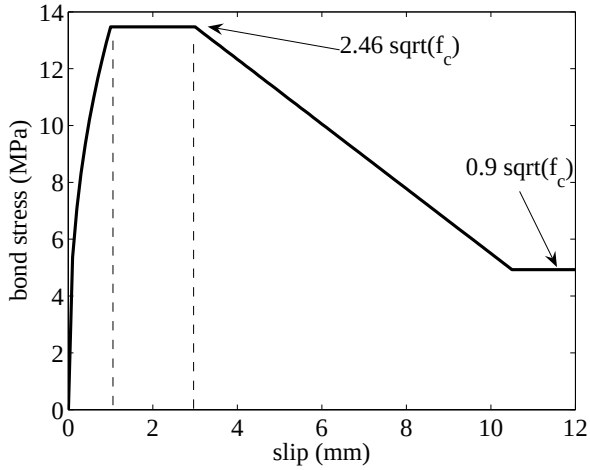

(a) Tangential response

Figure 3.13: Bond slip response

assumed to be developed at 10.5 mm slip. The bond response, in direction parallel to the bar, for concrete with compressive strength of 30 MPa is shown in Figure 3.13.

Anchorage bond zone response simulation

Good correlation was observed between simulated and experimental anchorage bond-zone response by Viwathanatepa et al. (1979). The comparison of the observed and the computed response for these models provides a means of evaluating the adequacy of the proposed bond model for predicting bond-zone response under severe loading conditions similar to those that develop under earthquake loading of reinforced concrete buildings. The geometry and material parameters of the model, as incorporated in a two-dimensional finite element model are represented in table 3.5.

The simulated anchorage bond specimen load-deformation response is shown in Figure 3.14(b), whereas the crack patterns (which were obtained similar to the one observed in the laboratory) are shown in Figure 3.14(a). The progression of cracks in the simulation was observed similar to the ones observed in the laboratory investigation. The kink in the simulated response is observed when a major conical crack is formed in the specimen.

Table 3.5: Anchorage bond-zone response by Viwathanatepa et al. (1979)

Model parameters	value
width of concrete block	25 in
height of concrete block	48 in
thickness of concrete block	10 in
anchored reinforcing bar nominal diameter	1 in
longitudinal reinforcing bar nominal diameter	0.875 in
transverse reinforcing bar nominal diameter	0.5 in
longitudinal steel ratio	0.019
compressive strength of concrete	4.72 ksi
tensile strength of concrete	0.51 ksi
fracture energy of concrete	0.001 kip/in
Poisson's ratio of concrete	0.175
Yield strength of the anchored reinforcing bar	68 ksi
Ultimate strength of the anchored reinforcing bar	102 ksi
Yield strength of transverse and longitudinal steel	72 ksi
Ultimate strength of transverse and longitudinal steel	102 ksi

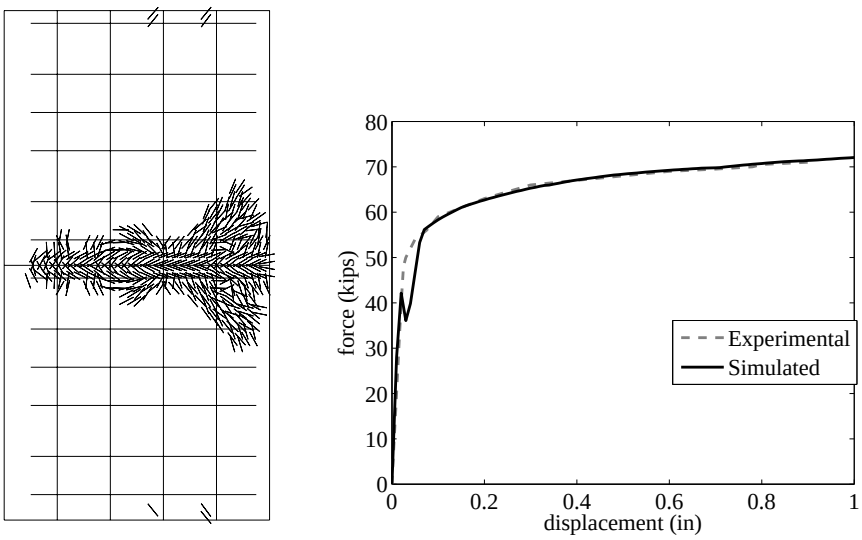

(a) Crack patterns (b) Load-deformation response

Figure 3.14: Anchorage bond slip response (Viwathanatepa et al. 1979)

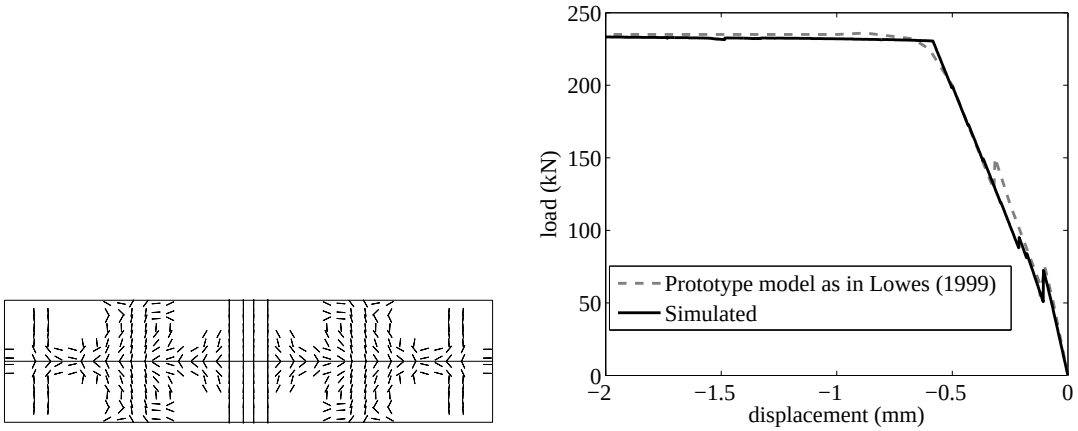

(a) Crack patterns (b) Load-deformation response

Figure 3.15: Flexural bond slip response

Flexural bond zone response simulation

Simulation of the flexural bending mechanism for bond slip was also carried out based on a specimen tested in Lowes (1999), which consists of a 25 mm bar anchored in a plain concrete prism 500 mm by 125 mm by 125 mm. The anchored bar is subjected to monotonically increasing elongation at both ends of the exposed bar. Concrete of 30 MPa compressive strength, 3 MPa tensile strength and an elastic modulus of 26 GPa was chosen for the study. The yield strength for the reinforcing steel was taken as 470 MPa with an ultimate tensile strength of 520 MPa, and an elastic modulus of 200 GPa. These geometry and material parameters were obtained from Lowes (1999). Good correlation was observed as regards to the crack patterns and also the load-deformation response analysis of the bond-zone prototype model in Lowes (1999), as shown in Figure 3.15.

3.5.3 Flexure tests of beams

Simulation of the flexural response of beams and columns is required to obtain accurate prediction of response at the joint perimeter and thereby, enable accurate simulation of the joint response mechanism. While beams and columns typically exhibit shear failure, shear-flexure failure or flexural failure, the beams and columns in the joint sub-assemblages included in the data-set exhibited flexural response only. Thus, flexure mechanism for beams

were considered as part of this simulation study.

The failure mechanism exhibited by a beam subjected to bending loads is typically determined by the shear demand-capacity ratio, where shear demand is determined by the maximum beam load and beam span and capacity is determined by concrete strength and transverse steel ratio. Beams with low shear demand-capacity ratio exhibit flexural response; high demand-capacity ratios exhibit shear failure and intermediate demand-capacity ratios exhibit flexural-shear failure.

Burns and Seiss (1962) sample was chosen for simulation which exhibited flexural response. Table 3.6 provides the geometry and material parameters for the specimen used in the test. The specimen was simulated using a displacement control loading applied at the top middle of the simply-supported beams. The concrete region in the specimen was modeled by using 8-node quadrilateral elements with a 2 by 2 gauss quadrature. A total of 720 concrete continuum elements with size of 1 by 1 mm was used in the simulation. The reinforcement was modeled as truss elements. The bond response was modeled as interface elements between the concrete and the reinforcing steel. Drucker-Prager plasticity was used as a material model for concrete in compression. Decomposed strain multiple fixed crack model with Hordijk softening was used to represent the behavior of concrete in tension. Von-Mises plasticity was used to represent the response of the reinforcing bars. The bond response parallel to the direction of the bar was calibrated based on the experimental data provided by Eligehausen and discussed in the previous section.

In table 3.6 L refers to the span length of the sample, h the in-plane height, b the out-of-plane width, f_c the concrete compressive strength, f_t the tensile strength of concrete, E_c the modulus of elasticity of concrete, G_f the fracture energy, $(\cdot)_b$ refers to bottom longitudinal steel parameters, $(\cdot)_t$ refers to top longitudinal steel parameters, $(\cdot)_s$ refers to stirrup steel parameters, f_y represents yield strength of reinforcing steel, f_u the ultimate strength of reinforcing steel, E_s the modulus of elasticity of steel, d_b the diameter of steel bars, and n_b the number of steel bars.

Table 3.6: Geometry and material parameters for flexural test specimen

Specimen	Burns and Seiss (1962)
L	144 in
h	20 in
b	8 in
f_c	4829 psi
f_t	350 psi
E_c	3500 ksi
G_f	1.5 lb/in
$(d_b)_t$	NA
$(n_b)_t$	NA
$(f_y)_t$	NA
$(f_u)_t$	NA
$(E_s)_t$	NA
$(d_b)_b$	0.71 in
$(n_b)_b$	2
$(f_y)_b$	44.9 psi
$(f_u)_b$	47 psi
$(E_s)_b$	29500 ksi
$(d_b)_s$	NA
$(f_y)_s$	NA
$(f_u)_s$	NA
$(E_s)_s$	NA

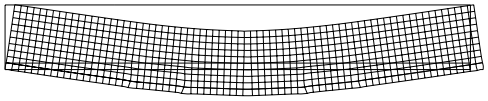

(a) Simulated specimen meshing and deflection

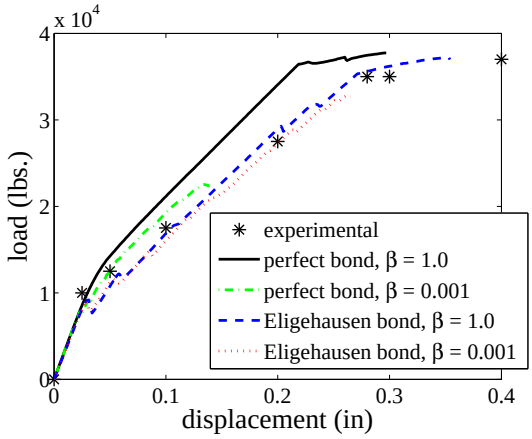

(b) Load-deformation response

(c) Crack patterns for perfect bond specimen

(d) Crack patterns for Eligehausen bond specimen

Figure 3.16: Flexure test of Burns and Seiss sample specimen

Discussion of results for the beam flexure tests

Figure 3.16 shows the crack patterns of the specimen as observed in the experimental investigation by Burns and Seiss (1962). The figure also shows a good correlation of the load-deformation response analysis. The simulated sample represented by *perfect bond* are those in which in which full/perfect bond has been considered, whereas *Eligehausen bond* refers to the specimen where bond model by Eligehausen has been considered. As expected it is observed that the perfect bond model has higher initial and pre-peak stiffness compared to the Eligehausen bond specimen. A difference in the crack pattern is also observed between the case of "perfect bond element" and the case of Eligehausen material bond model. If the bond is not perfect, then the cracking is not continuous and much more discrete. It is also observed that *shear retention* represented by β does not play a significant role in the stiffness response at the pre-peak region. But, numerical convergence problems were observed if the shear retention value was near to zero.

3.6 Simulation of joint response

The objective in this chapter was to develop a continuum model of the joint region to study the behavioral mechanisms within the joint region and also to observe the effect of variation of modeling parameters on the joint global and behavioral response. To fulfill this objective two idealized joint specimen are chosen from the data set in chapter 2 and are subjected to monotonic displacement controlled loading.

Simulated test specimen with loading and boundary conditions is shown in Figure 3.17. Constant axial load was applied at the column top using load-control. A monotonically increasing lateral load was applied at the top of the column by displacement-control. The joint region along with a plastic hinge region (taken equal to the depth of beam/column section) was discretized with concrete continuum elements. Four node quadrilateral elements with 2 by 2 gauss-quadrature integration was considered for the continuum elements. The size of the element used was 10 mm by 10 mm. The total number of concrete continuum elements used was 4500. Embedded reinforcement elements representing stirrups were also used within the concrete continuum region. The longitudinal bars in beams and columns were modeled as 2 dof bar elements which were connected to the concrete elements through a line interface bond element. Beams and columns outside the connection region was represented by elastic line elements with an effective stiffness, equal to that of cracked concrete as per ACI 318-05. The elastic line elements were specially connected to the concrete continuum elements so that there was proper transfer of moments from the beam/column line elements to the continuum elements.

Since fracture energy data was not provided in the experimental literature, the fracture energy for the specimen was taken as 0.16 N/mm with a characteristic length as 10 mm which is same as the element dimension. An elasto-plastic von-Mises model was utilized to represent the behavior of reinforcing steel. Eligehausen bond model was utilized for material modeling of the bond element. An elastic material model as well as Drucker-Prager model was used for concrete in compression. Decomposed strain multiple fixed crack model with Hordijk model for tension softening was used to represent the response of concrete in tension.

Two specimen from Oka and Shiohara (1992) were chosen for purpose of simulation,

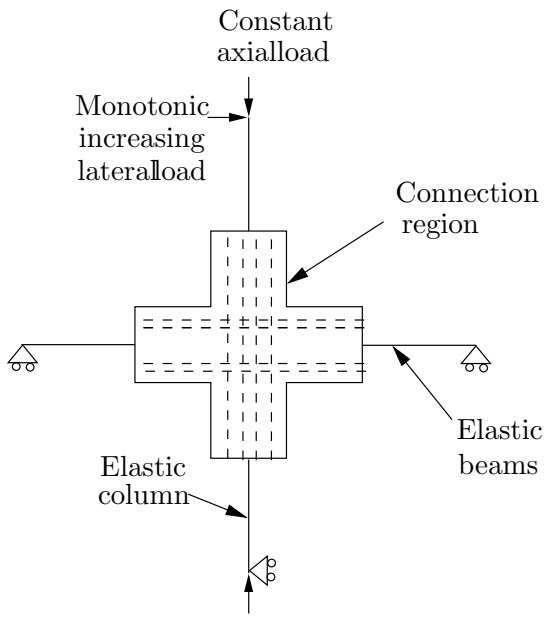

Figure 3.17: Simulated joint specimen with loading and boundary conditions

namely *OSJ5* and *OSJ10*. The particular specimen series was chosen since it consists of a number of specimen as well as have specimen which exhibit all the three different types of failure mechanisms observed for beam-column joints. Both specimen had a higher than average joint shear stress and bond stress demand (see table A.5). The concrete compressive stress was significantly different for the two specimen. Details of the geometric and material properties of the two specimen can be found in table A.1 and A.2.

The software used for simulation was DIANA 9.1 and each of the specimen had a total of 11458 dof. The simulation was carried out in Dell Server PE1800 computer (Microsoft Windows Server 2003) with Intel(R) Xeon(TM) CPU 3.60 GHz and 4.0 GB RAM.

3.6.1 Discussion of results for joint simulation

Simulation was carried out for specimen *OSJ5* which exhibited a BYJF type of failure. An elastic material model for concrete was considered in compression. The other material and element specifications are provided in the previous subsection. The cracked gauss points at different displacement levels are shown in Figure 3.18. The crack patterns indicate that cracks initiate at the corner regions and propagates along the joint interface. Finally at a

later displacement level, diagonal cracks are observed in the joint region.

Figure 3.19 shows simulated and observed load deformation response of specimen *OSJ5*. Good correlation could be observed in the pre-peak region. The simulated load-deformation response was observed not to soften after the observed peak strength was achieved. This anomalous behavior could be partly explained due to usage of elastic material model for concrete.

The mechanism of failure in a BYJF specimen is complicated. Failure initiation starts with the yielding of the beam longitudinal steel, after which failure could be either due to anchorage/bond failure of the longitudinal beam bars or could be due to shear failure within the joint region or it could also be due to simultaneous activation of both the failure mechanisms. In the literature for *OSJ5* specimen, shear failure after yielding of beam longitudinal steel is observed but bond/anchorage response is not documented. In the simulated response, Figure 3.20 shows distribution of compressive stress in x direction at a displacement level of 56 mm. The regions shown in red color are those in which the magnitude of the compressive stress is more than the magnitude of the concrete compressive stress of 79.2 MPa. Since the stress in the concrete core was not above the concrete compressive stress in the simulated model, the simulated model did not predict a shear failure after beam yielding.

However, stress of concrete at the perimeter of joint was more than the concrete compressive stress. The material response of concrete was provided as elastic, but if a material model for concrete with strength degradation was provided then that would have influenced the load-deformation response of the specimen and a softening response might have been obtained. The stress strain response of a concrete element at the top, and a longitudinal bottom reinforcement on the right hand interface of the joint reveals that concrete stress is much higher compared to the concrete compressive stress and reinforcing steel has reached yielding (Figure 3.21).

The distribution of steel stresses along the top reinforcement bar at 5% drift is shown in Figure 3.22(a). The y-axis represents the stress in x-direction in MPa, whereas the x-axis represents the distance in mm measured from one one end of the plastic hinge region in the beams to the other end of the plastic hinge. Thereby, distance 300 to 600 represent the

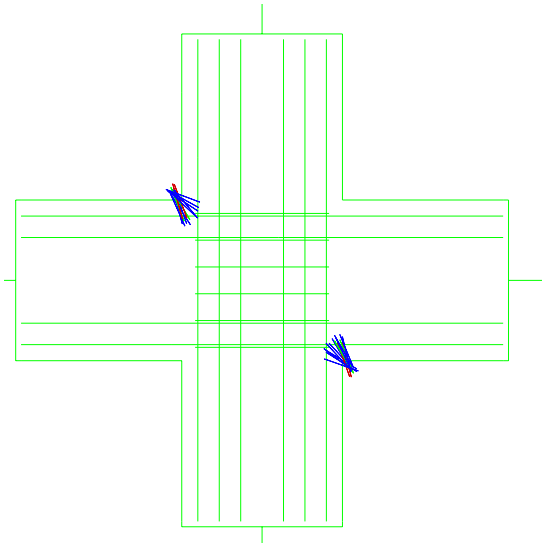

(a) At displacement step 10

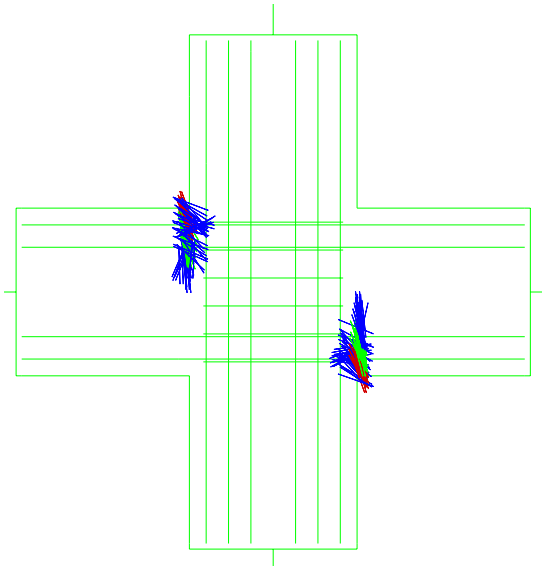

(b) At displacement step 18

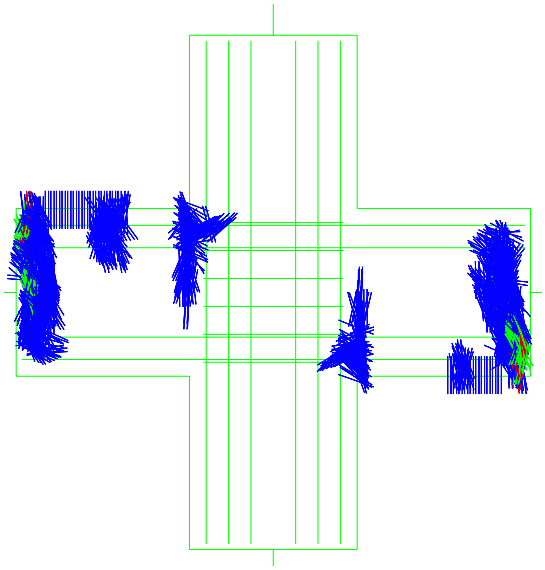

(c) At displacement step 40

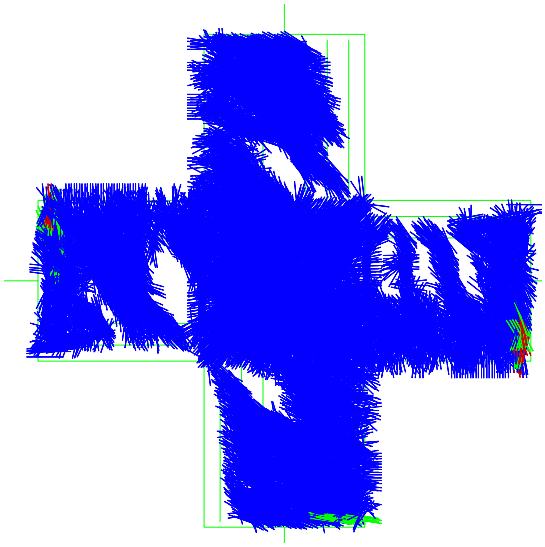

(d) At displacement step 500

Figure 3.18: Cracked gauss points at different displacements demands

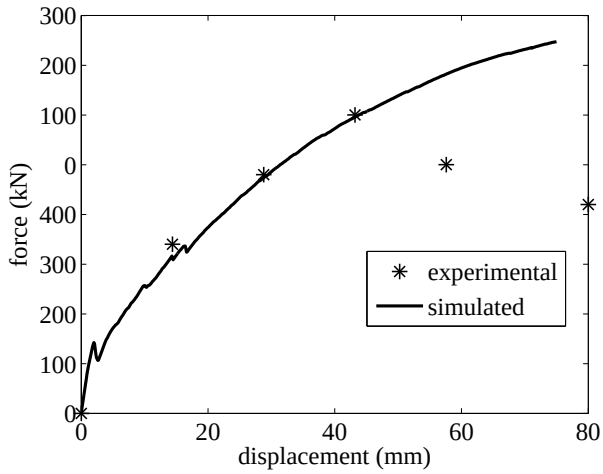

Figure 3.19: Load deformation response of *OSJ5* specimen

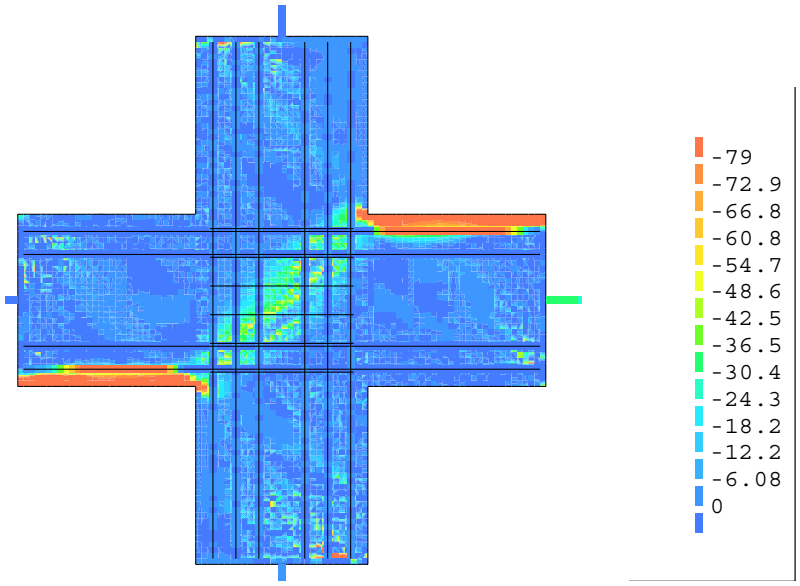

Figure 3.20: Distribution of compressive σ_{xx} at displacement level of 56 mm for *OSJ5*

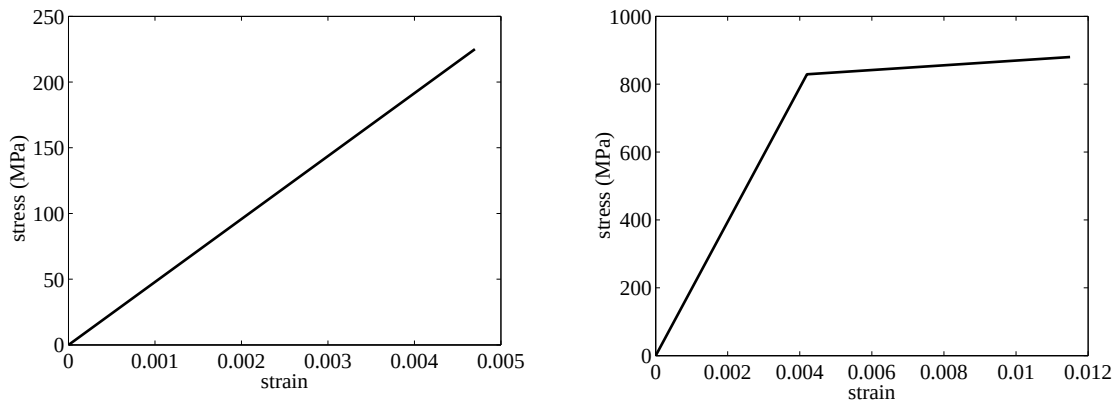

(a) Concrete compressive response at extreme top right element

(b) Tensile response of right-bottom longitudinal steel

Figure 3.21: Stress-strain response of concrete and steel at the right interface of the joint

joint region. The bond response at the joint perimeter is shown in Figure 3.22(b). These figures suggest that in order to obtain a degradation in strength due to bond-loss, a varying bond stress distribution response should be provided in the joint region. Currently in the simulated specimen, Eligehausen bond model with a maximum bond stress of 2.46 $\sqrt{f_c}$ is provided for all the bond elements, which is clearly an overestimated value to be used for bond stress within the joint. The maximum bond stress value in Eligehausen bond model experiment was obtained by applying tensile force to a reinforcing bar anchored to a concrete block. The stress distribution in a joint is more complex than the simple idealization of anchorage failure in Eligehausen experiment and thereby proper bond stress values are to be estimated.

Thereby with the the present software restrictions, the failure mechanism of a BYJF specimen, *OSJ5* could not be correlated well with the experimental observations. Two aspects were identified which would improve the simulation response behavior: 1) better model to represent the strength deterioration in concrete and 2) better model to represent the bond stress - bar slip response along the reinforcement bar. Too much effort was not utilized to model better material models for concrete and bond in DIANA 9.1 since these simulations took more than 7 days in the computer specified above and thereby cannot be successfully utilized for the purpose of PBSD of joints.

Another sample, specimen *OSJ10*, which exhibits a joint shear failure was also simulated

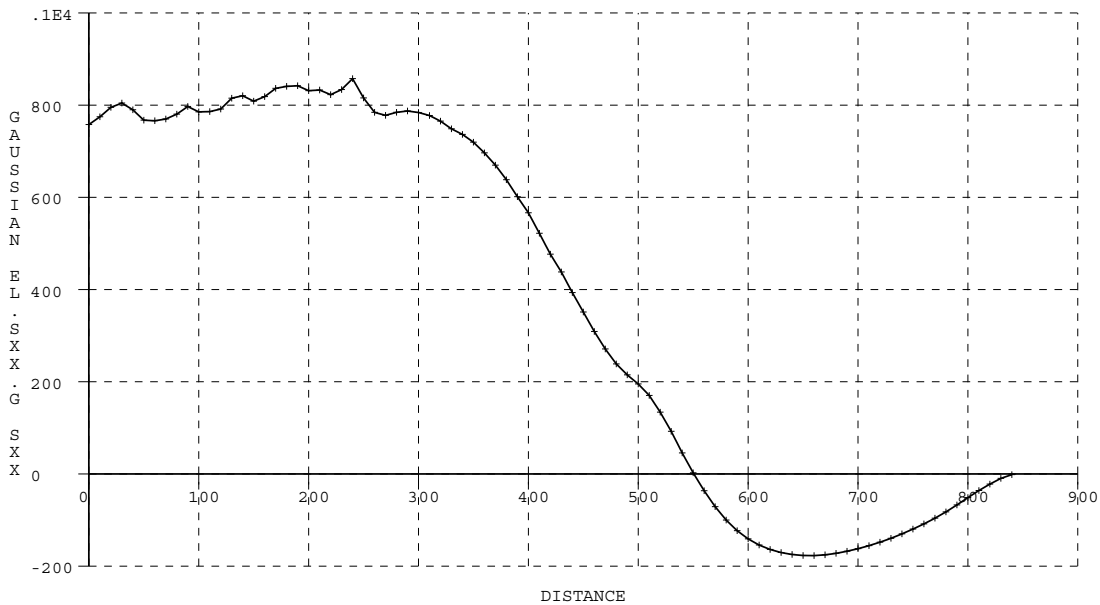

(a) Steel stress distribution along top reinforcement bar in beam

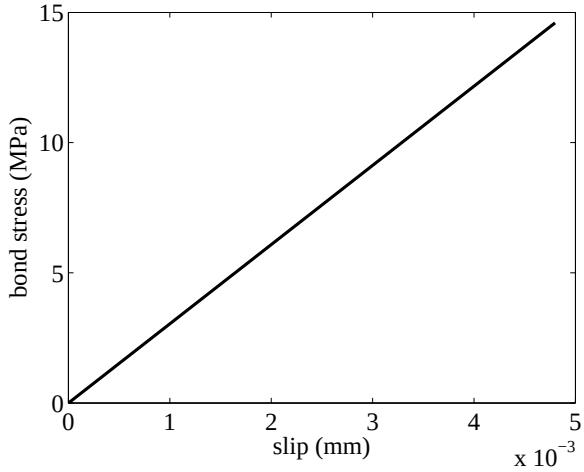

(b) Bond stress-slip relation at the joint interface

Figure 3.22: Stress-strain response of concrete and steel at the right interface of the joint

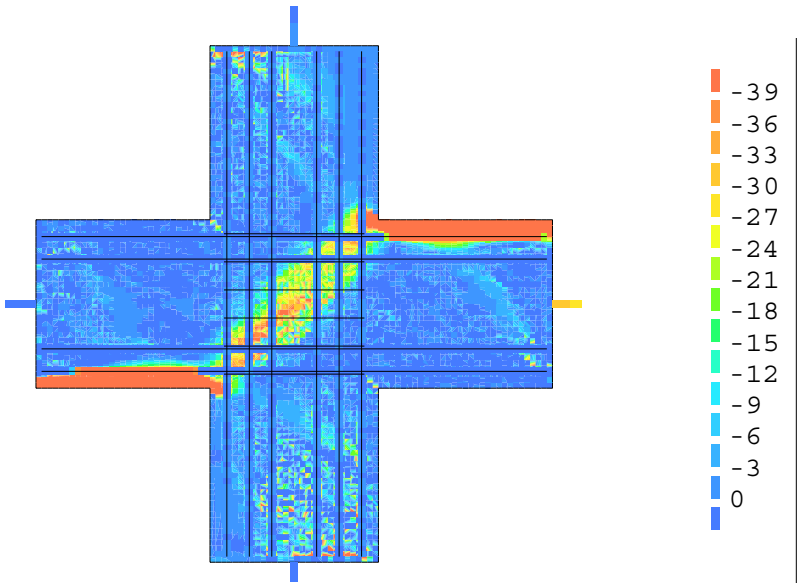

Figure 3.23: Distribution of compressive σ_{xx} at displacement level of 60 mm for *OSJ10*

and compared with experimental observations. A high compressive stress is expected within the joint region for a sample representing joint shear failure. This was observed in the simulated specimen response (see Figure 3.23). The compressive stress at the interior of the joint is more than the concrete compressive stress suggesting that instead of using an elastic model for concrete in compression, if a material model with strength degradation is used for concrete, a good correlation could be obtained between simulated and observed load-deformation response (see Figure 3.24).

The crack patterns observed in *OSJ10* correlates well with the crack pattern propagation obtained from simulation (see Figure). Cracks initiate at the joint corner perimeter and then progresses diagonally in the joint region. Note the pattern of cracks observed in the simulation of *OSJ10* differs significantly with the pattern of cracks observed in the simulation of *OSJ5*.

Good correlation between observed and simulated load-deformation response could be observed in Figure 3.24 but could not be obtained in the post-peak region. Good correlation in the post-peak regime could be obtained if strength reduction model for concrete is considered instead of the currently used elastic model for compression. Thereby, Drucker-Prager model for compression is being used to obtain better response.

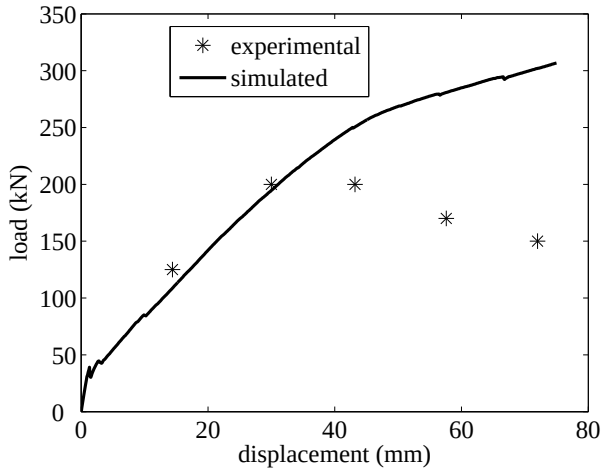

Figure 3.24: Load deformation response of *OSJ10* specimen

Analysis was carried out of the *OSJ10* specimen just by changing the concrete compressive response to that of Drucker-Prager model and keeping all other parameters the same. The analysis could not be completed due to numerical convergence problems. The load-deformation of the sample response is shown in Figure 3.26(a). It can be noted in here that the displacement level at which convergence problem issues is significantly smaller to the total displacement level of the specimen. The reason for lack of numerical convergence is due to the weird response of the concrete tensile region as shown in Figure 3.26(b). The response should have followed the Hordijk tensile softening curve but element convergence could not be attained at the crack. The numerical algorithm in DIANA fails stating that stresses in the main and the crack material are unequal.

Similar observations were also made by Wang et al. (1990) who concluded that the problem of convergence for multiple-fixed crack model with plasticity is similar to the numerical convergence problems associated with multi-surface plasticity models. It is well known that a standard radial return-mapping algorithm fails for multi-surface plasticity problems due to presence of more than one plasticity yield surfaces in its vicinity. In this problem too, multiple yield surfaces of cracking and crushing of concrete originate at a local level, thereby resulting in numerical convergence failures.

Thereby, even though we could represent one response of concrete, i.e. cracking but both

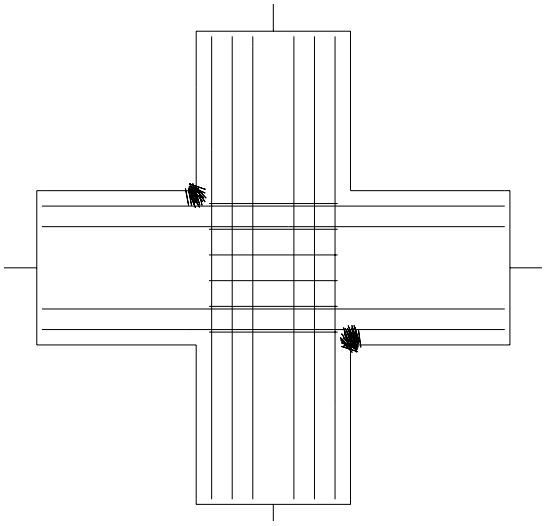

(a) At displacement step 7

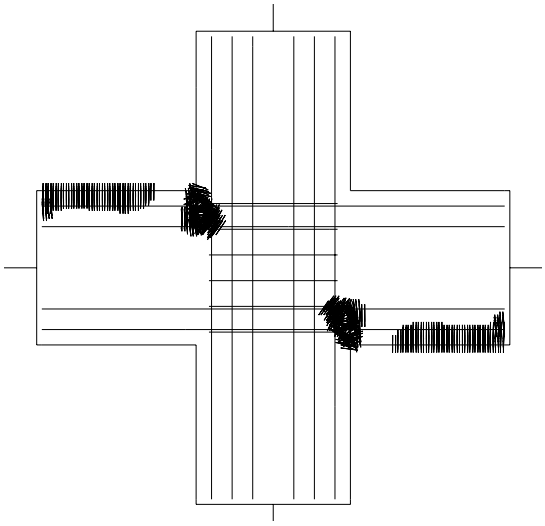

(b) At displacement step 12

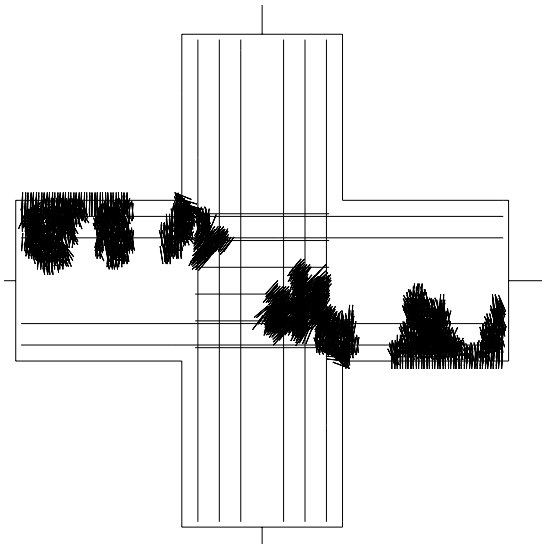

(c) At displacement step 20

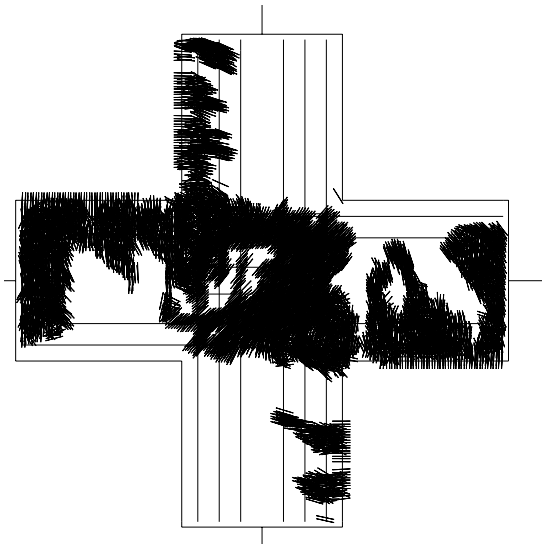

(d) At displacement step 75

Figure 3.25: Cracked gauss points at different displacements demands

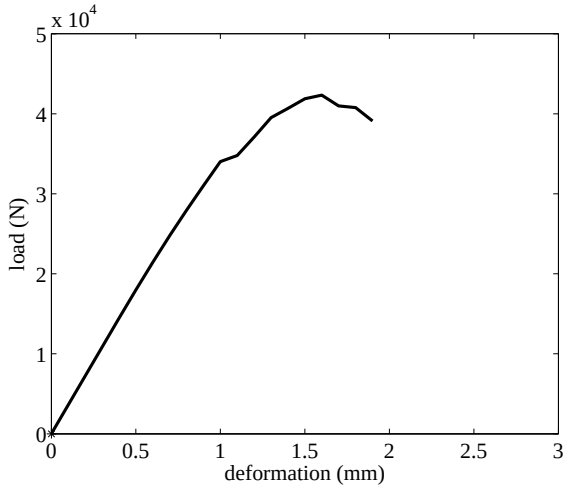

(a) load-deformation response

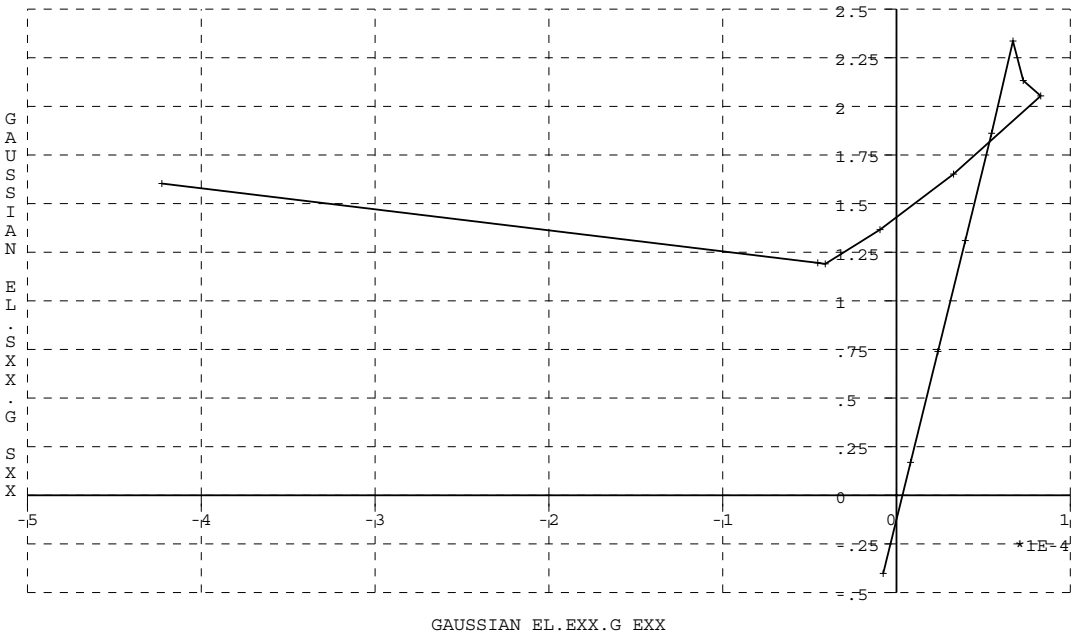

(b) Response of concrete in tensile region

Figure 3.26: Simulated response of OSJ10 with Drucker-Prager plasticity in compression

the responses cracking and crushing of concrete could not be captured simultaneously. Due to numerical unstable algorithms, and lack of better material models in DIANA 9.1 and also due to huge amount of computational time required for one analysis (approximately 7 days to run one analysis on computer specified above) the investigation with the continuum methodology is being abandoned. This methodology might be recommended for local interaction behavior study at a smaller scale but should not be used as an analytical method for performance based design method for joints.

3.7 Conclusion

In this chapter state of art nonlinear continuum finite element was utilized to develop a model for the interior joint region. The model relies on the constitutive models for constituent materials: concrete, steel and bond. These material models were calibrated using a number of benchmark studies. It was observed that multiple fixed crack model performed better in comparison to either the single fixed crack model and the rotating crack model. Shear retention also contributed to a great extent in the load-deformation analysis of different benchmark samples. The presence of bond was also observed not to influence the global load-deformation behavior in the pre-peak regime even though distinctive crack patterns were obtained for the case of perfect bond and Eligehausen bond model.

This study helped us to better understand the behavior of the joint specimen and can be used as a great tool to study the local behavioral characteristics of the joint region like the bond interaction or the shear panel response. The pattern of crack formation also laid the foundation as well as supported previous research (Paulay 1989) for later developments of diagonal strut model in chapters 4 and 5.

Even though continuum formulation can be utilized to simulate the response of an experimental observation but it depends upon a lot of modeling parameters which does not have any physical meaning. These modeling parameters can alter the response behavior of the specimen, given the same geometry and the material properties for the specimen. Thereby an improved understanding of these modeling parameters is required for the continuum formulation of the any reinforced concrete structure.

The continuum methodology is plagued with convergence problems and requires huge

amount of computational time as well as complexity. Thereby, this methodology cannot be used as an analytical tool for performance based design and analysis tool for reinforced concrete joints. Development of computationally stable and robust continuum methods for analysis calls for further research in this area.

Chapter 4

COMPONENT BASED MODELING OF JOINT REGION

4.1 Introduction

The advent of performance-based design has placed an emphasis on simulating the nonlinear response of structures subjected to seismic excitation (Filippou and Fenves 2004). Given the potential impact of joint nonlinearity on system response, (as discussed in previous chapter) a number of researchers have proposed joint models for use in simulating structural response to earthquake loading. A primary requirement of this type of model is the need for compatibility with other component models that make up the structure. Here these models are beam column line elements. Additionally the joint model should include nonlinear response relationships that are to be calibrated by the user on the basis of fundamental material parameters along with specimen geometry. The models, unlike the continuum models developed in chapter 3, should also be computationally efficient, robust and transparent in simulating controlling parameters.

This chapter presents a review of previous joint models, followed by the development of a model which extends the previous work by Lowes and Altoontash (2003). The chapter ends with a comprehensive evaluation and validation of the model using experimental data set described in chapter 2.

4.2 Literature review of previous joint models

Finite element models of beam-column joints, apart from the continuum approach discussed in chapter 3, are assumed to fall into two categories: Implicit models and explicit macroscopic models.

Implicit models: The stiffness and strength loss due to joint damage is modeled by modifying beam and column elements. Typically, nonlinear springs or plastic-hinges or both are added at the member ends. Such models are useful to determine the overall

impact of nonlinear joint action on structural response. These models are also difficult to calibrate since the joint action is split between the adjacent beams and columns. On the other hand, these models are computationally less demanding and can be easily incorporated into any finite element program. Since these models does not consider an explicit representation of the joint region, these do not satisfy the joint kinematics and thereby can not be used for detailed investigation of mechanisms governing the joint inelastic behavior.

Explicit macroscopic models: These models consider an explicit representation of the joint region. Inelastic mechanisms governing joint behavior such as bar-slippage through the joint, shear failure in the joint core form the backbone for these models. These models satisfy joint kinematics and also can be used as separate macroscopic elements in frame models composed of line elements. The models in this category also vary in their level of discretization of the joint region, complexity, robustness and accuracy with which it is able to capture the precise mechanism of failure within the joint region.

A brief overview of these two types of joint models follows. The model developed as part of the work falls in the second category.

4.2.1 Implicit joint models

In these approach, the beam and/or column models are calibrated to account for the inelastic action of the beam-column joints into which they frame. In most cases one of the primary inelastic response mechanisms observed in joints (shear or bar-slip) is considered. The reason can be traced to the geographical locations: North-American design practices results in beam-column connections that are relatively characterized by large bond-slip, whereas New-Zealand design practice results in connection with strong bond conditions and higher shear deformations (Pantazopoulou and Bonacci 1994). Thereby a mixed type of analytical modeling effort for the RCBC joints (concentrating on the global response) was observed amongst researchers around the globe.

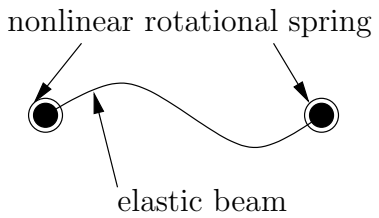

Figure 4.1: One component frame model, Giberson (1969)

One component frame model

The model (Figure 4.1) is a beam element with two nonlinear rotational springs attached to two ends of a perfectly elastic element (Giberson 1969). The springs account for nonlinear action due to beam flexure and joint deformation. The inelastic moment-rotation relationship of the rotational spring, which idealizes the joint region, was determined assuming the point of contraflexure at the center of the member. The one component frame models suffered from one primary drawback, which was the rotation of the equivalent rotational spring is uniquely determined as a function of the moment acting on the spring. In other words, the one component model uses the initially assumed moment distribution shape and the fixed point of contraflexure in the member, instead of the current moment distribution along the member when calculating member end rotations.

Two component frame model

The model by Otani (1974) consists of two parallel flexible line elements (an elastic and an inelastic element), two inelastic rotational springs at the ends of the flexible line elements, and two rigid line elements outside of the rotational springs (Figure 4.2). The concept of two parallel flexible line elements follows from works by Clough et al. (1965) in which a steel frame was idealized as an elastoplastic element to represent yielding characteristics and fully elastic element to represent strain hardening characteristics of steel members.

In the model by Otani, the beam column joint core is modeled by an infinitely rigid part outside of the rotational springs in the beam/column element. Rotational springs, placed outside the joint core, simulates the rotation at the member ends due to slip of longitudinal reinforcement within the joint core. Bond stress was assumed to be constant

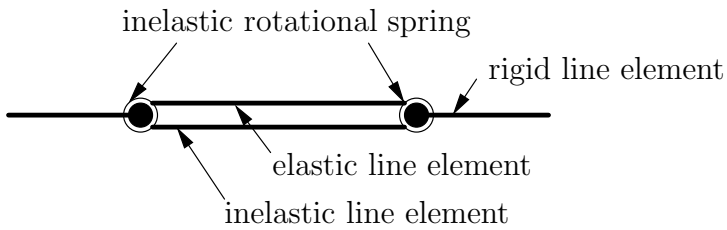

Figure 4.2: Two component frame model, Otani (1974)

along the development length and the compressive reinforcement was assumed not to slip. The rotation due to slip was evaluated as the elongation of the tensile reinforcement along the development length divided by the distance in between the tensile and compressive reinforcing bars. Takeda hysteretic rule (Takeda et al. 1970) was simplified into a bilinear backbone curve to represent the response of these springs. Joint shear deformation response was neglected in this model. A modified Takeda hysteretic material model was calibrated for the inelastic line elements so as to consider in a lumped manner the characteristic behaviors of reinforced concrete frame members: cracking of concrete, yielding and strain hardening of reinforcing steel, stiffness degradation due to bond slip and cracks within the member.

Anderson and Townsend (1977) improved the Otani model to include simulation of the shear deformation response. The study by Anderson and Townsend primarily showed that stiffness degradation in the material model for the rigid region, depicting the joint region, is an essential requirement to predict the inelastic cyclic response of a structure since in model by Otani the response was elasto-plastic with no strength and stiffness degradation.

The two-component frame models were based upon the assumption of constant bond stress along the development length and reinforcing bar embedment length was considered enough to develop steel forces of required magnitude, both of which seemed to contradict experimental observations. The assumption of no slip-through of the bars within the joint thereby lead to an interaction between the two joint end sections such that no unique moment-rotation relationship could be derived for one end of the joint without taking into account the effect of the other end.

Zero length concentrated inelastic rotational spring model

El-Metwally and Chen (1988) developed a model in which a zero length rotational spring was

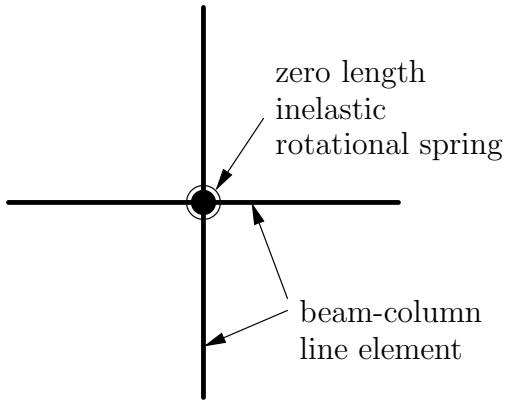

Figure 4.3: Zero length concentrated inelastic rotational spring model, El-Metwally and Chen (1988)

placed between beams and columns to characterize the inelastic behavior within the joint. Figure 4.3 shows an idealization of the model. Thermodynamics of an irreversible process was used to develop a moment-rotation relationship for the rotational spring. The model is defined by three parameters: the joint's initial stiffness and ultimate moment capacity, and an internal variable that represents the energy dissipated by the joint. Energy dissipated by the joint is assumed to be due to deterioration of bond for reinforcing bars anchored in the joint and the hysteretic behavior of the cracked reinforced concrete section at the joint interface. Bond stress-slip envelope curve by Morita and Kaku (1984) was used.

However the model was unable to capture the strength and stiffness loss due to shear loading of the joint.

Panel zone model

Alath and Kunnath (1995) proposed a model in which the joint was modeled as a rigid link with a rotational spring connected to its end, as shown in Figure 4.4. The rotational springs are calibrated by an inelastic shear-deformation relationship which includes degrading effects. The rigid links, connected to the beam/column line elements, are capable of independent rotation. A modified set of empirical relations by Umemura and Aoyama (1969) was utilized to represent the shear backbone envelope for the hysteretic model response (Kunnath et al. 1992) of the panel region. Simulation of inelastic response due to

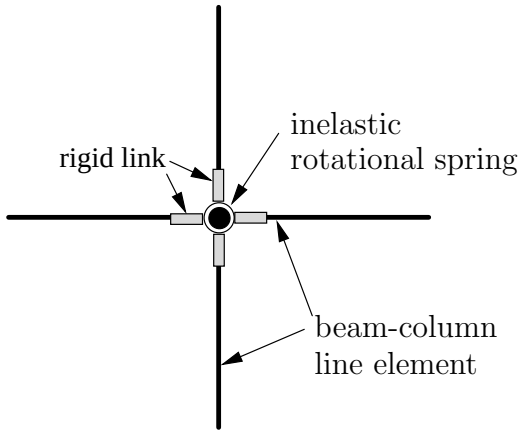

Figure 4.4: Panel zone model, Alath and Kunnath (1995)

bar-slip was not included in this model formulation.

Shear beam element model

Uma and Prasad (1996) modeled the joint region using a flexural rigid shear beam element placed in series with traditional beam/column flexural elements, as shown in Figure 4.5. The inelastic shear response of the beam/ column element was calibrated using the softened truss theory (Belarbi and Hsu 1995). Stress-strain relationship proposed by Sheikh and Uzumeri (1982) was utilized for confined concrete within the joint region with softening of concrete in compression proposed by Vecchio and Collins (1986) to account for cracks in perpendicular direction. Slippage of reinforcing bars was not considered explicitly but was incorporated in terms of increased pinching in the hysteretic response of the components (Uma and Prasad 2004).

Model with rotational spring for shear and bond slip

Biddah and Ghobarah (1999) proposed a two spring joint element in which one spring represented the inelastic shear response of the joint and the other represented bond-slip within the joint region, as shown in Figure 4.6. The softened truss model (Hsu 1988) was used to characterize the force-deformation relationship of the shear spring. The softened truss model theory includes: a) equilibrium equations assuming steel bars to resist only axial

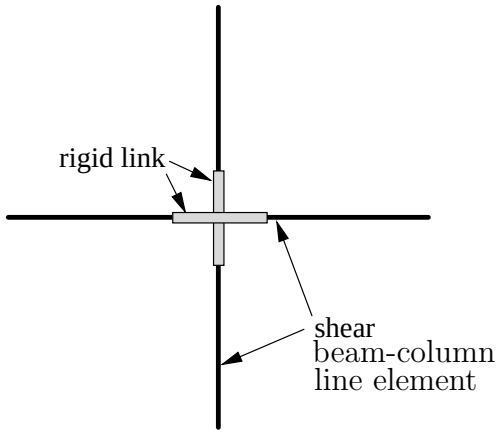

Figure 4.5: Shear beam element model, Uma and Prasad (1996)

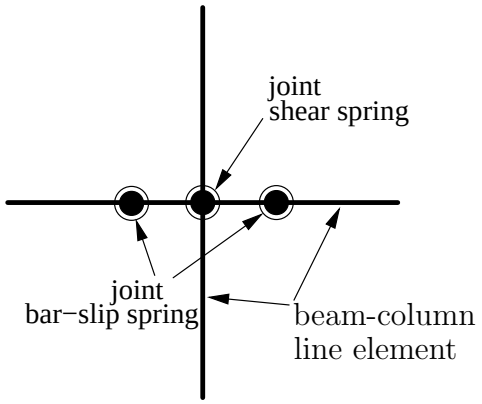

Figure 4.6: Rotational spring model for both shear panel and bar-slip components, Biddah and Ghobarah (1999)

stresses, b) compatibility equation of Collins (1978) to determine the angle of inclination of the concrete struts, and c) constitutive laws of the materials. Softening of concrete in compression due to cracking in the perpendicular direction was simulated using the expression proposed by Vecchio and Collins (1986). A simple bilinear hardening relation, based on experimental results (Kaku and Morita 1978), was used to represent the moment-rotation relationship of the rotational springs representing bond-slip within the joint. The model developed by Chung et al. (1987) was adopted to represent the hysteretic behavior of the rotational springs representing bond slip.

Summary

The implicit models were computationally efficient but the calibration of the model was difficult and sometimes did not correspond directly to any physical mechanism. The implicit models typically required calibration of rotational springs and/or the rigid offsets. The rotational springs cannot capture the kinematics of a finite-area 2d joint, whereas rotational springs in combination with rigid offsets can capture shear deformation but not axial deformation. The constitutive models required for the rotational springs and/or the rigid offsets were difficult to calibrate and was not typically a direct function of fundamental material and geometric properties. However, it should be remembered that these models were not developed for local mechanism behavior study. The primary intention of these models was to include the effect of the joint in the entire global frame response, which it satisfied with reasonable accuracy.

4.2.2 Explicit macroscopic joint models

This group of models are typically macroscopic super-elements, in which the finite size of the joint is modeled along with the different mechanisms that determine joint response. These macroscopic models provides us a better representation of the inelastic mechanisms governing joint response. These are also used along with conventional frame elements to study the global behavioral response of frame structures. A brief overview of a number of macroscopic joint models are being presented in this subsection.

Elmorsi-Kianoush-Tso model

Elmorsi et al. (2000) proposed a joint element comprising a panel zone and four transition zones (Figure 4.7). The panel zone is represented by a 12 node inelastic plane stress element. Each of the four transition elements are represented by 10 node inelastic plane stress transition elements which are connected to the adjacent beam and column elastic line elements. The transition elements, represents the plastic hinges, where most of the nonlinearities were assumed to occur, were extended to a distance of one full depth of the member that is connected to it. Flexural reinforcement in the beams, columns and joint

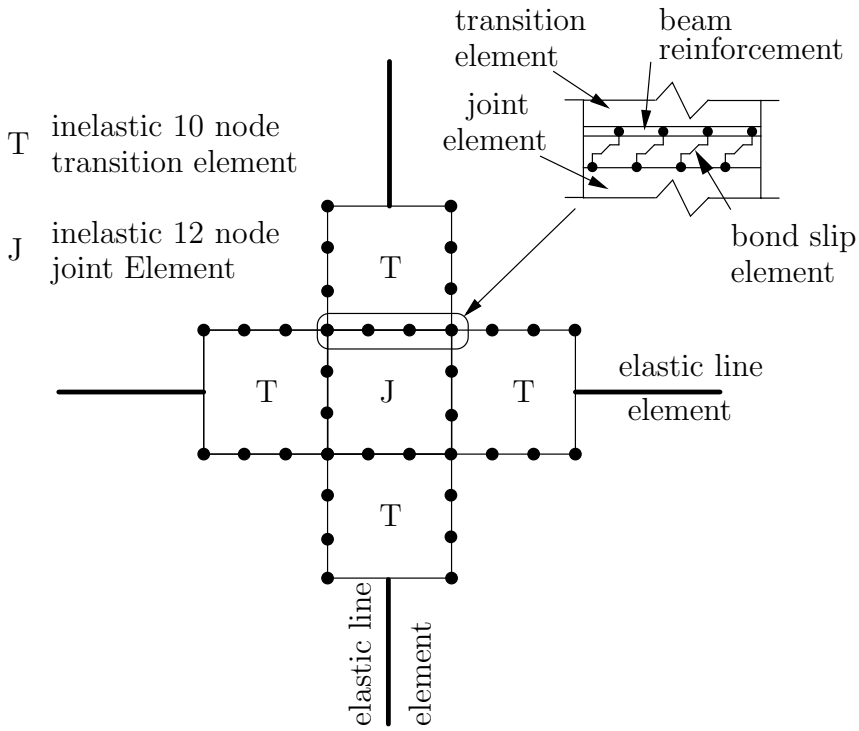

Figure 4.7: Elmorsi-Kianoush-Tso joint model (2000)

panels, placed at upper and lower extreme fibers of the adjacent plane stress elements, are represented using inelastic truss elements. Both the transition elements and panel zones are comprised of concrete material with reinforcing bars connected to it through bond-slip elements.

The constitutive model for concrete is based upon the concept of orthogonal fixed cracks. The normal stress-strain relation of concrete is based upon well-accepted empirical uniaxial curves for concrete along with reduction in compressive strength to account for cracks in perpendicular direction (Vecchio and Collins 1986). The important aspects of the concrete behavior considered in the normal stress function are tension stiffening, compression hardening and softening, degradation of concrete strength and stiffness in direction parallel to crack, and compression unloading and reloading. A new varying shear stress-strain function was defined to consider the effect of interface shear stiffness.

Material model used for reinforcing steel is similar to the relationship used by Menegotto and Pinto (1977) and includes the aspects of yielding, strain hardening, Bauschinger effect

as well as cyclic unloading and reloading rules.

Contact elements were introduced in between the nodes of the flexural reinforcement and the adjacent plane stress elements to account for bar-slippage. The assumed bond-slip model is essentially similar to the one by Eligehausen et al. (1983) with modifications proposed by Filippou (1986).

Fleury-Reynouard-Merabet model

The component-based model by Fleury et al. (2000) follows from the assumption that can coexist in a joint are a) yielding of the main longitudinal reinforcing bars in beams and /or columns at the perimeter of the joint, b) slip of reinforcing steel anchored in the joint and opening of cracks at the joint perimeter, c) distortion of joint due to diagonal cracking, d) shearing of reinforcement at the interface (dowel action). Thus the model, shown in Figure 4.8 consists of: a) two four-noded quadrilateral elements placed in parallel that describe the behavior of concrete and the transverse reinforcing steel in joint core in a smeared manner, b) a mesh of quadrilateral elements of small width representing beam longitudinal steel anchored in the joint and the bond between concrete and steel, c) two elements allowing the connection of beams to the joint, d) two noded bar elements for column longitudinal steel crossing the connection, e) kinematic constraints between the degrees of freedom to ensure comtability.

Concrete material model was simulated using a smeared fixed orthogonal crack model (Merabet et al. 1995). Plasticity theory, with isotropic hardening and associated flow, was used to simulate the response of un-cracked concrete. The Ottosen criterion was used to determine the elastic domain in compression as well as in tension.

A simple elastoplastic law with linear isotropic hardening model was adopted for reinforcing steel. Bauschinger effect was neglected in the model for reinforcing steel.

The bond model is based on the uniaxial bond-slip relation proposed by Eligehausen et al. (1983) with modifications by Monti et al. (1997).

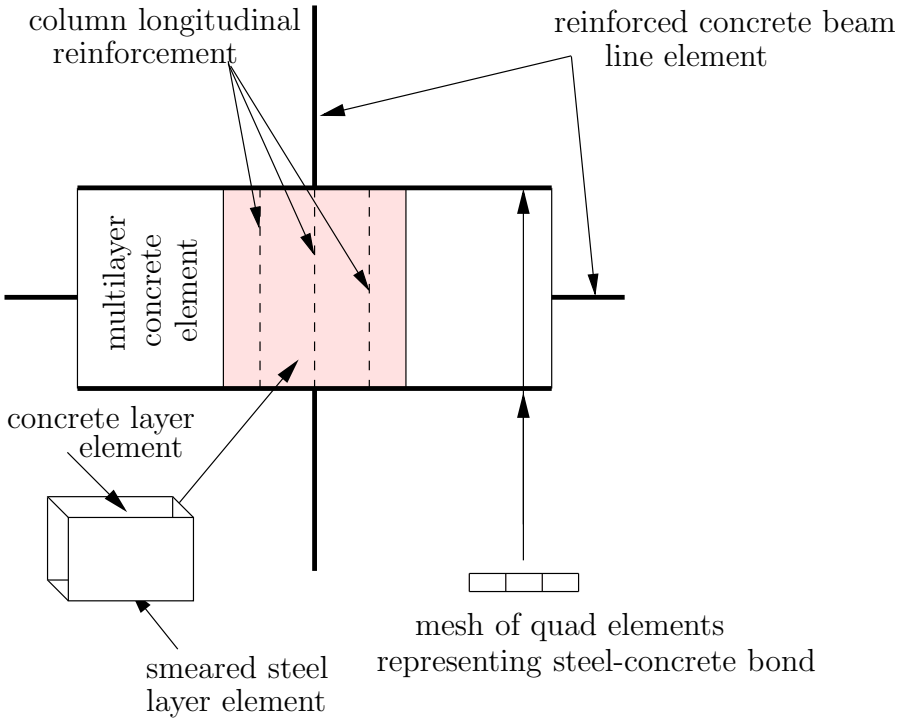

Figure 4.8: Fleury-Reynouard-Merabet joint model (2000)

Youssef-Ghobarah model

Youssef and Ghobarah (2001) proposed a model in which the joint was represented by four rigid members that enclose the joint, with pin connection between the between these rigid elements and with shear springs connecting the diagonal. The impact of bar-slip within the joint and concrete crushing at the joint perimeter was represented using three concrete and three steel springs at each face of the connection region between the beams and columns and the joint panel. Figure 4.9 shows an idealization of the model. The reinforcement steel in the form of a group of bars, was represented by steel springs which idealize the relationship between the force in the steel bars and the bond slip. The concrete spring represents the relationship between the axial force on the concrete strut and the axial displacement of the strut. The shear springs represent the shear response in the joint core.

The material model for concrete is represented by Kent and Park (1971) model for concrete in compression and exponential tensile softening curve with a smooth transition from tension to compression region (Youssef and Ghobarah 1999).

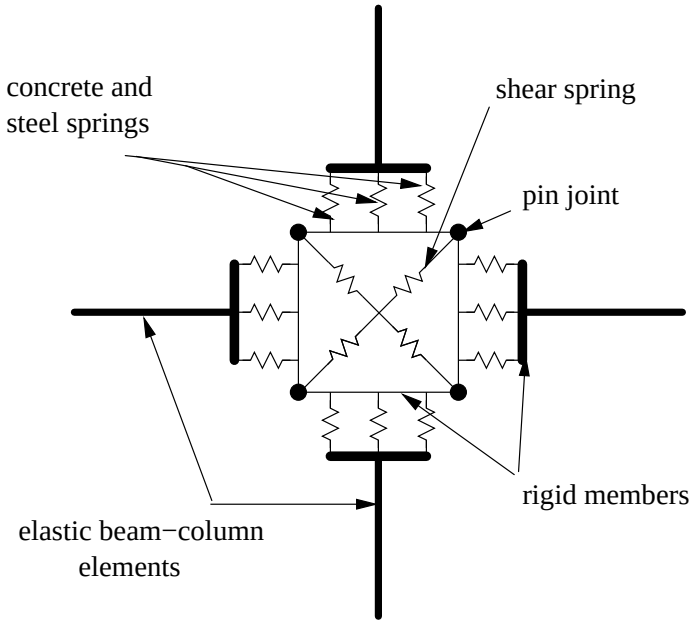

Figure 4.9: Youssef-Ghobarah joint model (2001)

Analytical material model by Giuriani et al. (1969) was used to represent the bond strength and slip relation. For solution of the governing equation for the bond-slip relation to determine the envelope for the steel springs a methodology similar to Filippou (1986) was utilized.

A new hysteretic material model was proposed for the shear-springs to represent the shear behavior of reinforced concrete members subjected to shear force and bending moment reversals (Ghobarah and Youssef 1999). Modified compressive field theory (Vecchio and Collins 1986) was utilized to define the backbone envelope of the curve.

Lowes-Altoontash model

Figure 4.10 shows an idealization of the model developed by Lowes and Altoontash (2003). The joint element has four exterior nodes each with three dof, thus the joint is compatible with traditional 2d beam-column elements. The joint model, comprises of eight zero-length bar slip springs, four interface shear springs and a panel that deforms only in shear. The shear-panel component simulates strength and stiffness loss due to shear failure of the joint core, bar-slip springs simulate stiffness and strength loss due to anchorage-zone damage, and

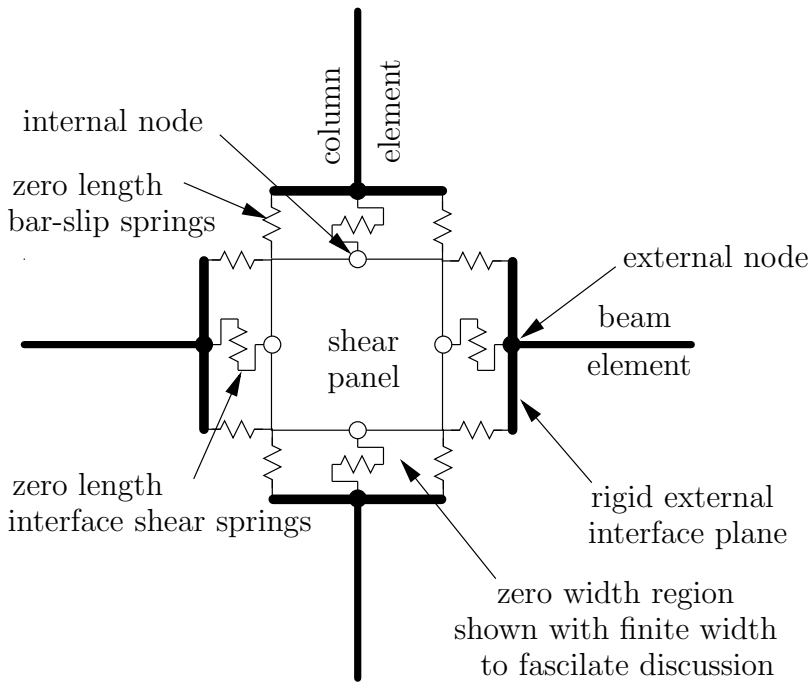

Figure 4.10: Lowes-Altoontash joint model (2003)

interface-shear springs simulates reduced capacity for shear transfer at the joint perimeter due to crack opening. The deformation of the component is based upon the displacement at the four internal dof in the shear panel along with the combination of displacements at the 12 exterior dof.

Modified compressive field theory (Vecchio and Collins 1986) was used to define the envelope of the shear panel. Joint transverse steel and column interior bars are assumed to contribute to shear panel stiffness and strength. Calibration of parameters in the hysteretic one-dimensional material model for the shear panel was developed using only the joint geometry and fundamental material parameters. The cyclic response parameters were calibrated based on experimental data.

A new bar-slip material model was proposed based on the assumption that bond stress within the joint is constant or piecewise constant and slip is entirely due to elongation of the steel. Bond strength and cyclic response parameters are proposed on the basis of experimental studies (Eligehausen et al. 1983, Viwathanatepa et al. 1979, Shima et al. 1987, Lowes 1999).

This element forms the basis for the new model development, a detailed discussion of the calibration of the joint component models are presented in section .

Altoontash-Deierlein model

Altoontash and Deierlein (2003) proposed a two dimensional joint element with four exterior nodes, constrained to a central node by multi-point constraints. These multi-point constraints are imposed at a global system level. The joint load-deformation response was determined by a shear panel and a set of rotational springs that connects the shear panel to the frame elements. Figure 4.11 represents an idealization of the model. The shear panel was assumed to deform only in shear and is represented by an internal central node with four kinematic degrees of freedom, with three degrees corresponding to rigid body motions and a fourth degree of freedom that was used to define the shear distortion of the joint. The central node is connected to the external nodes by four multi-point constraints. The rotational springs at the external nodes of the shear panel represents, in a lumped sense, the bar-slip in between the reinforcing steel and the concrete along with the material inelasticity in the plastic hinge region. This joint model has been extended to a 3d representation and can also take into account large deflections (Altoontash 2004).

The material model used for modeling the panel core region is the modified compressive field theory (Vecchio and Collins 1986). The bond-slip material mode proposed in Lowes and Altoontash (2003) was utilized to represent the behavior of the bond-slip springs at the joint perimeter.

LaFave-Shin model

Figure 4.12 shows an idealization of the joint model proposed by LaFave and Shin (2005). The model comprises of four rigid link elements located on the perimeter of the joint. The links are connected via hinges and load-deformation response is simulated via three nonlinear rotational springs embedded in one of the four hinges. This model was implemented in DRAIN-2DX and Element 10 developed by Foutch et al. (2003) was used for the nonlinear rotational springs. These springs are intended to simulate the nonlinear response of joint

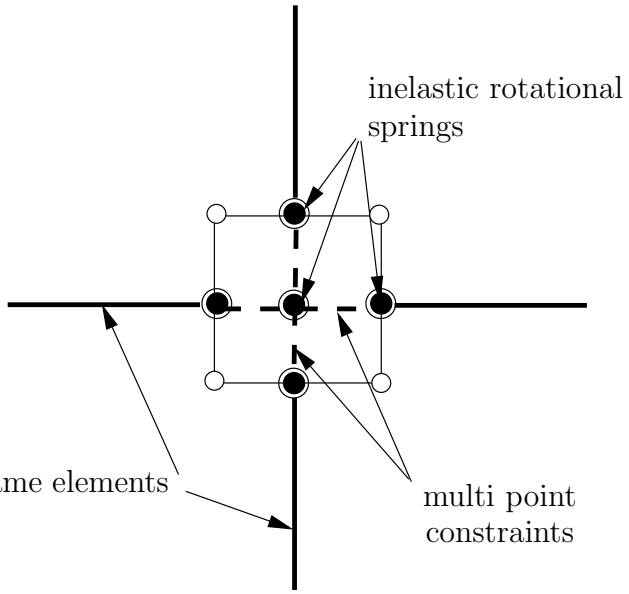

Figure 4.11: Altoontash-Deierlein joint model (2003)

core under shear loading. Additional rotational springs are placed between the beam ends and the joint to simulate the inelastic action due to bar-slip and the plastic hinge region in the beams (DRAIN 2DX Element 10 and Element 2 respectively).

Modified compression field theory (Vecchio and Collins 1986) was used to determine the moment curvature relationship of the three nonlinear springs attached in parallel to represent the shear behavior within the joint. The bond-slip rotational springs were calibrated using the formulation proposed by Morita and Kaku (1984).

Tajiri-Shiohara-Kusuhara model

Figure 4.13 shows the joint element proposed by Tajiri et al. (2006). This connection macro-element model is represented by four nodes, twelve degree of freedom. The super-element represents the behavior of the joint along with the plastic hinge regions of the beams and columns adjacent to the joint region. In this element formulation, the nonlinear response of the joint core was represented by a number of axial springs connecting rigid bodies. The axial springs represent the behavior of concrete, reinforcing steel and bond zone response. The rigid bodies represent concrete sections that remain plane after deformation.

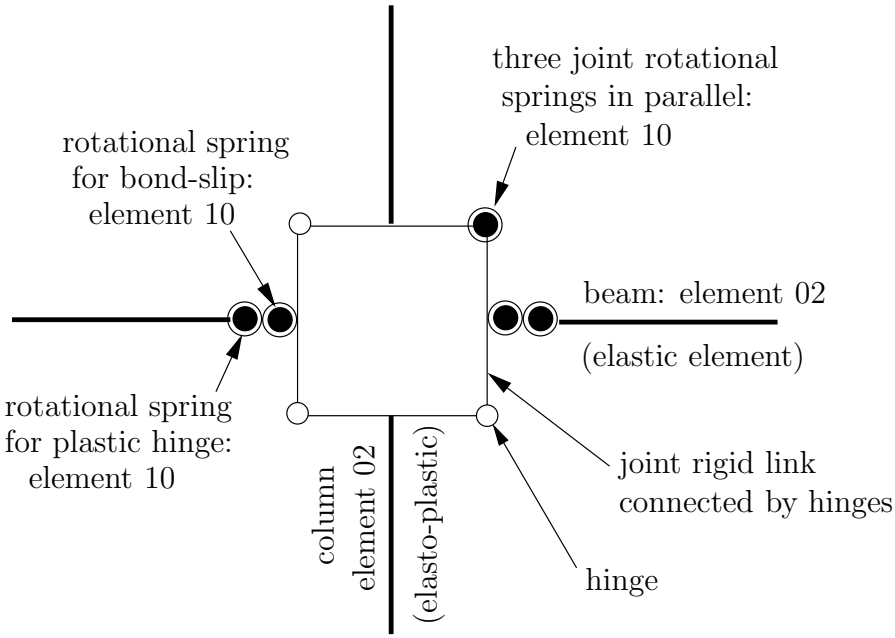

Figure 4.12: LaFave-Shin joint model (2005)

Concrete springs within the joint and also within the plastic hinge region of the beams and columns are modeled using a modified stress-strain relationship of Park et al. (1982). The unloading stiffness of the constitutive relationship for concrete assumes no stiffness degradation. A modified version of Ramberg and Osgood (1943) was utilized for the constitutive relationship of steel springs. The model proposed by Morita and Kaku (1975) was used to represent the bond-slip relationship. The diagonal arrangement of concrete springs in the joint regions takes into account the smeared cracking within the joint core and thereby no cracked concrete models were utilized in this research.

Summary

A number of joint models have been proposed in the past. However, relatively limited data sets were used in the development and validation of these models. To create a computationally efficient, robust joint model that can be used for joints with a wide range design, geometric and material parameters, a new joint model was developed for the study. This new model represents a modification of the model proposed by Lowes and Altoontash (2003). This model was developed and validated using the data set presented in chapter 2.

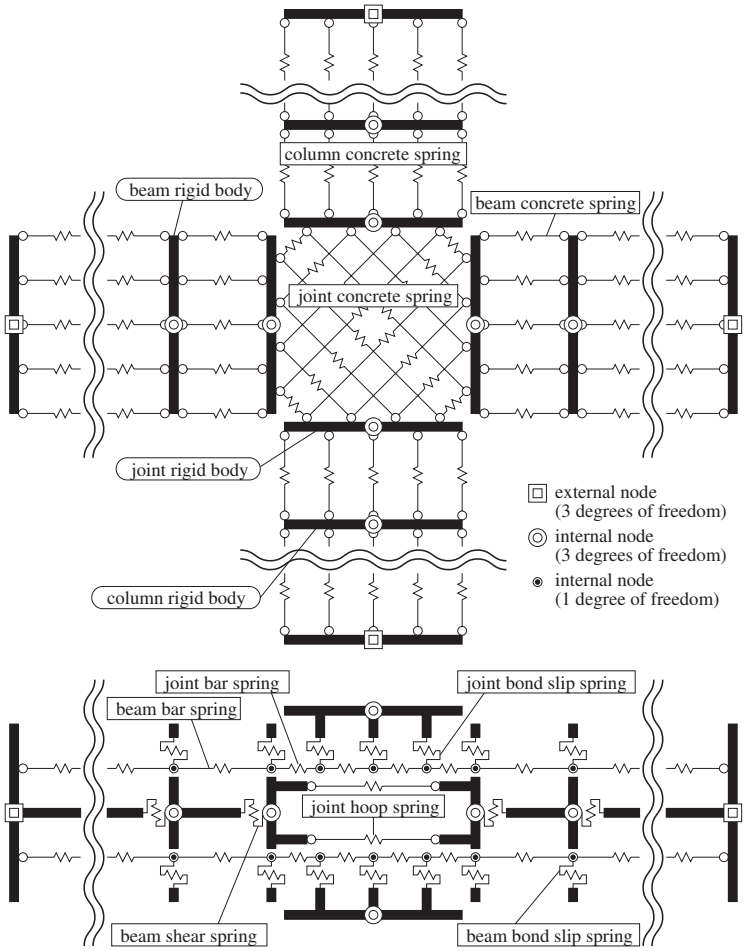

Figure 4.13: Tajiri-Shiohara-Kusuhara joint model (2006)

4.3 Proposed super-element model for the joint (Mitra and Lowes 2007): Element formulation

Both the Mitra-Lowes and Lowes-Altoontash joint models employ a four node, twelve degree-of-freedom element for use in modeling the response of reinforced concrete beam-column joints in two-dimensional structural analysis. The joint element for both the models represents a super-element comprising a shear-panel component that simulates strength and stiffness loss due to failure of the joint core, eight bar-slip springs that simulate stiffness and strength loss due to anchorage-zone damage, and four interface-shear springs that simulate reduced capacity for shear transfer at the joint perimeter due to crack opening. The new element formulation moves the bar-slip springs, which in the Lowes-Altoontash model are located at the perimeter of the joint element, to the centroid of the beam and column flexural tension and compression zones (Figure 4.14). This results in improved simulation of forces in the bar-slip springs. The new joint model also includes improved constitutive models for the shear panel component and modifications to the material model for bar-slip springs.

The new joint element formulation is basically a generalization of the Lowes-Altoontash model which in turn can be obtained as a special case of the new joint element formulation. The formulation of the new joint model has been described in detail in the following subsections.

4.3.1 Kinematics

The deformation of the joint element components is defined by the displacements and rotations of the external and internal nodes. The shear panel component is assumed to deform only in shear and the shear deformation is defined by four internal nodes. Small displacements and rotations are assumed in the super-element formulation. A positive bar-slip spring deformation is associated with tensile force applied to the bars. For the shear panel component a positive shear deformation is associated with clockwise arrangement of the shear forces at the internal nodes in the joint core. For the interface-shear springs, a positive shear deformation is associated with a positive external and zero internal displacement.

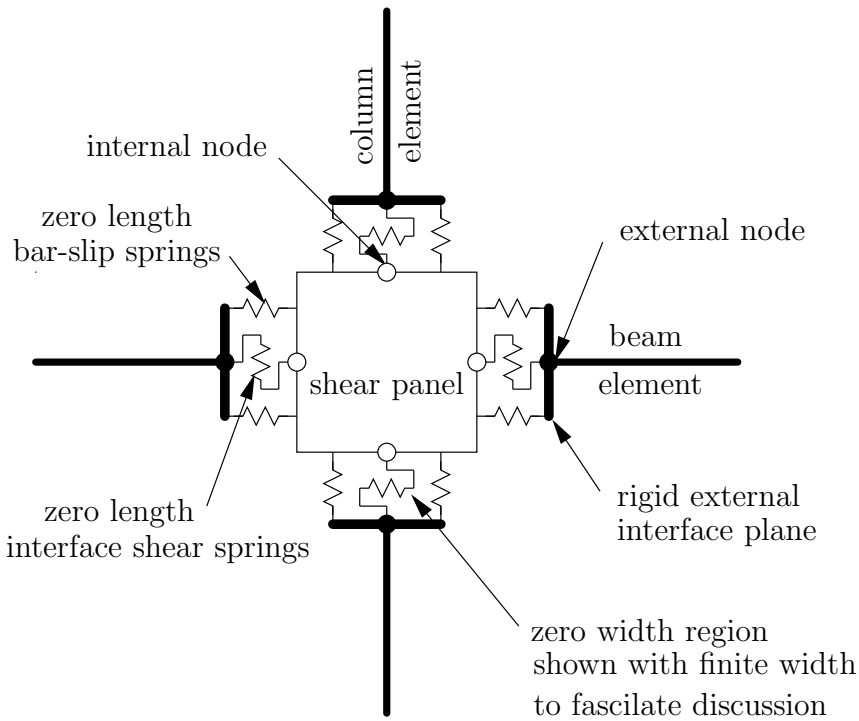

Figure 4.14: Mitra-Lowes joint model

Determination of the element material state requires the solution of a nonlinear system to determine the internal element translations that satisfy element equilibrium. Eq. 4.1 represents the relationship between the component deformations $\underline{\Delta}$, to the external nodal displacements and rotations, u_i and internal nodal displacements, v_i. Figure 4.15 shows the component deformations and the external and internal nodal displacements.

$$\Delta_1 = -u_2 + \frac{\hat{w}}{2}u_3 + \frac{\hat{w}}{2}\left(\frac{v_4 - v_2}{w}\right) + \frac{v_4 + v_2}{2} \tag{4.1a}$$

$$\Delta_2 = -u_2 - \frac{\hat{w}}{2}u_3 + \frac{\hat{w}}{2}\left(\frac{v_2 - v_4}{w}\right) + \frac{v_4 + v_2}{2} \tag{4.1b}$$

$$\Delta_3 = u_1 - v_1 \tag{4.1c}$$

$$\Delta_4 = u_4 + \frac{\hat{h}}{2}u_6 - \frac{\hat{h}}{2}\left(\frac{v_1 - v_3}{h}\right) - \frac{v_1 + v_3}{2} \tag{4.1d}$$

$$\Delta_5 = u_4 - \frac{\hat{h}}{2}u_6 - \frac{\hat{h}}{2}\left(\frac{v_3 - v_1}{h}\right) - \frac{v_1 + v_3}{2} \tag{4.1e}$$

$$\Delta_6 = u_5 - v_2 \tag{4.1f}$$

$$\Delta_7 = u_8 - \frac{\hat{w}}{2}u_9 + \frac{\hat{w}}{2}\left(\frac{v_2 - v_4}{w}\right) - \frac{v_2 + v_4}{2} \tag{4.1g}$$

$$\Delta_8 = u_8 + \frac{\hat{w}}{2}u_9 - \frac{\hat{w}}{2}\left(\frac{v_2 - v_4}{w}\right) - \frac{v_2 + v_4}{2} \tag{4.1h}$$

$$\Delta_9 = u_7 - v_3 \tag{4.1i}$$

$$\Delta_{10} = -u_{10} - \frac{\hat{h}}{2}u_{12} + \frac{\hat{h}}{2}\left(\frac{v_1 - v_3}{h}\right) + \frac{v_1 + v_3}{2} \tag{4.1j}$$

$$\Delta_{11} = -u_{10} + \frac{\hat{h}}{2}u_{12} - \frac{\hat{h}}{2}\left(\frac{v_1 - v_3}{h}\right) + \frac{v_1 + v_3}{2} \tag{4.1k}$$

$$\Delta_{12} = u_{11} - v_4 \tag{4.1l}$$

$$\Delta_{13} = -\frac{v_1}{h} + \frac{v_2}{w} + \frac{v_3}{h} - \frac{v_4}{w} \tag{4.1m}$$

where w represents the total width of the joint, h the total height of the joint, $\hat{w}$ represents the distance between the tension compression couple (or distance between bar-slip springs) in columns and $\hat{h}$ the distance between the tension compression couple (or distance between bar-slip springs) in beams. Thereby, the vector of component deformations $\underline{\Delta}$ is defined as a function of the vector of internal and external nodal displacements, $\underline{\mathbb{U}}$, through the kinematic matrix $\underline{\underline{\mathbb{A}}}$ as follows:

$$\underline{\Delta} = \underline{\underline{\mathbb{A}}} \cdot \underline{\mathbb{U}} \tag{4.2}$$

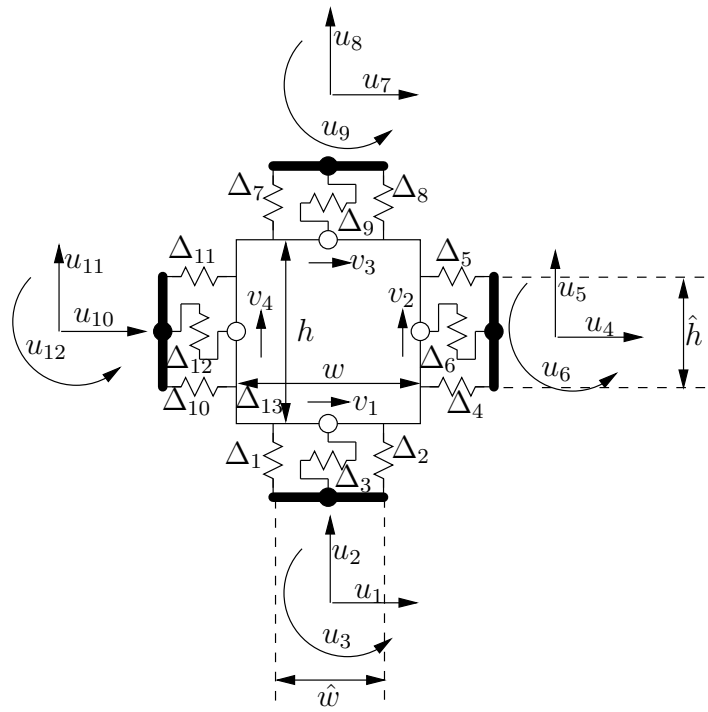

Figure 4.15: Component deformations

where $\underline{\Delta}$ is the vector of joint element component deformations;

$$\underline{\Delta} = (\Delta_1, \Delta_2, \ldots, \Delta_{12}, \Delta_{13})^T \tag{4.3}$$

$\underline{\mathbb{U}}$ in Eq 4.2 is the vector of external and internal generalized nodal displacements:

$$\underline{\mathbb{U}} = (u_1, u_2, \ldots, u_{11}, u_{12}, v_1, v_2, v_3, v_4)^T \tag{4.4}$$

The kinematic transformation matrix, $\underline{\underline{\mathbb{A}}}$ is defined as:

$$\underline{\underline{\mathbb{A}}} = \begin{bmatrix}
0 & -1 & \frac{\hat{w}}{2} & 0 & 0 & 0 & 0 & 0 & 0 & 0 & 0 & 0 & 0 & \frac{(w-\hat{w})}{2w} & 0 & \frac{(w+\hat{w})}{2w} \\
0 & -1 & -\frac{\hat{w}}{2} & 0 & 0 & 0 & 0 & 0 & 0 & 0 & 0 & 0 & 0 & \frac{(w+\hat{w})}{2w} & 0 & \frac{(w-\hat{w})}{2w} \\
1 & 0 & 0 & 0 & 0 & 0 & 0 & 0 & 0 & 0 & 0 & 0 & -1 & 0 & 0 & 0 \\
0 & 0 & 0 & 1 & 0 & \frac{\hat{h}}{2} & 0 & 0 & 0 & 0 & 0 & 0 & -\frac{\left(h+\hat{h}\right)}{2h} & 0 & -\frac{\left(h-\hat{h}\right)}{2h} & 0 \\
0 & 0 & 0 & 1 & 0 & -\frac{\hat{h}}{2} & 0 & 0 & 0 & 0 & 0 & 0 & -\frac{\left(h-\hat{h}\right)}{2h} & 0 & -\frac{\left(h+\hat{h}\right)}{2h} & 0 \\
0 & 0 & 0 & 0 & 1 & 0 & 0 & 0 & 0 & 0 & 0 & 0 & 0 & -1 & 0 & 0 \\
0 & 0 & 0 & 0 & 0 & 0 & 0 & 1 & -\frac{\hat{w}}{2} & 0 & 0 & 0 & 0 & -\frac{(w-\hat{w})}{2w} & 0 & -\frac{(w+\hat{w})}{2w} \\
0 & 0 & 0 & 0 & 0 & 0 & 0 & 1 & \frac{\hat{w}}{2} & 0 & 0 & 0 & 0 & -\frac{(w+\hat{w})}{2w} & 0 & -\frac{(w-\hat{w})}{2w} \\
0 & 0 & 0 & 0 & 0 & 0 & 1 & 0 & 0 & 0 & 0 & 0 & 0 & 0 & -1 & 0 \\
0 & 0 & 0 & 0 & 0 & 0 & 0 & 0 & 0 & -1 & 0 & -\frac{\hat{h}}{2} & \frac{\left(h+\hat{h}\right)}{2h} & 0 & \frac{\left(h-\hat{h}\right)}{2h} & 0 \\
0 & 0 & 0 & 0 & 0 & 0 & 0 & 0 & 0 & -1 & 0 & \frac{\hat{h}}{2} & \frac{\left(h-\hat{h}\right)}{2h} & 0 & \frac{\left(h+\hat{h}\right)}{2h} & 0 \\
0 & 0 & 0 & 0 & 0 & 0 & 0 & 0 & 0 & 0 & 1 & 0 & 0 & 0 & 0 & -1 \\
0 & 0 & 0 & 0 & 0 & 0 & 0 & 0 & 0 & 0 & 0 & 0 & -\frac{1}{h} & \frac{1}{w} & \frac{1}{h} & -\frac{1}{w}
\end{bmatrix} \tag{4.5}$$

and elements of $\underline{\Delta}$, $\underline{\mathbb{U}}$ and $\underline{\underline{\mathbb{A}}}$ are shown in Figure 4.15.

4.3.2 Equilibrium Equations

There exists a complimentary set of 16 internal and external nodal resultants to the set of 16 internal and external nodal displacements. Nodal resultants are computed directly from the component forces by imposing equilibrium at the external and internal nodes. The

equilibrium equations for the joint are given as

$$F_1 = f_3 \tag{4.6a}$$

$$F_2 = -f_1 - f_2 \tag{4.6b}$$

$$F_3 = \frac{\hat{w}}{2}\left(f_2 - f_1\right) \tag{4.6c}$$

$$F_4 = f_4 + f_5 \tag{4.6d}$$

$$F_5 = f_6 \tag{4.6e}$$

$$F_6 = \frac{\hat{h}}{2}\left(f_4 - f_5\right) \tag{4.6f}$$

$$F_7 = f_9 \tag{4.6g}$$

$$F_8 = f_7 + f_8 \tag{4.6h}$$

$$F_9 = \frac{\hat{w}}{2}\left(f_8 - f_7\right) \tag{4.6i}$$

$$F_{10} = -f_{10} - f_{11} \tag{4.6j}$$

$$F_{11} = f_{12} \tag{4.6k}$$

$$F_{12} = \frac{\hat{h}}{2}\left(f_{11} - f_{10}\right) \tag{4.6l}$$

$$\Phi_1 = -f_3 - \frac{1}{2}\left(1 + \frac{\hat{h}}{h}\right)\left(f_4 - f_{10}\right) - \frac{1}{2}\left(1 - \frac{\hat{h}}{h}\right)\left(f_5 - f_{11}\right) - \frac{f_{13}}{h} \tag{4.6m}$$

$$\Phi_2 = -f_6 - \frac{1}{2}\left(1 + \frac{\hat{w}}{w}\right)\left(f_8 - f_1\right) - \frac{1}{2}\left(1 - \frac{\hat{w}}{w}\right)\left(f_7 - f_2\right) + \frac{f_{13}}{w} \tag{4.6n}$$

$$\Phi_3 = -f_9 - \frac{1}{2}\left(1 + \frac{\hat{h}}{h}\right)\left(f_5 - f_{11}\right) - \frac{1}{2}\left(1 - \frac{\hat{h}}{h}\right)\left(f_4 - f_{10}\right) + \frac{f_{13}}{h} \tag{4.6o}$$

$$\Phi_4 = -f_{12} - \frac{1}{2}\left(1 + \frac{\hat{w}}{w}\right)\left(f_7 - f_2\right) - \frac{1}{2}\left(1 - \frac{\hat{w}}{w}\right)\left(f_8 - f_1\right) - \frac{f_{13}}{w} \tag{4.6p}$$

In a matrix representation of Eq. 4.6, the vector of external, $\underline{\mathbb{F}}$ and internal $\underline{\Phi}$ nodal resultant forces is defined as a function of a vector of component forces $\underline{f}$ through the transpose of the kinematic matrix $\underline{\underline{\mathbb{A}}}$ as follows:

$$\left\{ \begin{array}{c} \underline{\mathbb{F}} \\ \underline{\Phi} \end{array} \right\} = \underline{\underline{\mathbb{A}}}^T \cdot \underline{f} \tag{4.7}$$

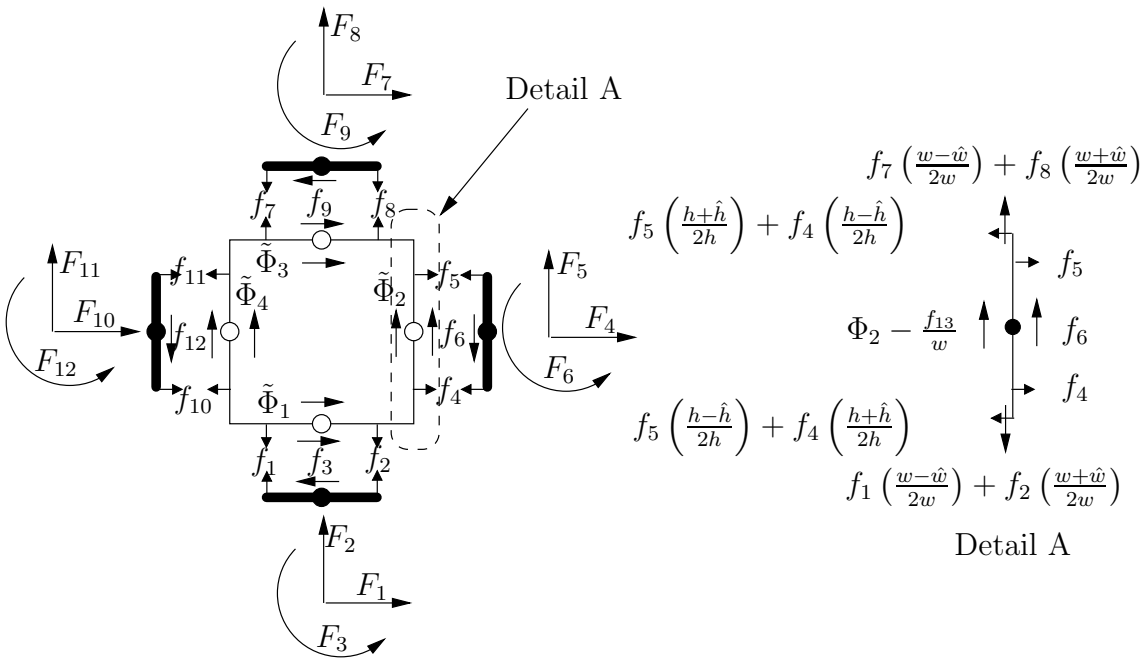

Figure 4.16: External and internal nodal forces and component forces

External nodal resultant force vector $\underline{\mathbb{F}}$ is represented as:

$$\underline{\mathbb{F}} = (F_1, F_2, \ldots, F_{11}, F_{13})^T \tag{4.8}$$

Internal nodal resultant force vector $\underline{\Phi}$ is represented as:

$$\underline{\Phi} = (\Phi_1, \Phi_2, \Phi_3, \Phi_4)^T \tag{4.9}$$

where f_i, F_i and Φ_i are as shown in figure 4.16.

4.3.3 Internal equilibrium of the beam-column joint element

Since the internal element nodes are unique to the joint element, an admissible element state is achieved when the internal nodal resultants are zero. This requires solution of the following system of coupled nonlinear equations.

$$0 = \underline{\Phi} = \underline{\underline{\tilde{A}}}^T \cdot \underline{f} \tag{4.10}$$

where $\underline{\underline{\tilde{A}}}$ refers to columns 13 through 16 of $\underline{\underline{\mathbb{A}}}$. This requirement is used to solve for the vector of internal nodal displacements, $\underline{v}$, by satisfying internal equilibrium within the element, and is accomplished by using the classical Newton-Raphson solution algorithm.

Definition of element tangent and resultant

Use of the above element formulation in a displacement based finite element analysis program requires the computation of external nodal resultant vector $\underline{\mathbb{R}}$ as well as the derivative of the resultants with respect to the external nodal displacements, which is typically the element tangent matrix. Vector of external nodal resultant forces $\underline{\mathbb{R}}$, is computed from the component force vector as

$$\underline{\mathbb{R}} = \underline{\mathbb{F}} = \underline{\underline{\hat{A}}}^T \cdot \underline{f} \tag{4.11}$$

where $\underline{\underline{\hat{A}}}$ represents columns 1 through 12 of $\underline{\underline{\mathbb{A}}}$. The derivative of the resultant vector, $\underline{\mathbb{R}}$, with respect to the external nodal displacement vector, $\underline{u}$, results in the element tangent matrix. This matrix is computed from the tangent of 13 model components and thereby requires a static condensation of the global element tangent matrix, $\underline{\underline{\mathrm{K}}}$.

$$\underline{\underline{K}} \left\{ \begin{array}{c} \underline{du} \\ \underline{dv} \end{array} \right\} = \left[\begin{array}{cc} \underline{\underline{K_{ee}}} & \underline{\underline{K_{ei}}} \\ \underline{\underline{K_{ie}}} & \underline{\underline{K_{ii}}} \end{array} \right] \left\{ \begin{array}{c} \underline{du} \\ \underline{dv} \end{array} \right\} = \left\{ \begin{array}{c} \underline{dF} \\ \underline{d\Phi} \end{array} \right\} = \left\{ \begin{array}{c} \underline{dR} \\ \underline{0} \end{array} \right\} \tag{4.12}$$

where

$$\underline{\underline{K}} = \underline{\underline{\mathbb{A}}}^T \cdot \underline{\underline{k}} \cdot \underline{\underline{\mathbb{A}}} \tag{4.13}$$

and $\underline{\underline{k}}$ is 13 by 13 matrix of component tangents.

$$k_{i,j} = \frac{df_i}{d\Delta_j}, \quad i = 1 \ldots 13, \quad j = 1 \ldots 13 \tag{4.14}$$

In the current formulation it is assumed that there is no coupling action between the components which constitute the super-element and thereby $\underline{\underline{k}}$ is diagonal. Thus, the 12 by 12

element tangent matrix is defined

$$\frac{\underline{\underline{dR}}}{\underline{\underline{du}}} = \underline{\underline{K_{ee}}} - \underline{\underline{K_{ei}}} \left[\underline{\underline{K_{ii}}} \right]^{-1} \underline{\underline{K_{ie}}} \tag{4.15}$$

4.4 One-dimensional hysteretic load-deformation response model

To facilitate implementation of the model, the load-deformation response of each of the components of the joint element is defined using the one-dimensional hysteretic model developed by Lowes and Altoontash (2003) along with modifications proposed in this thesis. The material model have been implemented in the open-source software program OpenSEES (http://opensees.berkeley.edu) along with some modifications and improvements (see Pinching4 uniaxial material model in OpenSEES). In this section the original hysteretic model developed by Lowes and Altoontash have been described in details.

This model consists of a multi-linear response envelope, a tri-linear unload-reload path and three damage rules that control the evolution of these paths (Figure 4.17). The multi-linear response envelope for each of the components in the joint is obtained as a function of the material and geometrical properties. The calibration procedures for the shear-panel and bar-slip components are described in the following sections. Due to lack of experimental data, the interface shear-slip spring components are assumed as elastic.

4.4.1 Material state definition

Figure 4.17 shows the four material states that define the material model. States 1 and 2, which represent the envelope to response loading, are defined as input parameters by the user and may be modified during the analysis to simulate hysteretic strength degradation. With each deformation reversal the load-paths for states 3 and 4 are redefined. The load deformation point at which reversal occurs defines one end point for state 3 (state 4); the state 3-state 2 (state 4-state 1) transition defined the other. Two additional load-deformation points define the state 3 (state 4) load path: the point reached when substantial unloading has occurred and the point at which substantial reloading has occurred. For state 3 (state 4) the load developed upon unloading is defined as a fraction of the minimum (maxi-

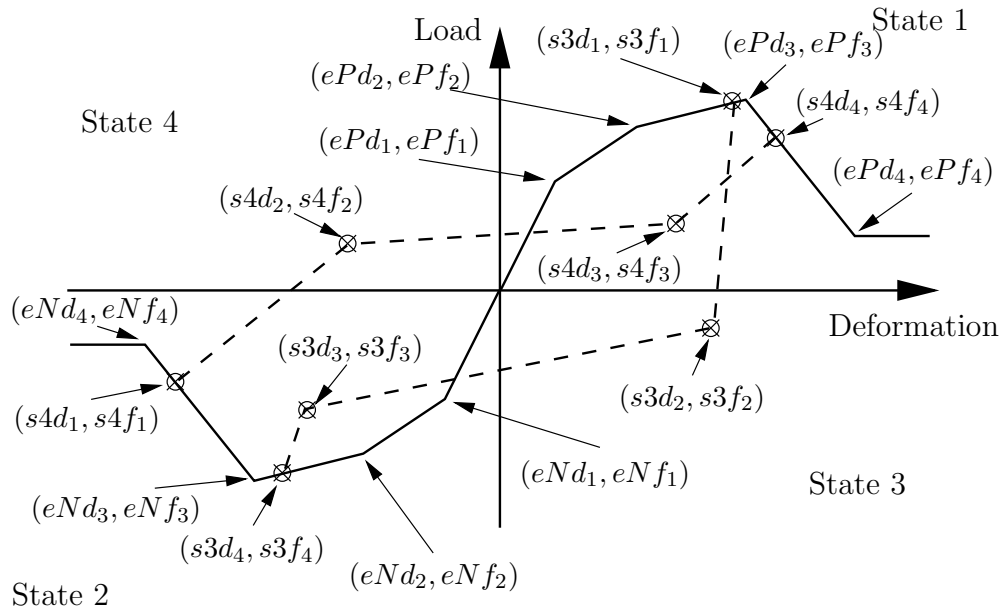

Figure 4.17: Hysteretic one-dimensional load-deformation model

mum strength) that can be developed. With the unloading stiffness defined, this establishes the end of the substantial unload phase. The load-deformation point at which substantial reloading occurs for state 3 (state 4) is defined as the fraction of the minimum (maximum) historic deformation demand and a fraction of the load developed at the minimum (maximum) deformation demand.

4.4.2 Hysteretic response

The impact of deformation history on response is determined by three damage rules. These damage rules control degradation in unloading stiffness (unloading stiffness degradation), deterioration in strength achieved at previously unachieved deformation demands (strength degradation), and deterioration in strength in the vicinity of maximum and minimum deformation demands (reloading strength degradation). Each of the three damage rules employs a damage index, δ, defined as follows

$$\delta = \left(\alpha_1 \left(\tilde{d}_{max}\right)^{\alpha_3} + \alpha_2 \left(\kappa\right)^{\alpha_4}\right) \leq \delta_{lim} \tag{4.16}$$

where

$$\tilde{d}_{max} = \max\left[\frac{d_{max}}{D_{max}}, \frac{d_{min}}{D_{min}}\right] \tag{4.17}$$

and α are parameters defined to fit experimental data, δ_{lim} is the maximum possible value of the damage index, d_{max} and d_{min} are the maximum and minimum historic deformation demands, D_{max} and D_{min} are the positive and negative deformations at which strength loss initiates in states 1 and 2, subscript i refers to the current load step, and κ is a measure of energy dissipated under cyclic loading as is defined in Eqs. 4.18a and 4.18b.

$$\kappa = \frac{E_i}{E_{monotonic}} \tag{4.18a}$$

$$\kappa = \sum\left|\frac{du}{4u_{\max}}\right| \tag{4.18b}$$

where E_i is the accumulated hysteretic energy defined as

$$E_i = \int_{load\,history} dE \tag{4.19}$$

with $E_{monotonic}$ taken equal to energy required to achieve D_{max} under monotonic loading, du is equal to the displacement in a load-deformation history, and $u_{\max}$ refers to the deformation achieved up to the current load step i. Thereby, κ is defined either as a function of hysteretic energy as defined in Eq. 4.18a or as a function of number of equivalent load-cycles using the analogy of rain-flow counting algorithm used in fatigue analysis in Eq. 4.18b.

The stiffness and strength degradation are defined as follows:

$$k_i = k_0\left(1 - \delta_i^k\right) \tag{4.20a}$$

$$f_{max,i} = f_{max,0}\left(1 - \delta_i^f\right) \tag{4.20b}$$

$$d_{max,i} = d_{max,0}\left(1 + \delta_i^d\right) \tag{4.20c}$$

where k is the unloading stiffness, δ_i^k is the unloading stiffness damage index, f_{max} is the maximum strength of the response envelope, δ_i^f is the strength damage index, d_{max} is the maximum historic deformation demand and target for reloading, δ_i^d is the reloading stiffness

damage index, and subscripts i and 0 refer, respectively, to load step i and the initial load step. Figure 4.4.2 shows the effect of each of these stiffness and strength degradation on the load-deformation response.

4.5 Shear panel model calibration using modified compressive field theory

Calibration of the one-dimensional hysteretic material model, discussed in the previous section, is required to define the response of the joint components. Knowledge of geometry and fundamental material properties have only been used to calibrate the material response of the joint components. This section describes the calibration of the shear panel component, as was done in Lowes and Altoontash (2003).

To simulate the strength and stiffness loss due to shear loading of the joint core, Lowes and Altoontash (2003) developed a calibration model for the shear panel based on modified compression field theory (MCFT) (Vecchio and Collins 1986). The assumptions employed in developing this model are as follows:

- Joint transverse reinforcement and all column longitudinal reinforcement are used to compute the stiffness and strength of the joint core.
- Concrete compression strength is reduced, using the factors provided by Stevens et al. (1991a), to model the impact of cyclic loading.
- Reinforcing steel exhibits strain hardening.
- In computing joint shear strength, the joint is assumed to deform only in shear.
- The gross dimension of the joint are used to compute joint shear stiffness and strength.

4.5.1 Evaluation of the MCFT for calibration of joint element shear panel component

Mitra and Lowes (2004), LaFave and Shin (2005), Lowes et al. (2005) show that that MCFT based model simulates well the response of joints with moderate volumes of transverse steel, but that the model is overly conservative for joints with little or no transverse steel. Figure 4.19 shows ratio of predicted, using MCFT with cyclic reduction, τ_{mcft_cyclic}, to observed, τ_{max}, joint shear strength versus ρ_j and ϕ. For detailed explanation of these parameters refer to section 2.3.2.

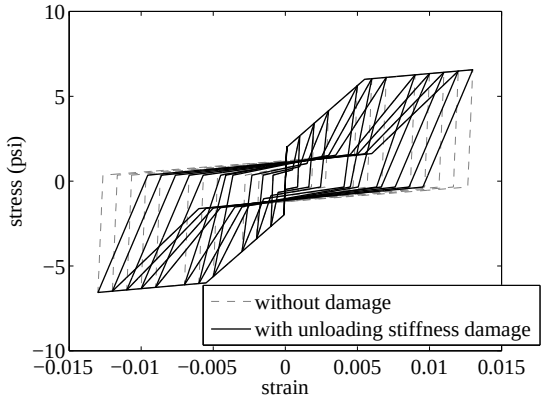

(a) with only strength degradation

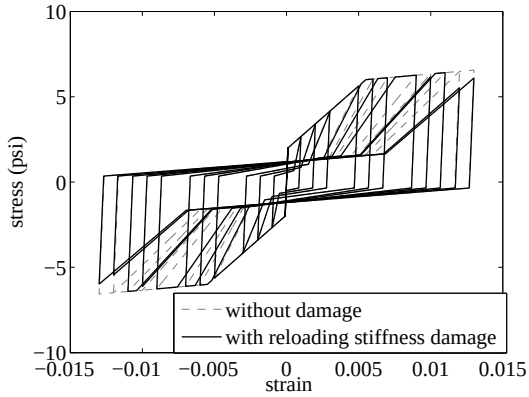

(b) with only reloading stiffness degradation

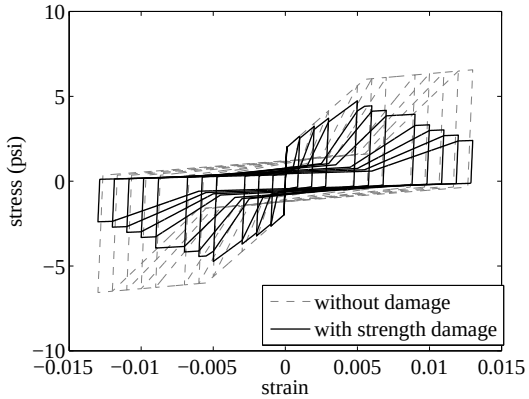

(c) with only unloading stiffness degradation

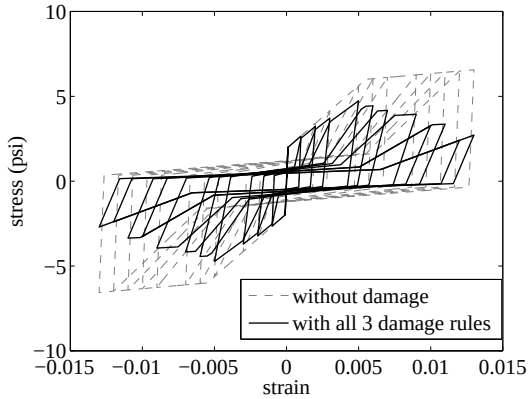

(d) with all three degradations

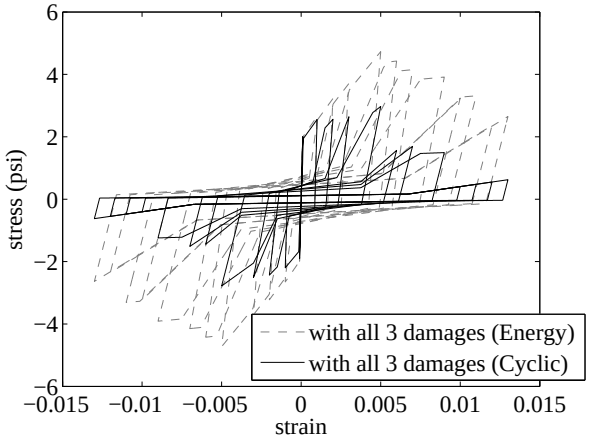

(e) variation with energy and cyclic damage criterion

Figure 4.18: Degradation rules used in the hysteretic response

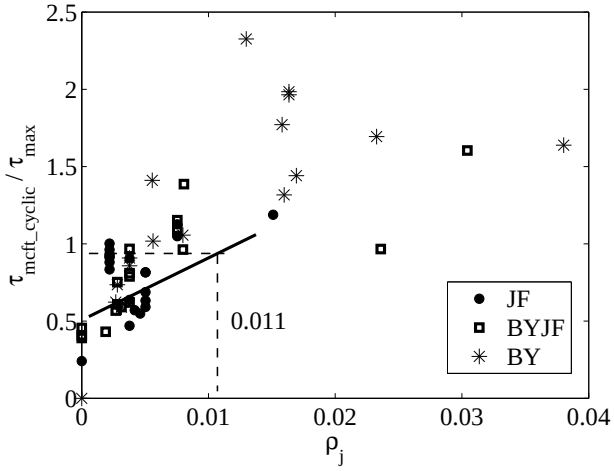

(a) with ρ_j

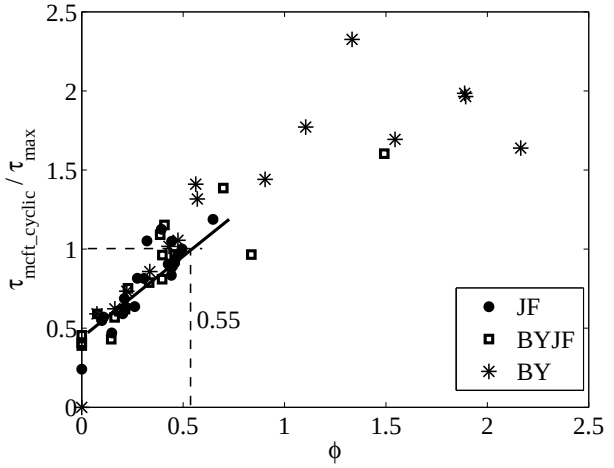

(b) with ϕ

Figure 4.19: Variation of the ratio of simulated shear stress using MCFT and cyclic reduction with observed shear stress

In evaluating these data, it is important to note that a perfect model would result in a ratio of simulated to observed strength of 1.0 for all joints that exhibits JF and some joints that exhibit BYJF and a ratio greater than 1.0 for some joints that exhibit BYJF and all joints that exhibit BY. This is because observed shear strength is limited by beam flexural strength for all joints that exhibit BY and some that exhibit BYJF. The figures 4.19(b) and 4.19(a) clearly indicate that the MCFT-based model with the reduction factor to account for cyclic loading under predicts the observed strength for joints that exhibit JF and BYJF. Moreover, the figure also shows that for joints that exhibit JF and BYJF, the ratio of simulated to observed shear strength is a function of the transverse reinforcement ratio. Since the transverse reinforcement ratio is included in the model, this dependence is unexpected and undesirable. Further, this dependence implies that the MCFT-based model under-predicts strength for joints with low transverse reinforcement ratios and over-predict strength for joints with higher transverse reinforcement ratios. Based upon these observations it is proposed that MCFT-based model with cyclic strength reduction is appropriate for use with joints that have ρ_j greater than 0.011 or ϕ greater than 0.55.

Application of the MCFT based model without reduction in strength due to cyclic loading results in improved prediction of the observed shear strength of the joints. Figure 4.20 shows ratio of shear strength predicted using the MCFT based model without strength reduction due to cyclic loading, $\tau_{mcft\_monotonic}$, to observed shear strength, τ_{max}, joint shear strength versus transverse steel ratio, ρ_j and ratio of total joint transverse steel capacity to joint shear force demand, ϕ. However, the data in Figure 4.20 indicate that the ratio of simulated to observed shear strength is still a function of the transverse reinforcement ratio. Based upon these observations it is proposed that MCFT-based model without cyclic strength reduction is appropriate for use with joints that have ρ_j greater than 0.0034 or ϕ greater than 0.29.

Since both the models, using and not using cyclic reduction with MCFT model, are undesirably dependent on ρ_j and ϕ, a model is required that will perform well over a broader range of ρ_j and ϕ values and is not strongly dependent upon those parameters.

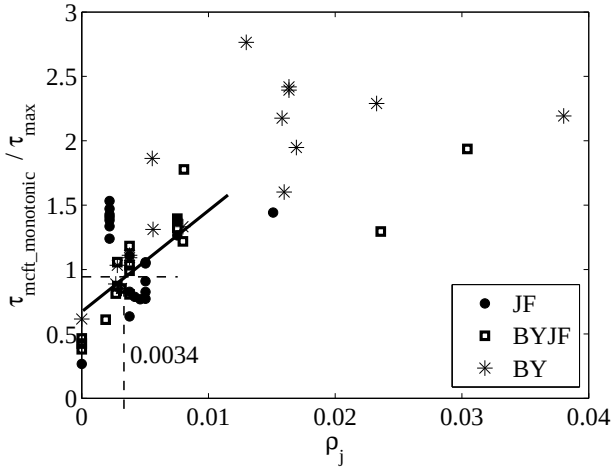

(a) with ρ_j

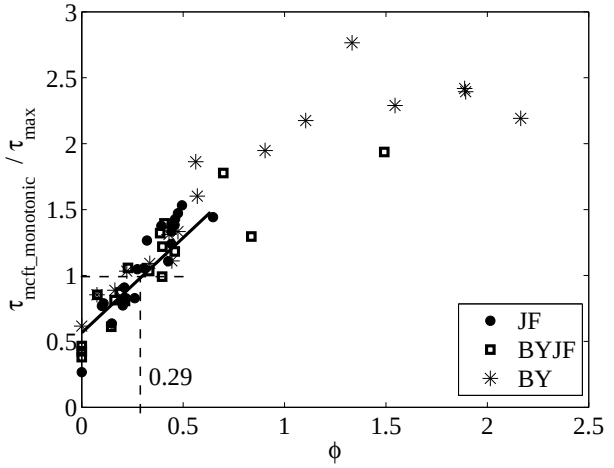

(b) with ϕ

Figure 4.20: Variation of the ratio of simulated shear stress using MCFT with observed shear stress

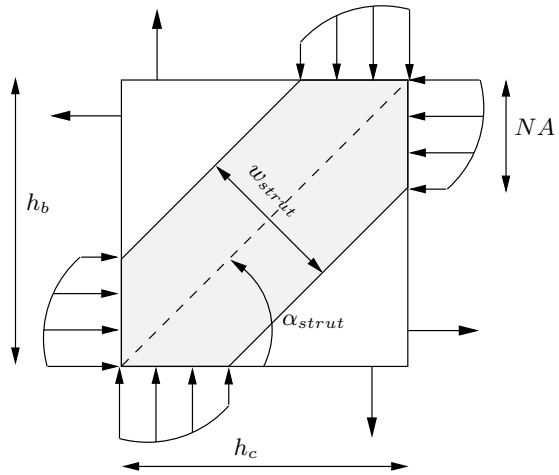

Figure 4.21: Diagonal compression strut model

4.6 Proposed diagonal compression strut mechanism for shear panel calibration of Mitra-Lowes joint model

For the current study, a new approach for calibrating the shear panel was developed employing the assumption that joint shear is primarily transferred via a concrete compression strut (Paulay et al. 1978) and that joint transverse reinforcement acts to increase the strength and deformation capacity of this strut. This new model enables simulation of response for joints with a wide range of ρ_j. Figure 4.21 shows an idealization of the strut-model that employs the following assumptions:

- The orientation and in-plane width of the strut are assumed to be constant and defined by the depth of the column and beam flexural compression zones, at a load level corresponding to the beams developing nominal flexural strength on opposite sides of the joint.
- Strut depth is defined as the maximum of the out-of-plane depth of the beam and column.
- The confined concrete model presented by Mander et al. (1988) defines the stress-strain response of the strut.
- Column longitudinal and joint horizontal reinforcing steel act to confine the joint core concrete; only the component of the confining force acting perpendicular to the

orientation of the compression strut is considered.

- Concrete compressive strength is reduced to account for cracking parallel to the axis of the strut and as well as cyclic loading.
- The joint carries shear only through the compression strut. By equating the horizontal (or vertical) load carried by the strut with that carried by a joint panel carrying uniform shear stress, panel shear stress may be related to strut stress as follows:

$$\tau_{strut} = f_{c\_strut} \frac{w_{strut} \cdot \cos \alpha_{strut}}{w} \tag{4.21}$$

where τ_{strut} is the shear stress in the shear-panel component, f_{c_strut} is the effective strut stress, w_{strut} is the in-plane width of the strut, α_{strut} the angle of inclination of the strut with the horizontal, and w is the in-plane width of the joint.

The effective strut stress f_{c_strut} is not equal to the compressive strength in concrete. In fact the compressive strength of concrete is reduced due to the presence of cracks and cyclic loading. This reduction in concrete compressive strength resulting in an effective strut stress is discussed in the following subsection.

4.6.1 Reduction in concrete compressive strength

The results of previous research indicate that concrete compressive strength is reduced due to tensile loading in the orthogonal direction and subsequent tensile cracking parallel to the direction of compressive loading (Vecchio and Collins 1986, Belarbi and Hsu 1995, Shirai and Noguchi 1989)and also due to cyclic loading (Stevens et al. 1991a). Figure 4.22 shows the ratio of observed to predicted concrete strut stress for the 13 joint sub-assemblage tests that 1) exhibited joint shear failure prior to or following beam yielding and 2) have shear strain data reported in the literature.

For each specimen, data are included for three points on the shear stress-strain history. In Figure 4.22 f_{c_obs} is computed as

$$f_{c\_obs} = \tau_{obs} \frac{w}{w_{strut} \cdot \cos \alpha_{strut}} \tag{4.22}$$

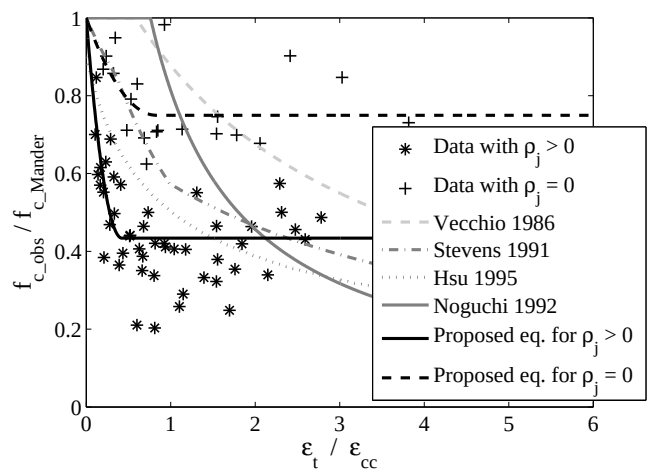

Figure 4.22: Reduction equations to the concrete compressive strength

where τ_{obs} is computed using Eq. 2.2 with actual, instead of maximum, moments and shears, and w, h, w_{strut} and α_{strut} are as defined previously. Figure 4.22 shows six models for predicting the reduction in compression strength resulting from load history. The reduction factor, ζ, for all the models are presented as follows. In the expressions below ε_t is the principal tensile strain computed from the laboratory shear strain data assuming the joint deforms only in shear, and ε_{cc} is the strain at the compressive strength per Mander et al. (1988)The first model (Vecchio 1986) is the original model proposed by Vecchio and Collins (1986) and is given as

$$\zeta = \frac{1}{0.8 + 0.34\left(\frac{\varepsilon_t}{\varepsilon_{cc}}\right)} \leq 1 \tag{4.23}$$

The second model (Stevens 1991) is a combination of the revised model by Vecchio and Collins (1986) model (eq. 4.24a modified by Stevens et al. (1991b) (eq. 4.24b) to account

for cyclic load history, and is given as

$$\zeta_1 = \frac{1}{0.9 + 0.27\left(\frac{\varepsilon_t}{\varepsilon_{cc}}\right)} \leq 1 \tag{4.24a}$$

$$\zeta_2 = \frac{1}{1.0 + 0.5\left(\frac{\varepsilon_t}{\varepsilon_{cc}}\right)} \leq 0.67 \tag{4.24b}$$

$$\zeta = \zeta_1 \cdot \zeta_2 \tag{4.24c}$$

The third model (Hsu 1995) is the model proposed by Belarbi and Hsu (1995), and is represented as

$$\zeta = \frac{0.9}{1.0 + 400\varepsilon_t} \leq 0.9 \tag{4.25}$$

The fourth model (Noguchi 1989) is the model proposed by Shirai and Noguchi (1989), and is represented as

$$\zeta = \frac{1}{0.27 + 0.96\left(\frac{\varepsilon_t}{\varepsilon_{cc}}\right)} \leq 1.0 \tag{4.26}$$

The fifth and sixth models are proposed here respectively to provide a better fit to the data for joints with transverse reinforcement ($\rho_j > 0$) and without transverse reinforcement ($\rho_j = 0$). Table 4.1 shows the root mean square error of each of these strength reduction equations when compared with the experimental joint shear stress-strain data. For joints with transverse reinforcement, the new strength-reduction model is defined

$$\frac{f_{c\_strut}}{f_{c\_Mander}} = 3.62\left|\frac{\varepsilon_t}{\varepsilon_{cc}}\right|^2 - 2.82\left|\frac{\varepsilon_t}{\varepsilon_{cc}}\right| + 1 for \left|\frac{\varepsilon_t}{\varepsilon_{cc}}\right| < 0.39 \tag{4.27a}$$

$$= 0.45 for \left|\frac{\varepsilon_t}{\varepsilon_{cc}}\right| \geq 0.39 \tag{4.27b}$$

and for joints without transverse reinforcement:

$$\frac{f_{c\_strut}}{f_{c\_Mander}} = 0.36\left|\frac{\varepsilon_t}{\varepsilon_{cc}}\right|^2 - 0.60\left|\frac{\varepsilon_t}{\varepsilon_{cc}}\right| + 1 for \left|\frac{\varepsilon_t}{\varepsilon_{cc}}\right| < 0.83 \tag{4.28a}$$

$$= 0.75 for \left|\frac{\varepsilon_t}{\varepsilon_{cc}}\right| \geq 0.83 \tag{4.28b}$$

where f_{c_strut} is the strut strength including strength reduction to account for tensile stress

Table 4.1: Root mean square error values (RMSE) for the concrete compressive strength reduction models

Redn. Eq.	RMSE
Vecchio 1986	0.40
Stevens 1991	0.26
Hsu 1995	0.20
Noguchi 1989	0.40
Proposed $\rho_j > 0$	0.08
Proposed $\rho_j = 0$	0.08

in the orthogonal direction and cyclic loading; f_{c_Mander} is the concrete compressive stress computed per Mander et al. (1988); ε_t is the principal tensile strain computed from the laboratory shear strain data assuming the joint deforms only in shear, and ε_{cc} is the strain at the compressive strength per Mander et al. (1988). Model parameters are defined to provide a best fit to the experimental data assuming the strength reduction factor is 1.0 for zero transverse strain and decreases quadratically to a limit value.

Evaluation of the proposed strength-reduction models shows that the new models provide a better fit to the data than do the models developed previously by other researchers (Vecchio and Collins 1986, Stevens et al. 1991b, Shirai and Noguchi 1989, Belarbi and Hsu 1995). This is attributed to the fact that the previous models were developed for use in simulating the response of concrete in large, uniformly reinforced, uniformly loaded panels, which is not representative of concrete in beam-column joints. Evaluation of the two new models shows that joints without transverse reinforcement exhibit less strength loss than do joints with transverse reinforcement. This is attributed to the fact that for joints without transverse reinforcement, out-of-plane bending of column longitudinal reinforcement provides some confinement of joint core concrete. This mechanism is not included in computing concrete compressive stress-strain response. A similar observation of lower reduction in compressive strength associated for the case with low transverse reinforcement has also been obtained in von Ramin and Matamoros (2006b).

Table 4.2: Comparison of the ratio of simulated to observed maximum shear stresses predicted by different models

Specimen exhibiting failure mechanism	Number	$\tau_{mcft\_monotonic}/\tau_{\max}$		$\tau_{mcft\_cyclic}/\tau_{\max}$		$\tau_{strut}/\tau_{\max}$	
		Mean	C.O.V.	Mean	C.O.V.	Mean	C.O.V.
JF	22	1.10	0.31	0.81	0.29	1.09	0.23
BYJF	18	1.02	0.42	0.81	0.43	1.09	0.13
BY	17	1.64	0.40	1.25	0.48	1.23	0.18

4.6.2 Evaluation of the newly proposed model for joint shear panel component calibration

Evaluation of the data in table 4.2 indicates that for joints that exhibit shear failure (JF or BYJF), the proposed model predicts the observed strength more accurately and with a smaller coefficient of variation than is achieved using the MCFT-based model.

Additionally, the data in Figure 4.23(a) show that the ratio of observed to predicted strength does not exhibit the same level of dependence on transverse steel ratio, ρ_j, that the MCFT-based model does. Similar results are observed when dependence on ϕ is considered, as has been shown in Figure 4.23(b). The data in table 4.2 and figure 4.23 indicate that the strut-based model is appropriate for use with joints with a wide range of transverse reinforcement ratios.

4.6.3 Simulation of stiffness deterioration under cyclic load

Using the above material model for the shear-panel component we obtain the multi-linear envelope (states 1 and 2) of the one-dimensional hysteretic load-deformation response envelope for the shear panel component. Calibration of the shear-panel response model also requires specification of the parameters defining the unload-reload path and stiffness and strength loss under cyclic loading. Assuming symmetry with respect to load direction, and using experimental shear stress-strain data (a reduced data set of 13 samples from chapter 2 where the joint stress strain response is provided by the experimental investigators), the following average values for the path parameters were determined: strain at which reloading occurs as a fraction of maximum (minimum) historic strain, $rDisp = 0.09$, stress at which reloading occurs as a fraction of the stress developed at maximum historic strain, $rForce = 0.21$, and ratio of stress developed upon unloading, from a negative (positive)

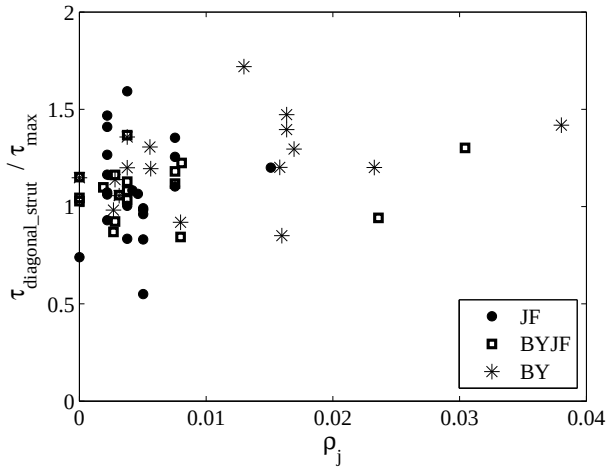

(a) with ρ_j

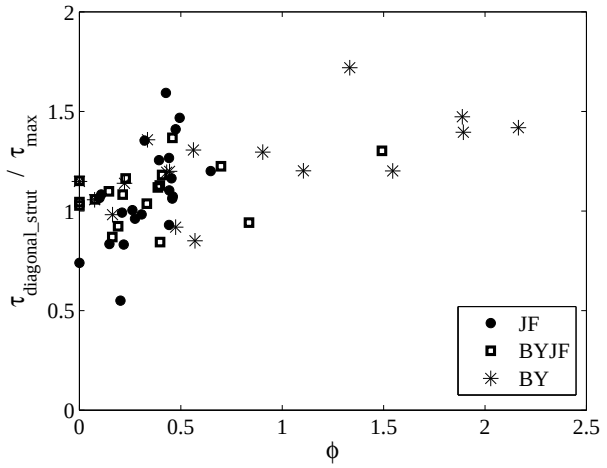

(b) with ϕ

Figure 4.23: Variation of the ratio of simulated shear stress using the new model with observed shear stress

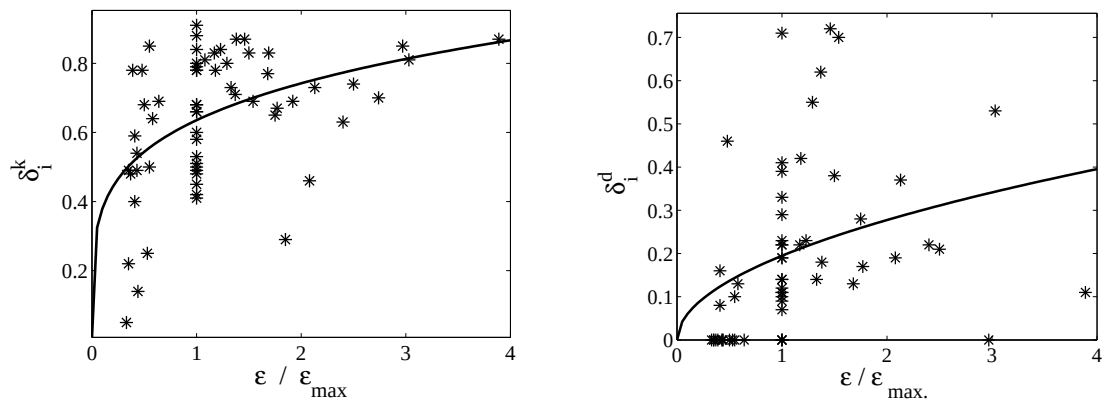

(a) for unloading stiffness degradation

(b) for reloading stiffness degradation

Figure 4.24: Damage degradation rules for the shear panel

stress to a maximum (minimum) of the stress envelope, $uForce = 0.0$.

In order to maintain calibration simplicity, both the unloading and reloading stiffness degradation has been determined primarily by maximum deformation demand. Figure 4.24 shows value of the unloading stiffness parameter, δ^k, and reloading stiffness parameter, δ_i^d, computed from experimental joint shear strain data versus the ratio of strain with the strain at maximum stress $\varepsilon/\varepsilon_{max}$. A reduced data set of 13 samples from chapter 2 with joint shear stress strain data provided were considered in the plots. Coefficients in the damage parameter equation Eq. 4.29 were computed to provide a best fit to the data, with the following results

$$\delta_i^k = 0.64\left(\tilde{d}_{max,i}\right)^{0.22} \leq 0.9 \tag{4.29}$$

$$\delta_i^d = 0.20\left(\tilde{d}_{max,i}\right)^{0.51} \leq 0.4 \tag{4.30}$$

where δ_i^k , δ_i^d and $\tilde{d}_{max}$ are as defined previously.

4.6.4 Simulation of strength deterioration under cyclic load

The envelope to the proposed joint-panel response model simulates strength loss due to crushing of the concrete strut as well as opening of cracks parallel to the strut. However, experimental data suggest that yielding of beam reinforcing steel causes damage to anchor-

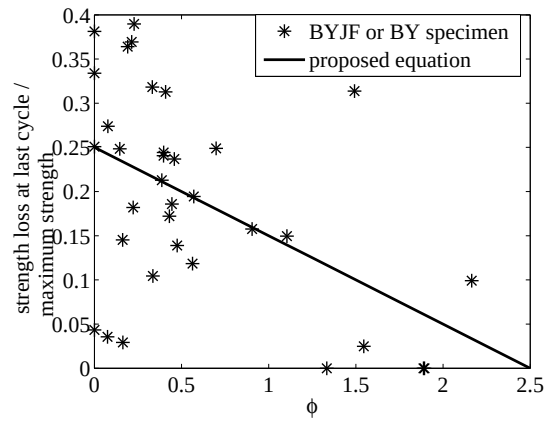

Figure 4.25: strength reduction with ϕ

age zone concrete that reduces joint shear capacity. This mechanism of strength loss is simulated using the hysteretic damage rules included in the material model. Strength loss is assumed to initiate once beam yielding occurs and maximum strength loss is defined to be a function of the joint shear capacity-demand ratio, ϕ, as shown in figure 4.25, with the result that

$$\delta_i^f = \alpha_1 \left(\tilde{d}_{max,i} - \tilde{d}_{yield} \right) \leq \delta_{lim}^f \qquad \forall \qquad \tilde{d}_{max,i} \geq \tilde{d}_{yield} \tag{4.31}$$

where

$$\alpha_1 = \frac{\delta_{lim}^f}{1 - \tilde{d}_{yield}} \tag{4.32a}$$

$$\tilde{d}_{yield} = \frac{d_{yield}}{D_{\max}} \tag{4.32b}$$

$$\delta_{\lim}^f = 0.25 - 0.10\phi \tag{4.32c}$$

with d_{yield} equal to the deformation demand associated with beams reaching yield and all other variables are as previously defined.

4.7 Bar-slip model calibration

The bar-slip springs included in the joint element are intended to simulate stiffness and strength loss associated with deterioration of beam- and column-bar anchorage in the joint. Lowes and Altoontash (2003) proposed a calibration model for the bar-slip springs on the

basis of an assumed bond-stress distribution within the joint and empirically derived bond strength values, and a slip limit of 3.0 mm beyond which springs exhibited a softening-type response, and cyclic-response parameters (which were defined using cyclic bond test data). Evaluation of this model using a data set in chapter 2 suggested that the model could be modified to improve accuracy, ensure numerical stability for the global system (Mitra and Lowes 2004). In this section, the bar-slip model prepared by Lowes and Altoontash (2003) is reviewed and improvements to this model are presented.

4.7.1 Lowes-Altoontash Bar slip model

In the study by Lowes and Altoontash (2003), a model was developed using data from experimental testing of anchorage-zone specimen and making some assumptions about bond-stress distribution within the joint. The simplified assumptions about joint anchorage-response are:

- Bond stress along the anchored length of the reinforcing bar is assumed to be uniform for reinforcement that remains elastic and piecewise uniform for reinforcement loaded beyond yield.
- Slip is assumed to define the relative movement of the reinforcement bar with respect to the perimeter of the joint and is a function of the strain distribution along the bar.
- Bar is assumed to exhibit zero slip at the point of zero bar stress.
- Based on studies by Eligehausen et al. (1983) and Lowes (1999) it was recommended that bond strength deteriorates once slip exceeds 3 mm (0.1 in) and the post peak stiffness is defined as equal to 10% of the initial stiffness.

Given these assumptions, the bar-stress versus bar-slip relationship is defined as follows:

$$
\begin{aligned}
d_{slip} &= \int_0^{l_{fs}} \tau_E \frac{\pi d_b}{A_b} \cdot \frac{1}{E} x \, dx \\
&= 2\frac{\tau_E}{E}\frac{l_{fs}^2}{d_b} \qquad \forall \, f_s < f_y \\
&= \int_0^{l_e} \frac{4}{d_b}\frac{\tau_E}{E} x \, dx + \int_{l_e}^{l_y+l_e} \left(\frac{f_y}{E} + \tau_y \frac{4}{d_b}\frac{(x-l_e)}{E_h} \right) dx \\
&= 2\frac{\tau_E}{E}\frac{l_e^2}{d_b} + \frac{f_y \cdot l_y}{E} + 2\frac{\tau_Y}{E_h}\frac{l_y^2}{d_b} \qquad \forall \, f_s \geq f_y
\end{aligned} \tag{4.33}
$$

with

$$l_{fs} = \frac{f_s}{\tau_{ET}} \cdot \frac{A_b}{\pi d_b} \; ; \tag{4.34a}$$

$$l_e = \frac{f_y}{\tau_{ET}} \cdot \frac{A_b}{\pi d_b} \; ; \tag{4.34b}$$

$$l_y = \frac{f_s - f_y}{\tau_{YT}} \cdot \frac{A_b}{\pi d_b} \tag{4.34c}$$

where f_s is the bar stress at the joint perimeter, f_y the yield strength of steel, E the elastic steel modulus, E_h the hardening modulus of steel assuming the steel response to be represented by a bilinear response, τ_E is the bond strength for elastic steel, τ_Y is the bond strength for yielded steel, A_b the nominal bar area, d_b the nominal bar diameter, l_e and l_y respectively the length of the reinforcing bar for which steel stress is less than and greater than the yield stress. For the case of $l_e + l_y$ greater than the width of the joint, the deterioration of bond strength under cyclic loading is more severe and it is appropriate to assume reduced bond strength in the elastic region of the reinforcing bar.

These average bond strength values were determined from previous experimental investigations of anchorage-zone specimens and structural sub-assemblages (Eligehausen et al. 1983, Viwathanatepa et al. 1979, Shima et al. 1987, Lowes 1999). The results of experimental testing indicate that bond strength is a function of the material state of the anchored bar as well as the concrete and transverse reinforcing steel in the vicinity of the bar. It was

Table 4.3: Average bond strengths as a function of steel stress state (adapted from Lowes and Altoontash (2003))

Bar Stress, f_s (f_y is yield strength, taken same for tension and compression)	Average bond strength in MPa. (f_c in MPa.)	Average bond strength in psi. (f_c in psi.)
Tension, $f_s < f_y$	$\tau_{ET} = 1.8\sqrt{f_c}$	$\tau_{ET} = 21\sqrt{f_c}$
Tension, $f_s < f_y$	$\tau_{YT} = 0.4\sqrt{f_c}$ *to* $0.05\sqrt{f_c}$	$\tau_{YT} = 4.8\sqrt{f_c}$ *to* $0.6\sqrt{f_c}$
Compression, $-f_s < f_y$	$\tau_{EC} = 2.2\sqrt{f_c}$	$\tau_{EC} = 26\sqrt{f_c}$
Compression, $-f_s > f_y$	$\tau_{YC} = 3.6\sqrt{f_c}$	$\tau_{YC} = 43\sqrt{f_c}$

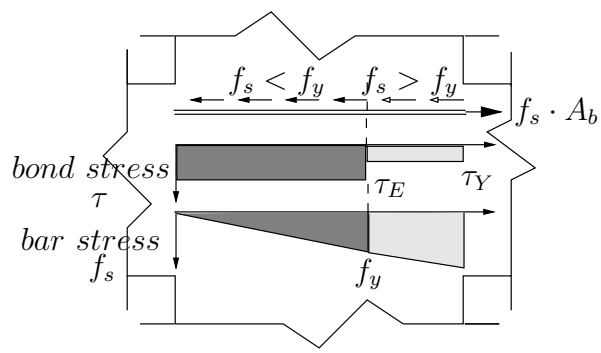

Figure 4.26: Bond stress and bar stress distribution for a bar anchored in beam-column joint

observed from experimental investigations that bond strength is relatively higher where there is a compressive stress field perpendicular to the reinforcing bar, and relatively lower where there is a tensile stress field. Moreover, bond strength also reduced for reinforcement carrying stress in excess of the tensile yield strength and increased for the case of reinforcement carrying compressive strength less than the yield strength of the bar in compression. Thus, Table 4.3 provides bond strength values for the four different bond-zone conditions that may develop within the joint region. Figure 4.26 represents the distribution of bond stress and bar stress within the anchored region of the reinforcing steel in the joint. A detailed discussion of what experimental tests were used to obtain the values in Table 4.3 are provided in Lowes and Altoontash (2003).

Bar slip spring constitutive model

Development of the bar-slip spring constitutive model requires definition of the relationship between bar stress and spring force. The axial and flexural forces from the beam and column

members are transferred to the joint through the tension and compression forces in the bar-slip springs. For tensile loading, it is appropriate to assume that all of the tensile force is carried by reinforcing steel. Thus, the total tensile force in the spring is transferred into the joint through bond. However, for compressive loading, the total compressive force is carried by the concrete and reinforcing steel. Thus, only a fraction of the compressive force is transferred to the joint through bond. Following this approach, concrete compression force, C_c, and the steel compression resultant force, C_s, are computed as

$$C_c = 0.85 f_c \beta c w \tag{4.35a}$$

$$C_s = f_s^c A_s^c = 0.003 \frac{c - d'}{c} E_s A_s^c \tag{4.35b}$$

where β is the scale factor to account for the use of a uniform concrete compressive stress distribution in place of a true stress distribution, c is the neutral axis depth of the section, w represents the width of the section, d' represents the depth to the centroid of the compression reinforcement, E_s is the reinforcing elastic steel modulus, A_s^c is the area of reinforcing steel carrying compression.

Assuming the centroid of the total concrete compression force is defined by the concrete-stress distribution, the compressive spring force, C is defined as

$$C = C_s + C_c = f_s^c A_s^c \left(1 + \frac{0.85 f_c d w}{E_s A_s^c} \frac{2\left(1 - j\right)}{0.003\beta \left(1 - \frac{\beta d'}{2d(1-j)}\right)} \right) \tag{4.36}$$

where d is the depth to tension reinforcement, jd is the tension-compression couple distance of a cross-section. Typically, in reinforced concrete section design, j is assumed as a constant value of 0.75 for columns and 0.85 for beams.

4.7.2 Proposed bar-slip model for Mitra-Lowes joint

Here, the model developed by Lowes and Altoontash (2003) is modified to improve accuracy, ensure numerical stability for the global system, and to ensure applicability for a wide range of design and demand parameters for interior reinforced-concrete beam-column joints. The

first issue considered in developing the new bar-slip model was initiation of strength loss in the bar-slip springs. A review of experimental data by Mitra and Lowes (2004) indicated the 3.0 mm slip limit proposed by Lowes and Altoontash (2003) was too conservative. To determine new criterion for initiation of strength loss, simulated bar-slip data for the joint sub-assemblages listed in Table B.2 that exhibited BY or BYJF were considered. Only joints that exhibit BY and BYJF were considered as the response of the joints could be expected to be controlled by bond, with strength loss in BYJF could either be due to bond or due to shear stress degradation in the joint panel. These tests were simulated using the modeling approach discussed in section 5.9 and the new joint element formulation with an elastic shear-panel component, elastic interface-shear components and bar-slip components calibrated as per Lowes and Altoontash (2003) with the exception that strength loss was not simulated. Figure 4.27(a) shows the simulated maximum slip in the beam bar-slip components. These data show no clear distinction between joints that exhibit BYJF and BY. Similar results were found when the ratio of the maximum slip to the slip associated with an anchorage length equal to the joint width was considered(Figure 4.27(b)). Thus, it was concluded that, for the given approach to modeling bar slip, a slip-based criterion cannot be used to initiate strength deterioration of the bar-slip components.

The second issue considered in developing the new model was numerical stability of the global solution algorithm. It was found that if multiple bar-slip springs exhibited a negative tangent stiffness, the joint element and global system developed multiple negative eigenvalues. Thus, the global system could not be solved using traditional nonlinear solution algorithms.

To address the above two issues, the new calibration model developed as part of this study employs the recommendations of Lowes and Altoontash (2003) but 1) delays initiation of bar-slip strength loss until reinforcing steel reaches ultimate strength and 2) simulates strength loss using a hysteretic damage rule rather than an envelope that exhibits softening. This strength-loss model is defined as

$$\delta_i^f = \alpha_1 \left(\tilde{d}_{max,i} - \tilde{d}_{ult} \right) \leq \delta_{lim}^f \qquad \forall \qquad \tilde{d}_{max,i} > \tilde{d}_{ult} \tag{4.37}$$

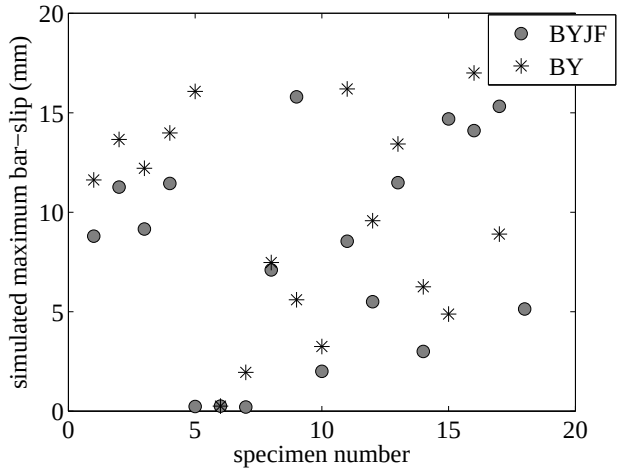

(a) Simulated maximum slip in bar-slip components

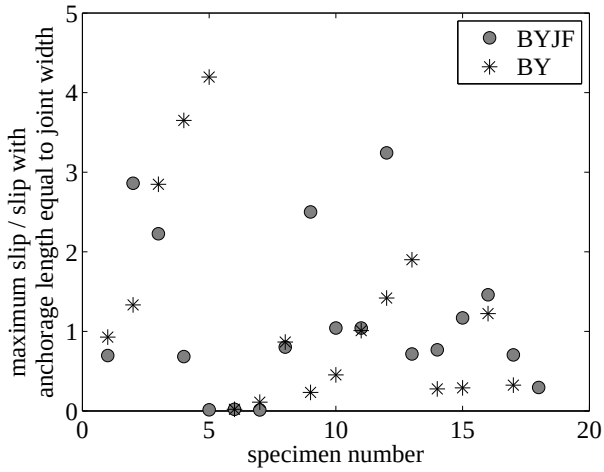

(b) Ratio of maximum slip to slip associated with an anchorage length equal to joint width

Figure 4.27: Slip based criterion for strength deterioration for Bar-Slip springs

where

$$\alpha_1 = \frac{\delta^f_{lim}}{1 - \tilde{d}_{ult}} \tag{4.38a}$$

$$\tilde{d}_{ult} = \max\left[\frac{d_{ult,comp}}{D_{min}}, \frac{d_{ult,ten}}{D_{max}}\right] \tag{4.38b}$$

where $d_{ult,comp}$ and $d_{ult,ten}$ refer to the deformation demand associated with longitudinal steel reaching ultimate strength in compression and tension, D_{min} and D_{max} define deformations associated with reinforcing steel reaching minimum and maximum strain capacity, and δ^f_{lim} is defined such that minimum strength is equal to the residual bond strength associated with development of a frictional mechanism.

The third issue considered in developing the new model was unload-reload response under cyclic loading. Lowes and Altoontash (2003) proposed unload-reload response parameters ($rDisp$, $rForce$, $uForce$) for bar-slip springs on the basis of bond-test data. These parameters resulted in a friction-type response, characterized by low strength and stiffness, for most of the unload-reload cycle. Bond test data show similar unload-reload response for tension and compression, and model parameters were defined to be equal. However, because bar-slip spring strength and stiffness was increased in compression to account for the contribution of concrete, the use of equal unload-reload response parameters resulted in overly rapid stiffness and strength gain for reloading from tension to compression. For joint sub-assemblages, this translated to an over-prediction of reloading strength and reduced "pinching" of joint load-deformation response curves.

In the new model, the model parameter $rForce$, which defines the force at which reloading occurs as a fraction of the force developed at minimum historic slip, is uniquely defined for tension and compression. For tension, $rForce_t$ is defined per the recommendation of Lowes and Altoontash (2003) to be 0.25. For compression, $rForce_c$:

$$rForce_c = rForce_t \frac{F^{ult}_{ten}}{F^{ult}_{comp}} \tag{4.39}$$

where F^{ult} is the ultimate strength in tension and compression (represented with subscripts $(.)_{ten}$ and $(.)_{comp}$ respectively). This results in a friction-type response being sim-

ulated for reloading in tension and compression as well as accurate simulation of sub-assemblage "pinching".

The material model has been implemented in the OpenSEES platform as Bar-Slip Material.

4.8 Application of the proposed calibration procedures

The previous sections present a series of calibration procedures that must be employed to simulate joint response. Following is the recommended process for creating a model of a particular joint with specific material and geometric properties:

1. Complete a moment-curvature analysis of the beams and column that frame into the joint. Here it is assumed that beams carry zero axial load while columns carry axial load associated with gravity loading.
2. From the moment-curvature analysis, determine i) the moment associated with first yield of beam reinforcing steel, ii) the distance between tension and compression resultants at nominal flexural strength (defined per ACI 318 (2005)), and iii) the neutral axis depth at nominal flexural strength.
3. Define joint element formulation parameters using joint geometry and distance between beam and column tension and compression resultants.
4. Using neutral axis depths for beams and columns, determine the width, w_{strut}, and angle, α_{strut}, of the concrete compression strut as shown in Figure 4.21.
5. Determine concrete compression strut response. This requires use of i) the concrete model by Mander et al. (1988) with concrete confinement determined by reinforcement geometry and strut angle, α_{strut} , ii) the concrete strength reduction models proposed here (Eqs. 4.27, 4.28), and iii) cyclic response parameters defined here (Eqs. 4.29, 4.31) and in Lowes and Altoontash (2003).
6. Determine bar-slip spring response using the basic model proposed by Lowes and Altoontash (2003) with strength reduction defined using Eqs. 4.37 and 4.39.
7. Interface-slip springs are defined to be stiff and elastic.

4.9 Simulation of laboratory tests

The joint element formulation and calibration procedures were evaluated through comparison of simulation and observed response for tests listed in Table B.3 and B.4. Numerical simulation of the laboratory tests was accomplished using the OpenSEES analysis platform (McKenna et al. 2005). OpenSEES is an object-oriented, open-source framework for finite element analysis that is currently under development by researchers at the Pacific Earthquake Engineering Research Center. OpenSEES was chosen for use because of the relative ease with which the new joint element formulation and material models could be introduced into the framework and because it includes nonlinear beam-column element formulations and global solution algorithms, thereby eliminating the need to develop these for the current study.

Figure 4.28 shows an idealization of the numerical model. Lateral loading was applied using displacement control at the top of the column. A constant column axial load was applied using load control. The boundary conditions are representative of those employed in the laboratory.

The nonlinear response of beams and columns was simulated using the OpenSEES "beamWithHinges" element formulation (Scott and Fenves 2006). This element formulation assumes a linear moment distribution and employs a numerical integration scheme that includes two quadrature points within the user-defined plastic hinges at the element ends and a single quadrature point at mid-span. At the interface with the joint, the plastic-hinge length was defined equal to half the height of the member section following Corley (1966). At the supports, since no inelastic action was expected, the plastic-hinge length was defined equal to zero. At mid-span, the element was assumed to be elastic with an effective moment of inertia defined per ACI318-05 Section 9.5.2.3.

A fiber-discretization was used to simulate flexural response within the plastic-hinges. Concrete material response was simulated using the OpenSEES "Concrete01" material model. The modified Kent-Park model (Park et al. 1982) with a degraded linear unloading/reloading stiffness (Karsan and Jirsa 1969) was used to define compression response, and zero tensile strength was assumed. The OpenSEES "Steel02" material model was used

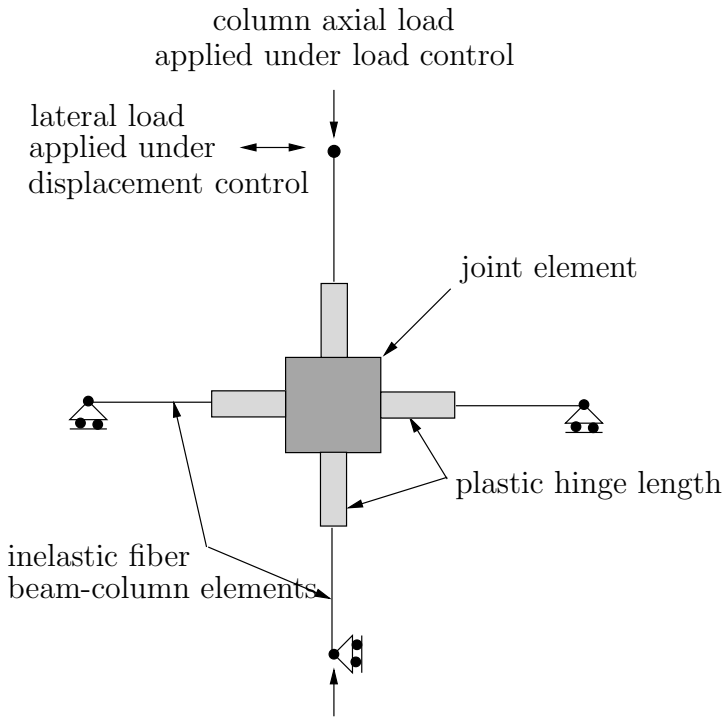

Figure 4.28: Numerical model of a typical building joint sub-assemblage tested in laboratory

to simulate the steel response; this model employs a bilinear envelope and a curvilinear unload-reload response.

C++ source code for the joint element formulation ("beamColumnJoint2d") and the material models ("Pinching4" and "BarSlip") presented in this manuscript are currently available on the OpenSEES website (http://opensees.berkeley.edu). Additionally, all of models are included in executable version of the OpenSEES code and documented in the OpenSEES User's Manual (Mazonni et al. 2006).

4.10 Comparison of simulated and observed response

The tests listed in Table B.3 were simulated using the new joint model, including the new joint element formulation and shear-panel and bar-slip spring calibration methods, following the calibration process outlined in the previous section. Tables 4.4 and 4.5 lists the mean and coefficient of variation of the ratio of observed to simulated response quantities for the 57 specimens that were simulated. A more extensive presentation of the simulation data

Table 4.4: Comparison of the ratio of simulated to observed stiffness values

Specimen	Number	Initial Stiffness (kN/mm)		Post yield stiffness (kN/mm)		Unloading stiffness max. load (kN/mm)	
		Mean	C.O.V.	Mean	C.O.V.	Mean	C.O.V.
All	57	1.06	0.15	1.07	0.27	1.03	0.13
JF	22	1.14	0.13			1.09	0.19
BYJF	18	1.07	0.15	1.00	0.22	1.02	0.10
BY	17	1.00	0.15	1.11	0.29	1.00	0.09

Table 4.5: Comparison of the ratio of simulated to observed strength and drift values

Specimen	No.	Drift at max. load		Max. column load kN		Strength at final drift level / max. strength		Average nominal Pinching ratio	
		Mean	C.O.V.	Mean	C.O.V.	Mean	C.O.V.	Mean	C.O.V.
All	57	1.12	0.27	1.03	0.17	1.04	0.20	1.04	0.12
JF	22	1.01	0.26	1.09	0.23	1.05	0.20	0.99	0.14
BYJF	18	1.21	0.32	1.00	0.09	1.03	0.25	1.03	0.13
BY	17	1.14	0.20	1.00	0.08	1.04	0.16	1.07	0.10

can be found in table B.3 and B.4.

Observations that can be drawn from the data in these tables include

Failure mechanisms: On average, the model simulates the correct inelastic failure mechanism, with 82% accuracy for specimen exhibiting JF, 89% accuracy for BYJF specimen and 94% accuracy for BY specimen.

Initial and unloading stiffness: The proposed model represents well the observed initial stiffness and the unloading stiffness at maximum load. For these measures, the average ratio of simulated to observed stiffness ranges from 1.03 to 1.06 with coefficients of variation less than 15%. The initial stiffness is a measure of stiffness of the adjacent beam-column elements when the joint responds elastically during initial load cycles. Unloading stiffness is a measure of stiffness deterioration exhibited by the shear-panel and/or the bar-slip component when the global system reaches maximum load.

Post-yield tangent stiffness: The proposed model predicts well the post-yield stiffness, with an average ratio of simulated to observed stiffness, for specimens that exhibit beam yielding prior to joint failure, of 1.0, with a coefficient of variation of 22%. For this analysis, 'yield' is defined by first yield of beam reinforcing steel, and stiffness are

not considered for joints that exhibit softening prior to yield. The post-yield stiffness is the result of several influencing factors including the degrading post-peak response of the shear panel, the hardening response of the bar-slip components, and the flexural stiffness of beams and columns. Given the complexity of the response, a coefficient of variation of 22% is considered relatively low.

Maximum strength: The model represents well the observed maximum strength of the sub-assemblage, with the average ratio of simulated to observed response equal to 1.03. The coefficient of variation of 17% on this average value also is considered to be relatively low given the wide variation in design parameters included in the data set.

Drift at maximum strength: The model simulates the drift at maximum strength with less accuracy than strength. For all of the specimens, the average ratio of simulated to observed drift is 1.12 with a coefficient of variation of 27%. One of the reasons for the higher level of variability in this response measure is that drift values are limited to the peaks of the drift history imposed in the laboratory; the difference between the peak drift imposed in two sequential cycles may be large.

Strength loss at final drift level: On average, the model predicts well the observed strength during the final load cycle, with an average ratio of simulated to observed strength of 1.04 and a coefficient of variation of 20%. These results validate the proposed shear-panel calibration model, including the proposed strength reduction model for joints that exhibit yielding of beam longitudinal reinforcing steel prior to joint failure.

Pinching ratio: is defined, using data from the cycle corresponding to maximum load, as the ratio of the strength at zero drift to the maximum strength. On average, the model closely predicts the observed pinching ratio with a mean of 1.04 and a coefficient of variation of 12%.

Figure 4.29 show load-displacement histories for the one of the laboratory sub-assemblages *OSJ10* that was considered to be the best case examples of simulating observed response. The grey lines at the background represent the experimental observations and fine black line at the top represents the simulated observation. Similarly, Figure 4.30 shows the load-displacement histories for a worst case sample, namely *PEER4150*. In specimen *PEER4150*

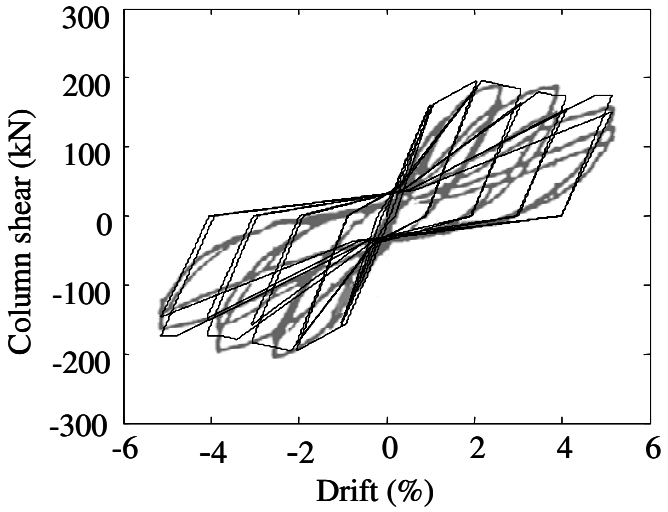

Figure 4.29: Best simulation of load-deformation data for 'JF' sample: *OSJ10*

the shear stress envelope of the joint core could not be obtained correctly based on our proposed process, which explains the difference in the maximum column load between the observed and the simulated response. Both the above samples, namely *OSJ10* and *PEER4150* represents joint shear failure samples ('JF'). Two 'BYJF' samples showing comparison of simulated and observed response are provided in Figures 4.31 and 4.32. A full listing of all the experimental and simulated load-deformation response is provided in appendix B and the simulated and observed load-deflection plots of the specimen are given in appendix D.

4.11 Conclusion

A model for use in simulating the response of reinforced concrete beam column joints was developed and evaluated using an extensive experimental data set. The model builds on a previously proposed model by Lowes and Altoontash (2003) and includes 1) a revised element formulation that provides accurate prediction of joint load mechanisms, 2) a new, more accurate, model for simulating joint shear response that is appropriate for use with a wide range of joint designs and simulates strength loss due to anchorage-zone damage within the joint, and 3) an improved method for simulating anchorage response of beam and column reinforcing steel that does not impede classical nonlinear solution algorithms and is not overly conservative in predicting failure. The model was implemented in the OpenSEES

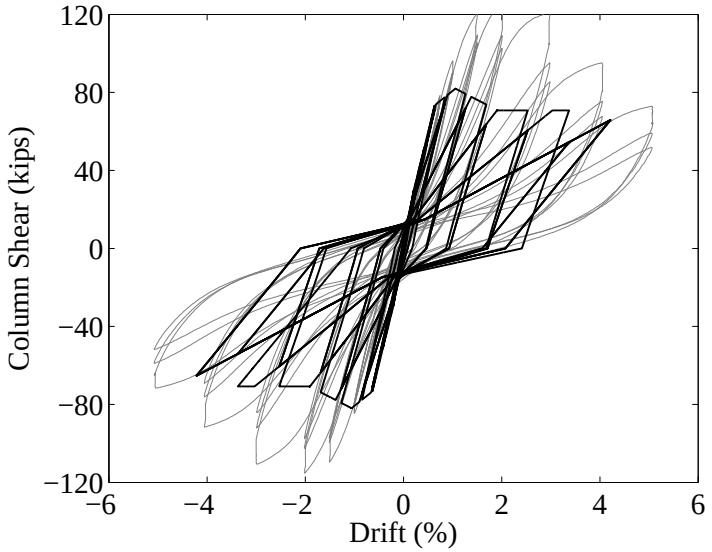

Figure 4.30: Worst simulation of load-deformation data for 'JF' sample: *PEER4150*

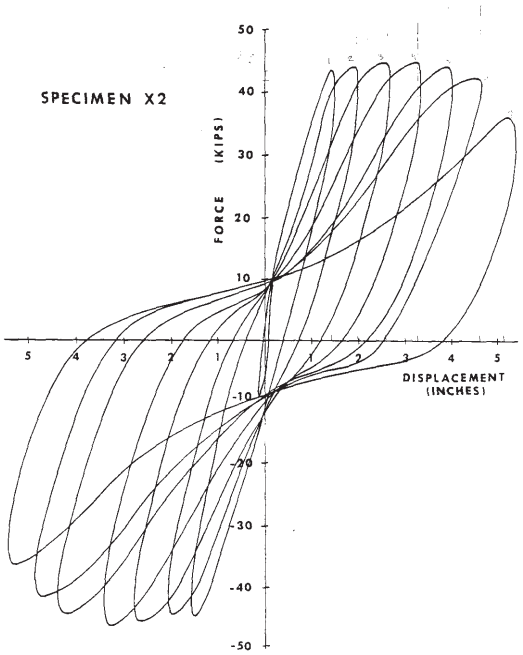

(a) Experimental

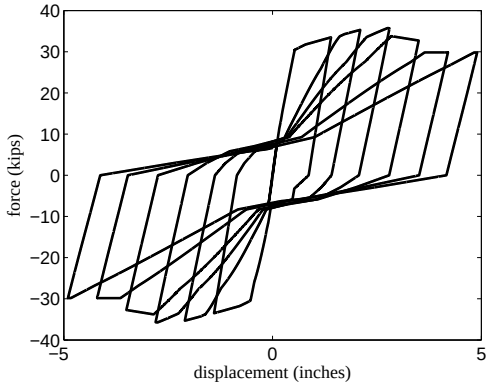

(b) Simulated

Figure 4.31: Load deformation response of a 'BYJF' specimen: *DW_X2*

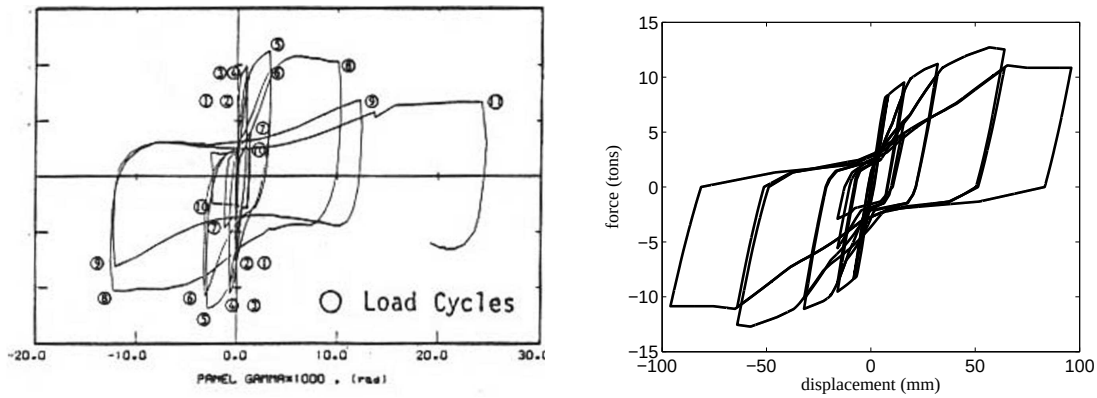

(a) Experimental (b) Simulated

Figure 4.32: Load deformation response of a 'BYJF' specimen: *OKA_J4*

analysis framework and is available for use by others (http://opensees.berkeley.edu). This component based model for the joint region is computationally robust and less demanding in regards to computational time and complexity compared to the continuum model. This model can also be utilized in 2 dimensional frame analysis of structures along with other conventional line elements. The component based model is also able to simulate the complete load-deformation relation and thereby outweighs the simplicity of the strut-and-tie model and also the probabilistic failure initiation model. This component based super-element for the joint can be utilized for performance based analysis of connection regions.

The model was evaluated by comparing simulated and observed response for 57 interior joint sub-assemblages tested in the laboratory. Joints had widely varying design characteristics and exhibited different failure modes: joint failure prior to beam yielding (JF), beam yielding prior to joint failure (BYJF) and beam yielding without joint failure (BY). Results indicate that the observed failure mode was simulated correctly for 89% of the specimens. Results indicate also that model represents well observed cyclic response characteristics including initial stiffness, unloading stiffness at maximum strength, maximum strength, strength loss at the final laboratory drift demand level, and pinching ratio.

The results of this study support several additional conclusions about modeling of the seismic response of interior building joints. First, a compression-strut model may be used to simulate the load-deformation response of the joint core; however, experimental data

indicate that response is significantly different for joints with and without transverse reinforcement. Second, accurate simulation of joint stiffness requires consideration of both nonlinear joint core response as well as bond-slip response of frame member longitudinal reinforcement anchored in the joint. In particular, sub-assemblage stiffness during unloading and reloading and the pinching of the sub-assemblage load-deformation response history are determined by simulation of bar-slip response. Third, strength loss in joints that exhibit beam-yielding cannot be predicted accurately by considering bond-slip response and employing a slip-based failure criterion. Fourth, accurate simulation of strength loss in joints that exhibit beam-yielding may be achieved by accounting for the impact of anchorage-zone damage on joint core strength.

Chapter 5

STRUT-AND-TIE MODELING OF JOINTS SUBJECTED TO SEISMIC LOADING

5.1 Introduction

Strut-and-tie models are discrete representations of actual stress fields resulting from applied load and support conditions. Like a real truss, a strut-and-tie model consists of compression members (struts) and tension members (ties) interconnected at nodes (referred to as nodal zones or nodal regions).

An admissible strut-and-tie model (STM) satisfies equilibrium at the nodes and does not load struts, ties or nodes beyond their capacities. A particular STM of a system provides a lower bound on the strength of the system since neither compatibility requirements nor explicit material constitutive relationships are considered in developing an STM. Thus, there is no unique solution and multiple admissible STM may be developed for each load case for any system. However, as a result of limited ductility in the structural concrete, there are only a small number of viable solutions for each design region.

Strut-and-tie models are used widely by engineers to dimension and detail reinforced concrete structures and this design methodology is included in most structural design codes around the world (ACI 318-05, AASHTO LRFD 1994, National Building Code of Canada 2005, EuroCode-2 1998). However, most of these design codes allow STM for non-seismic applications but not for seismic applications. The objective of the research presented here is to extend the applicability of STM, as defined in ACI 318-05, to performance-based-seismic design of joints. To accomplish this, STM were developed for several joints in the data set (see chapter 2) at peak load level and the stresses in the strut, nodal and bond stresses were compared to ACI prescribed limits. It was observed that modifications to the ACI requirements are required for seismic applications.

The layout of this chapter follows from the research objectives. In section 5.2 background

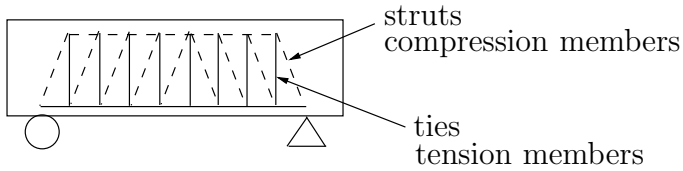

(a) Ritter's model

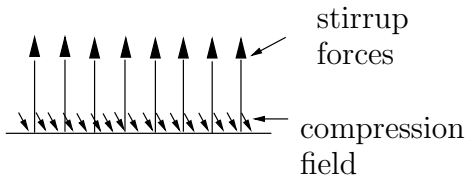

(b) Mörsch's model

Figure 5.1: STM for a simply supported beam

on STM applied for non-seismic applications is presented. Section 5.3 reviews the previous research to apply STM for seismic design of joints. Section 5.4 presents the developmental work on seismic design recommendations for joints.

5.2 Previous research on Strut and Tie modeling

5.2.1 Review of STM

Pioneering work by Ritter (1899) and Mörsch (1909) to develop the truss analogy laid the foundation for modern strut-and-tie models (STM). The early truss analogy assumed concrete to be incapable of resisting tension and was used primarily to idealize the flow of forces in a cracked beam. Ritter idealized a simply supported concrete beam as a truss in which the top compression block of the beam section was analogous to the top chord of the truss, the longitudinal reinforcement at the bottom truss to the bottom chord of the truss, the transverse stirrups to the vertical components, and discrete compressive concrete zones in between to the diagonal members of the truss. Mörsch (1909) expanded on Ritter's model by proposing that the diagonal compressive stress in concrete need not be a discrete zone, as proposed by Ritter (1899), but could be a continuous field in equilibrium with discrete stirrup forces (see Figure 5.1).

Thereby, in a STM, struts represents compression fields in concrete. The centerline of the strut is aligned with the orientation of the principal compressive stress. The idealized

shape of a strut in a plane (2D) member is assumed to be prismatic, bottle shaped or fan shaped (ACI 318-05). Struts can be strengthened by steel reinforcements, in which case they are termed as reinforced struts. Ties, typically represent reinforcing steel, though occasionally models have been proposed that include concrete ties, in which the orientation of the tie is aligned with the principal tensile stress. Forces are transferred between struts and ties at the nodes; thus, nodal regions represent multidirectional states of stress.

An important breakthrough in application of STM to discontinuity regions (D-regions) in structures was accomplished by Schlaich et al. (1987). Following Schlaich's lead, STM became a tool to examine the flow of stresses within a region of the structure where traditional Bernoulli-Euler beam theory is not valid and shear deformation are not negligible, thereby enabling simplified analysis for all regions of the structure. Since then, researches have taken a four-fold approach to advancing STM.

1. Development of empirically based recommendations for the effective strength of concrete struts and the effective strength of concrete in nodal regions. Concrete in these regions may crack under loading and thus would not be expected to develop full strength. Most of the research to date has considered monotonic loading and design for non-seismic loads. Prominent studies include Schlaich et al. (1987), Alshegeir (1992), Adebar and Zhou (1993), Yun and Ramirez (1996), Bergmeister et al. (1991), MacGregor (1997). The results obtained from these studies have been partly incorporated into ACI 318-05 Appendix A. Recently, ACI committee 445 began investigating the application of STM to seismic loading of structures. Here, it could be expected that further reduction of concrete strength as well as other prescriptive requirements might be necessary. Preliminary studies of this study (Lowes 1999, Sritharan et al. 2000, Sritharan and Ingham 2003, von Ramin and Matamoros 2006a, Alcocer and Uribe 2006) indicate that application of STM to seismic design of structural components requires lower effective concrete strength. Even though researchers have proposed different strength reduction values for different D-regions such as for bridge joints, deep beams, but, no research, till now, have been performed to check the validity of these recommended strength reduction factors for interior joints subjected to seismic

loading. The research work discussed in this chapter addresses this issue.

2. Including modeling of material response and the requirement of strain compatibility to ensure a unique analytical solution for design of structures (Hwang and Lee 1999; 2000; 2002, Yun 2000a).
3. Development of computer software for STM. CAST developed by Tjhin and Kuchma (2002) from University of Illinois at Urbana-Champagne and NL-STM developed by Yun (2000a) from Korea. CAST is a stand-alone software package for design that relies on the conventional approach of using equilibrium and yield criterion to determine the appropriate STM. The user provides a truss arrangement and the externally applied loads, and CAST produces the forces in each component of the truss. NL-STM is a software package that consists of three parts: 1) a non-linear finite element program PLANE that is used to solve 2d continuum mechanics problems, 2) a nonlinear finite element program TRUSS that takes stress from the PLANE analysis and uses them to develop a truss model of the structure and solves the truss, 3) a final component that enables the user to dimension struts, nodes and ties from the analysis results.
4. Application of topological optimization methods, in which various optimization approach such as maximum stiffness and minimum volume are used to develop the most feasible configuration for the loaded structure (Biondini et al. 2001). After the configuration was finalized finite-element methods or enhanced STM with strain compatibility and material constitutive relation were utilized to develop a unique solution for the problem.

The research presented here falls within the first category above, in that restrictions are sought for strut, tie and nodal strengths for seismic design of reinforced interior beam-column joints. Additional background information addressing this topic is presented in the following sub-sections.

5.2.2 Current code practice and state-of-art research to advance STM for monotonic loading of interior joints

Design using STM relies on specified capacities for struts, ties and nodes. These strengths are provided by the structural design codes (ACI 318-R05, AASHTO LRFD 1994, National

Table 5.1: ACI 318R05 specified values for effective compressive strength in the strut

Clause No.	Criterion	β Value
A.3.2.1	Prismatic strut of uniform cross-section area over it's length	0.85
A.3.2.2a	Bottle-shaped struts with reinforcement satisfying A.3.3	0.64
A.3.2.2b	Bottle-shaped struts of normal-weight concrete without reinforcement satisfying A.3.3	0.51

building Code of Canada 2005, EuroCode-2 1998). In this thesis ACI318-05 recommendations are evaluated. The effective compressive strength of the strut, f_{ce}, is related to the actual concrete compressive strength, f_c, through a strut strength reduction factor, β.

$$f_{ce} = \beta \cdot f_c \tag{5.1}$$

Table 5.1 specifies values for β as recommended in ACI318-05. It should be pointed out here that these specified factors in table 5.1 are developed for non-seismic applications.

While designing a structure, different types of D-regions (such as deep beams, corbels, squat shear walls, pile cap, beam-column joints) depending upon geometry and loading condition can be envisaged. In this thesis reinforced concrete beam-column joint regions are being investigated. It had been pointed out by Vollum and Newman (1999) that it is relatively straightforward to develop STM if the node dimensions can be related to the width of the supports and positions of reinforcement (e.g. deep beams); but that is not the case with beam-column joints. The complications that result in application of STM to model interior beam-column joints have been explored here:

- *Strut and nodal zone geometry*: Definition of the strut geometry is sometimes uncertain. ACI 318-05 recommends defining the strut width on the basis of the geometry of the structure. However, for interior joints, a wide range of diagonal strut widths meet geometric constraints. Similarly in an internal joint nodal zone, more than three members intersect and defining the dimensions of the node is difficult.

- *Strut and node capacity*: The ultimate strength of struts and nodal zones are determined by the shape and geometry of the strut and nodes, the level of confinement provided, stress field in the structure (such as tension perpendicular to the strut stress results in lower strength) and the cyclic demand history. Thus, the performance of one specific D-region will be different from that of another. The effective strength reduction factors provided in ACI 318-05 are applicable to all D-regions. Thus, research is required to determine if modification of these factors are required for these values to be appropriate for joints.
- *Bond stress of longitudinal reinforcements*: In real structure force transfer between the reinforcing steel and the concrete occurs gradually over a finite, but significant length of reinforcing steel. However in a STM, force transfer occur at the nodes over a very short length of the reinforcing bar. This implies high bond stress at the nodes. Appropriate limits on joint bond demands are necessary which requires further research.

A very few studies have addressed STM of interior reinforced concrete building joints; these include Kim and Mander (2000) and Hwang and Lee (2000). Both of these studies evaluated the recommendations of ACI-ASCE 352 using laboratory testing of joint subassemblages subjected to monotonic loading. The following sections provides a detailed review of these studies.

Kim and Mander (2000) model

Kim and Mander (2000) concluded that the post-elastic behavior of beam-column connections can be effectively modeled using a STM approach with a fan-shaped crack pattern. The theoretical framework proposed in their study was validated with an experimental test of a knee joint.

STM of a interior beam-column joint region by Kim and Mander (2000) was developed assuming that interior column bars do not contribute to the load transfer mechanism within the joint region. Thus, the model comprises one diagonal strut that spans the extreme corners of the joint in combination with other struts located between horizontal ties, and

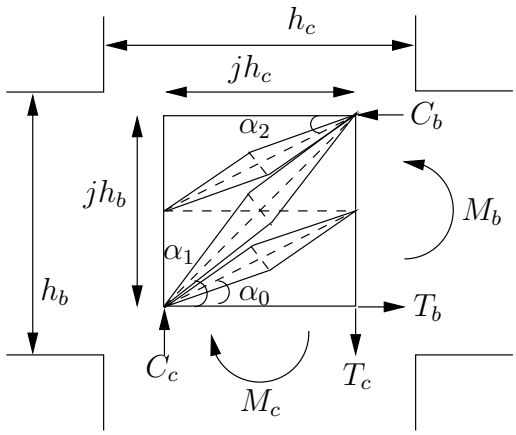

(a) with only one set of horizontal tie

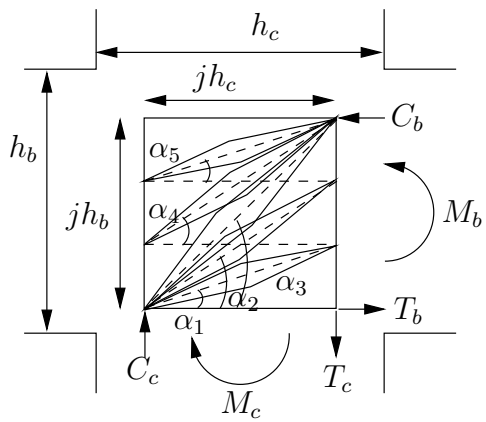

(b) with two sets of horizontal ties

Figure 5.2: Kim-Mander STM for interior beam-column joint

ties aligned with beam longitudinal steel and extreme layers of column steel. Struts are assumed shaped as rhomboids, with maximum widths located at the center line of the joint panel and minimum widths at the corner of the joint panel. The interior beam-column joint strut arrangement and area is shown in Figure 5.2.

The section area of the ith strut was obtained as

$$A_{cdi} = \frac{\cos\alpha_i}{2\,(1+n)\,(1+\cos^2\alpha_i)} d \cdot jh_b \tag{5.2}$$

where α_i is the angle measured from the axis of the ith. strut to the horizontal line, that is

$$\alpha_i = \tan^{-1}\left[\left(1 - \frac{i}{1+n}\right)\frac{jh_b}{jh_c}\right] \tag{5.3}$$

in which n is the number of layers of transverse steel in the joint, d is the out-of-plane thickness of the strut taken equal to the maximum out-of-plane width of the beams or columns, h_b and h_c are respectively the in-plane width of the beams and columns respectively, jh_b and jh_c are respectively, the distance between internal tension-compression couples in beams and columns at the perimeter of the joint, taken equal to the distance between the center layers of longitudinal steel. The term j in jh_b and jh_c is a constant factor between 0 and 1.

This modeling approach neglected the role of internal column longitudinal bars and is primarily based upon the assumption that only the transverse steel in the joint region contributes to the resistance against crack formation within the joint region by confining the strut. However, if interior column longitudinal column reinforcement does not yield under column flexural load then this reinforcement has additional capacity to carry load and may be included in the STM. This modeling approach also makes an assumption of considering the farthest longitudinal steel layers in case of specimen having two layers of steel, which is also not considered to be a good proposition. In this model, the area of the strut has also been determined empirically without any basis in order to satisfy code specified strength limits.

Hwang and Lee (2000) model

A softened STM was proposed by Hwang and Lee (2000) for determination of the shear strength capacity of interior beam-column joints for seismic resistance. The analytical model for the joint region is based on the concept of force transfer through struts and ties and satisfies equilibrium, compatibility and the constitutive laws of cracked reinforced concrete. In the Hwang-Lee model three different joint shear resisting mechanisms, the *Diagonal*, *Horizontal* and *Vertical* mechanisms contribute to joint shear strength. Figure 5.3 shows all the three mechanisms.

In Figure 5.3, h_{b_r} and h_{c_r} are the distances between the extreme longitudinal reinforce-

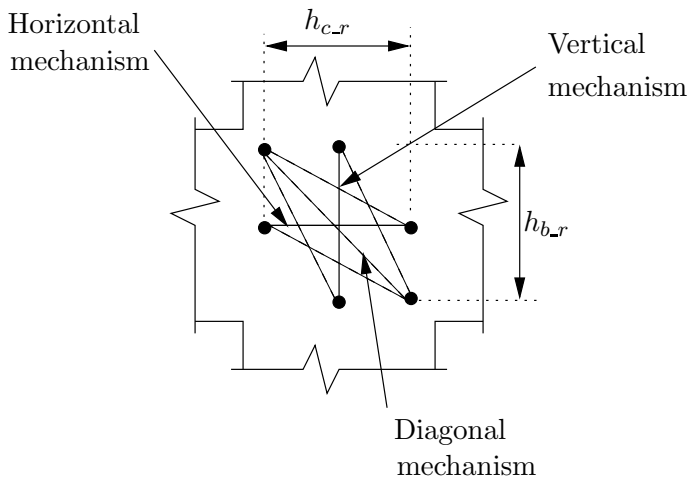

Figure 5.3: Hwang-Lee STM for interior beam-column joint

ment in the beams and columns, respectively. The effective area of the diagonal strut, A_{str}, is defined as

$$A_{str} = a_s \cdot b_s \tag{5.4}$$

where a_s is the depth of the diagonal strut and b_s is the width of the diagonal strut, which is considered as the effective width of the joint per ACI 318 (1995). The depth of the diagonal strut, a_s, was taken equal to the depth of the flexural compression zone of an elastic column per the recommendations of Zhang and Jirsa (1982), Paulay and Priestley (1992) and is represented as

$$a_s = \left(0.25 + 0.85\frac{N}{A_g f_c}\right) h_c \tag{5.5}$$

where N is the axial force acting on the column, f_c is the concrete compressive strength, A_g is the gross area of the column section, and h_c is the thickness of the column in the direction of loading. In this research, an empirical algorithm is proposed to determine the effective number of internal column longitudinal steel layers and transverse hoop steel layers that contribute to load transfer in the joint region, given the actual total number of transverse steel hoop layers and interior column longitudinal bars in the specimen . This empirical algorithm of determining the effective number lacks any proper physical or behavioral justification.

The primary intention of the previous two described research paper was to determine

an analytical model for the joint region. So, the research area of effective strength of struts and nodal stresses were not explored. ACI specified effective strength limits were used to define strut strengths.

5.3 Proposed STM for interior beam-column joints

To investigate the response of building joints to seismic loading and develop a methodology for the application of strut-and-tie modeling for seismic design of building joints, a series of STM were created for 75 representative joint specimen in the data set, described in chapter 2. These models included a single strut model, a distributed strut model, and a combined strut model. Each of these models are described in details in the sub sections that follow.

Each of the three types of STM were developed using the same basic assumptions:

- Load transfer occurs only at the nodes.
- Only equilibrium and component strengths (strut, tie and nodes) are considered in developing the STM.
- The problem is assumed to be two-dimensional in nature. The out-of-plane depth of the struts is taken equal to the maximum of the column and the beam out-of-plane depths.
- The STM is created using the axial load and maximum lateral load applied to the joint sub-assemblage in the laboratory.
- Node shapes are defined by the intersection of struts and ties of specified dimensions.
- Ties representing top or bottom beam longitudinal reinforcement are located at the centroid of the bars. The in-plane width of the ties is defined equal to the total width of bar layers, limited by the cover region to the bars.
- The strength of the ties representing beam and column longitudinal steel is limited by the ultimate strength of the reinforcing bars. The strength of the ties representing joint transverse steel is defined by the yield strength of the bars.

5.3.1 Single-Strut model

Paulay et al. (1978) proposed that bond strength is lost in a joint subjected to multiple

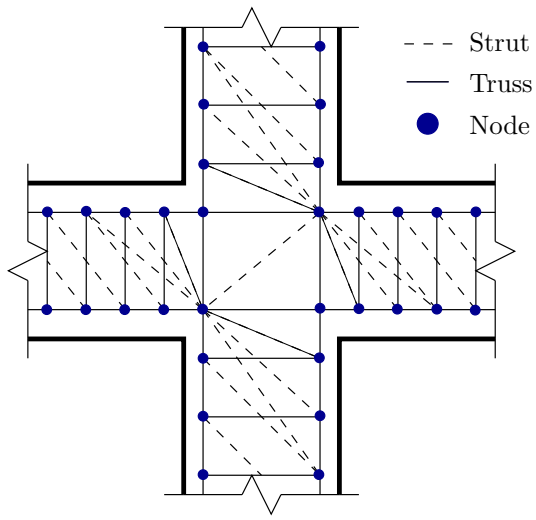

Figure 5.4: Single strut STM

earthquake load cycles and as a result, load is transferred within the joint primarily through a single concrete strut. The single-strut model developed as part of this study follows from this load-transfer mechanism, idealized by Paulay et al. (1978).

Figure 5.4 shows the single-strut model. In addition to the assumptions listed in section 5.3 to develop the single-strut model it was assumed that:

- Joint transverse steel were not modeled explicitly.
- Interior column longitudinal bars were not modeled explicitly.

Strut and node dimensions were defined by the depth of the flexural compression zones in beams and columns framing into the joint at nominal moment. For beams, the width of the compression zone was taken equal to the neutral axis depth at nominal moment. For columns, which were assumed to carry axial load, it was taken as the maximum of the neutral axis depth obtained from the section analysis and the depth obtained for the flexural compression zone for elastic column (Paulay and Priestley 1992) in Eq. 5.5, since column typically does not reach nominal moment prior to beams reaching the nominal moment. The strut width was determined from the width of the above defined compression zones in the beams and columns framing into the joint, as the square root of the summation of the square of these two widths.

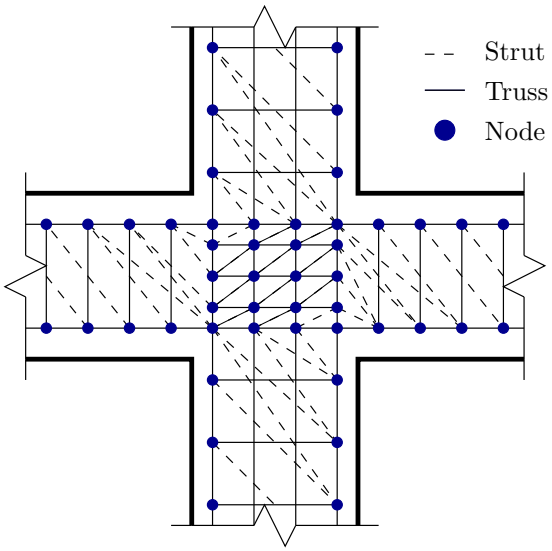

Figure 5.5: Distributed truss STM

5.3.2 Distributed-truss model

Paulay et al. (1978) proposed that prior to loss of bond strength within the joint region, force transfer occurs through distributed truss mechanism formed by the mesh of joint transverse steel and column longitudinal steel. The distributed truss model is shown in Figure 5.5. The capacity of this STM is defined by the yield strength of the joint transverse reinforcements, and was observed to be substantially less than the observed maximum strength of the sub-assemblage in the laboratory. This result is consistent with Paulay et al.'s proposition that the distributed truss mechanism represents joint load transfer at low load levels at which the bond stress within the joint is approximately uniform. Given the lower capacity of this STM, this modeling strategy was not pursued further in the study.

5.3.3 Combined strut-truss model

The combined strut-truss model (Figure 5.6) represents a combination of the two previous models. The stress in the joint transverse steel is at or below yield strength and stress in the beam longitudinal reinforcement bar is approximately equal to the ultimate strength.

For this STM, since most are located at the intersection of many struts and ties, current structural design codes (ACI 318-05, ACI-ASCE 352) do not provide adequate guidance for

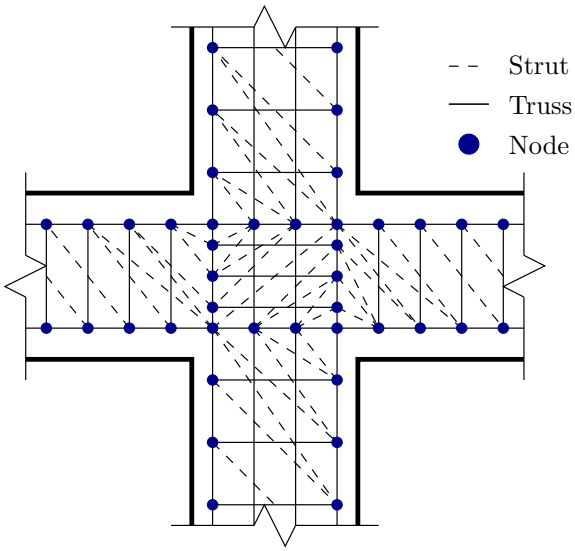

Figure 5.6: Combined strut-truss STM

determining strut dimension. Strut width is required to determine the strength demand on the concrete strut. However, with many struts in the joint perimeter region it is difficult to use geometric constraints to determine the strut width of joints. Thus, for the current study three approaches were used to determine strut width and concrete stress.

1. The width of the strut was defined equal to the total diagonal length of the joint (st_1 in Figure 5.7(a)). Total strut load was defined as the summation of all the compressive strut loads in the joint crossing the diagonal. This is an unconservative approach to assessing strut stress demands as the entire joint would not be activated in transferring loads. As expected, this approach results in very wide struts, small concrete stress demands and small strut strength reduction factors. This approach provides a lower bound on the strut strength reduction factor.

2. The strut width was determined by the spacing of the column longitudinal bars and the joint transverse steel (st_2 in Figure 5.7(b)). Total strut load was defined as the summation of the primary diagonal strut force and the average of the additional strut forces in the joint region. Since this approach depends on the relative spacing of the internal column longitudinal bars and the joint transverse steel, very small strut widths will be obtained if there are many interior column longitudinal bars

or joint transverse steel within the joint. Similarly, very wide strut widths will be obtained for sparse distributions of column longitudinal steel and/or joint transverse steel. The proposition of strut widths being dependent on the number of interior column longitudinal bars and/or joint transverse steel and not on the compressive load within the joint region is not appealing since it results in higher values of strut strength reduction factors, irrespective of the load in the joint, for specimen with a large number of interior column longitudinal steel.

3. Strut width was defined by the depth of the compressive zones in the beams and columns (st_3 in Figure 5.7(c)), as was done in the single strut model. The depth of the compression zone in the beams was taken equal to the depth of the neutral axis, obtained from section analysis at nominal flexural strength per ACI 318-05. For the columns, the depth of the compression zone was defined as the maximum of the depth obtained from the section analysis at nominal flexural strength and the depth obtained for the flexural compression zone for elastic column (Paulay and Priestley 1992), since column typically does not reach nominal moment prior to beams reaching the nominal moment. The strut width was determined from the depth of the above defined compression depths in the beams and columns framing into the joint, as the square root of the summation of the square of these two depths. The total strut force was defined equal to the summation of individual strut forces within the strut width region in the joint. This approach resulted in strut stresses which were average strut stress within the joint region.

Figure 5.7 represents the above different methods of determination of strut width within the joint region. Results obtained using these different methods for determination of strut width have been discussed in the following section.

5.4 Discussion of results obtained from proposed STM of interior joints

The single strut and combined strut-truss model described in the previous section were used to model seventy-five of the joint sub-assemblage specimen in the data-set presented in chapter 2. A typical STM for a single strut model and a combined strut-truss model is

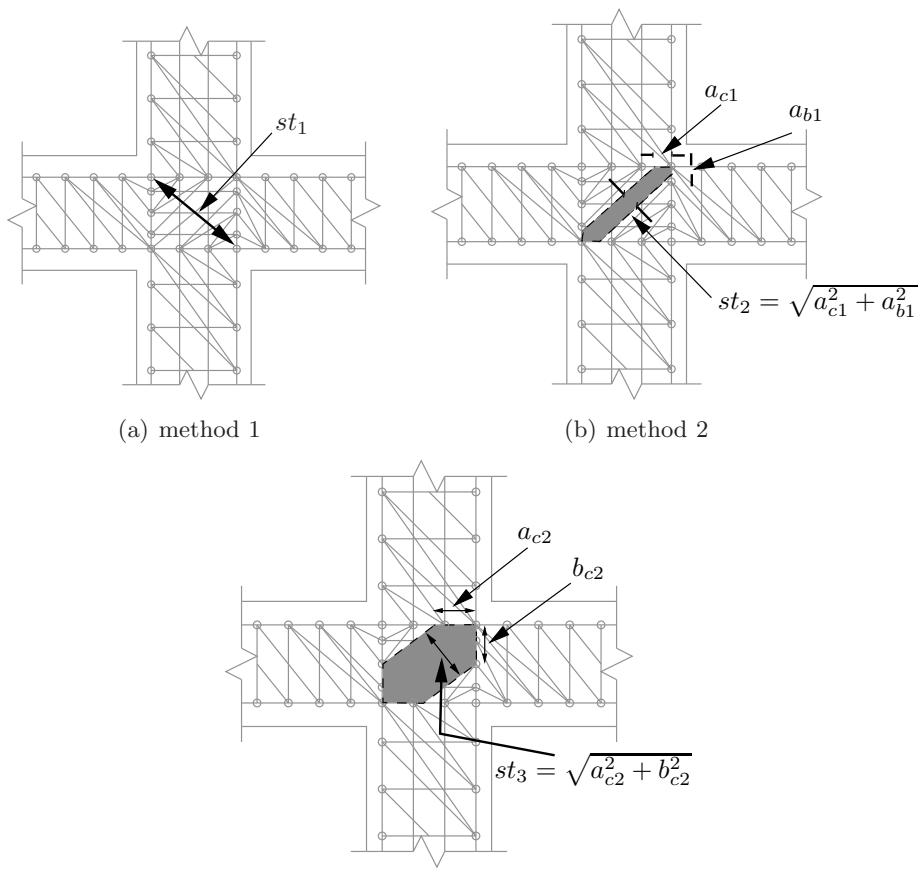

(a) method 1

(b) method 2

(c) method 3

Figure 5.7: Different methods for strut width determination in combined mechanism

shown in Figures 5.4 and 5.4 respectively. The zoomed figure of the joint region for each of the specimen with the combined strut-truss model is provided in Appendix E.

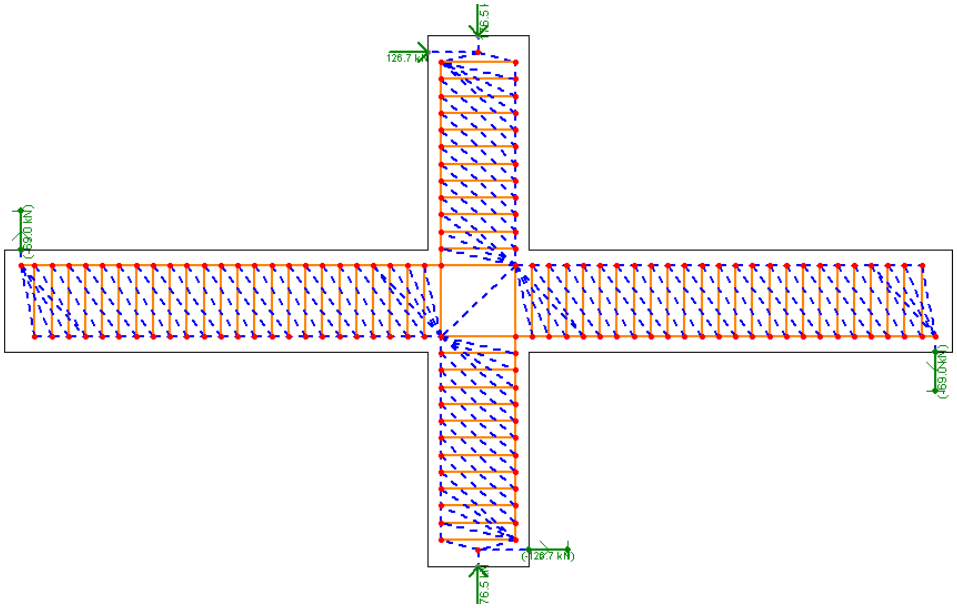

Figure 5.8: Typical single strut model for Specimen *EKOA_HC*

The seventy-five specimens chosen span the range of material and geometric parameters included in the data set. Simulation of each of these specimen were performed using the single strut and combined strut-truss model. Forces were determined in each of the struts and ties when the specimen is subjected to a combination of maximum lateral load and axial load. Results obtained from the study were used to evaluate the current ACI318-05 recommendations for strut and nodal capacities. New recommendations for strut and nodal stress for seismic design were developed using the results of the STM effort.

5.4.1 STM provision for struts and nodes in interior joint region

STM provisions for nodes and struts used in design and analysis of reinforced concrete structures depend on ACI318-05 recommended values for compressive strength of concrete. The efficiency factors recommended by ACI318-05 for struts are given in table 5.1. Several efficiency factors for nodal stresses are also provided in ACI318-05 Appendix A, based on the type of intersecting elements at the nodes.

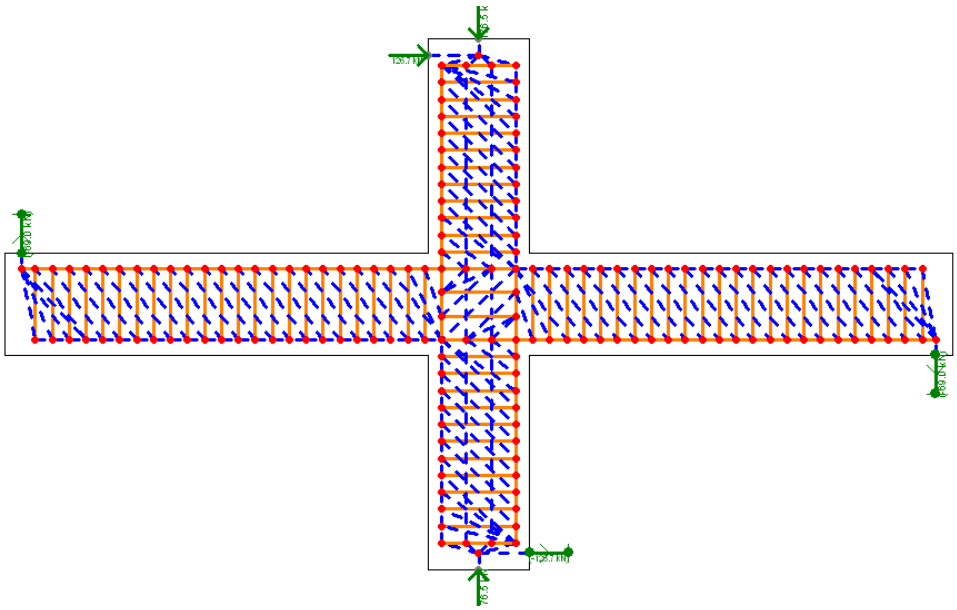

Figure 5.9: Typical combined strut-truss model for Specimen *EKOA_HC*

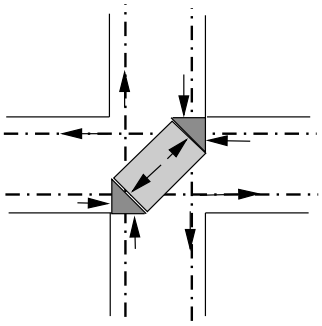

Figure 5.10: CCC node in interior beam-column joint

Node at an interior joint corner can be classified as a CCC node (see Figure 5.10) in which there are three compression members. ACI318-05 recommends an efficiency factor of 0.85 for CCC nodes. The total compressive force acting on the node is divided by the cross-sectional area of the inclined face of the node to obtain the nodal stresses. The in-plane width of the nodal region is the same as the strut width of the joint, and the out-of-plane depth of the joint is the maximum of the beam and column out-of-plane depths.

These reduction factor recommendations for struts and nodes in ACI318-05 are being investigated in this chapter as regards to their applicability for interior beam-column joints subjected to seismic loading.

Determination of strut strength reduction factor

Seventy-five specimen sub-assemblage (refer Chapter 2) spanning the entire range of design, geometric and material parameters in the entire data-set were analyzed using STM. Models were developed using both the single-strut and combined strut-truss methods (section 5.3.1 and 5.3.3 respectively) and the basic modeling procedures are discussed in section 5.3. Each of the specimen were modeled and example STM's are included in Appendix E. Using the results of these analyses, the maximum strut stress factor, β, and nodal bond stress factor were computed. The results are presented in the following paragraphs.

The compressive strength reduction factor for the main diagonal strut, β, was obtained for the case of single strut model with strut width obtained from the compression zone in the beams and columns at nominal yield strength. Figure 5.4 shows the typical model. Figure 5.11(a) shows the β factors for the diagonal strut in the single-strut mechanism. It also shows different recommended ACI318-05 limits, as given in table 5.1. Different symbols have been used to represent different failure mechanisms within the joint (see section 2.4). Since the strut strength reduction values were determined at maximum lateral load, thereby no distinctive difference in values of β could be obtained in between 'BY' and 'BYJF' specimens and thereby these two types of specimens have been marked by the same symbol. The plot shows that the recommended values by ACI318-05 are un-conservative and a value of 0.4 is being proposed for the compressive strength reduction factor in the main diagonal strut in the joint. ACI318-05 employs a β value of 0.85. A reduced value of β, as observed from our research, could be expected for joints subjected to repetitive loading, as is the case for seismic loading.

The combined strut-truss model was used to determine appropriate β values. As discussed in section 4.3.3 there are three possible approaches for defining strut stress for the confined strut model. All three approaches were considered and it was found that results of strut strength reduction factor obtained from the first approach, in which strut width is defined by the entire diagonal width, were very small. The other two approaches of consideration of the strut width (one based on geometry and other based on compression zone region) for determination of β have been investigated. The plots for the β factors obtained

from these two methods are shown in Figures 5.11(b) and 5.11(c) respectively. Plots in the figures use different symbols for joint failure mechanism (defined by Section 2.4) and also show ACI318-05 limits for strut strength. It was observed that the ACI318-05 recommended values were un-conservative.

As discussed before, ACI318-05 was originally developed for non-seismic applications, so obviously the values proposed for reduction of compressive strength in the strut region are un-conservative for seismic loading of structures. The values of strut strength reduction factors obtained from the basis of geometry (in which the spacing of interior column bars and the joint transverse steel were utilized to determine the strut width) are observed to result in values that sometimes exceed 1. This can be explained based on the amount and distribution of steel within the joint core. If there are many layers of transverse steel or many internal column longitudinal bars, this results in smaller strut widths and thus, higher values for β. This dependency of β on number and arrangement of steel within the joint core is undesirable, thus this method was not considered further in the study.

The case of combined STM with compression zones used for determination of the strut width represents a reliable method for determination of β factors. The results obtained in Figure 5.11(c) suggest a value of 0.4 for β which can be used as a conservative estimate for prevention of failure within the reinforced concrete beam-column joint region.

In Figure 5.11(c) no difference between β values for joints that fail in a brittle manner prior to beam yielding ('JF' specimen) and those that fail in a ductile manner following beam yielding ('BYJF' and 'BY' specimen) can be detected. To investigate the issue further, β values were plotted in Figure 5.12 which lists a reduced subset of specimen in Figure 5.11(c). The reduced data set in which it was possible to determine the extent of strength loss in the final load cycle was considered, since the entire load-deformation response could not be obtained for all the experimental investigations. Figure 5.12 shows β values with tests defined as 1)'JS' specimen for which the failure is initiated by joint shear but the strength loss at the last cycle is less than 20% of the maximum strength, 2)'JSF' specimen for which failure is initiated by joint shear and which exhibits a strength loss of more than 20% from the maximum strength 3)'BY' specimen for which the strength at the last cycle is more than 80% of the maximum strength, and 4)'BYJF' specimen for which there is more than

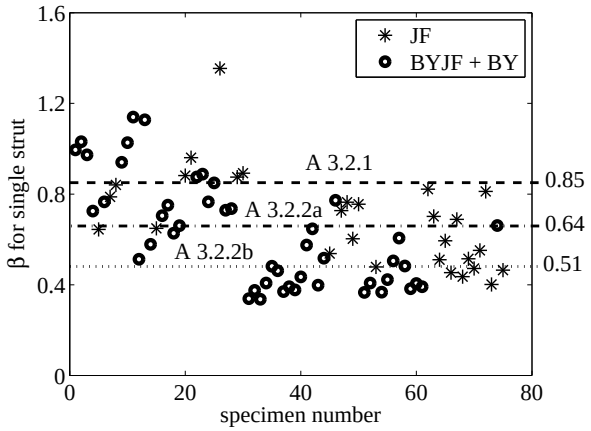

(a) Single strut mechanism

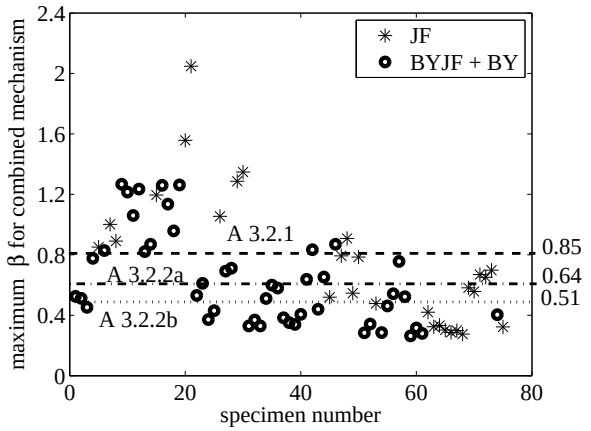

(b) Combined strut-truss mechanism (strut width defined by geometry)

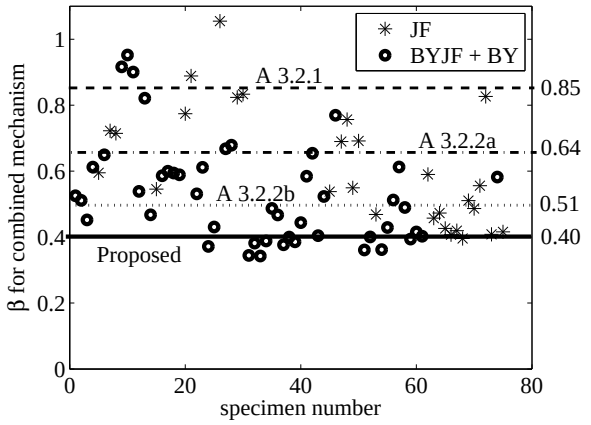

(c) Combined strut-truss mechanism (strut width based on compressive zone depth)

Figure 5.11: β factors for struts in joints

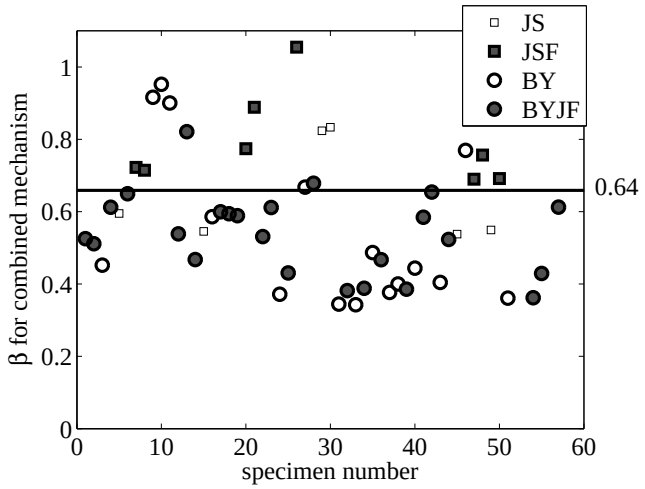

Figure 5.12: Combined strut-truss mechanism (strut width based on compressive zone depth)

20% reduction in strength in the last cycle from the maximum strength. Thereby, within this 4 sets of data the primary distinction would be between the specimen that exhibit failure i.e. 'JSF' (or those that exhibit brittle mechanism of failure) and 'BYJF' (those that exhibit ductile mechanism of failure). The reason why the 'JS' and 'BY' specimen were not experimentally loaded till failure is unknown. Figure 5.12 suggests a β factor of 0.64 for the main diagonal strut in the joint region below which brittle failure in the joint region will not be observed. This proposed limit below which brittle failure would not occur have been discussed in details later (section 5.4.2) in which specimen were evaluated with respect to drift capacity of the specimen.

Determination of nodal compressive stress reduction factor

ACI318-05 Appendix A limits nodal stress on the basis of type of forces acting on the nodal region. and ACI-ASCE 352 provides limits on nodal stress based on the type of forces acting on a nodal region. A nodal region is usually defined as the region where three different force directions meet. For the case of an interior joint, there are more than three forces acting on a region. However in the corner nodal region of an internal joint, it can be considered to be as a CCC node. The recommended reduction value for compressive stress in a CCC node as per ACI318-05 is 0.85. The nodal stresses are obtained for the simulated specimen in

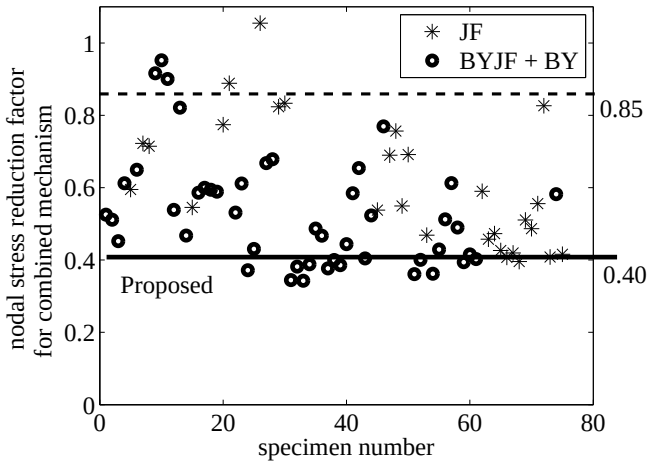

Figure 5.13: Nodal strut compressive strength reduction factor

the data-set and recommendations are provided for nodal stress values in an interior joint subjected to seismic loading.

Figure 5.10 shows the forces acting on the nodal region of an interior joint. As explained in section 5.4.1, the nodal stress obtained for a CCC node in an interior beam column joint is exactly identical to the strut stress values. Thereby a similar proposition of 0.40 can also be made for nodal compressive strength reduction factors in an interior beam column joint subjected to seismic loading. Figure 5.13 represents ACI318-05 recommended and the proposed value. No distinction could be obtained between specimen with different type of failure mechanism. The lower value of nodal stress reduction factor is justifiable since the specimen are subjected to seismic loading and ACI318-05 only provides recommendations for non-seismic application.

Determination of bond stress of longitudinal reinforcement bars

The combined STM approach for interior joint was used to determine the bond stress of longitudinal reinforcement bars. The difference of tensile forces in the reinforcement bars at the nodes constitute the total bond force. The total tensile force is divided by the total circumferential area of the bar and the development length in order to obtain the bond stress. Development length of the bars was considered to be the spacing between the

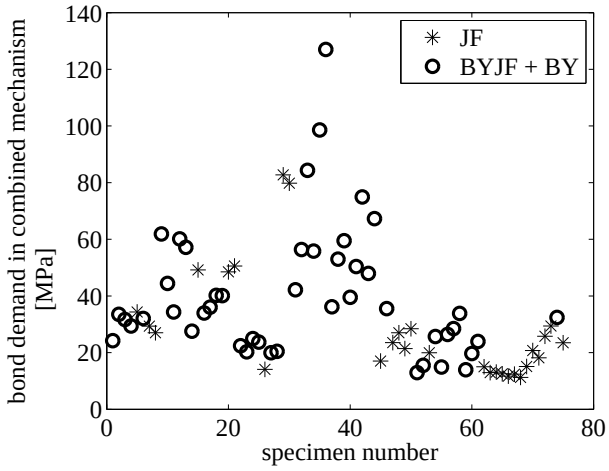

Figure 5.14: Bond demand in an interior joint

internal column longitudinal bars. The bond stress was normalized with the square root of the compressive strength of concrete. Figure 5.14 shows the normalized bond stress of the simulated specimen. No distinction could be observed between specimen with different type of failure mechanism.

5.4.2 Development of STM provisions for seismic design of joints

Current ACI318-05 Appendix A guidelines for application of STM are intended for non-seismic applications and are superseded by Chapter 21 of the ACI Building Code (ACI318 2005). To extend STM for seismic design it is necessary to ensure that components have adequate strength and can maintain the deformation required to develop this strength under multiple load cycles. One approach to ensure this is to define strut and node strengths on the basis of deflection demands (Sritharan et al. 2000, von Ramin and Matamoros 2006b). In the current study, this approach was explored to establish a relation between the measured demand parameters, such as maximum strut stress, β, and bond stress, and measured performance capacity measures, such as drift capacity and strength loss at last cycle.

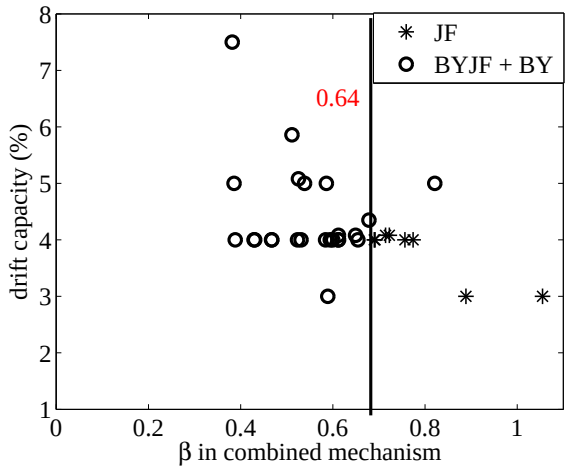

Figure 5.15: Combined strut-truss STM β with drift capacity

Investigation of the impact of demand on drift capacity

Drift capacity is defined as the maximum inter-story drift experienced by joint sub-assemblies in cycles prior to which an increase in drift demand results in more than 20% reduction in strength from the maximum. If a specimen did not exhibit loss of more than 20%, even in the last cycle of experimental loading, it was not included in this phase of study. Specimen that exhibit "brittle" response could be expected to have lower drift capacity than those that exhibit "ductile" response. Combined strut-truss mechanism was considered for this investigation. The strut width is obtained from compressive zone depth of the adjacent beam and column sections at nominal yield strength. The relationship between the demand parameters, strut stress reduction factor and bond stress normalized with square root of compressive strength of concrete, is being investigated here with the performance measure of drift capacity, in the following paragraphs.

Figure 5.15 shows the relationship between the drift capacity and strut strength reduction factors (β). A reduced data set was considered since only those specimen samples were considered which experienced more than 20% reduction in strength from the maximum. It was observed, as expected, that specimen with a ductile mechanism (BYJF+BY) exhibited a higher drift capacity in comparison to the ones exhibiting a brittle mechanism (JF) of failure. It was also observed that specimen exhibiting JF had a higher value of β in compar-

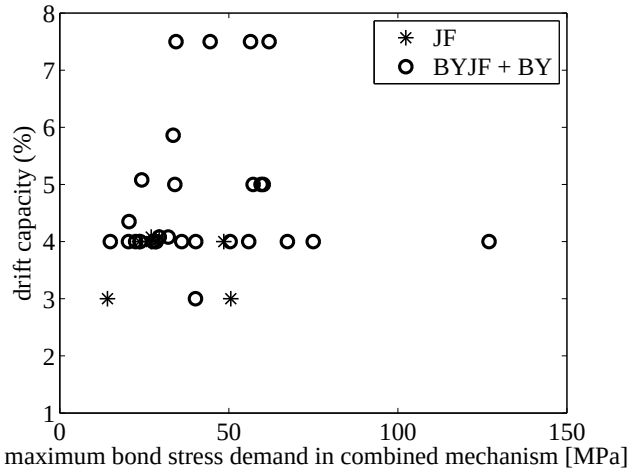

Figure 5.16: Nodal bond stress with drift capacity

ison to the ones which exhibited BYJF or BY. A limit value on β of 0.64 is being proposed which precludes JF specimen (or brittle mechanism of failure) and ensures drift capacity greater than 4% with only one exception.

Nodal bond stress represent another demand parameter for interior beam column joint sub-assemblage subjected to seismic loading. Calculation of nodal bond stress has been presented in the previous subsection. The strut-truss combined mechanism was used to investigate the relationship between nodal bond stress and drift capacity. Figure 5.16 presents the relationship between nodal bond stress and drift capacity. These data indicate that bond stress does not determine joint failure mechanism.

Investigation of the impact of demand on strength loss in last drift cycle

The severity of strength loss in the final drift cycle can be considered a performance measure. Figure 5.17 show strength loss, as a % of maximum strength for the last load cycle versus strut stress demand, β. The data in Figure 5.17 shows an increased value of β for specimens in which joint failure precedes beam yielding. Since failure in a specimen is defined as reduction in strength of more than 20% from the maximum, a dotted line in Figure 5.17 shows the region above the 20% strength reduction. The Figure also shows the proposed line of 0.64 which separates the ductile mode of failure to the brittle mode of failure.

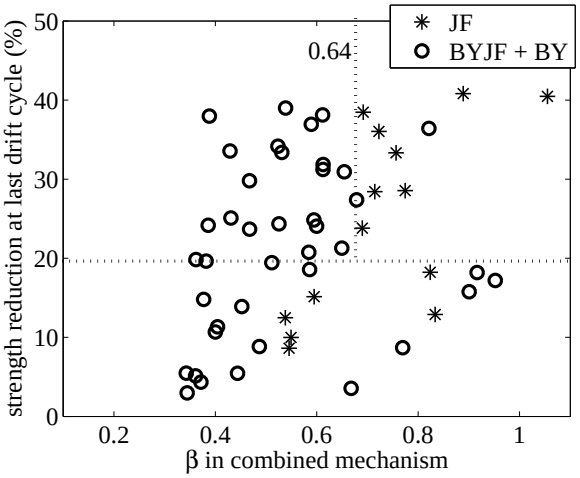

Figure 5.17: Combined strut-truss STM β with strength reduction at last drift cycle

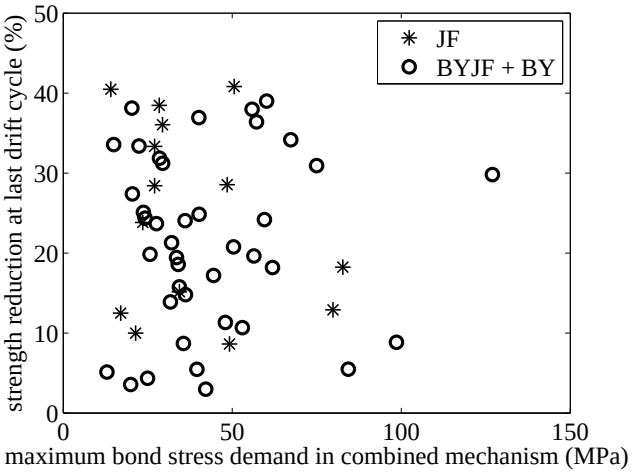

Figure 5.18: Bond demand at nodes with strength reduction at last drift cycle

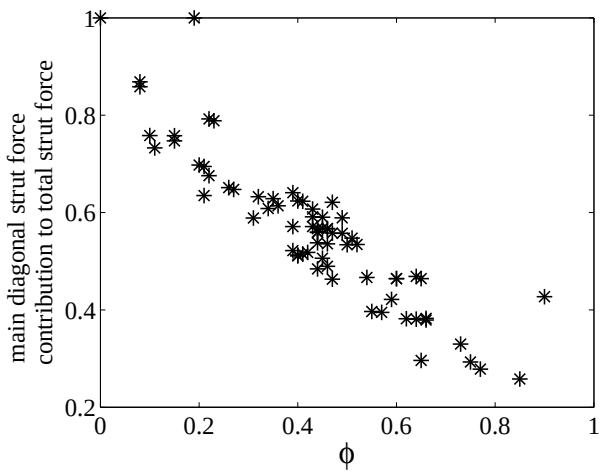

Figure 5.19: Main diagonal strut force contribution with ϕ

Figure 5.18 show strength loss, as a % of maximum strength for the last load cycle versus strut stress demand, β. No relation between strength reduction in the last drift cycle and bond demand at the nodes can be observed.

5.4.3 Behavioral mechanisms observed in the combined STM for joint

The combined strut-truss mechanism comprises a single strut and number of distributed truss. When cracking originates in a specimen, it is hypothesized that it follows the distributed strut mechanism, since a distributed truss mechanism is only viable when the stresses in the joint transverse steel is below yield stress. Later as the column lateral load reaches its maximum, it either follows a single strut mechanism or a combined strut-truss mechanism. So, at maximum strength and in the post peak region, it exhibits either a single strut or a combined strut-truss mechanism whereas in the pre-peak region it exhibits a distributed truss mechanism. A similar observation was also made by Paulay et al. (1978) for interior beam column joints in which the authors proposed that there are two possible mechanisms of transfer of load within the joint: single-strut mechanism or the distributed truss mechanism and there are possible interactions in between these two mechanisms.

The data in Figure 5.19 show that with increase in ϕ (transverse steel strength expressed as a ratio of the total shear force in the joint) the contribution of the main diagonal strut

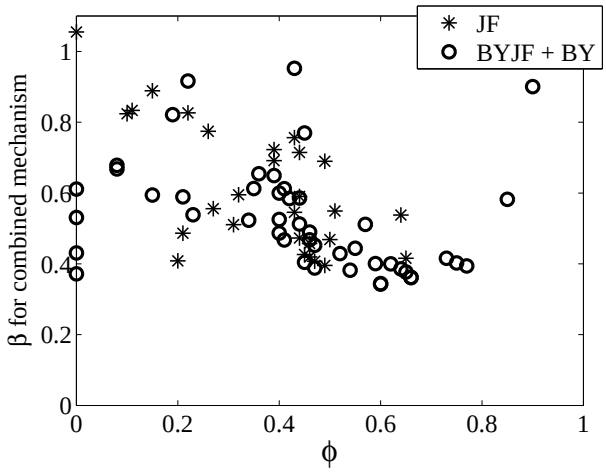

(a) β versus ϕ

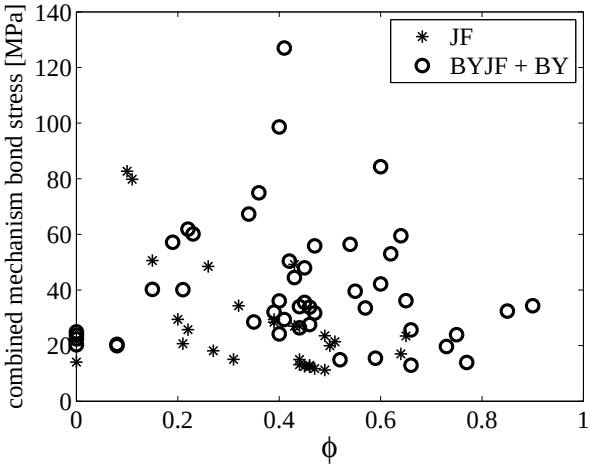

(b) bond demand versus ϕ

Figure 5.20: Relationship of ϕ with β and bond demand

to the total strut force decreases. This suggests that at lower values of ϕ the main diagonal strut force contribution is more significant and the single strut mechanism dominates the response. Whereas, for larger ϕ values, the combined strut-truss mechanism contributes more significantly to joint load transfer at post-peak load levels.

Figure 5.20(a) shows the relation between strut strength reduction factor, β to ratio of joint transverse steel strength to total shear demand, ϕ. Figure 5.20(b) shows the relation between bond stress to ratio of joint transverse steel strength to total shear demand, ϕ. No relation could be observed between theses demand and performance measures.

5.5 Summary

Strut-and-tie models were developed for 75 joints from the data set which spanned the wide range of material and geometric parameters for reinforced-concrete interior beam-column joints. The STM followed ACI318-05 Appendix A recommendations and specifications with the exception that the strut strength reduction factors were not restricted. Three models, namely single-strut, distributed-truss and combined strut-truss, were considered for the analysis. Ultimately, the combined strut-truss model was employed for further evaluation. In the combined strut-truss model, three different propositions were made for determining the strut widths of the main diagonal compression strut in the joint, which are 1) the total diagonal length of the joint, 2) based on spacing of interior column longitudinal bars and stirrups, and 3) based on width of compressive region of beams and columns at nominal moment. Ultimately the third approach was considered the best approach and was employed to further evaluate strut-stress values, nodal stress values and nodal bond stress values. These strut-stress values, nodal stress and bond stress values were evaluated against ACI318-05 recommendations and relationships were investigated between the above joint demand parameters with several joint performance measures such as drift capacity and strength loss at the last cycle to determine appropriate recommendations in application of STM to performance based design of interior joints.

5.6 Conclusion

Several conclusions were obtained from the above research:

- A strut strength reduction factor of 0.40 is proposed to ensure joints do not exhibit significant strength loss under seismic loading.
- A strut strength reduction factor of 0.64 is proposed to ensure that joints have sufficient strength to develop the yield strength of beams.
- As transverse steel increases the diagonal strut contribution in the combined mechanism decreases.
- Lower strut stress demand results in higher drift capacity.
- No relation could be obtained in between strut strength reduction factor with strength loss at last cycle.
- No relation could be obtained between bond strength with response mechanism, drift capacity and strength loss at last cycle.

Chapter 6

CONCLUSION AND FUTURE RECOMMENDATIONS FOR RESEARCH

6.1 Summary of research activities

This thesis documents a study of the behavior and modeling of reinforced-concrete beam-column joints under seismic loading. Four different types of models of varying complexity were developed, calibrated and evaluated using an experimental data set comprising joints with wide range of geometric, material and design parameters. The experimental data set and each of the model development efforts are summarized in the following paragraphs.

A data set was assembled comprising of 110 previous experimental investigations of reinforced beam-column joint sub-assemblages. The data set includes only two-dimensional interior building joint sub-assemblages without slabs, beam eccentricity, or out-of-plane beams for which response is determined by beam flexural yielding and/or joint failure. The data set include joints with a wide range of design parameters, but does not include joints with plain round (smooth) reinforcing steel bars. The data set includes only sub-assemblages subjected to quasi-static cyclic loading in the laboratory for which there is enough data recorded for the purpose of modeling and comparison with the simulated observations. A qualitative evaluation of the data set was performed to determine critical design parameters. In the data set, a brittle response is associated with joint failure prior to beam yielding whereas a ductile mechanism is associated with beam yielding prior to joint failure.

Using the data set, a probabilistic failure-initiation model was developed to determine the type of failure mechanism (brittle versus ductile) that could be expected for a joint with a specific set of design parameters. A result of this modeling effort was to develop a simplistic model that can be used to predict failure with an uncertainty of 10%. Another result of this modeling effort is quantification of the relative importance of different design

parameters in determining whether a joint will exhibit brittle or ductile response.

To provide further understanding of interaction of different inelastic mechanisms within the joint region, a two-dimensional continuum finite element modeling of joints was explored using DIANA 9.1. The joint model comprised of standard four-node quadrilateral elements to represent concrete, two-node bar elements to represent reinforcing steel, and interface bond elements placed between reinforcing bar and concrete. Drucker-Prager plasticity with a linear tension cutoff, a specified hardening/softening envelope, and tension-softening envelope was used to represent concrete behavior. Reinforcing steel was modeled using J2 plasticity with isotropic hardening. The one-dimensional slip model proposed by Eligehausen et al. (1983) was used for the bond model. To improve understanding of the software, constitutive models and simulation of reinforced concrete behavior, a series of benchmark analyses of relatively simple plain and reinforced concrete components were performed initially. Good correlation could be observed between the simulated and the experimental results. To improve understanding of the joint behavior, a series of analyses of two joint: 1) OSJ10 exhibiting 'JF' mechanism and 2) OSJ5 exhibiting 'BYJF' mechanism were done with different constitutive models for concrete and bond to capture the inelastic mechanisms of cracking, crushing of concrete and bond-slip behavior of the reinforcing steel. The modeling effort provided only limited improvement in understanding of joint behavior at a very high computational cost.

Performance-based design requires accurate prediction of component load and deformation demands. With the objective of developing a computationally robust strategy for predicting the load-deformation response of joints, a component-based super-element model for joint was developed. The joint super-element is a four-node, twelve degree-of-freedom element that can be used in 2D frame analysis of structures. The joint element comprises of a shear-panel component that simulates strength and stiffness loss due to failure of the joint core, eight bar-slip springs that simulate stiffness and strength loss due to anchorage-zone damage, and four interface-shear springs that simulate reduced capacity for shear transfer at the joint perimeter due to crack opening. The joint represents two primary failure mechanisms: shear failure of the joint core and anchorage failure of the reinforcing steel. This joint element was build on the previous work by Lowes and Altoontash (2003) and uses the

experimental data set to revise the previous element formulation and calibration methods. The new joint element includes 1) a revised element formulation that provides accurate prediction of joint load mechanisms, 2) a new, more accurate, model for simulating joint shear response that is appropriate for use with a wide range of joint designs and simulates strength loss due to anchorage zone damage within the joint, and 3) an improved method for simulating anchorage response of beam and column reinforcing steel that does not impede nonlinear solution algorithms and is not overly conservative in predicting failure. This modeling effort provided an efficient computationally robust analytical tool for modeling of 2D reinforced beam column joints in frame structures subjected to seismic loading.

To enable the PBSD of joints recommendations for a strut-and-tie modeling of the joints were developed. A strut-and-tie model represents the flow of forces through a joint and provides a basis for designing the components, including the reinforcing steel to carry these forces. Here the recommendations of ACI 318-05 were evaluated for application to seismic design of joints. For most of the joints in the data set, a simple and refined strut-and-tie model was developed at the maximum lateral load. Strut, tie and nodal bond stress demands were determined and the relationship between demands and performance measures (e.g. drift capacity, strength loss at final load cycle) were evaluated. Ultimately modifications to ACI 318-05 design codes were developed for PBSD of joints.

6.2 Conclusions about the behavior and modeling of joints

The research presented here supports a number of conclusions about the seismic behavior and modeling of reinforced-concrete beam-column joints. The following conclusions enable the advancement of PBSD of joints.

- The probabilistic modeling strategy provides a first-hand estimate of the factors responsible for failure initiation within the joint region and also identifies the relative importance of the factors in determination of the failure initiation mechanism in the joint region.
- The state-of-art commercial continuum finite element packages (e.g. DIANA 9.1) even though could be utilized to study individual inelastic mechanisms, but cannot be used

for study of complex interaction of different inelastic mechanisms due to very high computational overhead (with regards to both complexity and time) and absence of stable, robust numerical algorithms for capturing different failure mechanisms simultaneously.

- A joint super-element component based model, which was developed and calibrated as part of the study, provides a good correlation between simulated and observed load-deformation response of reinforced-concrete beam-column joints and thus can be utilized as a computationally efficient and robust model in 2D analysis of frame structures subjected to seismic loading.
- New recommendations were developed for PBSD of joints utilizing strut-and-tie modeling strategy, since the recommendations by ACI 318-05 design codes were found to be inadequate.

6.3 Comparison of different modeling strategies and their application

The research presented here focussed on four methods of varying complexity for modeling joints under seismic loading. All of these models have a place in PBSD and comparison of these models provides additional insight into joint behavior and design.

The probabilistic model is simple to use and provides a measure of the likelihood a joint will exhibit a specific failure mode. As such, it is an ideal tool for a quick evaluation of the performance of an existing structure or even a newly designed system. However, it provides no insight into load-deformation response of the specimen subjected to cyclic loading. Continuum finite element analysis provides a detailed understanding of the mechanism that controls response. However this cannot be done using the state-of-art commercial software available today. Additionally it seems likely that the computational demands and time required for model creation and evaluation of results will make this type of modeling more appropriate for research than for use by a practicing engineer. For application in the design office as well as in research, the strut-and-tie model for design and component-based super-element model for prediction of load-deformation response of the specimen are better choices. The strut-and-tie model requires the introduction of a number of assumptions and provides a crude representation of joint response. As such it has the potential for significant

inaccuracy and requires introduction of a high level of conservatism for application in design. While the strut-and-tie model provides sufficient information for design, it cannot be used to generate the load-deformation response history required for PBSD of an entire structure. Here, the component-based joint super-element is required. This model uses fewer assumptions about behavior and can be used to determine the mechanism by which a joint loses strength and stiffness. Additionally the results of this study suggest that the model provides relatively accurate prediction of response as well as enables efficient simulation of 2D frame response.

Of the models developed and calibrated as part of the study, the joint super-element appears to most significantly advance the PBSD of joints, while the probabilistic model appears to provide the greatest amount of information (about the influence of joint demand parameters on the joint response) for the smallest investment of modeling time. From the perspective of design by engineers, the strut-and-tie method provides important conservative recommendations about joint demands and establishes relationship between demand and performance measures for joints.

6.4 Recommendations for future research

Several recommendations can be made based on the work done in this thesis.

The binomial probabilistic model (discrete choice logit model) can be extended to a multinomial discrete choice model in which the dependent variables would be the different failure mechanisms (such as 1) only beam yielding at 4% drift, 2) beam yielding followed by failure at 4% drift, 3) joint failure prior to beam yielding) instead of just failure initiation mechanisms. Moreover within the framework of probabilistic approach a drift capacity model or a maximum strength reduction model can be developed for different failure mechanisms within the joint region.

The research on continuum finite element methods for joints have not been pursued further in the thesis due to huge amount of computational overhead associated with the commercial software DIANA 9.1. Introduction of better numerical algorithms, constitutive models, and elements might pave the way for a better understanding of the interaction of different inelastic mechanisms within the joints. The coupling action between the damage

due to bar-slip and shear response within the joint calls for further research with more improved concrete constitutive models and numerically stable algorithms.

Improvements can be made in the calibration of the components in the super-element model such that it is applicable to a wider range of data sets including exterior, knee and T-shaped joints. A three dimensional joint formulation needs to be developed that can not only consider all these cases but also considers the case of eccentric joints and joints with slabs or transverse beams attached to it, since it has been observed experimentally that the slabs or transverse beams significantly affects the behavior of the joint regions.

Topological optimization of struts and ties within the joint region would pave the way for a better understanding of the transfer of forces within the joint region with a wide variety of material and geometry variations. The resultant truss model obtained from the topological optimization could then be analyzed within the framework of nonlinear finite element analysis of trusses to obtain a clear load-deformation response analysis of joints. Currently, in this research it has been assumed that the force transfer within the joint region is a mechanism between the diagonal strut method and the distributed truss method, based on experimental investigation and research. Topological optimization might lead to some entirely new picture of force transfer within the joint region.

The modeling hierarchy presented in here for reinforced concrete beam-column joints could be utilized to study other different components of a reinforced concrete structure subjected to seismic loading such as coupling beams, shear walls etc. Usually most of the research on a structural component is primarily related to experimental investigations and/or some analytical methodology. But, extensive validation of an analytical methodology utilizing the work of other researchers is usually very rare. Developing a data-set for other structural components and performing an extended study of the behavior of that component will pave the way for better design standards for performance based design of structures.

BIBLIOGRAPHY

ACI Committee 318. Building code requirements for structural concrete (ACI 318-05) and commentary (ACI 318-R05). Technical report, American Concrete Institute, Farmington Hills, MI, 2005.

ACI-ASCE Joint Committee 352. Recommendations for design of beam-column connections in monolithic reinforced concrete structures (ACI 352-R02). Technical report, American Concrete Institute, Farmington Hills, MI, 2002.

T. M. Abu-Lebdeh and G. Z. Voyiadjis. Plasticity damage model for concrete under cyclic multiaxial loading. *Journal of the Engineering Mechanics, ASCE*, 119(7):1465–1484, 1993.

P. Adebar and Z. Zhou. Bearing strengths of compressive struts confined by plain concrete. *ACI Structural Journal*, 90(5):534–541, 1993.

S. Alath and S. K. Kunnath. Modeling inelastic shear deformation in RC beam-column joints. In *Tenth Conference on Engineering Mechanics*, pages 822–825, University of Colorado, Boulder, 1995.

S. M. Alcocer and C. M. Uribe. Application of strut-and-tie modeling to seismic design of deep beams. *ACI SP 236*, 2006.

D. A. Alire. Seismic evaluation of existing unconfined reinforced concrete beam-column joints. Master's thesis, Department of Civil Engineering, University of Washington, Seattle, 2002.

A. Alshegeir. *Analysis and design of disturbed regions with strut-tie models*. PhD thesis, School of Civil Engineering, Purdue University, West Lafayette, Indiana, 1992.

A. Altoontash. *Simulation and damage models for performance assessment of reinforced concrete beam-column joints*. PhD thesis, Department of Civil Engineering, Stanford University, CA, 2004.

A. Altoontash and G. D. Deierlein. A versatile model for beam-column joints. In *ASCE Structures Congress, Seattle, WA*, 2003.

J. Anderson and W. H. Townsend. Models for RC frames with degrading stiffness. *Journal of the Structural Division, ASCE*, 103(ST12):2361–2376, 1977.

S. P. Anderson, A. de Palma, and J. F. Thisse. *Discrete choice theory of product differentiation*. MIT Press, Cambridge, Massachusetts, London, England, 1992.

F. Armero. Localized anisotropic damage of brittle materials. In D. R. J. Owen, E. Oñate, and E. Hinton, editors, *Computational plasticity: Fundamentals and application, Proc.*

COMPLAS V,, pages 635–640. International Center for Numerical Methods in Engineering, Barcelona, 1997.

F. Armero and K. Garikipati. Recent advances in the analysis and numerical simulation of strain localization in inelastic solids. In D. R. J. Owen and E. Oñate, editors, *Computational plasticity: Fundamentals and application, Proc. COMPLAS IV,*, pages 547–561. International Center for Numerical Methods in Engineering, Barcelona, 1995.

O. M. Atrach. Behavior of interior and exterior beam-column joints under earthquake conditions. Master's thesis, Department of Civil Engineering, University of Toronto, Ontario, 1992.

S. A. Attaalla and M. S. Agbabian. Performance of interior beam-column joints cast from high strength concrete under seismic loads. *Advances in structural engineering*, 7(2): 147–157, 2004.

J. P. Bardet. Lode dependencies for isotropic pressure-sensitive elastoplastic material. *Journal of Applied Mechanics*, 57:498–506, 1990.

S. B. Batdorf and B. Budianski. A mathematical theory of plasticity based on concept of slip. Technical Report 1871, National Advisory Committee for Aeronautics, Washington, D. C., 1949.

Z. P. Bažant. Comment on orthotropic materials for concrete and geomaterials. *Journal of Engineering Mechanics, ASCE*, 109(3):849–865, 1983.

Z. P. Bažant. Size effect in blunt fracture: Concrete, rock, metal. *Journal of Engineering Mechanics, ASCE*, 110:518–535, 1984.

Z. P. Bažant and F. C. Caner. Microplane model m5 with kinematic and static constraints for concrete fracture and anelasticity i: Theory. *Journal of Engineering Mechanics, ASCE*, 131(1):30–41, 2005.

Z. P. Bažant and T. P. Chang. Instability of nonlocal continuum and strain averaging. *Journal of Engineering Mechanics, ASCE*, 103(11):1119–1149, 1984.

Z. P. Bažant and M. Jirásek. Nonlocal integral formulation of plasticity and damage: survey of progress. *Journal of Engineering Mechanics*, 110(10):1441–1450, 2002.

Z. P. Bažant and B. H. Oh. Crack band theory for fracture of concrete. *Material Construction (RILEM)*, 16:155–177, 1983.

Z. P. Bažant and B. H. Oh. Microplane model for progressive fracture of concrete and rocks. *Journal of Engineering Mechanics, ASCE*, 111(4):559–582, 1985.

Z. P. Bažant and J. Ožbolt. Nonlocal microplane model for fracture, damage and size effects in structures. *Journal of Engineering Mechanics, ASCE*, 116(11):2485–2505, 1990.

Z. P. Bažant and P. A. Pfeiffer. Determination of fracture energy from size effect and brittleness number. *ACI Materials*, 86(6):463–480, 1987.

Z. P. Bažant and J. Planas. *Fracture and size effect in concrete and other quasi-brittle materials*. CRC Press, LLC, Boca Raton, FL, 1998.

Z. P. Bažant and P. C. Prat. Microplane model for brittle plastic material i: Theory. *Journal of Engineering Mechanics, ASCE*, 114(10):1672–1688, 1988.

Z. P. Bažant, Y. Xiang, and P. C. Prat. Microplane model for concrete i: Stress-strain boundaries and finite strain. *Journal of Engineering Mechanics, ASCE*, 122(3):245–254, 1996.

Z. P. Bažant, F. C. Caner, I. Carol, M. D. Adley, and S. A. Akers. Microplane model m4 for concrete i: Formulation with work conjugate deviatoric stress. *Journal of Engineering Mechanics, ASCE*, 126(9):944–953, 2000.

C. W. Beckingsale. *Post elastic behavior of reinforced concrete beam-column joints*. PhD thesis, Department of Civil Engineering, University of Canterbury, Christchurch, New Zealand, 1980.

A. Belarbi and T. C. Hsu. Constitutive laws of softened concrete in biaxial tension-compression. *ACI Structural Journal*, pages 562–573, 1995.

T. Belytschko, J. Fish, and B. E. Engelmann. A finite element with embedded localization zones. *Computational methods in applied mechanics and engineering*, 70:59–89, 1988.

T. Belytschko, Y. Y. Lu, and L. Gu. Element free galerkin methods. *International Journal for Numerical Methods in Engineering*, 37:229–256, 1994.

M. Ben-Akiva and S. R. Lerman. *Discrete choice analysis: theory and application to predict travel demand*. MIT Press, Cambridge, MA, 1985.

K. Bergmeister, J. E. Breen, and J. O. Jirsa. Dimensioning of nodes and development of reinforcement. In C. Meyer and H. Okamura, editors, *IABSE Colloquium, Structural Concrete, Stuttgart, Germany*, pages 551–564, 1991.

D. Besdo. Ein beitrag zur nichtlinearen theorie des cosserat kontinuums. *Acta Mechanica*, 20:105–131, 1974.

A. Biddah and A. Ghobarah. Modeling of shear deformation and bond slip in reinforced concrete joints. *Structural Engineering and Mechanics*, 7(4):413–432, 1999.

F. Biondini, F. Bontempi, and P. G. Malerba. Stress path adapting strut-and-tie models in cracked and uncracked RC elements. *Structural Engineering and Mechanics*, 12(6): 685–698, 2001.

G. R. Birss. The elastic behavior of earthquake resistant reinforced concrete interior beam-column joints. Technical Report Research report 78-13, Department of Civil Engineering, University of Canterbury, New-Zealand, 1978.

J. Blaauwendraad. Realizations and restrictions - application of numerical models to concrete structures. In C. Meyer and H. Okamura, editors, *Finite Element Analysis of Reinforced Concrete Structures, Proceedings US-Japan Seminar ASCE*, pages 557–578, 1985.

J. Blaauwendraad and H. J. Grootenboer. Essenials for discrete crack analysis. In *IABSE Reports 34, Colloquium for Advanced Mechanics of Reinforced Concrete, Delft University Press, The Netherlands*, pages 263–272, 1981.

R.W.G. Blakeley, L.M. Megget, and M.J.N. Priestley. Seismic performance of two full size reinforced concrete beam-column joint units. *Bulletin of the New-Zealand National Society for Earthquake Engineering*, 8(1):38–69, 1975.

J. E. Bolander and S. Berton. Cohesive zone modeling of fracture in irregular lattices. In V. C. Li, editor, *Fracture Mechanics of Concrete Structures, Ia-FramCOS*, pages 989–994, 2004.

J. Bonacci and J. K. Wight. Displacement based assessment of reinforced concrete frames in earthquakes. In J. K. Wight and M. E. Kreger, editors, *ACI Special Publications SP 162: M. A. Sozen Symposium: A tribute from his students*, pages 117–138. ACI, Farmington Hills, Michigan, 1996.

J. F. Bonacci and S. J. Pantazopoulou. Parametric investigation of joint mechanics. *ACI Structural Journal*, 90(1):61–71, 1993.

B. Bresler and K. S. Pister. Strength of concrete under combined stresses. *ACI Journal*, 55:321–345, 1958.

B. Bresler and A. C. Scordelis. Shear strength of reinforced concrete beams. *Journal of American Concrete Institute*, 60:51–72, 1963.

N. H. Burns and C. P. Seiss. Load-deformation characteristics of beam-column connections in reinforced concrete. Technical Report Civil Engineering Studies, SRS No. 234, Department of Civil Engineering, University of California, Berkeley, 1962.

B. Carter, P. Wawrzynek, and A. Ingraffea. Automated 3d crack growth simulation. *International Journal for Numerical Methods in Engineering*, 47:229–253, 1998.

J. Cervenka. *Mixed mode discrete crack propagation in concrete structures*. PhD thesis, Department of Civil Engineering, University of Colorado, Boulder, Colorado, 1994.

M. Cervera and J. Oliver. Seismic evaluation of concrete dams via continuum damage models. *Earthquake Engineering and Structural Dynamics*, 24:1225–1245, 1995.

J. L. Chaboche. Continuum damage mechanics: Part 1 - General concepts. *Journal of Applied Mechanics ASME*, 55:59–64, 1988.

W. F. Chen. *Plasticity in reinforced concrete*. McGraw-Hill New York, 1982.

W. F. Chen and D. J. Han. *Plasticity for structural engineers*. Springer-Verlag, New York Inc., 1988.

Y. S. Chung, C. Meyer, and M. Shinozuka. Seismic damage assessment of reinforced concrete members. Technical Report NCEER-87-0022, State University of New-York at Buffalo, 1987.

Y. S. Chung, M. Shinozuka, and C. Meyer. Sarcf users guide - seismic analysis of reinforced concrete frames. Technical Report NCEER-88-0044, State University of New-York at Buffalo, 1988.

R. W. Clough, K. L. Benuska, and E. L. Wilson. Inelastic earthquake response of tall buildings. In *Third World Conference on Earthquake Engineering, New-Zealand*, volume 11, pages 68–89, 1965.

M. P. Collins. Towards a rational theory for reinforced concrete members in shear. *Journal of the Structural Division, ASCE*, 104:649–666, 1978.

R. J. Cope, P. V. Rao, L. A. Clark, and P. Norris. Modeling of reinforced concrete behavior for finite element analysis of bridge slabs. In C. Taylor et al., editor, *Numerical Methods for Nonlinear Problems 1*, pages 457–470. Pineridge Press, Swansea, 1980.

W. G. Corley. Rotational capacity of reinforced concrete beam. *Journal of the Structural Division, ASCE*, 92(ST5), 1966.

H. A. W. Cornelissen, D. A. Hordijk, and H. W. Reinhardt. Experimental determination of crack softening characteristics of normal-weight and light-weight concrete. *Heron*, 31 (2):1–22, 1986.

E. Cosserat and F. Cosserat. *Théorie des Corps Déformables*. Herman, Paris, 1909.

J. V. Cox. Development of a plasticity bond model for reinforced concrete - theory and validation for monotonic applications. Technical Report TR-2036-SHR, Naval Facilities Engineering Service Center, Port Hueneme, CA, 1994.

M. A. Crisfield. Snap-through and snap-back response in concrete structures and the dangers of under-integration. *International Journal of Numerical Methods in Engineering*, 22:751–756, 1986.

M. A. Crisfield and J. Wills. Analysis of RC panels using different concrete models. *Journal of Engineering Mechanics ASCE*, 115(3):578–597, 1989.

D. Darwin. Reinforced concrete. In J. Isenberg, editor, *Finite element analysis of reinforced concrete structures*, pages 203–232. ASCE, Detroit, Michigan, 1995.

D. Darwin and D. A. Pecknold. Nonlinear biaxial stress-strain law for concrete. *Journal of Engineering Mechanics Division ASCE*, 103(2):229–241, 1977.

R. de Borst. Fracture in quasi-brittle materials: a review of continuum damage based approaches. *Engineering Fracture Mechanics*, 69:95–112, 2002.

R. de Borst. Simulation of strain localization: a reappraisal of cosserat continuum. *Engineering Computations*, 8:317–332, 1991.

R. de Borst and H. B. Mühlhaus. Gradient dependent plasticity: formulation and algorithmic aspects. *International Journal for Numerical Methods in Engineering*, 35:521–539, 1992.

R. de Borst and P. Nauta. Non orthogonal cracks in smeared finite element model. *Engineering Computations*, 2:35–46, 1986.

R. de Borst, L. J. Sluys, H. B. Mulhaus, and J. Pamin. Fundamental issues in finite element analysis of localization of deformation. *Engineering Computations*, 10:99–121, 1993.

R. de Borst, J. Pamin, and L. J. Sluys. Computational issues in gradient plasticity. In H. B. Mühlhaus, editor, *Continuum models for materials with microstructure*, pages 159–200. John Wiley and Sons, Ltd. London, 1995.

A. K. de Groot, G. M. A. Kusters, and T. Monnier. Numerical modeling of bond slip behavior. *Heron*, 26(1b), 1981.

J. H. P. de Vree, W. A. M. Brekelmans, and M. A. J. van Gils. Comparison of non-local approaches in continuum damage mechanics. *Computers and Structures*, 55:581–588, 1995.

K. Dörr. Bond behavior of ribbed reinforcement under transversal pressure. In *Proceedings, IASS Symposium on "Nonlinear behavior of reinforced concrete structures", Vol. 1, Preliminary report*. Werner Verlag, Dusseldorf, Germany, 1978.

A. J. Durrani and J. K. Wight. Experimental and analytical study of beam to column connections subjected to reverse cyclic loading. Technical Report UMEE 82 R3, Department of Civil Engineering, University of Michigan, 1982.

E. N. Dvorkin, A. M. Cuitiño, and G. Gioia. Finite elements with displacement interpolated embedded localization lines insensitive to mesh size and distortion. *International Journal for Numerical Methods in Engineering*, 30:541–564, 1990.

S. E. El-Metwally and W. F. Chen. Moment rotation modeling of reinforced-concrete beam-column connections. *ACI Structural Journal*, 85(4):384–394, 1988.

R. Eligehausen, E. P. Popov, and V. V. Bertero. Local bond stress slip relationship of deformed bars under generalized excitations. Technical Report UCB/EERC 83-23, Earthquake Engineering Research Center, University of California, Berkeley, 1983.

M. Elmorsi, M. R. Kianoush, and W. K. Tso. Nonlinear analysis of cyclically loaded reinforced concrete structures. *ACI Structural Journal*, 95(6):725–739, 1998.

M. Elmorsi, M. R. Kianoush, and W. K. Tso. Modeling bond-slip deformations in reinforced concrete beam-column joints. *Canadian Journal of Civil Engineering*, 27(3):490–505, 2000.

Y. Endoh, T. Kamura, S. Otani, and H. Aoyama. Behavior of RC beam-column connections using light-weight concrete. *Transactions of Japan Concrete Institute*, 13:319–326, 1991.

A. C. Eringen. Simple microfluids. *International Journal of Engineering Science*, 2:205–217, 1964.

A. C. Eringen. Mechanics of micromorphic materials. In *Proceedings, Eleventh International Congress of Applied Mechanics, Berlin*, pages 131–138. Springer, 1966.

A. C. Eringen. Theories of nonlocal plasticity. *International Journal of Engineering Science*, 21:741–751, 1983.

A. C. Eringen and D. G. B. Edelen. On nonlocal elasticity. *International Journal of Engineering Science*, 10:233–248, 1972.

G. Etse and M. Nieto. Coserat continua based microplane modeling: Theory and numerical analysis. *Latin American Applied Research*, 34(4):229–240, 2004.

G. Etse, M. Nieto, and P. Steinmann. A micropolar microplane theory. *International Journal of Engineering Science*, 41:1631–1648, 2003.

P. H. Feenstra. *Computational aspects of biaxial stress in plain and reinforced concrete*. PhD thesis, Department of Civil Engineering, Delft University of Technology, Delft, The Netherlands, 1993.

P. H. Feenstra and R. de Borst. Constitutive model for reinforced concrete. *Journal of Engineering Mechanics, ASCE*, 121(5):586–595, 1995.

F. C. Filippou. A simple model for reinforcing bar anchorages under cyclic excitations. *Journal of Structural Engineering, ASCE*, 112:1639–1659, 1986.

F. C. Filippou and G. L. Fenves. Methods of analysis for earthquake-resistant structures. In Y. Bozorgnia and V. V. Bertero, editors, *Earthquake Engineering: From engineering seismology to performance-based engineering*. CRC, Boca Raton, Florida, 2004.

F. C. Filippou, E. P. Popov, and V. V. Bertero. Modeling of RC joints under cyclic excitation. *Journal of Structural Engineering, ASCE*, 109(11):2666–2684, 1983.

F. Fleury, J. M. Reynouard, and O. Merabet. Multi-component model of reinforced concrete joints for cyclic loading. *Journal of Engineering Mechanics ASCE*, 126(8):804–811, 2000.

D. A. Foutch and S. Shi. Connection element (type 10) for DRAIN2DX. Technical report, Internal Report, Department of Civil Engineering, University of Illinois, Urbana-Champagne, 1997.

D. A. Foutch, S. Shi, and S. Y. Yun. *Element 10: A stiffness and strength degrading elemnet developed for teh SAC steel program*. http://nisee.berkeley.edu/software/drain2dx, 2003.

G. Frantziskonis and C. S. Desai. Constitutive model with strain softening. *International Journal for Solids and Structures*, 23(6):733–750, 1987.

S. Fujii and S. Morita. Comparison between interior and exterior RC beam-column joint behavior. In *ACI Special Publications SP 123-12: Design of beam-column joints for seismic resistance*, pages 145–165. ACI, Farmington Hills, Michigan, 1991.

P. G. Gambarova, G. P. Rosati, and B. Zasso. Steel to concrete bond after concrete splitting: test results. *Materials and Structures*, 22(127):35–47, 1989a.

P. G. Gambarova, G. P. Rosati, and B. Zasso. Steel to concrete bond after concrete splitting: constitutive laws and interface deterioration. *Materials and Structures*, 22(127):347–356, 1989b.

P. Gardoni, A. Der Kiureghian, and K. M. Mosalam. Probabilistic capacity models and fragility estimates for reinforced concrete columns based on experimental observations. *Journal of Engineering Mechanics, ASCE*, 128(10):1024–1038, 2002.

O. J. Gastebled. *Fracture in reinforced concrete - computational and analytical studies*. PhD thesis, Department of Civil Engineering, Heriot-Watt University, Edinburgh, Scotland, 1999.

A. Ghobarah and M. Youssef. Modeling of reinforced concrete structural walls. *Engineering Structures*, 21:912–923, 1999.

M. F. Giberson. Two nonlinear beams with definitions of ductility. *Journal of the Structural Division, ASCE*, 95(ST2):137–157, 1969.

E. Giuriani, G. Plizzari, and C. Schumm. Role of stirrups and residual tensile strength of cracked concrete on bond. *Journal of Structural Engineering, ASCE*, 117(1):1–18, 1969.

V. S. Gopalratnam and S. P. Shah. Softening response of plain concrete in direct tension. *ACI Structural Journal*, 3:310–323, 1985.

Y. Goto. Cracks formed in concrete around tension bars. *ACI Journal, Proceedings*, 68(4), 1971.

S. Govindjee, G. J. Kay, and J. C. Simo. Anisotropic modeling and numerical simulation of brittle damage in concrete. *International Journal for Numerical Methods in Engineering*, 38:3611–3633, 1995.

A. E. Green. Micromaterials and multipolar continuum mechanics. *International Journal of Engineering Science*, 3:533–537, 1965.

A. E. Green and R. S. Rivlin. Multipolar continuum mechanics. *Archive for Rational Mechanics and Analysis*, 17:113–147, 1964a.

A. E. Green and R. S. Rivlin. Simple force and stress multipoles. *Archive for Rational Mechanics and Analysis*, 16:325–353, 1964b.

W. H. Greene. *Econometric analysis*. Pearson Education, Singapore, 2000.

A. K. Gupta and H. Akbar. Cracking in reinforced concrete analysis. *Journal of Structural Engineering, ASCE*, 110(8):1735–1746, 1984.

S. Hakuto, R. Park, and H. Tanaka. Effect of deterioration of bond on beam-bars passing through interior beam-column joints on flexural strength and ductility. *ACI Structural Journal*, 96(5):858–864, September-October 1999.

S. Hakuto, R. Park, and H. Tanaka. Seismic load tests on interior and exterior beam-column joints with substandard reinforcing details. *ACI Structural Journal*, 97(1):11–25, 2000.

J.F. Hall. Northridge earthquake preliminary reconnaissance report. Technical report, EERI, January 1994.

N.W. Hanson and H.W. Connor. Seismic resistance of reinforced concrete beam-column joints. *Journal of Structural Engineering Division, ASCE*, 93(ST5):533–559, 1967.

F. Hayashi. *Econometrics*. Princeton University Press, 2000.

K. Hayashi, M. Teraoka, A. A. Mollick, and Y. Kanoh. Bond properties of main reinforcing bars and restoring force characteristics in RC interior beam column subassemblages using high strength materials. In *Proceedings, Second US-Japan-New Zealand-Canada multilateral meeting on structural performance of high strength concrete in seismic regions, Honolulu, Hawaii*, pages 15–27, 1994.

Y. Higashi and Y. Ohwada. Failing behaviors of reinforced concrete beam-column connections subjected to lateral load. *Memoris of Faculty of Technology Tokyo Metropolitan University, Tokyo, Japan*, 19:91–101, 1969.

A. Hillerborg. The theoritical basis of a method to determine the fracture energy gf of concrete. *Materials and Structures*, 106(18):773–782, 1985.

A. Hillerborg, M. Modeer, and P. E. Petersson. Analysis of crack formation and crack growth in concrete by means of fracture mechanics and finite elements. *Cement and Concrete Research*, 6:773–782, 1976.

G. Hofstetter and H. A. Mang. *Computational mechanics of reinforced concrete structures*. Vieweg and Sohn Verlagsgesellschaft mbH, Weisbaden, Germany, 1995.

D. A. Hordijk. *Local approach to fatigue of concrete*. PhD thesis, Department of Civil Engineering, Delft University of Technology, Delft, The Netherlands, 1991.

S. S. Hsieh, E. C. Ting, and W. F. Chen. A plasticity-fracture model for concrete. *International Journal of Solids and Structures*, 18(3):181–197, 1982.

T. T. C. Hsu. Softened truss model theory for shear and torsion. *ACI Structural Journal*, 85(6):624–634, 1988.

T. T. C. Hsu. *Unified theory of reinforced concrete*. CRC Press, LLC, Boca Raton, FL, 1993.

T. T. C. Hsu and R. R. H. Zhu. Softened membrane model for reinforced concrete elements in shear. *ACI Structural Journal*, 99(4):460–469, 2002.

B. P. Hughes and R. Gregory. Concrete subjected to high rates of loading in compression. *Magazine of Concrete Research*, 24(78):25–36, 1972.

B. P. Hughes and R. Gregory. Compressive strength and ultimate strain of concrete under impact loading. *Magazine of Concrete Research*, 30(105):189–199, 1978.

S. Hungspreug. *Local bond between steel bar and concrete under high intensity cyclic loading.* PhD thesis, Department of Civil Engineering, Cornell University, Ithaca, NY, 1981.

S. J. Hwang and H. J. Lee. Analytical models for predicting shear strengths of interior reinforced concrete beam-column joints for seismic resistance. *ACI Structural Journal*, 97(1):35–44, 2000.

S. J. Hwang and H. J. Lee. Strength prediction for discontinuity regions by softened strut and tie model. *Journal of Structural Engineering, ASCE*, 128(12):1519–1526, 2002.

S. J. Hwang and H. J. Lee. Analytical models for predicting shear strengths of exterior reinforced concrete beam-column joints for seismic resistance. *ACI Structural Journal*, 96(5):846–857, 1999.

T. Ichinose. Shear reinforcement of reinforced concrete inelastic interior beam-column joints. *Bulletin of the New-Zealand National Society for Earthquake Engineering*, 20(2):116–126, 1987.

A. R. Ingraffea and V. Saouma. Numerical modeling of discrete crack propagation in reinforced and plain concrete. In C. Meyer and H. Okamura, editors, *Fracture mechanics of concrete*, pages 171–225. Martinus Nijhoff Publishers, Dordrecht, 1985.

Y. Jenq and S. P. Shah. Two parameter fracture model for concrete. *Journal of Engineering Mechanics, ASCE*, 111(10):1227–1241, 1985.

M. Jirásek. Comparative study on finite elements with embedded discontinuities. *Computer Methods in Applied Mechanics and Engineering*, 188:307–330, 2000.

O. Joh, Y. Goto, and T. Shibata. Influence of transverse joint, beam reinforcement and relocation of plastic hinge region on beam-column joint stiffness determination. In *ACI Special Publications SP 123-12: Design of beam-column joints for seismic resistance*, pages 187–223. ACI, Farmington Hills, Michigan, 1991.

T. Kaku and S. Morita. Bond behavior of beam bars in the joint of reinforced concrete frames. *Annual Meeting of the Architectural Institute of Japan, AIJ*, pages 1777–1778, 1978.

I. D. Karsan and J. O. Jirsa. Behavior of concrete under compressive loading. *Journal of the Structural Division, ASCE*, 95(ST12):1519–1526, 1969.

W. Kaufmann and P. Marti. Structural concrete: cracked membrane model. *Journal of Structural Engineering*, 124(12):1466–1475, 1998.

D. C. Kent and R. Park. Flexural members with confined concrete. *Journal of the Structural Division, ASCE*, 97(ST7):1969–1990, 1971.

M. Keuser and G. Mehlhorn. Finite element models for bond problems. *Journal of Structural Engineering, ASCE*, 113(10):2160–2173, 1987.

J. H. Kim and J. B. Mander. Seismic detailing of reinforced concrete beam-column connections. *Structural Engineering and Mechanics*, 10(6):589–601, 2000.

K. Kitayama, S. Otani, and H. Aoyama. Earthquake resistant design criteria for reinforced concrete interior beam-column joints. In *Pacific Conference on Earthquake Engineering, Wairakei, New Zealand*, pages 315–326, 1987.

M. Klisinski, K. Runesson, and S. Sture. Finite elements with inner softening band. *Journal of the Engineering Mechanics, ASCE*, 117:575–587, 1991.

M. D. Kotsovos and M. N. Pavlovic. *Structural concrete: Finite element analysis for limit state design*. Thomas Telford Ltd., 1995.

R. Kozul and D. Darwin. Effects of aggregate type, size and content on concrete strength and fracture energy. Technical Report SM 43, The University of Kansas Center for Research, Inc., 1997.

H. Krawinkler and S. Mohasseb. Effects of panel zone deformations on seismic response. *Journal of Construction Steel Research*, (8):233–250, 1987.

E. Kuhl, P. Steinmann, and I. Carol. A thermodynamically consistent approach to microplane theory. part ii. *International Journal of Solids and Structures*, 38:2933–2952, 2001.

S. K. Kunnath, A. M. Reinhorn, and R. F. Lobo. Idarc version 3.0: Program for inelastic damage analysis of RC structures. Technical Report Technical Report NCEER-92-0022, State University of New-York at Buffalo, 1992.

H. B. Kupfer and K. H. Gerstle. Behavior of concrete under biaxial stress. *Journal of Engineering Mechanics ASCE*, 99(4):853–866, 1973.

Y. Kurose. Recent studies on reinforced concrete beam column joints in Japan. Technical Report PMFSEL Report No. 87-8, Department of Civil Engineering, University of Texas at Austin, 1987.

J. M. LaFave and M. Shin. Discussion of "Modeling reinforced concrete beam-column joints subjected to cyclic loading" by L. N. Lowes & A. Altoontash. *Journal of Structural Engineering, ASCE*, 131(6):992–993, 2005.

S. S. Lai, G. T. Will, and S. Otani. Model for inelastic biaxial bending of concrete members. *Journal of Structural Engineering, ASCE*, 110(11):2563–2583, 1984.

J. P. Laible, R. N. White, and P. Gergeley. Experimental investigation of seismic shear transfer across cracks in concrete nuclear containment vessels. *ACI Special Publications*, 53(9):203–226, 1977.

R. Larsson and K. Runesson. Element embedded localization band based on regularized displacement discontinuity. *Journal of Engineering Mechanics, ASCE*, 122:402–411, 1996.

R. Larsson, K. Runesson, and S. Sture. Embedded localization band in undrained soil based on regularized strong discontinuity - theory and FE analysis. *International Journal of Solids and Structures*, 33:3081–3101, 1996.

J. Lee and G. L. Fenves. A plastic damage model for cyclic loading of concrete structures. *Journal of Engineering Mechanics, ASCE*, 124:892–900, 1998.

Y. H. Lee and K. Willam. Mechanical properties of concrete in uniaxial compression. *ACI Materials Journal*, 94(6):457–471, 1997.

J. Lemaitre. *A course on damage mechanics*. Springer-Verlag, New York Inc., 1992.

R. T. Leon. Shear strength and hysteretic behavior of interior beam-column joints. *ACI Structural Journal*, 87(1):3–11, 1990.

H. Lippmann. Eine cosserat des plastischen flie ßens. *Acta Mechanica*, 8:255–284, 1969.

H. R. Lotfi. *Finite element analysis of fracture in concrete and masonry structures*. PhD thesis, Department of Civil, Environmental and Architectural Engineering, University of Colorado, Boulder, Colorado, 1992.

H. R. Lotfi and P. B. Shing. Embedded representation of fracture in concrete with mixed finite elements. *International Journal for Numerical Methods in Engineering*, 38:1307–1325, 1995.

L. N. Lowes. Finite element analysis of RC beam-column bridge connections. In P. B. Shing and T. Tanabe, editors, *Modeling of inelastic behavior of RC structures under seismic loads*, pages 276–296. ASCE, Detroit, Michigan, 2001.

L. N. Lowes. Modeling the response of reinforced-concrete bridge beam-column joints subjected to earthquake loading. *Transportation Research Record*, 1814:253–261, 2002.

L. N. Lowes. *Finite element modeling of reinforced concrete beam-column bridge connections*. PhD thesis, Department of Civil Engineering, University of California, Berkeley, California, 1999.

L. N. Lowes and A. Altoontash. Modeling reinforced concrete beam-column joints subjected to cyclic loading. *Journal of Structural Engineering, ASCE*, 129(12):1686–1697, 2003.

L. N. Lowes and J. P. Moehle. Evaluation and retrofit of beam-column T-joints in older reinforced concrete bridge structures. *ACI Structural Journal*, 96(4):519–532, 1999.

L. N. Lowes, A. Altoontash, and N. Mitra. Closure to "Modeling reinforced concrete beam-column joints subjected to cyclic loading" by L. N. Lowes & A. Altoontash. *Journal of Structural Engineering, ASCE*, 131(6):993–994, 2005.

J. Lubliner, J. Oliver, S. Oller, and E. Oñate. A plastic damage model for concrete. *International Journal of Solids and Structures*, 25(3):299–326, 1989.

L. A. Lutz and P. Gergeley. Mechanics of bond and slip of deformed bars in concrete. *ACI Journal*, 64:711–721, 1967.

J. G. MacGregor. *Reinforced concrete: mechanics and design*. Prentice Hall Inc., NJ, 3 edition, 1997.

J. Mainz, S. Stckl, and H. Kupfer. Fe calculations concerning the bond behavior of deformed bars in concrete. In *Proceedings of International Conference of Bond in Concrete, Riga, Latvia, CEB, Vol. 1*, pages 12.17–12.26, 1992.

L. J. Malvar. Bond of reinforcement under controlled confinement. Technical Report TR-1833-SHR, Naval Facilities Engineering Service Center, Port Hueneme, CA, 1991.

L. J. Malvar and M. E. Fourney. A three dimensional application of smeared crack approach. *Journal of Engineering Fracture Mechanics*, 35:251–260, 1990.

L. J. Malvar and G. E. Warren. Fracture energy for three-point bend tests on single-edged notched beams. *Experimental Mechanics*, 28:266–272, 1988.

J. B. Mander, M. J. N. Priestley, and R. Park. Theoretical stress-strain model for confined concrete. *Journal of Structural Engineering, ASCE*, 114(8):1804–1825, 1988.

O. L. Manzoli and P. B. Shing. Stress hybrid finite elements with multiple embedded cracks. In V. C. Li, C. K. Y. Leung, K. J. Willam, and S. L. Billington, editors, *Fracture mechanics of concrete structures, Vol. 1*, pages 123–130, 2004.

P. Marti. Basic tools of reinforced concrete beam design. *ACI Journal*, 82(1):46–56, 1985.

J. Martin, J. Stanton, N. Mitra, and L. N. Lowes. Experimental testing to determine concrete fracture energy using a simple laboratory test set-up. *ACI Materials Journal*, submitted, 2006.

J. Mazars and G. Pijaudier-Cabot. Continuum damage theory: Application to concrete. *Journal of Engineering Mechanics Division ASCE*, 115:345–365, 1989.

S. Mazonni, F. McKenna, M. H. Scott, G. L. Fenves, and et al. *OpenSees user command language manual, Version 1.7.2*. http://opensees.berkeley.edu/OpenSees/manuals/usermanual/index.html, 2006.

D.L. McFadden. Conditional logit analysis of qualitative choice analysis. In P. Zarembka, editor, *Frontiers of econometrics*, pages 105–142, 1974.

F. McKenna, G. L. Fenves, and et al. *OpenSees: Open System for Earthquake Engineering Simulation, Version 1.6.2*. http://opensees.berkeley.edu, 2005.

G. Mehlhorn and M. Keuser. Isoparametric contact elements for analysis of reinforced concrete structures. In *Finite Element Analysis of Reinforced Concrete, ASCE, Proceedings of a Seminar sponsored by Japan Society for the promotion of Science and UNSF, Tokyo, Japan*, pages 329–347, 1985.

P. K. Mehta and P. J. M. Monteiro. *Concrete: Structure, Properties and Materials*. Prentice Hall Inc., NJ, 2 edition, 1993.

D. F. Meinheit and J. O. Jirsa. The shear strength of reinforced concrete beam-column joints. Technical Report CESRL Report No. 77-1, University of Texas at Austin, 1977.

M. Menegotto and P. E. Pinto. Slender RC members in biaxial bending. *Journal of the Structural Division, ASCE*, 103(ST3):587–605, 1977.

O. Merabet, M. Djerroud, G. Heinfling, and J. M. Reynouard. Intégration d'un modèle élastoplastique fissurable pour le béton dans le code Aster. Technical Report Rapport Intermédiaire No. INSA/1/943/001, INSA, Lyon, France, 1995.

A. Mikame, K. Uchida, and H. Noguchi. Study of compressive deterioration of cracked concrete. In J. Isenberg, editor, *International Proceedings on Finite Element Analysis of Reinforced Concrete*, 1991.

J.R. Milburn and R. Park. Behavior of reinforced concrete beam-column joints designed to nzs 3101. Technical Report 82-7, University of Canterbury, Christchurch, New Zealand, 1982.

R. D. Mindlin. Microstructure in linear elasticity. *Archive for Rational Mechanics and Analysis*, 16:51–78, 1964.

R. D. Mindlin. Second gradient of strain and surface tension in linear elasticity. *International Journal of Solids and Structures*, 1:417–438, 1965.

R. D. Mindlin and H. F. Tiersten. Effects of couple stress in linear elasticity. *Archive for Rational Mechanics and Analysis*, 11:415–448, 1962.

N. Mitra and L. N. Lowes. Evaluation and advancement of a reinforced concrete beam-column joint model. In *Thirteenth World Conference on Earthquake Engineering, Vancouver, B.C. Canada*, number 1001, 2004.

N. Mitra and L. N. Lowes. Evaluation, calibration and verification of a reinforced concrete beam-column joint model. *Journal of Structural Engineering, ASCE*, 133(1):105–120, 2007.

T. Miyahara, T. Kawakami, and K. Maekawa. Nonlinear behavior of cracked reinforced concrete plate element under uniaxial compression. In *Proceedings of JSCE*, volume 387, pages 249–258, 1987.

M. Monti, F. C. Filippou, and E. Spacone. Finite element for anchored bars under cyclic load reversals. *Journal of Structural Engineering, ASCE*, 123(5):614–623, 1997.

S. Morita and S. Fujii. Bond slip models in finite element analysis. In *Proceedings of the Japan-USA seminar on Finite Element Analysis of Reinforced Concrete Structures, ASCE, Tokyo*, pages 348–363, 1985.

S. Morita and T. Kaku. Local bond stress-slip relationship and repeated loading. In *Proceedings, IABSE Symposium on "Resistance and ultimate deformability of structures acted on by well defined repeated loads", Lisboa*, pages 221–227, 1973.

S. Morita and T. Kaku. Bond slip relationship under repeated loading. *Transactions of the AIJ*, 229:15–24, 1975.

S. Morita and T. Kaku. Slippage of reinforcement in beam-column joint if reinforced concrete frame. In *Eighth World Conference on Earthquake Engineering, San-Francisco, CA, USA*, pages 477–484, 1984.

E. Mörsch. *Concrete-Steel Construction*. E. P. Goodrich, Translator, McGraw-Hill Book Company, New-York, 1909.

W. G. Mosier. Seismic assessment of reinforced concrete beam-column joints. Master's thesis, Department of Civil Engineering, University of Washington, Seattle, 2000.

H. B. Mühlhaus. Application of cosserat theory in numerical solution of limit load problems. *Archive of Applied Mechanics (Ingenieur Archiv)*, 59(2):124–137, 1989.

H. B. Mühlhaus and E. C. Aifantis. A variational principle for gradient plasticity. *International Journal of Solids and Structures*, 28(7):845–857, 1991.

D. Ngo and A. C. Scordelis. Finite element analysis of reinforced concrete beams. *Journal of American Concrete Institute*, 64(14):152–163, 1967.

H. Noguchi. Nonlinear finite element analysis of reinforced concrete beam-column joints. In *IABSE Colloquium, Delft, The Netherlands*, pages 639–653, 1981.

H. Noguchi and T. Kashiwazaki. Experimental studies on shear performances of RC interior column-beam joints. In *Tenth World Conference on Earthquake Engineering, Madrid, Spain*, pages 3163–3168, 1992.

U. Ohlsson and Th. Olofsson. Mixed mode fracture and anchor bolts in concrete: analysis with inner softening bands. *Journal of the Engineering Mechanics, ASCE*, 123:1027–1033, 1997.

K. Oka and H. Shiohara. Tests on high-strength concrete interior beam-column joint subassemblages. In *Tenth World Conference on Earthquake Engineering, Madrid, Spain*, pages 3211–3217, 1992.

J. Oliver. An analysis of strong discontinuities in multiplicative finite strain plasticity and their relation with the numerical simulation of strain localization in solids. *International Journal of Solids and Structures*, 33:2863–2885, 1996a.

J. Oliver. A consistent characteristic length for smeared crack models. *International Journal for Numerical Methods in Engineering*, 28:461–474, 1989.

J. Oliver. Continuum modeling of strong discontinuities in solid mechanics. In D. R. J. Owen and E. Oñate, editors, *Computational plasticity: Fundamentals and application, Proc. COMPLAS IV,*, pages 455–479. International Center for Numerical Methods in Engineering, Barcelona, 1995.

J. Oliver. Modeling strong discontinuities in solid mechanics via strain softening constitutive equation, part 1: Fundamentals, part 2: Numerical simulation. *International Journal for Numerical Methods in Engineering*, 39:3575–3624, 1996b.

J. Oliver and D. G. Pulido. On the use of strain softening damage constitutive equations to model cracking of concrete. In R. de Borst, H. Bićanić, H. Mang, and G. Meschke, editors, *Computational modeling of concrete structures*, pages 363–372. Balkema, Rotterdam, 1998.

J. Oliver, M. Cervera, and O. Manzoli. On the use of strain softening models for simulation of strong discontinuities in solids. In R. de Borst and E. van der Giessen, editors, *Material instabilities in solid*. Wiley, Chichester, 1998.

Th. Olofsson, M. Klisinski, and P. Nedar. Inner softening bands: a new approach to localization in finite elements. In H. Mang, H. Bićanić, and R. de Borst, editors, *Computational modeling of concrete structures*, pages 373–382. Pineridge Press, Swansea, 1994.

S. Otani. Inelastic analysis of RC frame structures. *Journal of the Structural Division, ASCE*, 100(ST7):1433–1449, 1974.

S. Otani, Y. Kobayashi, and H. Aoyama. Reinforced concrete interior beam-column joints under simulated earthquake loading. In *US-New Zealand-Japan seminar on design of reinforced concrete beam-column joints, Monterey, CA*, 1984.

N. S. Ottosen. A failure criterion for concrete. *Journal of Engineering Mechanics Division, ASCE*, 103(EM4):527–535, 1977.

J. Ožbolt and R. Eligehausen. Simulation of cycling bond behavior. In Z. P. et al. Bažant, editor, *Proceedings of the first international conference on fracture mechanics of concrete structures, Breckenridge, CO*, pages 912–917. Elsevier Science Publishers Ltd., Essex, England, 1992.

D. Palermo and F. J. Vecchio. Compression field modeling of reinforced concrete subjected to reverse loading: formulation. *ACI Structural Journal*, 100(5):616–625, 2003.

J. Pamin. *Gradient dependent plasticity in numerical simulation of localization phenomena*. PhD thesis, Department of Civil Engineering, Delft University of Technology, Delft, The Netherlands, 1994.

X. B. Pang and T. T. C. Hsu. Fixed-angle softened truss model for reinforced concrete. *ACI Structural Journal*, 93(2):197–207, 1996.

S. J. Pantazopoulou and J. F. Bonacci. Consideration of questions about beam-column joints. *ACI Structural Journal*, 89(1):27–36, 1992.

S. J. Pantazopoulou and J. F. Bonacci. On earthquake resistant reinforced concrete frame connections. *Canadian Journal of Civil Engineering*, 21:307–328, 1994.

R. Park and J.R. Milburn. Comparison of recent new zealand and united states seismic design provisions for reinforced concrete beam-column joints and test results from four units designed according to the new zealand code. *Bulletin of the New Zealand National Society of Earthquake Engineering*, 16(1):3–24, 1983.

R. Park and D. Ruitong. A comparison of the behavior of reinforced concrete beam column joints designed for ductility and limited ductility. *Bulletin of the New-Zealand national society for Earthquake Engineering*, 21(4):255–278, 1988.

R. Park, M. J. N. Priestley, and W. D. Gill. Ductility of square confined reinforced concrete columns. *Journal of the Structural Division, ASCE*, 108(ST4):929–950, 1982.

Y. J. Park, A. M. Reinhorn, and S. K. Kunnath. Idarc: Inelastic damage analysis of reinforced concrete frames and shear-wall structures. Technical Report Technical Report NCEER-87-0008, State University of New-York at Buffalo, 1987.

G. J. Parra-Montesionos and J. K. Wight. Prediction of strength and shear distortion in RC beam-column joints. In S. A. Sheikh and O. Bayrak, editors, *ACI Special Publications SP 197: S. M. Uzumeri Symposium: Behavior and design of concrete structures for seismic performance*, pages 191–204. ACI, Farmington Hills, Michigan, 2002.

T. Paulay. Equilibrium criteria for reinforced concrete beam-column joints. *ACI Structural Journal*, 86(6):635–643, 1989.

T. Paulay and P. J. Loeber. Shear transfer by aggregate interlock. *ACI Special Publications*, 42(1):1–15, 1977.

T. Paulay and M. J. N. Priestley. *Seismic design of reinforced concrete and masonry buildings*. John Wiley and Sons, Inc., 1992.

T. Paulay, R. Park, and M. J. N. Priestley. Reinforced concrete beam column joints under seismic action. *ACI Structural Journal*, 75(6):585–593, 1978.

R. H. J. Peerlings, R. de Borst, W. A. M. Brekelmans, and J. H. P. de Vree. Gradient enhanced damage for quasibrittle materials. *International Journal for Numerical Methods in Engineering*, 39:3391–3403, 1996.

S. P. Pessiki, C. Conley, P. Gergely, and R. N. White. Seismic behavior of lightly reinforced concrete column and beam-column joint details. Technical Report NCEER-90-0014, National Center for Earthquake Engineering Research, State University of New York at Buffalo, New York, 1990.

P. E. Petersson. Fracture energy of concrete: method of determination. *Cement and Concrete Research*, 10(1):79–89, 1980a.

P. E. Petersson. Fracture energy of concrete: practical performance and experimental results. *Cement and Concrete Research*, 10(1):91–101, 1980b.

S. Popovics. A numerical approach to the complete stress strain curve for concrete. *Cement and Concrete Research*, 3(5):583–599, 1973.

V. Prakash, G. H. Powell, and S. Campbell. *DRAIN-2DX base program description and user guide*. http://nisee.berkeley.edu/software/drain2dx, 1993.

E. Pramono and K. Willam. Fracture energy based plasticity formulation of plain concrete. *Journal of the Engineering Mechanics Division, ASCE*, 115(6):1183–1203, 1989.

W. Ramberg and W. R. Osgood. Description of stress strain curves by three parameters. Technical Report 902, National advisory committee on aeronautics, 1943.

Y. R. Rashid. Ultimate strength analysis of prestressed concrete pressure vessels. *Nuclear Engineering and Design*, 7:334–344, 1968.

G. Rehm. The fundamental law of bond. In *Proceedings of the symposium on bond and crack formation in reinforced concrete, Stockholm, Vol. 2, RILEM*, pages 491–498, 1957.

H. W. Reinhardt. Fracture mechanics of an elastic softening material like concrete. *Heron*, 29(2):1–22, 1984.

H. W. Reinhardt, J. Blauuwendraad, and E. Vos. Prediction of bond between steel and concrete by numerical analysis. *Materials and Structures*, 17(100):311–320, 1984.

L. Resende and J. B. Martin. A progressive damage continuum model for granular materials. *Computer Methods in Applied Mechanics and Engineering*, 42:1–18, 1984.

W. Ritter. Die bauwise hennebique (construction techniques handbook). Technical report, Schweizerische Bauzeitung, 1899.

C. A. Ross, J. W. Tedesco, and S. T. Kuennen. Effect of strain rate on concrete strength. *ACI Materials Journal*, 92(1):37–47, 1995.

C. A. Ross, D. M. Jerome, J. W. Tedesco, and M. L. Hughes. Moisture and strain rate effects on concrete strength. *ACI Materials Journal*, 93(3):293–300, 1996.

J. G. Rots. *Computational modeling of concrete fracture*. PhD thesis, Department of Civil Engineering, Delft University of Technology, Delft, The Netherlands, 1988.

J. G. Rots and J. Blaauwendraad. Crack models for concrete: Discrete or smeared ? fixed, multidirectional or rotating ? *Heron*, 34(1):334–344, 1989.

J. G. Rots, P. Nauta, G. M. A. Kusters, and J. Blaauwendraad. Smeared crack approach and fracture localization in concrete. *Heron*, 30(1):1–48, 1985.

J. Schlaich and G. Anagnostou. Stress fields for nodes of strut and tie models. *Journal of Structural Engineering, ASCE*, 116(1):13–23, 1990.

J. Schlaich and K. Schäfer. Design and detailing structural concrete using strut-tie models. *The Structural Engineer*, 69(6):113–125, 1991.

J. Schlaich, K. Schäfer, and M. Jennewein. Towards a consistent design of structural concrete. *PCI Journal*, 32(3):74–150, 1987.

M. H. Scott and G. L. Fenves. Plastic hinge integration methods for force based beam-column elements. *Journal of Structural Engineering, ASCE*, 132(2):244–252, 2006.

S. A. Sheikh and S. M. Uzumeri. Analytical model for concrete confinement in tied columns. *Journal of the Structural Division, ASCE*, 108:2703–2722, 1982.

H. Shima, L. L. Chou, and H. Okamura. Bond characteristics in the post yield range of deformed bars. *Concrete Library of Japan Society of Civil Engineering*, 10:113–124, 1987.

M. Shin and J. M. LaFave. Modeling of cyclic joint shear deformation contributions in RC beam column connections to overall frame behavior. *Structural Engineering and Mechanics*, 18(5):645–669, 2004.

H. Shiohara. New model for shear failure of RC interior beam-column connections. *Journal of Structural Engineering, ASCE*, 127(2):152–160, 2001.

J. M. Shipman and K. H. Gerstle. Bond deterioration in concrete panels under load cycles. *ACI Journal*, 76(2):311–325, 1979.

S. Shirai and H. Noguchi. Compressive deterioration of cracked concrete. In *ASCE Structures Congress 1989: Design, Analysis and Testing, New-York*, pages 1–10, 1989.

J. C. Simo and J. W. Ju. Stress and strain based continuum damage models - i. formulation. *International Journal of Solids and Structures*, 23:821–840, 1987.

J. C. Simo and J. Oliver. A new approach to the analysis and simulation of strain softening in solids. In Z. P. et al. Bažant, editor, *Fracture and damage in quasibrittle materials*, pages 25–39. E. and F. N. Spon, London, 1994.

L. J. Sluys. Discontinuous modeling of shear banding. In D. R. J. Owen, E. Oñate, and E. Hinton, editors, *Computational plasticity: Fundamentals and application, Proc. COMPLAS V,*, pages 735–744. International Center for Numerical Methods in Engineering, Barcelona, 1997.

L. J. Sluys and A. H. Berends. 2d/3d modeling of crack propagation with embedded discontinuity elements. In R. de Borst, H. Bićanić, H. Mang, and G. Meschke, editors, *Computational modeling of concrete structures*, pages 399–408. Balkema, Rotterdam, 1998.

P. Sluys. *Wave propagation, localization and dispersion in softening solids*. PhD thesis, Department of Civil Engineering, Delft University of Technology, Delft, The Netherlands, 1992.

D. Soleimani, E.P. Popov, and V.V. Bertero. Hysteretic behavior of reinforced concrete beam-column sub-assemblages. *Journal of the American Concrete Institute*, 76-48(11): 1179–1195, November 1979.

B. Spencer and P. B. Shing. Stress hybrid embedded crack element for analysis of concrete fracture. In K. Willam and T. Tanabe, editors, *ACI Special Publications SP 205: Finite element analysis of reinforced concrete structures*, pages 323–347. ACI, Farmington Hills, Michigan, 2001.

B. W. Spencer. *Finite element with embedded discontinuities for modeling reinforced concrete members*. PhD thesis, Department of Civil, Environmental and Architectural Engineering, University of Colorado, Boulder, Colorado, 2002.

L. Spievak, P. Wawrzynek, D. Lewicki, and A. Ingraffea. Automated 3d crack growth simulation. *Engineering Fracture Mechanics*, 68(1):53–76, 2001.

S. Sritharan and J. M. Ingham. Application of strut-and-tie concepts to concrete bridge joints in seismic regions. *PCI Journal*, 30:66–90, 2003.

S. Sritharan, M. J. N. Priestley, and F. Seible. Nonlinear finite element analyses of concrete bridge joint systems subjected to seismic actions. *Finite elements in analysis and design*, 36:215–233, 2000.

P. Steinmann. An improved FE expansion for micropolar localization analysis. *Communications in Numerical Methods in Engineering*, 10:1005–1012, 1994.

P. Steinmann. Theory and numerics of ductile micropolar elastoplastic damage. *International Journal for Numerical Methods in Engineering*, 38:583–606, 1995.

N. J. Stevens, S. M. Uzumeri, and M. P. Collins. Reinforced concrete subjected to reversed cyclic shear-experiments and constitutive model. *ACI Structural Journal*, 88(2):135–146, 1991a.

N. J. Stevens, S. M. Uzumeri, M. P. Collins, and G. T. Will. Constitutive model for reinforced concrete finite element analysis. *ACI Structural Journal*, 88(1):49–59, 1991b.

M. Suidan and W. C. Schnobrich. Finite element analysis of reinforced concrete. *Journal of the Structural Division, ASCE*, 99:2109–2122, 1973.

N. Sukumar, N. Möes, B. Moran, and T. Belytschko. Extended finite element method for three dimensional crack modeling. *International Journal for Numerical Methods in Engineering*, 48(1):1549–1570, 2001.

S. Tajiri, H. Shiohara, and F. Kusuhara. A new macroelement of reinforced concrete beam column joint for elasto-plastic plane frame analysis. In *Eighth National Conference of Earthquake Engineering, San Francisco, California*, number 1, 2006.

T. Takeda, M. A. Sozen, and N. N. Nielsen. Reinforced concrete response to simulated earthquakes. *Journal of the Structural Division, ASCE*, 96(ST12):2557–2573, 1970.

R. Tano, M. Klisinski, and Th. Olofsson. Stress locking in inner softening band method: a study of the origin and how to reduce the effect. In R. de Borst, H. Bićanić, H. Mang, and G. Meschke, editors, *Computational modeling of concrete structures*, pages 329–335. Balkema, Rotterdam, 1998.

T. P. Tassios. Theories of bond between concrete and steel under load cycles idealizing seismic action. In *Proceedings, AICAP-CEB Symposium, Rome, Italy*, pages 67–122, 1979.

G. I. Taylor. Plastic strain in metals. *Journal of the Institute of Metals*, 62:307–324, 1938.

M. Teraoka, Y. Kanoh, K. Tanaka, and K. Hayashi. Strength and deformation behavior of RC interior beam-column joint using high strength concrete. In *Proceedings, Second US-Japan-New Zealand-Canada multilateral meeting on structural performance of high strength concrete in seismic regions, Honolulu, Hawaii*, pages 1–14, 1994.

M. Teraoka, Y. Kanoh, K. Hayashi, and S. Sasaki. Behavior of interior beam-and-column subassemblages in an RC frame. In A. Azizinamini, D. Darwin, and C. French, editors, *Proceedings, First International Conference on High Strength Concrete, Kona, Hawaii*, pages 93–108, 1997.

E. Thorenfeldt, A. Tomaszewicz, and J. J. Jensen. Mechanical properties of high strength concrete and application in design. In *Symposium for utilization of high strength concrete, Tapir, Trondheim, Norway*, pages 149–159, 1987.

B. Thürlimann, J. Grob, and P. Luchinger. Torsion, biegung und schub in stahlbetontragern (torsion, flexure and shear in reinforced concrete girders). Technical report, Institute of Structural Engineering, ETH, Zurich, 1975.

T. N. Tjhin and D. A. Kuchma. Computer based tools for design by strut-and-tie methods:advances and challenges. *ACI Structural Journal*, 99(5):586–594, 2002.

R. A. Toupin. Elastic materials with couple stress. *Archive for Rational Mechanics and Analysis*, 11:385–414, 1962.

R. A. Toupin. Theories of elasticty with couple stress. *Archive for Rational Mechanics and Analysis*, 17:85–112, 1964.

S. R. Uma and A. M. Prasad. Seismic evaluation of RC moment resisting frame structures considering joint flexibility. In *Thirteenth World Conference on Earthquake Engineering, Vancouver, B.C. Canada*, number 2799, 2004.

S. R. Uma and A. M. Prasad. Analytical modeling of RC beam-column connections under cyclic load. In *Eleventh World Conference on Earthquake Engineering, Acapulco, Mexico*, number 1869, 1996.

H. Umemura and H. Aoyama. Evaluation of inelastic seismic deflection of RC frames based on tests of members. In *Fourth World Conference on Earthquake Engineering, Chile*, 1969.

J. van Mier. *Fracture processes of concrete*. CRC Press, LLC, Boca Raton, FL, 1997.

J. G. M. van Mier. *Strain softening of concrete under multiaxial loading conditions*. PhD thesis, Department of Civil Engineering, Eindhoven University of Technology, Eindhoven, The Netherlands, 1984.

I. Vardoulakis. Shear banding and liquefaction in granular materials on the basis of a cosserat continuum theory. *Archive of Applied Mechanics (Ingenieur Archiv)*, 59(2):106–113, 1989.

I. Vardoulakis and E. C. Aifantis. A gradient flow theory of plasticity for granular materials. *Acta Mechanica*, 87:197–217, 1991.

F. J. Vecchio. Disturbed stress field model for reinforced concrete: formulation. *Journal of Structural Engineering, ASCE*, 126(9):1070–1077, 2000.

F. J. Vecchio and M. P. Collins. The modified compression-field theory for reinforced concrete elements subjected to shear. *ACI Structural Journal*, 83(22):219–231, 1986.

F. J. Vecchio and M. P. Collins. Compression response of cracked reinforced concrete. *Journal of Structural Engineering, ASCE*, 119(12):3590–3610, 1993.

S. Viwathanatepa, E. P. Popov, and V. V. Bertero. Effects of generalized loadings on bond of reinforcing bars embedded in confined concrete blocks. Technical Report UCB/EERC-79/22, Earthquake Engineering Research Center, University of California, Berkeley, 1979.

R. L. Vollum and J. B. Newman. Strut and tie models for analysis/design of external beam-column joints. *Magazine of Concrete Research*, 51(6):415–425, 1999.

M. von Ramin and A. B. Matamoros. Effect of cyclic loading on the shear strength of reinforced concrete members. *ACI SP 236*, 2006a.

M. von Ramin and A. B. Matamoros. Shear strength of reinforced concrete members subjected to monotonic loads. *ACI Structural Journal*, 103(1):83–92, 2006b.

R. A. Vonk. *Softening of concrete loaded in compression*. PhD thesis, Department of Civil Engineering, Eindhoven University of Technology, Eindhoven, The Netherlands, 1992.

G. Z. Voyiadjis and R. J. Dorgan. Gradient formulation in coupled damage plasticity. *Archives of Mechanics*, 53:565–597, 2001.

S. G. Walker. Seismic performance of existing reinforced concrete beam-column joints. Master's thesis, Department of Civil Engineering, University of Washington, Seattle, 2001.

N. Wang. *Nonlinear fracture analysis of bond strength*. PhD thesis, Department of Civil Engineering, University of Calgary, Canada, 1993.

Q. B. Wang, P. L. J. Van Der Vorm, and J. Blaauwendraad. Failure of reinforced concrete panels - how accurate the models must be ? In N. Bićanić, editor, *Computer aided analysis and design of concrete structures*, pages 153–163. Pineridge Press, Swansea, U.K., 1990.

S. P. Washington, M. G. Karlaftis, and F. L. Mannering. *Statistical and econometric methods for transportation data analysis*. Chapman and Hall, CRC, 2003.

G. T. Will, S. M. Uzumeri, and S. K. Sinha. Application of finite element method to analysis of reinforced concrete beam-column joints. In *Proceedings of Specialty Conference on Finite Element Method in Civil Engineering, CSCE, EIC, Canada*, pages 745–766, 1972.

K. Willam and A. Dietsche. Regularization of localized failure computations. In E. Oñate, E. Hinton, and D. R. J. Owen, editors, *Proceedings of International Conference on Computational Plasticity COMPLAS III*, pages 2185–2204. Pineridge Press, Swansea, 1992.

K. Willam, N. Bićanic, and S. Sture. Composite fracture model for strain softening and localized failure of concrete. In E. Hinton and D. R. J. Owen, editors, *Computational Modeling of Reinforced Concrete Structures*, pages 122–153. Pineridge Press, Swansea, 1986.

K. Willam, E. Pramono, and S. Sture. Fundamental issues of smeared crack models. In S. P. Shah and S. E. Swartz, editors, *SEM-RILEM International Conference on Fracture of Concrete and Rock, SEM, Bethel*, pages 192–207, 1987.

K. Willam, T. Stankowski, K. Runesson, and S. Sture. Simulation issues of distributed and localized failure computations. In J. Mazars and Z. P. Bažant, editors, *Cracking and damage: Strain localization and size effect*, pages 363–378. Elsevier Applied Science, 1989.

K. Willam, A. Dietsche, M. M. Iordache, and P. Steinmann. Localization in micropolar continua. In H. B. Mühlhaus, editor, *Continuum models for materials with microstructure*, pages 297–339. John Wiley and Sons, Ltd. London, 1995.

K. J. Willam and E. P. Warnke. Constitutive model for triaxial behavior of concrete. In *Seminar on Concrete Structures subjected to Triaxial Stresses, IABSE Proc. 19, Paper III-1, Bergamo, Italy, May 1974*, 1975.

J. M. Wooldridge. *Econometric analysis of cross section and panel data*. The MIT Press, Cambridge, Massachusetts, 2002.

B. L. Yang, Y. F. Dafalias, and L. R. Herrmann. Bounding surface plasticity model for concrete. *Journal of the Engineering Mechanics, ASCE*, 111(3):359–380, 1985.

D. Z. Yankelevsky, M. A. Adin, and D. N. Farhey. Mathematical model for bond-slip behavior under cyclic loading. *ACI Structural Journal*, 89(6):692–698, 1992.

B. Yao. *Finite element analysis of distributed discrete concrete cracking*. PhD thesis, Department of Civil Engineering, University of Alberta, Canada, 1992.

S. Yazdani and H. L. Schreyer. Combined plasticity and damage mechanics model for plain concrete. *Journal of Engineering Mechanics Division, ASCE*, 116(7):1435–1450, 1990.

J. H. Yon, N. M. Hawkins, and A. S. Kobayashi. Strain-rate sesnsitivity of concrete material properties. *ACI Materials Journal*, 89(2):146–153, 1992.

M. Youssef and A. Ghobarah. Modeling of rc beam-column joints and structural walls. *Journal of Earthquake Engineering*, 5(1):93–111, 2001.

M. Youssef and A. Ghobarah. Strength deterioration due to bond slip and concrete crushing in modeling of reinforced concrete members. *ACI Structural Journal*, 96(6):956–967, 1999.

Y. M. Yun. Computer graphics for nonlinear strut-tie model approach. *Journal of Computing in Civil Engineering ASCE*, 14(2):127–133, 2000a.

Y. M. Yun. Nonlinear strut-tie model approach for structural concrete. *ACI Structural Journal*, 97(4):200–210, 2000b.

Y. M. Yun and J. A. Ramirez. Strength of struts and nodes in strut-tie model. *Journal of Structural Engineering, ASCE*, 112(1):20–29, 1996.

S. S. S. Zaid. *Behavior of reinforced concrete beam-column connections under earthquake loading*. PhD thesis, Department of Architecture, University of Tokyo, Japan, 2001.

H. M. Zbib and E. C. Aifantis. A gradient dependent flow theory of plasticity: application to metal and soil instability. *Applied Mechanics Review*, 42:295–304, 1989.

L. Zhang and J. O. Jirsa. A study of shear behavior for reinforced concrete beam column joints. Technical Report PMFSEL Report No. 82-1, Department of Civil Engineering, University of Texas at Austin, 1982.

L. Zhu, K. J. Elwood, and T. Haukaas. Assessment of expected failure mode for reinforced concrete columns. In *Eighth U.S. National Conference on Earthquake Engineering, San-Francisco, CA*, number 1001, 2006.

Appendix A

EXPERIMENTAL SPECIMEN DATA

Table A.1: Specimen geometry data

Specimen		Joint geometry (mm)			Beam geometry (mm)			Column geometry			aspect
		height	width	depth	length	depth	cover	length	depth	cover	ratio
		H_j	W_j	D_j	L_b	D_b	C_b	L_c	D_c	C_c	ι
Durrani &	X1	420	362	362	2498	280	51	2251	362	51	1.16
Wight	X2	420	362	362	2498	280	51	2251	362	51	1.16
(1982)	X3	420	362	362	2498	280	51	2251	362	51	1.16
Otani,	J1	300	300	300	2440	200	51	1280	300	51	1.00
Kobayashi	J2	300	300	300	2440	200	51	1280	300	51	1.00
& Aoyama	J3	300	300	300	2440	200	51	1280	300	51	1.00
(1984)	J4	300	300	300	2440	200	51	1280	300	51	1.00
	J5	300	300	300	2440	200	51	1280	300	51	1.00
	J6	300	300	300	2440	200	51	1280	300	51	1.00
Meinheit	U1	458	458	331	4883	280	35	3662	331	38	1.00
& Jirsa	U2	458	458	331	4883	280	35	3662	331	38	1.00
(1977)	U3	458	458	331	4883	280	35	3662	331	38	1.00
	U5	458	458	331	4883	280	35	3662	331	38	1.00
	U6	458	458	331	4883	280	35	3662	331	38	1.00
	U12	458	458	331	4883	280	35	3662	331	38	1.00
	U13	458	458	331	4883	280	35	3662	331	38	1.00
Walker,	PEER14	509	458	407	4069	407	38	2174	407	38	1.11
(2001) &	PEER22	509	458	407	4069	407	38	2174	407	38	1.11
Alire	PEER0850	509	458	407	4069	407	25	2174	407	25	1.11
(2002)	PEER0995	509	458	407	4069	407	25	2174	407	25	1.11
	PEER4150	509	458	407	4069	407	25	2174	407	25	1.11
Park &	U1	457	406	305	4238	229	42	2473	305	43	1.13
Ruitong	U2	457	406	305	4238	229	45	2473	305	44	1.13
(1988)	U3	457	406	305	4238	229	42	2473	305	43	1.13

continued on next page

continued from previous page

		H_j	W_j	D_j	L_b	D_b	C_b	L_c	D_c	C_c	ι
	U4	457	406	305	4238	229	45	2473	305	44	1.13
Noguchi &	J1	300	300	300	2700	200	35	1470	300	40	1.00
Kashiwazaki	J3	300	300	300	2700	200	35	1470	300	40	1.00
(1992)	J4	300	300	300	2700	200	35	1470	300	40	1.00
	J5	300	300	300	2700	200	35	1470	300	40	1.00
	J6	300	300	300	2700	200	35	1470	300	40	1.00
Oka &	J1	300	300	300	2860	240	30	1440	300	30	1.00
Shiohara	J2	300	300	300	2860	240	30	1440	300	30	1.00
(1992)	J4	300	300	300	2860	240	30	1440	300	30	1.00
	J5	300	300	300	2860	240	30	1440	300	30	1.00
	J6	300	300	300	2860	240	30	1440	300	30	1.00
	J7	300	300	300	2860	240	30	1440	300	30	1.00
	J8	300	300	300	2860	240	30	1440	300	30	1.00
	J10	300	300	300	2860	240	30	1440	300	30	1.00
	J11	300	300	300	2860	240	30	1440	300	30	1.00
Kitayama,	J1	300	300	300	2700	200	30	1470	300	30	1.00
Otani &	J6	300	300	300	2700	200	30	1470	300	30	1.00
Aoyama	C1	300	300	300	2700	200	30	1470	300	30	1.00
(1987)	C3	300	300	300	2700	200	30	1470	300	30	1.00
Park &	U1	457	406	305	5740	229	30	3217	305	42	1.13
Milburn (1983)	U2	457	406	305	5740	229	30	3217	305	42	1.13
Endoh, Kamura	HC	300	300	300	2700	200	30	1470	300	40	1.00
Otani &	HLC	300	300	300	2700	200	30	1470	300	40	1.00
Aoyama	LA1	300	300	300	2700	200	35	1470	300	40	1.00
(1991)	A1	300	300	300	2700	200	35	1470	300	40	1.00
Higashi &	SD35Aa-4	300	200	200	2000	150	30	1700	200	30	1.50
Ohwada	SD35Aa-7	300	200	200	2000	150	30	1700	200	30	1.50
(1969)	SD35Aa-8	300	200	200	2000	150	30	1700	200	30	1.50
	LSD35Aa-1	300	200	200	2000	150	30	1700	200	30	1.50
	LSD35Aa-2	300	200	200	2000	150	30	1700	200	30	1.50
	LSD35Ab-1	300	200	200	2000	150	30	1700	200	30	1.50
	LSD35Ab-2	300	200	200	2000	150	30	1700	200	30	1.50
Beckingsale	U11	610	457	457	4877	356	41	3354	457	43	1.33
(1980)	U12	610	457	457	4877	356	41	3354	457	43	1.33
Atalla &	SHC1	203	178	127	2102	127	20	832	127	20	1.14
Agababian	SHC2	203	178	127	2102	127	20	832	127	20	1.14
(2004)	SOC3	203	178	127	2102	127	20	832	127	20	1.14
Birss, Park	B1	610	457	457	5177	356	35	3430	457	40	1.33
& Paulay (1978)	B2	610	457	457	5177	356	35	3430	457	40	1.33

continued on next page

continued from previous page

		H_j	W_j	D_j	L_b	D_b	C_b	L_c	D_c	C_c	ι
Teraoka,	HJ1	400	400	400	3000	300	35	2000	400	40	1.00
Kanoh,	HJ2	400	400	400	3000	300	35	2000	400	40	1.00
Hayashi	HJ3	400	400	400	3000	300	35	2000	400	40	1.00
& Sasaki	HJ4	400	400	400	3000	300	35	2000	400	40	1.00
(1997)	HJ5	400	400	400	3000	300	35	2000	400	40	1.00
	HJ6	400	400	400	3000	300	35	2000	400	40	1.00
	HJ7	400	400	400	3000	300	35	2000	400	40	1.00
	HJ8	400	400	400	3000	300	35	2000	400	40	1.00
	HJ9	400	400	400	3000	300	35	2000	400	40	1.00
	HJ10	400	400	400	3000	300	35	2000	400	40	1.00
	HJ11	400	400	400	3000	300	35	2000	400	40	1.00
	HJ12	400	400	400	3000	300	35	2000	400	40	1.00
	HJ13	400	400	400	3000	300	35	2000	400	40	1.00
	HJ14	400	400	400	3000	300	35	2000	400	40	1.00
Hayashi,	NO43	400	400	400	3000	300	45	2000	400	45	1.00
Teraoka,	NO44	400	400	400	3000	300	45	2000	400	45	1.00
Mollick	NO45	400	400	400	3000	300	45	2000	400	45	1.00
& Kanoh	NO46	400	400	400	3000	300	45	2000	400	45	1.00
(1994)	NO47	400	400	400	3000	300	45	2000	400	45	1.00
	NO48	400	400	400	3000	300	45	2000	400	45	1.00
	NO49	400	400	400	3000	300	45	2000	400	45	1.00
	NO50	400	400	400	3000	300	45	2000	400	45	1.00
	HNO8	400	400	400	3000	300	45	2000	400	45	1.00
	HNO9	400	400	400	3000	300	45	2000	400	45	1.00
	HNO10	400	400	400	3000	300	45	2000	400	45	1.00
Teraoka,	HNO1	400	400	400	2800	300	45	1800	400	45	1.00
Kanoh,	HNO2	400	400	400	2800	300	45	1800	400	45	1.00
Tanaka &	HNO3	400	400	400	2800	300	45	1800	400	45	1.00
Hayashi	HNO4	400	400	400	2800	300	45	1800	400	45	1.00
(1994)	HNO5	400	400	400	2800	300	45	1800	400	45	1.00
	HNO6	400	400	400	2800	300	45	1800	400	45	1.00
Zaid	S1	300	300	300	2390	200	35	1020	300	35	1.00
(2001)	S2	300	300	300	2390	300	35	1020	300	35	1.00
	S3	300	300	300	2390	200	35	1020	300	35	1.00
Joh,	B1	350	300	300	3000	150	30	1750	300	30	1.17
Goto &	B2	350	300	300	3000	280	30	1750	300	30	1.17
Shibata	B8HH	350	300	300	3300	200	30	1750	300	30	1.17
(1991)	B8HL	350	300	300	3300	200	30	1750	300	30	1.17
	B8LH	350	300	300	3300	200	30	1750	300	30	1.17

continued on next page

continued from previous page											
		H_j	W_j	D_j	L_b	D_b	C_b	L_c	D_c	C_c	ι
	B8MH	350	300	300	3300	200	30	1750	300	30	1.17
	B9	350	300	300	3300	200	30	1750	300	30	1.17
	B10	350	300	300	3300	200	30	1750	300	30	1.17
	B11	350	300	300	3300	200	30	1750	300	30	1.17
Fujii &	A1	250	220	220	2000	160	25	1500	220	30	1.14
Morita	A2	250	220	220	2000	160	25	1500	220	30	1.14
(1991)	A3	250	220	220	2000	160	25	1500	220	30	1.14
	A4	250	220	220	2000	160	25	1500	220	30	1.14

where height of the joint, H_j, is equal to the in-plane height of the beam section; width of the joint, W_j, is equal to the in-plane height of the column section, D_c and D_b are the out-of-plane depth of the column and beam section respectively, and D_j is the depth of the joint taken equal to the maximum of D_b and D_c. L_b is the total length of beams and L_c the total height of the columns. The term ι is defined in chapter 2 and represents the aspect ratio of the joint.

Table A.2: Specimen material data (concrete compressive strength and beam reinforcement details)

Specimen	Concrete	Beam reinforcement details									
	f_c	Top longitudinal			Bottom longitudinal			Transverse			ϖ
		d_{b_bt}	f_{y_bt}	nb_{bt}	d_{b_bb}	f_{y_bb}	nb_{bb}	A_{s_bhp}	f_{y_bhp}	sp_{bhp}	
	MPa	mm	MPa		mm	MPa		mm^2	MPa	mm	
DW-X1	34.34	22	331	4	19	345	4	71	337	89	1.31
DW-X2	33.66	22	331	4	19	345	4	71	337	89	1.31
DW-X3	31.03	22	331	3	19	345	3	71	337	89	1.31
OKA-J1	25.70	13	401	8	13	401	4	28	368	50	2.00
OKA-J2	24.03	13	401	8	13	401	4	28	368	50	2.00
OKA-J3	24.03	13	401	8	13	401	4	28	368	50	2.00
OKA-J4	25.70	13	401	8	13	401	4	28	368	50	2.00
OKA-J5	28.74	13	401	8	13	401	4	28	368	50	2.00
OKA-J6	28.74	13	346	4	13	346	3	28	368	100	1.33
MJ-U1	26.21	32	449	3	25	406	3	71	485	89	1.79
MJ-U2	41.79	32	449	3	25	406	3	71	485	89	1.79
MJ-U3	26.62	32	449	3	25	406	3	71	485	89	1.79
MJ-U5	35.86	32	449	3	25	406	3	71	485	89	1.79
MJ-U6	36.76	32	449	3	25	406	3	71	485	89	1.79
MJ-U12	35.17	32	449	3	25	406	3	71	485	89	1.79
MJ-U13	41.31	32	449	3	25	406	3	71	485	89	1.79
W-PEER14	31.77	22	423	4	16	503	4	129	662	89	1.65
W-PEER22	38.41	22	528	6	22	528	4	129	662	89	1.50
A-PEER0850	34.97	22	504	2	22	504	2	129	536	89	1.00
A-PEER0995	60.46	22	504	5	22	504	3	129	536	89	1.67
A-PEER4150	32.99	29	541	6	29	545	6	129	536	89	0.99
PR-U1	45.89	16	294	5	16	294	2	28	282	80	2.50
PR-U2	36.00	28	314	2	20	300	2	38	364	80	2.05
PR-U3	36.19	16	294	5	16	294	2	28	282	80	2.50
PR-U4	40.10	28	314	2	20	300	2	38	364	80	2.05
NK-J1	70.00	13	718	9	13	718	7	28	955	50	1.29
NK-J3	107.00	13	718	10	13	718	10	28	955	50	1.00
NK-J4	70.00	13	718	9	13	718	7	28	955	50	1.29
NK-J5	70.00	13	718	10	13	718	10	28	955	50	1.00
NK-J6	53.50	13	718	8	13	718	7	28	955	50	1.14

continued on next page

continued from previous page

	f_c	d_{b_bt}	f_{y_bt}	nb_{bt}	d_{b_bb}	f_{y_bb}	nb_{bb}	A_{s_bhp}	f_{y_bhp}	sp_{bhp}	ϖ
OS-J1	81.20	13	638	9	13	638	7	28	1374	50	1.29
OS-J2	81.20	13	1456	8	13	1456	8	28	1374	50	1.00
OS-J4	72.80	13	515	10	13	515	10	28	1374	50	1.00
OS-J5	72.80	13	839	9	13	839	7	28	1374	50	1.29
OS-J6	79.20	13	676	9	13	676	7	28	775	50	1.29
OS-J7	79.20	13	676	7	13	676	5	28	857	50	1.40
OS-J8	79.20	19	370	9	19	370	7	28	775	50	1.29
OS-J10	39.20	13	700	9	13	700	7	28	598	50	1.29
OS-J11	39.20	19	372	9	19	372	7	28	401	50	1.29
KOA-J1	25.69	13	401	8	13	401	4	28	368	50	2.00
KOA-J6	25.69	13	346	4	13	346	3	28	324	100	1.33
KOA-C1	25.60	10	320	12	10	320	6	28	324	50	2.00
KOA-C3	25.60	10	320	12	10	320	6	28	324	50	2.00
PM-U1	41.30	16	315	8	16	315	8	79	321	89	1.00
PM-U2	46.90	20	307	4	20	307	4	79	321	125	1.00
EKOA-HC	41.48	10	374	12	10	374	12	28	420	50	1.00
EKOA-HLC	40.60	10	368	12	10	368	12	28	373	50	1.00
EKOA-LA1	34.81	13	801	8	13	801	4	28	420	40	2.00
EKOA-A1	30.60	13	780	8	13	780	4	28	422	40	2.00
HO-SD35Aa-4	30.40	10	419	3	10	419	3	13	350	50	1.00
HO-SD35Aa-7	38.05	10	400	3	10	400	3	13	350	50	1.00
HO-SD35Aa-8	38.05	10	400	3	10	400	3	13	350	50	1.00
HO-LSD35Aa-1	41.09	10	400	3	10	400	3	13	350	50	1.00
HO-LSD35Aa-2	41.09	10	400	3	10	400	3	13	350	50	1.00
HO-LSD35Ab-1	41.09	10	400	3	10	400	3	13	350	50	1.00
HO-LSD35Ab-2	41.09	10	400	3	10	400	3	13	350	50	1.00
B-U11	35.90	19	298	8	19	298	4	31	330	76	2.00
B-U12	34.60	19	298	6	19	298	6	31	330	76	1.00
AA-SHC1	56.54	10	413	3	10	413	3	32	551	76	1.00
AA-SHC2	59.55	10	413	3	10	413	3	32	551	76	1.00
AA-SOC3	47.20	10	413	3	10	413	3	32	551	76	1.00
BPP-B1	27.90	20	288	8	20	288	8	33	398	75	1.00
BPP-B2	31.52	20	288	8	20	288	8	33	398	75	1.00
TKHS-HJ1	53.98	19	382	4	19	382	4	32	312	75	1.00
TKHS-HJ2	53.98	16	624	4	16	624	4	32	312	75	1.00
TKHS-HJ3	53.98	19	858	2	19	858	2	32	347	85	1.00
TKHS-HJ4	53.98	19	382	6	19	382	6	32	608	100	1.00
TKHS-HJ5	53.98	19	645	4	19	645	4	32	608	100	1.00
TKHS-HJ6	53.98	19	858	3	19	858	3	32	608	75	1.00

continued on next page

continued from previous page

	f_c	d_{b_bt}	f_{y_bt}	nb_{bt}	d_{b_bb}	f_{y_bb}	nb_{bb}	A_{s_bhp}	f_{y_bhp}	sp_{bhp}	ϖ
TKHS-HJ7	88.33	22	422	6	22	422	6	32	608	75	1.00
TKHS-HJ8	88.33	22	599	4	22	599	4	32	608	75	1.00
TKHS-HJ9	88.33	19	858	4	19	858	4	32	608	75	1.00
TKHS-HJ10	88.33	16	611	8	16	611	8	32	608	80	1.00
TKHS-HJ11	88.33	22	441	8	22	441	8	32	608	60	1.00
TKHS-HJ12	88.33	22	604	8	22	604	8	32	608	50	1.00
TKHS-HJ13	117.77	18	623	8	18	623	8	32	608	60	1.00
TKHS-HJ14	117.77	22	604	8	22	604	8	32	608	50	1.00
HTMK-NO43	54.27	19	383	4	19	383	4	28	312	75	1.00
HTMK-NO44	54.27	16	624	4	16	624	4	28	312	75	1.00
HTMK-NO45	54.27	22	599	4	22	599	4	28	312	75	1.00
HTMK-NO46	54.27	19	858	2	19	858	2	79	347	85	1.00
HTMK-NO47	54.27	19	382	6	19	382	6	28	755	100	1.00
HTMK-NO48	54.27	19	645	4	19	645	4	28	755	100	1.00
HTMK-NO49	54.27	22	599	5	22	599	5	28	755	100	1.00
HTMK-NO50	54.27	19	858	3	19	858	3	28	755	75	1.00
HTMK-HNO8	87.97	22	422	6	22	422	6	28	755	75	1.00
HTMK-HNO9	87.97	22	599	4	22	599	4	28	755	75	1.00
HTMK-HNO10	87.97	19	858	4	19	858	4	28	755	75	1.00
TKTH-HNO1	88.72	16	611	8	16	611	8	28	604	80	1.00
TKTH-HNO2	88.72	16	611	8	16	611	8	28	604	60	1.00
TKTH-HNO3	88.72	22	442	8	22	442	8	28	604	60	1.00
TKTH-HNO4	88.72	22	605	8	22	605	8	28	604	50	1.00
TKTH-HNO5	116.98	18	623	8	18	623	8	28	604	60	1.00
TKTH-HNO6	116.98	22	605	8	22	605	8	28	604	50	1.00
Z-S1	24.02	10	390	5	10	390	5	32	390	50	1.00
Z-S2	24.02	12	355	12	12	355	12	32	390	50	1.00
Z-S3	24.02	16	465	5	16	465	5	32	390	50	1.00
JGS-B1	21.20	13	371	3	13	371	3	28	307	100	1.00
JGS-B2	22.54	13	371	3	13	371	3	28	307	100	1.00
JGS-B8HH	25.61	13	404	3	13	404	3	28	377	50	1.00
JGS-B8HL	27.41	13	404	3	13	404	3	28	377	100	1.00
JGS-B8LH	26.90	13	404	3	13	404	3	28	377	50	1.00
JGS-B8MH	28.11	13	404	3	13	404	3	28	377	50	1.00
JGS-B9	25.60	13	404	3	13	404	3	28	377	100	1.00
JGS-B10	24.90	13	404	3	13	404	3	28	377	100	1.00
JGS-B11	25.90	13	404	3	13	404	3	28	377	100	1.00
FM-A1	40.22	10	1069	8	10	1069	8	28	291	80	1.00
FM-A2	40.22	10	409	8	10	409	8	28	291	80	1.00

continued on next page

continued from previous page											
	f_c	d_{b_bt}	f_{y_bt}	nb_{bt}	d_{b_bb}	f_{y_bb}	nb_{bb}	A_{s_bhp}	f_{y_bhp}	sp_{bhp}	ϖ
FM-A3	40.22	10	1069	8	10	1069	8	28	291	80	1.00
FM-A4	40.22	10	1069	8	10	1069	8	28	291	80	1.00

where f_c represents concrete compressive stress, $(\cdot)_{bt}$ represents the parameters for top longitudinal beam bar, $(\cdot)_{bb}$ represents parameters for bottom longitudinal beam bars and $(\cdot)_{bhp}$ represent parameters for longitudinal beam hoop steel. The terms d_b represents the diameter of the longitudinal bar, f_y represents the yield stress of the bar, nb the number of bars, sp the spacing of hoop steel, A_s the cross-sectional area of the transverse steel. The term $varpi$ has been defined in chapter 2 and represents the ratio of top longitudinal beam bar force the bottom longitudinal beam bar force at yield.

Table A.3: Specimen material data (Column and joint reinforcement details)

Specimen	Column reinforcement						Joint reinforcement				
	Longitudinal			Transverse			Hoop				
	d_{b_col} mm	f_{y_col} MPa	nb_{col}	A_{s_chp} mm^2	f_{y_chp} MPa	sp_{chp} mm	d_{b_jhp} mm	f_{y_jhp} MPa	sp_{jhp} mm	n_{jhp}	config.
DW-X1	25	414	8	129	352	89	13	352	153	2	2SD
DW-X2	25	414	8	129	352	89	13	352	76	3	2SD
DW-X3	22	331	8	129	352	89	13	352	153	2	2SD
OKA-J1	13	401	16	28	368	80	6	368	75	3	2S
OKA-J2	13	401	16	28	368	80	6	368	75	3	4S
OKA-J3	13	401	16	28	368	80	6	368	25	7	4S
OKA-J4	13	401	16	28	368	80	6	368	75	3	2S
OKA-J5	13	401	10	28	368	80	6	368	75	3	2S
OKA-J6	10	362	12	28	368	50	6	368	50	5	2S
MJ-U1	22	457	8	129	409	89	13	409	153	2	2S
MJ-U2	32	449	8	129	409	89	13	409	153	2	2S
MJ-U3	36	402	10	129	409	89	13	409	153	2	2S
MJ-U5	32	449	8	129	409	89	13	409	153	2	2S
MJ-U6	32	449	8	129	409	89	13	409	153	2	2S
MJ-U12	32	449	8	129	409	89	16	423	51	6	2S
MJ-U13	32	449	8	129	409	89	13	409	51	6	2S
W-PEER14	22	423	8	129	662	89	0	0	0	0	0
W-PEER22	29	538	8	129	662	89	0	0	0	0	0
A-PEER0850	13	537	8	129	536	89	0	0	0	0	0
A-PEER0995	19	505	8	129	536	89	0	0	0	0	0
A-PEER4150	29	545	10	129	536	89	0	0	0	0	0
PR-U1	16	498	8	28	282	60	12	283	75	5	2SD
PR-U2	20	476	8	38	364	60	12	283	80	5	2SD
PR-U3	16	498	8	28	282	60	6	282	75	5	2SD
PR-U4	20	476	8	38	364	60	10	320	80	5	2SD
NK-J1	13	718	20	28	955	40	6	955	50	3	4S
NK-J3	13	718	22	28	955	40	6	955	50	3	4S
NK-J4	13	718	20	28	955	40	6	955	50	3	4S
NK-J5	13	718	24	28	955	40	6	955	50	3	4S
NK-J6	13	718	20	28	955	40	6	955	50	3	4S

continued on next page

continued for previous page

	d_{b_col}	f_{y_col}	nb_{col}	A_{s_chp}	f_{y_chp}	sp_{chp}	d_{b_jhp}	f_{y_jhp}	sp_{jhp}	n_{jhp}	config.
OS-J1	13	638	24	28	1374	50	6	1374	50	5	2S
OS-J2	13	1456	24	28	1374	50	6	1374	50	5	2S
OS-J4	13	515	24	28	1374	50	6	1374	50	5	2S
OS-J5	13	839	24	28	1374	50	6	1374	50	5	2S
OS-J6	13	676	24	28	775	50	6	775	100	3	2S
OS-J7	13	676	24	28	857	50	6	857	50	5	2S
OS-J8	19	370	24	28	775	50	6	775	50	5	2S
OS-J10	13	700	24	28	598	50	6	598	50	5	2S
OS-J11	19	372	24	28	401	50	6	401	50	5	2S
KOA-J1	13	401	16	28	375	80	6	368	70	3	2S
KOA-J6	10	320	12	28	375	80	6	324	50	5	2S
KOA-C1	13	422	16	28	335	50	6	324	70	3	2S
KOA-C3	13	422	16	28	335	50	10	324	45	5	4S
PM-U1	24	473	6	79	321	60	16	320	52	8	3S
PM-U2	24	473	6	79	321	60	16	320	65	6	3S
EKOA-HC	16	369	12	28	420	50	6	282	60	2	2S
EKOA-HLC	16	360	12	28	373	50	6	290	60	2	2S
EKOA-LA1	16	550	16	28	420	40	6	286	45	3	2S
EKOA-A1	16	539	16	28	422	40	6	320	45	3	2S
HO-SD35Aa-4	10	419	8	13	350	40	4	350	60	5	2S
HO-SD35Aa-7	10	400	8	13	350	40	4	350	60	5	2S
HO-SD35Aa-8	10	400	8	13	350	40	4	350	60	5	2S
HO-LSD35Aa-1	10	400	8	13	350	40	4	350	60	5	2S
HO-LSD35Aa-2	10	400	8	13	350	40	4	350	60	5	2S
HO-LSD35Ab-1	10	400	8	13	350	40	4	350	60	5	2S
HO-LSD35Ab-2	10	400	8	13	350	40	4	350	60	5	2S
B-U11	22	423	12	127	336	50	13	336	68	8	4S
B-U12	22	422	12	127	336	50	13	336	68	8	4S
AA-SHC1	13	413	4	32	551	51	6	551	100	1	2S
AA-SHC2	13	413	4	32	551	51	6	551	50	2	2S
AA-SOC3	13	413	4	32	551	51	6	551	50	2	2S
BPP-B1	24	427	12	127	346	120	13	346	153	4	4S
BPP-B2	24	427	12	33	398	120	7	398	153	4	4S
TKHS-HJ1	19	383	12	71	347	100	10	347	50	8	2S
TKHS-HJ2	19	383	12	71	347	100	10	347	50	8	2S
TKHS-HJ3	19	383	12	71	347	100	10	347	50	8	2S
TKHS-HJ4	19	646	12	71	347	100	10	347	50	8	2S
TKHS-HJ5	19	646	12	71	347	100	10	347	50	8	2S
TKHS-HJ6	19	646	12	71	347	100	10	347	50	8	2S

continued on next page

continued for previous page

	d_{b_col}	f_{y_col}	nb_{col}	A_{s_chp}	f_{y_chp}	sp_{chp}	d_{b_jhp}	f_{y_jhp}	sp_{jhp}	n_{jhp}	config.
TKHS-HJ7	19	646	12	71	347	100	8	681	50	8	2SD
TKHS-HJ8	19	646	12	71	347	100	8	681	50	8	2SD
TKHS-HJ9	19	646	12	71	347	100	8	681	50	8	2SD
TKHS-HJ10	21	614	12	71	343	50	8	681	50	8	2SD
TKHS-HJ11	21	442	12	71	343	50	8	681	50	8	2SD
TKHS-HJ12	21	614	12	71	343	50	8	681	50	8	2SD
TKHS-HJ13	21	614	12	71	343	50	8	681	50	8	2SD
TKHS-HJ14	21	614	12	71	343	50	8	681	50	8	2SD
HTMK-NO43	19	383	12	79	347	100	10	347	50	8	2S
HTMK-NO44	19	383	12	79	347	100	10	347	50	8	2S
HTMK-NO45	19	383	12	79	347	100	10	347	50	8	2S
HTMK-NO46	19	383	12	79	347	100	10	347	50	8	2S
HTMK-NO47	19	645	12	79	347	100	10	347	50	8	2S
HTMK-NO48	19	645	12	79	347	100	10	347	50	8	2S
HTMK-NO49	19	645	12	79	347	100	10	347	50	8	2S
HTMK-NO50	19	645	12	79	347	100	10	347	50	8	2S
HTMK-HNO8	19	645	12	79	347	100	8	797	50	8	2SD
HTMK-HNO9	19	645	12	79	347	100	8	797	50	8	2SD
HTMK-HNO10	19	645	12	79	347	100	8	797	50	8	2SD
TKTH-HNO1	22	610	12	79	343	50	8	681	50	8	2SD
TKTH-HNO2	22	610	12	79	343	50	8	681	50	8	2SD
TKTH-HNO3	22	442	12	79	343	50	8	681	50	8	2SD
TKTH-HNO4	22	610	12	79	343	50	8	681	50	8	2SD
TKTH-HNO5	22	610	12	79	343	50	8	681	50	8	2SD
TKTH-HNO6	22	610	12	79	343	50	8	681	50	8	2SD
Z-S1	19	450	12	32	390	40	6	390	60	4	2S
Z-S2	19	450	12	32	390	40	6	390	60	4	2S
Z-S3	19	450	12	32	390	40	6	390	60	4	2S
JGS-B1	13	371	8	28	307	50	6	307	88	3	2S
JGS-B2	13	371	8	28	307	50	6	307	88	6	4S
JGS-B8HH	13	404	14	28	377	50	5	1320	43	6	4S
JGS-B8HL	13	404	14	28	377	50	5	1320	43	6	4S
JGS-B8LH	13	404	14	28	377	50	6	377	88	3	2S
JGS-B8MH	13	404	14	28	377	50	6	377	45	5	2S
JGS-B9	13	404	14	28	377	50	5	1320	43	6	4S
JGS-B10	13	404	14	28	377	50	5	1320	43	6	4S
JGS-B11	13	404	14	28	377	50	5	1320	43	6	4S
FM-A1	13	644	16	28	291	80	6	291	60	3	2S
FM-A2	13	388	16	28	291	80	6	291	60	3	2S

continued on next page

continued for previous page											
	d_{b_col}	f_{y_col}	nb_{col}	A_{s_chp}	f_{y_chp}	sp_{chp}	d_{b_jhp}	f_{y_jhp}	sp_{jhp}	n_{jhp}	config.
FM-A3	13	644	16	28	291	80	6	291	60	3	2S
FM-A4	13	644	16	28	291	80	6	291	45	4	4S

where $(\cdot)_{col}$ represents parameters for the longitudinal column steel, $(\cdot)_{chp}$ represents parameters for the column hoop steel, $(\cdot)_{jhp}$ represents parameters for the joint stirrup steel. The terms d_b represents the diameter of the longitudinal bar, f_y represents the yield stress of the bar, nb the number of bars, sp the spacing of hoop steel, A_s the cross-sectional area of the transverse steel, n the actual number of hoop steel in that region. The term $config$ represents the pattern of arrangement of the stirrup steel in the joint, where S refers to a square orientation, SD refers to a square and diamond orientation and numbers associated with them represents the number of legs of the stirrups.

Table A.4: Specimen drift and load data

Specimen	Ax ld		Drft mx	Lat ld		Fail	Str los	Fail	Drft	Str lss	Drft
	Ttl	Rat	lat ld	mx	yld	int	lst cyc	mech	cap	drft cap	lst cyc
	P	p	D_{mx}	V_{mx}	V_{yld}	F_{int}	Sl_{mx}	F_{mch}	D_{cap}	Sl_{dcap}	D_{lst}
	N		%	N	N		%		%	%	%
DW-X1	244750	0.05	2.54	191350	128015	B	24.36	BYJF	5.08	16.28	5.93
DW-X2	244750	0.06	3.38	200250	128030	B	19.45	BY	5.86	19.45	5.86
DW-X3	214490	0.05	3.67	160200	97660	B	13.89	BY	5.88	13.89	5.88
OKA-J1	176168	0.08	5.00	114509	77338	B	18.19	BY	7.50	18.19	7.50
OKA-J2	176168	0.08	5.00	118532	77271	B	17.20	BY	7.50	17.20	7.50
OKA-J3	176168	0.08	5.00	131582	77271	B	15.77	BY	7.50	15.77	7.50
OKA-J4	704672	0.30	2.50	111860	77338	B	39.00	BYJF	5.00	8.30	7.50
OKA-J5	176168	0.07	3.78	133447	77939	B	36.41	BYJF	5.00	1.00	7.50
OKA-J6	528504	0.20	2.50	98067	50040	B	30.00	BYJF	5.00	15.00	7.50
MJ-U1	1588650	0.40	NA	108160	162460	J	NA	JF	NA	NA	NA
MJ-U2	1602000	0.25	NA	158222	163393	J	NA	JF	NA	NA	NA
MJ-U3	1584200	0.39	NA	121139	162485	J	NA	JF	NA	NA	NA
MJ-U5	213600	0.04	NA	152042	163005	J	NA	JF	NA	NA	NA
MJ-U6	2683350	0.48	NA	163785	163062	J	NA	JF	NA	NA	NA
MJ-U12	1615350	0.30	NA	192524	162960	B	NA	BYJF	NA	NA	NA
MJ-U13	1570850	0.25	NA	153896	163361	J	NA	JF	NA	NA	NA
W-PEER14	590293	0.10	2.83	267227	157761	B	33.38	BYJF	4.00	11.60	5.00
W-PEER22	713869	0.10	1.89	359606	325198	B	38.13	BYJF	4.00	18.75	5.00
A-PEER0850	649789	0.10	2.83	209328	188279	B	4.34	BY	5.00	4.34	5.00
A-PEER0995	1123581	0.10	2.53	415800	281781	B	25.08	BYJF	4.00	16.00	5.00
A-PEER4150	612988	0.10	1.69	560700	732233	J	40.48	JF	3.00	4.00	5.00
PR-U1	110000	0.02	4.25	80300	40463	B	0.00	BY	4.25	0.00	4.25
PR-U2	134000	0.03	3.03	111700	71433	B	15.00	BY	4.25	15.00	4.25
PR-U3	110000	0.02	2.43	79400	40244	B	12.00	BY	4.25	12.00	4.25
PR-U4	134000	0.03	3.03	106500	71925	B	25.00	BYJF	3.64	2.00	4.25
NK-J1	756000	0.12	2.04	236470	233613	B	31.23	BYJF	4.08	15.34	5.10
NK-J3	1155600	0.12	3.06	300000	316469	J	15.15	JF	5.10	15.15	5.10
NK-J4	756000	0.12	3.06	249700	233613	B	21.29	BYJF	4.08	6.00	5.10
NK-J5	756000	0.12	3.06	245690	312147	J	36.04	JF	4.08	16.68	5.10
NK-J6	577800	0.12	3.06	217760	229945	J	28.42	JF	4.08	17.34	5.10

continued on next page

continued for previous page

	P	p	D_{mx}	V_{mx}	V_{yld}	F_{int}	Sl_{mx}	F_{mch}	D_{cap}	Sl_{dcap}	D_{lst}
OS-J1	834000	0.11	3.00	257000	198703	B	23.68	BYJF	4.00	10.89	5.00
OS-J2	834000	0.11	3.00	276000	506902	J	8.63	JF	5.00	8.63	5.00
OS-J4	834000	0.13	3.00	265000	221177	B	18.58	BY	5.00	18.58	5.00
OS-J5	834000	0.13	3.00	297000	257380	B	24.06	BYJF	4.00	8.42	5.00
OS-J6	834000	0.12	3.00	274000	208393	B	24.84	BYJF	4.00	12.04	5.00
OS-J7	834000	0.12	3.00	219000	164031	B	10.00	BY	5.00	10.00	5.00
OS-J8	834000	0.12	2.00	311000	254093	B	36.94	BYJF	3.00	10.62	5.00
OS-J10	417000	0.12	2.00	196000	210975	J	28.55	JF	4.00	17.35	5.00
OS-J11	417000	0.12	2.00	232000	244500	J	40.82	JF	3.00	10.78	5.00
KOA-J1	176520	0.08	4.35	114738	78065	B	15.00	BY	6.12	15.00	6.12
KOA-J6	176520	0.08	2.18	82000	49024	B	32.00	BYJF	4.08	12.50	6.12
KOA-C1	176520	0.08	4.35	100000	82526	B	3.00	BY	7.14	3.00	7.14
KOA-C3	176520	0.08	4.35	98039	82526	B	2.00	BY	7.14	2.00	7.14
PM-U1	511418	0.10	4.18	128735	121437	B	10.00	BY	6.56	10.00	6.56
PM-U2	580763	0.10	4.18	140065	107011	B	31.00	BYJF	6.56	1.00	8.44
EKOA-HC	176520	0.05	4.35	126702	107566	B	3.56	BY	6.53	3.56	6.53
EKOA-HLC	176520	0.05	2.18	126702	105766	B	27.40	BYJF	4.35	5.00	6.53
EKOA-LA1	176520	0.06	4.08	159848	144630	J	18.24	JF	6.67	18.24	6.67
EKOA-A1	176520	0.06	4.08	150042	139698	J	12.89	JF	6.67	12.89	6.67
HO-SD35Aa-4	78453	0.06	1.18	25497	31359	J	NA	JF	NA	NA	NA
HO-SD35Aa-7	78453	0.05	1.18	24615	30186	J	NA	JF	NA	NA	NA
HO-SD35Aa-8	156906	0.10	2.35	25497	30186	J	NA	JF	NA	NA	NA
HO-LSD35Aa-1	78453	0.05	1.18	24811	30211	J	9.00	JF	NA	NA	NA
HO-LSD35Aa-2	156906	0.10	2.35	23732	30237	J	NA	JF	NA	NA	NA
HO-LSD35Ab-1	78453	0.05	1.18	24468	30237	J	NA	JF	NA	NA	NA
HO-LSD35Ab-2	156906	0.10	2.35	22800	30237	J	NA	JF	NA	NA	NA
B-U11	311000	0.04	3.81	181223	116981	B	NA	BY	NA	NA	NA
B-U12	311000	0.04	3.81	180706	165556	B	NA	BY	NA	NA	NA
AA-SHC1	58000	0.05	NA	17000	40021	J	NA	JF	NA	NA	NA
AA-SHC2	58000	0.04	NA	16800	38998	J	NA	JF	NA	NA	NA
AA-SOC3	58000	0.05	NA	16000	39015	J	NA	JF	NA	NA	NA
BPP-B1	311000	0.05	1.91	242000	229428	B	6.44	BY	3.60	6.44	3.60
BPP-B2	2890000	0.44	1.69	242500	229767	B	12.86	BY	3.18	12.86	3.18
TKHS-HJ1	1725970	0.20	4.00	197114	166820	B	2.98	BY	7.50	2.98	7.50
TKHS-HJ2	1725970	0.20	4.00	219669	196137	B	19.64	BY	7.50	19.64	7.50
TKHS-HJ3	1725970	0.20	2.00	197114	190573	B	5.47	BY	7.50	5.47	7.50
TKHS-HJ4	1725970	0.20	2.00	253012	235735	B	37.98	BYJF	4.00	18.58	7.50
TKHS-HJ5	1725970	0.20	3.00	296161	284383	B	8.83	BY	7.50	8.83	7.50
TKHS-HJ6	1725970	0.20	3.00	286354	283042	B	29.81	BYJF	4.00	10.00	7.50

continued on next page

continued for previous page

	P	p	D_{mx}	V_{mx}	V_{yld}	F_{int}	Sl_{mx}	F_{mch}	D_{cap}	Sl_{dcap}	D_{lst}
TKHS-HJ7	2824315	0.20	2.00	375595	351568	B	14.80	BY	7.50	14.80	7.50
TKHS-HJ8	2824315	0.20	4.00	395208	354580	B	10.68	BY	7.50	10.68	7.50
TKHS-HJ9	2824315	0.20	2.00	382459	380483	B	24.18	BYJF	5.00	14.20	8.00
TKHS-HJ10	2824315	0.20	2.00	444241	356161	B	5.46	BY	8.00	5.46	8.00
TKHS-HJ11	2824315	0.20	2.00	580554	470316	B	20.76	BYJF	4.00	12.30	8.00
TKHS-HJ12	2824315	0.20	3.00	680582	641715	B	30.94	BYJF	4.00	12.20	8.00
TKHS-HJ13	3765754	0.20	4.00	541327	437466	B	11.33	BY	8.00	11.33	8.00
TKHS-HJ14	3765754	0.20	3.00	713924	672078	B	34.17	BYJF	4.00	20.00	8.00
HTMK-NO43	1600000	0.18	4.00	197114	162138	B	5.13	BY	7.00	5.13	7.00
HTMK-NO44	1600000	0.18	NA	219914	188208	B	NA	NA	NA	NA	NA
HTMK-NO45	1600000	0.18	NA	261838	331618	J	NA	JF	NA	NA	NA
HTMK-NO46	1600000	0.18	2.00	197114	184035	B	19.84	BY	7.00	19.84	7.00
HTMK-NO47	1600000	0.18	2.00	253012	225833	B	33.57	BYJF	4.00	10.78	7.00
HTMK-NO48	1600000	0.18	NA	295671	271719	B	NA	NA	NA	NA	NA
HTMK-NO49	1600000	0.18	4.00	373633	381483	B	31.86	BYJF	4.00	0.00	7.00
HTMK-NO50	1600000	0.18	NA	286109	272340	B	NA	NA	NA	NA	NA
HTMK-HNO8	2824315	0.20	NA	375104	335413	B	NA	NA	NA	NA	NA
HTMK-HNO9	2824315	0.20	NA	394963	339503	B	NA	NA	NA	NA	NA
HTMK-HNO10	2824315	0.20	NA	382459	363721	B	NA	NA	NA	NA	NA
TKTH-HNO1	2353596	0.17	2.00	448262	386072	J	12.49	JF	8.00	12.49	8.00
TKTH-HNO2	2353596	0.17	3.00	644395	386072	B	8.69	BY	8.00	8.69	8.00
TKTH-HNO3	2353596	0.17	2.00	588399	501934	J	23.82	JF	4.00	19.10	8.00
TKTH-HNO4	2353596	0.17	3.00	672442	680576	J	33.34	JF	4.00	8.00	8.00
TKTH-HNO5	2353596	0.13	3.00	560352	481759	J	9.99	JF	8.00	9.99	8.00
TKTH-HNO6	2353596	0.13	3.00	728536	697384	J	38.47	JF	4.00	15.40	8.00
Z-S1	100000	0.05	3.00	73000	80935	J	17.81	JF	4.00	17.81	4.00
Z-S2	100000	0.05	3.00	79000	209837	J	4.00	JF	4.00	4.00	4.00
Z-S3	100000	0.05	2.00	131000	223265	J	15.30	JF	4.00	15.30	4.00
JGS-B1	308909	0.16	3.00	59821	53367	B	9.83	BYJF	5.00	9.83	5.00
JGS-B2	308909	0.15	2.00	64724	55045	B	0.00	BYJF	5.00	0.00	5.00
JGS-B8HH	353000	0.15	3.00	65000	58439	B	38.46	BYJF	5.00	4.60	5.50
JGS-B8HL	353000	0.14	2.50	68000	58615	B	30.88	BYJF	4.00	11.76	5.50
JGS-B8LH	353000	0.15	3.00	68000	58565	B	26.47	BYJF	5.00	11.76	5.50
JGS-B8MH	353000	0.14	2.50	65000	58683	B	23.07	BYJF	4.00	7.70	5.50
JGS-B9	353000	0.15	5.00	75750	58439	B	0.00	BY	5.50	0.00	5.50
JGS-B10	353000	0.16	5.00	84000	58371	B	6.67	BY	5.50	6.67	5.50
JGS-B11	353000	0.15	5.00	85700	58468	B	5.40	BY	5.50	0.00	5.50
FM-A1	147150	0.08	2.00	48069	162139	J	12.30	JF	3.33	12.30	3.33
FM-A2	147150	0.08	3.33	44636	63546	J	0.00	JF	3.33	0.00	3.33

continued on next page

continued for previous page											
	P	p	D_{mx}	V_{mx}	V_{yld}	F_{int}	Sl_{mx}	F_{mch}	D_{cap}	Sl_{dcap}	D_{lst}
FM-A3	441450	0.23	2.00	48069	162139	J	18.39	JF	3.33	18.39	3.33
FM-A4	441450	0.23	2.00	49050	162139	J	16.02	JF	3.33	16.02	3.33

where P represents the total axial load applied to the specimen, p (as described in chapter 2) the axial load ratio, D_{mx} represents the observed drift at maximum applied lateral load, V_{mx} the observed maximum lateral load, V_{yld} the lateral load at nominal yield of the beam section, F_{int} the failure initiation mechanism (explained in chapter 2), Sl_{max} the observed strength loss from the maximum strength at the last cycle, F_{mch} the mechanism of failure in the joint (explained in chapter 2), D_{cap} the drift capacity (explained in chapter 2), Sl_{dcap} the strength loss at drift capacity, and D_{lst} the drift at the last cycle. The term NA represents data not available.

Table A.5: Specimen demand parameters

Specimen	Joint shear stress				Bond demands		Hoop steel			Int. col. steel
	τ_{max_ACI} MPa	τ_{max} MPa	τ_{nom} MPa	τ $\sqrt{MPa}$	ξ	μ	ρ_j	ϕ	φ	φ_c
DW-X1	6.40	5.22	4.07	0.70	19	1.73	0.798	0.40	0.51	0.68
DW-X2	6.70	5.47	3.95	0.68	19	1.75	1.597	0.57	0.79	0.70
DW-X3	5.36	4.37	3.00	0.54	19	1.82	0.798	0.47	0.69	0.56
OKA-J1	4.32	3.49	2.76	0.54	24	1.67	0.281	0.22	0.28	1.22
OKA-J2	4.48	3.61	2.73	0.56	24	1.73	0.562	0.43	0.57	1.24
OKA-J3	4.97	4.01	2.73	0.56	24	1.73	1.693	0.90	1.33	1.24
OKA-J4	4.22	3.40	2.76	0.54	24	1.67	0.281	0.23	0.28	1.22
OKA-J5	5.04	4.06	2.82	0.53	24	1.58	0.281	0.19	0.28	0.00
OKA-J6	3.70	2.98	1.84	0.34	24	1.37	0.422	0.43	0.70	0.62
MJ-U1	5.38	4.47	6.63	1.30	18	4.28	0.503	0.31	0.21	0.71
MJ-U2	7.87	6.53	6.73	1.04	18	3.39	0.503	0.21	0.20	1.44
MJ-U3	6.03	5.00	6.63	1.29	18	4.25	0.503	0.27	0.21	2.43
MJ-U5	7.57	6.28	6.69	1.12	18	3.66	0.503	0.22	0.21	1.45
MJ-U6	8.15	6.76	6.70	1.10	18	3.62	0.503	0.20	0.20	1.45
MJ-U12	9.58	7.95	6.69	1.13	18	3.70	2.359	0.84	0.99	1.45
MJ-U13	7.66	6.36	6.72	1.05	18	3.41	1.510	0.65	0.61	1.45
W-PEER14	4.97	4.01	4.07	0.72	29	2.05	0.000	0.00	0.00	0.39
W-PEER22	6.69	5.39	6.36	1.03	21	2.33	0.000	0.00	0.00	0.53
A-PEER0850	3.89	3.14	4.46	0.75	21	2.33	0.000	0.00	0.00	0.15
A-PEER0995	7.73	6.24	6.24	0.80	21	1.77	0.000	0.00	0.00	0.22
A-PEER4150	10.43	8.41	13.32	2.32	16	3.33	0.000	0.00	0.00	0.25
PR-U1	3.08	2.52	1.55	0.23	25	1.14	1.298	1.33	2.17	0.93
PR-U2	4.29	3.51	2.25	0.37	20	2.40	1.580	1.10	1.73	0.95
PR-U3	3.05	2.50	1.52	0.25	25	1.28	0.557	0.56	0.92	0.94
PR-U4	4.09	3.35	2.26	0.36	20	2.28	0.807	0.70	1.03	0.95
NK-J1	10.84	8.82	9.20	1.10	23	1.86	0.754	0.41	0.39	0.92
NK-J3	13.75	11.19	12.41	1.20	23	1.50	0.754	0.32	0.29	0.68
NK-J4	11.44	9.31	9.20	1.10	23	1.86	0.754	0.39	0.39	0.92
NK-J5	11.26	9.16	12.11	1.45	23	1.86	0.754	0.39	0.30	0.70
NK-J6	9.98	8.12	8.98	1.23	23	2.13	0.754	0.44	0.40	0.94
OS-J1	11.58	9.41	8.05	0.89	24	1.50	0.377	0.46	0.54	0.89
OS-J2	12.43	10.11	18.57	2.06	23	3.50	0.377	0.43	0.23	0.92

continued on next page

continued for previous page

	τ_{max_ACI}	τ_{max}	τ_{nom}	τ	ξ	μ	ρ_j	ϕ	φ	φ_c
OS-J4	11.94	9.71	8.98	1.05	24	1.28	0.377	0.44	0.48	0.65
OS-J5	13.38	10.88	10.01	1.17	24	2.08	0.377	0.40	0.43	0.94
OS-J6	12.34	10.04	8.36	0.94	24	1.61	0.188	0.15	0.17	0.91
OS-J7	9.87	8.02	6.67	0.75	24	1.61	0.377	0.34	0.40	1.14
OS-J8	14.01	11.39	10.85	1.22	16	1.32	0.377	0.21	0.22	0.87
OS-J10	8.83	7.18	8.16	1.30	24	2.37	0.377	0.26	0.23	0.97
OS-J11	10.45	8.50	10.25	1.64	16	1.89	0.377	0.15	0.12	0.92
KOA-J1	5.26	4.28	3.47	0.68	23	1.71	0.269	0.16	0.20	1.02
KOA-J6	3.76	3.06	2.17	0.43	23	1.48	0.377	0.33	0.47	0.51
KOA-C1	4.58	3.73	2.58	0.51	30	1.05	0.269	0.16	0.24	1.44
KOA-C3	4.49	3.66	2.58	0.51	30	1.05	2.326	1.54	2.18	1.44
PM-U1	6.96	5.76	6.06	0.94	25	1.29	3.801	2.16	2.06	0.51
PM-U2	7.57	6.27	5.20	0.76	20	1.47	3.041	1.49	1.80	0.59
EKOA-HC	5.81	4.72	4.45	0.69	31	0.92	0.314	0.08	0.08	0.74
EKOA-HLC	5.81	4.72	4.38	0.69	31	0.92	0.314	0.08	0.08	0.73
EKOA-LA1	7.32	5.96	5.60	0.95	24	2.87	0.462	0.10	0.11	1.32
EKOA-A1	6.88	5.59	5.41	0.98	24	2.98	0.419	0.11	0.11	1.34
HO-SD35Aa-4	3.19	2.61	3.49	0.63	20	1.90	0.220	0.44	0.33	0.31
HO-SD35Aa-7	3.08	2.52	3.41	0.55	20	1.62	0.220	0.46	0.34	0.31
HO-SD35Aa-8	3.19	2.61	3.41	0.55	20	1.62	0.220	0.44	0.34	0.31
HO-LSD35Aa-1	3.10	2.54	3.30	0.52	20	1.56	0.220	0.45	0.35	0.32
HO-LSD35Aa-2	2.97	2.43	3.43	0.53	20	1.56	0.220	0.47	0.34	0.31
HO-LSD35Ab-1	3.06	2.51	3.43	0.53	20	1.56	0.220	0.46	0.34	0.31
HO-LSD35Ab-2	2.85	2.34	3.43	0.53	20	1.56	0.220	0.49	0.34	0.31
B-U11	4.22	3.46	2.65	0.44	24	1.03	1.635	1.89	2.46	0.87
B-U12	4.21	3.45	3.70	0.63	24	1.05	1.635	1.89	1.76	0.62
AA-SHC1	2.57	2.07	5.34	0.71	19	2.06	0.506	0.76	0.29	0.00
AA-SHC2	2.54	2.04	5.16	0.67	19	2.01	1.013	1.53	0.61	0.00
AA-SOC3	2.42	1.95	5.17	0.75	19	2.26	1.013	1.61	0.61	0.00
BPP-B1	5.83	4.78	5.07	0.96	23	1.20	0.727	0.70	0.66	0.55
BPP-B2	5.84	4.79	5.11	0.91	23	1.12	0.190	0.21	0.20	0.54
TKHS-HJ1	5.05	4.11	3.82	0.52	21	1.24	0.710	0.60	0.64	0.71
TKHS-HJ2	5.63	4.58	4.29	0.58	25	1.70	0.710	0.54	0.58	0.63
TKHS-HJ3	5.05	4.11	4.10	0.56	21	2.77	0.710	0.60	0.60	0.66
TKHS-HJ4	6.48	5.27	5.42	0.74	21	1.24	0.710	0.47	0.46	0.84
TKHS-HJ5	7.59	6.17	6.20	0.84	21	2.09	0.710	0.40	0.40	0.74
TKHS-HJ6	7.33	5.97	6.02	0.82	21	2.77	0.710	0.41	0.41	0.76
TKHS-HJ7	9.62	7.82	8.00	0.85	18	1.23	0.852	0.65	0.64	0.57
TKHS-HJ8	10.12	8.23	7.72	0.82	18	1.75	0.852	0.62	0.66	0.59

continued on next page

continued for previous page

	τ_{max_ACI}	τ_{max}	τ_{nom}	τ	ξ	μ	ρ_j	ϕ	φ	φ_c
TKHS-HJ9	9.80	7.97	8.10	0.86	21	2.17	0.852	0.64	0.63	0.56
TKHS-HJ10	11.38	9.26	7.80	0.83	25	1.30	0.852	0.55	0.65	0.68
TKHS-HJ11	14.87	12.09	10.57	1.13	18	1.29	0.852	0.42	0.48	0.36
TKHS-HJ12	17.43	14.18	13.95	1.48	18	1.77	0.852	0.36	0.37	0.38
TKHS-HJ13	13.86	11.28	9.56	0.88	23	1.26	0.852	0.45	0.53	0.56
TKHS-HJ14	18.29	14.87	14.15	1.30	18	1.53	0.852	0.34	0.36	0.38
HTMK-NO43	5.05	4.11	3.64	0.49	21	1.23	0.785	0.66	0.75	0.75
HTMK-NO44	5.63	4.58	4.07	0.55	25	1.69	0.785	0.59	0.67	0.67
HTMK-NO45	6.71	5.45	7.17	0.97	18	2.24	0.785	0.50	0.38	0.38
HTMK-NO46	5.05	4.11	3.94	0.54	21	2.77	0.785	0.66	0.69	0.69
HTMK-NO47	6.48	5.27	5.19	0.71	21	1.23	0.785	0.52	0.52	0.88
HTMK-NO48	7.57	6.16	5.82	0.79	21	2.08	0.785	0.44	0.47	0.79
HTMK-NO49	9.57	7.78	8.40	1.14	18	2.24	0.785	0.35	0.32	0.54
HTMK-NO50	7.33	5.96	5.76	0.78	21	2.77	0.785	0.46	0.47	0.79
HTMK-HNO8	9.61	7.81	7.75	0.83	18	1.24	0.857	0.77	0.78	0.59
HTMK-HNO9	10.12	8.23	7.35	0.78	18	1.76	0.857	0.73	0.82	0.62
HTMK-HNO10	9.80	7.97	7.73	0.82	21	2.17	0.857	0.75	0.78	0.59
TKTH-HNO1	9.91	8.00	7.27	0.77	25	1.30	0.857	1.00	0.71	0.80
TKTH-HNO2	14.25	11.51	7.27	0.77	25	1.30	0.857	0.69	0.71	0.80
TKTH-HNO3	13.01	10.51	9.80	1.04	18	1.29	0.857	0.77	0.52	0.43
TKTH-HNO4	14.87	12.01	12.73	1.35	18	1.77	0.857	0.66	0.40	0.46
TKTH-HNO5	12.39	10.01	9.08	0.84	23	1.26	0.857	0.83	0.57	0.64
TKTH-HNO6	16.11	13.01	13.11	1.21	18	1.54	0.857	0.63	0.39	0.44
Z-S1	2.03	1.60	1.89	0.39	30	1.33	0.355	0.69	0.59	3.00
Z-S2	2.19	1.73	4.84	0.99	26	1.42	0.355	0.64	0.23	1.17
Z-S3	3.64	2.87	5.04	1.03	19	2.53	0.355	0.39	0.22	1.13
JGS-B1	2.85	2.33	2.26	0.49	23	1.74	0.215	0.25	0.26	0.41
JGS-B2	3.09	2.52	2.37	0.50	23	1.69	0.431	0.92	0.97	0.39
JGS-B8HH	3.14	2.56	2.51	0.50	23	1.73	0.609	2.70	2.76	1.22
JGS-B8HL	3.28	2.68	2.52	0.48	23	1.67	0.609	2.58	2.74	1.22
JGS-B8LH	3.28	2.68	2.52	0.49	23	1.69	0.215	0.27	0.28	1.22
JGS-B8MH	3.14	2.56	2.52	0.48	23	1.65	0.419	0.46	0.47	1.21
JGS-B9	3.66	2.98	2.51	0.50	23	1.73	0.609	2.31	2.76	1.22
JGS-B10	4.06	3.31	2.50	0.50	23	1.75	0.609	2.09	2.76	1.22
JGS-B11	4.14	3.38	2.51	0.49	23	1.72	0.609	2.05	2.76	1.22
FM-A1	5.25	4.31	14.21	2.24	23	3.65	0.428	0.24	0.07	0.63
FM-A2	4.87	4.00	6.22	0.98	23	1.40	0.428	0.25	0.16	0.86
FM-A3	5.25	4.31	14.21	2.24	23	3.65	0.428	0.24	0.07	0.63
FM-A4	5.35	4.40	14.21	2.24	23	3.65	1.142	0.62	0.19	0.63

where all the specimen demand parameters have been defined in chapter 2.

Appendix B

RESULTS OBTAINED FROM STM AND COMPONENT BASED SIMULATION

Table B.1: Results of strut-and-tie simulation

Specimen	ϕ	strength loss at last cycle Sl_{max}	drift capacity D_{cap}	SSM β_s	Combined mechanism: Main diag. contrib. $Diag_{ctrb}$	β_c	Max. bond stress B_{c_max}
DW-X1	0.40	24.36	5.08	0.99	0.51	0.53	24.20
DW-X2	0.57	19.45	5.86	1.03	0.39	0.51	33.52
DW-X3	0.47	13.89	5.88	0.97	0.46	0.45	31.70
OKA-J1	0.22	18.19	7.50	0.94	0.79	0.92	61.89
OKA-J2	0.43	17.20	7.50	1.03	0.61	0.95	44.44
OKA-J3	0.90	15.77	7.50	1.14	0.43	0.90	34.36
OKA-J4	0.23	39.00	5.00	0.51	0.79	0.54	60.16
OKA-J5	0.19	36.41	5.00	1.13	1.00	0.82	57.18
MJ-U1	0.31	NA	NA	0.51	0.59	0.51	15.08
MJ-U2	0.21	NA	NA	0.47	0.63	0.49	20.72
MJ-U3	0.27	NA	NA	0.55	0.65	0.56	18.15
MJ-U5	0.22	NA	NA	0.81	0.68	0.83	25.77
MJ-U6	0.20	NA	NA	0.40	0.70	0.41	29.42
MJ-U12	0.84	NA	NA	0.66	0.26	0.58	32.43
MJ-U13	0.65	NA	NA	0.46	0.30	0.42	23.47
W-PEER14	0.00	33.38	4.00	0.88	1.00	0.53	22.41
W-PEER22	0.00	38.13	4.00	0.89	1.00	0.61	20.28
A-PEER0850	0.00	4.34	5.00	0.77	1.00	0.37	24.93
A-PEER0995	0.00	25.08	4.00	0.85	1.00	0.43	23.73
A-PEER4150	0.00	40.48	3.00	1.35	1.00	1.06	14.09
NK-J1	0.41	31.23	4.08	0.73	0.51	0.61	29.40
NK-J3	0.32	15.15	5.10	0.64	0.63	0.59	34.35
NK-J4	0.39	21.29	4.08	0.77	0.52	0.65	32.07
NK-J5	0.39	36.04	4.08	0.79	0.57	0.72	29.37

continued on next page

continued from previous page

	ϕ	Sl_{max}	D_{cap}	β_s	$Diag_{ctrb}$	β_c	B_{c_max}
NK-J6	0.44	28.42	4.08	0.84	0.48	0.71	27.03
OS-J1	0.46	23.68	4.00	0.58	0.49	0.47	27.55
OS-J2	0.43	8.63	5.00	0.65	0.57	0.55	49.20
OS-J4	0.44	18.58	5.00	0.70	0.56	0.59	34.00
OS-J5	0.40	24.06	4.00	0.75	0.51	0.60	36.04
OS-J6	0.15	24.84	4.00	0.63	0.76	0.59	40.21
OS-J8	0.21	36.94	3.00	0.66	0.69	0.59	40.12
OS-J10	0.26	28.55	4.00	0.88	0.65	0.77	48.49
OS-J11	0.15	40.82	3.00	0.96	0.75	0.89	50.58
EKOA-HC	0.08	3.56	6.53	0.73	0.86	0.67	19.96
EKOA-HLC	0.08	27.40	4.35	0.74	0.87	0.68	20.47
EKOA-LA1	0.10	18.24	6.67	0.88	0.76	0.82	82.72
EKOA-A1	0.11	12.89	6.67	0.89	0.73	0.83	79.82
HO-SD35Aa-4	0.44	NA	NA	0.82	0.57	0.59	14.99
HO-SD35Aa-7	0.46	NA	NA	0.70	0.57	0.46	12.93
HO-SD35Aa-8	0.44	NA	NA	0.51	0.56	0.47	13.14
HO-LSD35Aa-1	0.45	9.00	NA	0.59	0.57	0.43	12.56
HO-LSD35Aa-2	0.47	NA	NA	0.45	0.56	0.41	11.73
HO-LSD35Ab-1	0.46	NA	NA	0.69	0.57	0.42	12.38
HO-LSD35Ab-2	0.49	NA	NA	0.44	0.56	0.40	11.25
TKHS-HJ1	0.60	2.98	7.50	0.34	0.46	0.34	42.17
TKHS-HJ2	0.54	19.64	7.50	0.38	0.47	0.38	56.40
TKHS-HJ3	0.60	5.47	7.50	0.34	0.46	0.34	84.33
TKHS-HJ4	0.47	37.98	4.00	0.41	0.62	0.39	55.86
TKHS-HJ5	0.40	8.83	7.50	0.48	0.62	0.49	98.60
TKHS-HJ6	0.41	29.81	4.00	0.46	0.62	0.47	126.99
TKHS-HJ7	0.65	14.80	7.50	0.37	0.46	0.38	36.18
TKHS-HJ8	0.62	10.68	7.50	0.39	0.38	0.40	53.00
TKHS-HJ9	0.64	24.18	5.00	0.38	0.38	0.39	59.51
TKHS-HJ10	0.55	5.46	8.00	0.43	0.40	0.44	39.55
TKHS-HJ11	0.42	20.76	4.00	0.58	0.52	0.58	50.38
TKHS-HJ12	0.36	30.94	4.00	0.65	0.61	0.65	74.96
TKHS-HJ13	0.45	11.33	8.00	0.40	0.51	0.40	47.94
TKHS-HJ14	0.34	34.17	4.00	0.52	0.61	0.52	67.31
HTMK-NO43	0.66	5.13	7.00	0.37	0.38	0.36	12.94
HTMK-NO44	0.59	NA	NA	0.41	0.42	0.40	15.49
HTMK-NO45	0.50	NA	NA	0.48	0.53	0.47	19.96
HTMK-NO46	0.66	19.84	7.00	0.37	0.38	0.36	25.67
HTMK-NO47	0.52	33.57	4.00	0.42	0.53	0.43	14.92

continued on next page

continued from previous page							
	ϕ	Sl_{max}	D_{cap}	β_s	$Diag_{ctrb}$	β_c	B_{c_max}
HTMK-NO48	0.44	NA	NA	0.51	0.54	0.51	26.40
HTMK-NO49	0.35	31.86	4.00	0.61	0.63	0.61	28.49
HTMK-NO50	0.46	NA	NA	0.48	0.54	0.49	33.84
HTMK-HNO8	0.77	NA	NA	0.38	0.28	0.39	13.96
HTMK-HNO9	0.73	NA	NA	0.41	0.33	0.42	19.68
HTMK-HNO10	0.75	NA	NA	0.39	0.29	0.40	23.94
TKTH-HNO1	1.00	12.49	8.00	0.54	0.47	0.54	17.01
TKTH-HNO2	0.69	8.69	8.00	0.77	0.59	0.77	35.56
TKTH-HNO3	0.77	23.82	4.00	0.73	0.59	0.69	23.54
TKTH-HNO4	0.66	33.34	4.00	0.76	0.59	0.76	27.02
TKTH-HNO5	0.83	9.99	8.00	0.60	0.55	0.55	21.42
TKTH-HNO6	0.63	38.47	4.00	0.76	0.64	0.69	28.42

where β_s represents the strength reduction factors obtained from using the single strut mechanism, β_c represents the strength reduction factor obtained from the combined strut-truss mechanism, $Diag_{ctrb}$ represents the contribution of the main diagonal strut force to the total strut force within the joint in the combined strut-truss mechanism. The definition and explanation of these parameters can be found in chapter 5 and term NA represents data not available.

Table B.2: Results of maximum joint shear stress prediction

Specimen	Failure mechanism	τ_{max} MPa	τ_{MCFT_mono} MPa		τ_{MCFT_cyc} MPa		τ_{strut} MPa	
	Obs_{fm}	Obs_{Tm}	Sim_{Mm}	$(\frac{Sim}{Obs})_{Mm}$	Sim_{Mc}	$(\frac{Sim}{Obs})_{Mc}$	Sim_{str}	$(\frac{Sim}{Obs})_{str}$
DW-X1	BYJF	5.22	6.37	1.22	5.03	0.96	4.41	0.84
DW-X2	BY	5.47	8.76	1.60	7.20	1.32	4.65	0.85
DW-X3	BY	4.37	5.83	1.33	4.62	1.06	4.02	0.92
OKA-J1	BY	3.49	3.60	1.03	2.56	0.73	3.97	1.14
OKA-J2	BY	3.61	4.73	1.31	3.67	1.02	4.31	1.19
OKA-J3	BY	4.01	7.80	1.95	5.77	1.44	5.19	1.30
OKA-J4	BYJF	3.40	3.60	1.06	2.56	0.75	3.96	1.16
OKA-J5	BYJF	4.06	3.54	0.87	2.47	0.61	3.75	0.92
MJ-U1	JF	4.47	4.72	1.06	3.64	0.81	4.39	0.98
MJ-U2	JF	6.53	5.94	0.91	4.49	0.69	6.48	0.99
MJ-U3	JF	5.00	5.24	1.05	4.08	0.82	4.81	0.96
MJ-U5	JF	6.28	5.19	0.83	3.97	0.63	5.22	0.83
MJ-U6	JF	6.76	5.23	0.77	4.00	0.59	3.72	0.55
MJ-U12	BYJF	7.95	10.30	1.30	7.68	0.97	7.49	0.94
MJ-U13	JF	6.36	9.17	1.44	7.55	1.19	7.63	1.20
W-PEER14	BYJF	4.00	1.86	0.46	1.82	0.45	4.18	1.04
W-PEER22	BYJF	5.39	2.29	0.43	2.10	0.39	6.20	1.15
A-PEER0850	BY	3.13	1.93	0.62	0.00	0.00	3.60	1.15
A-PEER0995	BYJF	6.23	2.37	0.38	2.54	0.41	6.40	1.03
A-PEER4150	JF	8.40	2.24	0.27	2.02	0.24	6.21	0.74
PR-U1	BY	2.52	6.98	2.76	5.87	2.33	4.34	1.72
PR-U2	BY	3.51	7.64	2.18	6.22	1.77	4.22	1.20
PR-U3	BY	2.50	4.65	1.86	3.52	1.41	3.26	1.31
PR-U4	BYJF	3.35	5.95	1.78	4.64	1.39	4.10	1.22
NK-J1	BYJF	8.82	12.30	1.40	10.16	1.15	10.41	1.18
NK-J3	JF	11.19	14.15	1.27	11.76	1.05	15.14	1.35
NK-J4	BYJF	9.31	12.30	1.32	10.16	1.09	10.41	1.12
NK-J5	JF	9.16	12.61	1.38	10.31	1.13	11.50	1.26
NK-J6	JF	8.12	11.29	1.39	8.52	1.05	8.96	1.10
OS-J1	BYJF	9.41	11.13	1.18	9.10	0.97	12.87	1.37
OS-J2	JF	10.11	11.20	1.11	9.15	0.91	16.10	1.59
OS-J4	BY	9.71	10.78	1.11	8.81	0.91	11.64	1.20

continued on next page

continued from previous page

	Obs_{fm}	Obs_{Tm}	Sim_{Mm}	$(\frac{Sim}{Obs})_{Mm}$	Sim_{Mc}	$(\frac{Sim}{Obs})_{Mc}$	Sim_{str}	$(\frac{Sim}{Obs})_{str}$
OS-J5	BYJF	10.88	10.78	0.99	8.81	0.81	12.27	1.13
OS-J6	BYJF	10.04	6.13	0.61	4.32	0.43	11.03	1.10
OS-J7	BY	8.02	8.76	1.09	6.88	0.86	10.89	1.36
OS-J8	BYJF	11.39	9.19	0.81	7.07	0.62	12.33	1.08
OS-J10	JF	7.18	5.94	0.83	4.57	0.64	7.21	1.00
OS-J11	JF	8.50	5.40	0.64	3.99	0.47	7.09	0.83
KOA-J1	BYJF	4.28	3.48	0.81	2.43	0.57	3.72	0.87
KOA-J6	BYJF	3.06	3.16	1.03	2.41	0.79	3.17	1.04
KOA-C1	BY	3.73	3.31	0.89	2.32	0.62	3.66	0.98
KOA-C3	BY	3.66	8.37	2.29	6.19	1.69	4.39	1.20
PM-U1	BY	5.76	12.63	2.19	9.44	1.64	8.17	1.42
PM-U2	BYJF	6.27	12.14	1.94	10.05	1.60	8.16	1.30
EKOA-HC	BY	4.72	4.03	0.85	2.79	0.59	4.99	1.06
EKOA-HLC	BYJF	4.72	4.03	0.85	2.79	0.59	5.00	1.06
EKOA-LA1	JF	5.96	4.58	0.77	3.27	0.55	6.35	1.07
EKOA-A1	JF	5.59	4.41	0.79	3.19	0.57	6.06	1.08
HO-SD35Aa-4	JF	2.61	3.24	1.24	2.18	0.83	2.43	0.93
HO-SD35Aa-7	JF	2.52	3.49	1.38	2.30	0.91	2.68	1.06
HO-SD35Aa-8	JF	2.61	3.49	1.34	2.30	0.88	3.31	1.27
HO-LSD35Aa-1	JF	2.54	3.58	1.41	2.34	0.92	2.96	1.16
HO-LSD35Aa-2	JF	2.43	3.58	1.47	2.34	0.96	3.43	1.41
HO-LSD35Ab-1	JF	2.51	3.58	1.43	2.34	0.93	2.69	1.07
HO-LSD35Ab-2	JF	2.34	3.58	1.53	2.34	1.00	3.43	1.47
B-U11	BY	3.46	8.36	2.42	6.86	1.98	5.09	1.47
B-U12	BY	3.45	8.25	2.39	6.77	1.96	4.81	1.40
Mean (C.O.V.)	JF		1.10 (0.31)		0.81 (0.29)		1.09 (0.23)	
	BYJF		1.02 (0.42)		0.81 (0.43)		1.09 (0.13)	
	BY		1.64 (0.40)		1.25 (0.48)		1.23 (0.18)	

where the explanation of each of these terms are provided in chapter 4. The term NA represents data not available.

Table B.3: Results of simulated and experimental comparison (failure mechanism and stiffness values)

Specimen	Failure mechanism		Initial stiffness		Post-yield		Unloading stiffness	
			kN/mm		stiffness kN/mm		at max. strength kN/mm	
	Obs_{fm}	Sim_{fm}	Obs_{is}	$(\frac{Sim}{Obs})_{is}$	Obs_{ps}	$(\frac{Sim}{Obs})_{ps}$	Obs_{us}	$(\frac{Sim}{Obs})_{us}$
DW-X1	BYJF	BYJF	4.90	0.83	0.00	NA	6.54	1.14
DW-X2	BY	BYJF	5.44	0.80	0.17	1.18	6.56	1.04
DW-X3	BY	BY	4.71	0.77	0.05	3.80	5.25	0.99
OKA-J1	BY	BY	5.31	1.04	0.45	1.18	7.63	1.05
OKA-J2	BY	BY	5.98	0.98	0.31	1.45	8.47	0.90
OKA-J3	BY	BY	5.88	0.98	0.31	2.00	6.58	1.03
OKA-J4	BYJF	BYJF	6.14	0.97	$\leq$ 0.00	NA	13.98	0.77
OKA-J5	BYJF	BYJF	5.31	1.10	0.68	0.93	6.67	1.03
MJ-U1	JF	JF	NA	NA	NA	NA	NA	NA
MJ-U2	JF	JF	NA	NA	NA	NA	NA	NA
MJ-U3	JF	JF	NA	NA	NA	NA	NA	NA
MJ-U5	JF	JF	NA	NA	NA	NA	NA	NA
MJ-U6	JF	JF	NA	NA	NA	NA	NA	NA
MJ-U12	BYJF	BYJF	NA	NA	NA	NA	NA	NA
MJ-U13	JF	JF	NA	NA	NA	NA	NA	NA
PR-U1	BY	BY	2.42	0.99	0.22	0.86	2.43	1.08
PR-U2	BY	BY	3.26	0.98	0.39	1.08	3.72	0.98
PR-U3	BY	BY	2.36	1.02	0.17	0.82	3.70	0.86
PR-U4	BYJF	BYJF	3.10	1.03	0.17	1.18	7.00	0.86
NK-J1	BYJF	BYJF	10.83	1.23	0.00	NA	9.46	1.00
NK-J3	JF	BY	10.61	1.29	$\leq$ 0.00	NA	8.57	1.33
NK-J4	BYJF	BYJF	10.34	1.29	0.00	NA	8.33	1.08
NK-J5	JF	JF	10.95	1.22	$\leq$ 0.00	NA	10.20	1.32
NK-J6	JF	JF	10.39	1.24	$\leq$ 0.00	NA	12.00	1.25
OS-J1	BYJF	BY	10.21	1.36	0.69	0.72	8.56	1.05
OS-J2	JF	JF	11.11	1.28	$\leq$ 0.00	NA	9.20	1.14
OS-J4	BY	BY	12.26	1.27	0.70	0.64	10.60	1.03
OS-J5	BYJF	BYJF	11.92	1.28	0.00	$\geq$ 10	8.49	1.12
OS-J6	BYJF	BYJF	12.26	1.16	0.68	0.62	7.82	1.03
OS-J7	BY	BY	10.21	1.12	0.43	1.07	7.30	0.90
OS-J8	BYJF	BYJF	17.03	1.06	0.00	1.00	15.55	1.07
OS-J10	JF	JF	7.78	1.16	$\leq$ 0.00	NA	9.30	1.00

continued on next page

continued from previous page

	Obs_{fm}	Sim_{fm}	Obs_{is}	$(\frac{Sim}{Obs})_{is}$	Obs_{ps}	$(\frac{Sim}{Obs})_{ps}$	Obs_{us}	$(\frac{Sim}{Obs})_{us}$
OS-J11	JF	JF	12.26	0.97	$\leq$ 0.00	NA	11.60	1.29
KOA-J1	BYJF	BYJF	5.52	0.94	$\leq$ 0.00	$\leq$ 0.00	5.74	1.08
KOA-J6	BYJF	BYJF	4.73	0.82	1.20	0.88	11.50	0.87
KOA-C1	BY	BY	5.52	0.82	0.31	1.35	7.10	0.99
KOA-C3	BY	BY	5.63	0.81	0.67	1.04	7.00	0.96
PM-U1	BY	BY	3.54	1.18	NA	NA	NA	NA
PM-U2	BYJF	BY	3.53	1.11	NA	NA	NA	NA
EKOA-HC	BY	BY	5.75	1.22	0.33	1.00	6.33	1.26
EKOA-HLC	BYJF	BYJF	5.75	1.20	0.80	0.94	7.92	1.06
EKOA-LA1	JF	JF	4.36	1.14	$\leq$ 0.00	NA	8.88	0.81
EKOA-A1	JF	JF	4.36	1.08	$\leq$ 0.00	NA	8.33	0.82
HO-SD35Aa-4	JF	JF	NA	NA	NA	NA	NA	NA
HO-SD35Aa-7	JF	JF	NA	NA	NA	NA	NA	NA
HO-SD35Aa-8	JF	BYJF	NA	NA	NA	NA	NA	NA
HO-LSD35Aa-1	JF	JF	1.24	1.16	NA	NA	2.48	0.97
HO-LSD35Aa-2	JF	BYJF	NA	NA	NA	NA	NA	NA
HO-LSD35Ab-1	JF	JF	NA	NA	NA	NA	NA	NA
HO-LSD35Ab-2	JF	BYJF	NA	NA	NA	NA	NA	NA
B-U11	BY	BY	7.81	0.99	0.29	1.14	4.18	0.97
B-U12	BY	BY	7.81	1.08	0.27	1.04	4.29	0.91
W-PEER14	BYJF	BYJF	11.67	0.95	0.65	1.23	10.28	1.02
W-PEER22	BYJF	BYJF	13.12	1.00	0.60	1.20	14.40	1.04
A-PEER0850	BY	BY	14.58	0.97	0.30	0.83	9.50	1.02
A-PEER0995	BYJF	BYJF	18.47	0.89	0.35	1.29	14.50	1.12
A-PEER4150	JF	JF	23.82	0.81	$\leq$ 0.00	NA	26.70	0.94
Mean (C.O.V)		All	1.06 (0.15)		1.07 (0.27)		1.03 (0.13)	
		JF	1.14 (0.13)				1.09 (0.19)	
		BYJF	1.07 (0.15)		1.00 (0.22)		1.02 (0.10)	
		BY	1.00 (0.15)		1.11 (0.29)		1.00 (0.09)	

where the explanation of each of these terms are provided in chapter 4. The term NA represents data not available.

Table B.4: Results of simulated and experimental comparison (strength and drift values)

Specimen	Max. Column load kN		Drift at max.		Strength loss at last cycle / max. strength		average pinching ratio	
	Obs_{mld}	$(\frac{Sim}{Obs})_{mld}$	Obs_{dmax}	$(\frac{Sim}{Obs})_{dmax}$	Obs_{sls}	$(\frac{Sim}{Obs})_{sls}$	Obs_{pr}	$(\frac{Sim}{Obs})_{pr}$
DW-X1	191	0.86	2.54	1.00	0.76	0.97	0.23	1.05
DW-X2	200	0.85	2.99	1.00	0.81	0.98	0.23	1.01
DW-X3	160	0.85	3.67	1.38	0.86	1.12	0.31	1.02
OKA-J1	115	1.12	5.00	1.00	0.82	1.12	0.19	1.00
OKA-J2	119	1.09	5.00	1.00	0.83	1.04	0.19	0.95
OKA-J3	132	1.02	5.00	1.00	0.84	1.14	0.17	1.13
OKA-J4	112	1.11	2.50	1.93	0.61	1.26	0.20	0.92
OKA-J5	133	0.88	3.78	1.00	0.64	1.24	0.15	1.03
MJ-U1	108	0.98	NA	NA	NA	NA	NA	NA
MJ-U2	158	0.99	NA	NA	NA	NA	NA	NA
MJ-U3	121	0.96	NA	NA	NA	NA	NA	NA
MJ-U5	152	0.83	NA	NA	NA	NA	NA	NA
MJ-U6	164	0.56	NA	NA	NA	NA	NA	NA
MJ-U12	193	0.94	NA	NA	NA	NA	NA	NA
MJ-U13	154	1.18	NA	NA	NA	NA	NA	NA
PR-U1	80	0.98	4.25	1.00	1.00	1.00	0.56	1.02
PR-U2	112	0.98	3.03	1.40	0.85	1.19	0.36	1.17
PR-U3	79	0.99	2.43	1.25	0.88	1.13	0.50	1.01
PR-U4	107	1.13	3.03	1.00	0.75	1.18	0.33	0.94
NK-J1	236	1.10	2.04	1.50	0.69	0.53	0.36	0.70
NK-J3	300	1.33	3.06	1.67	0.85	1.27	0.27	1.27
NK-J4	250	1.12	3.06	1.00	0.79	0.55	0.28	1.02
NK-J5	246	1.26	3.06	0.73	0.64	1.24	0.18	0.94
NK-J6	218	1.10	3.06	0.67	0.72	1.17	0.20	1.02
OS-J1	257	1.03	3.00	1.00	0.76	1.26	0.25	1.12
OS-J2	276	1.58	3.00	0.97	0.92	1.00	0.22	0.82
OS-J4	265	1.02	3.00	1.00	0.81	1.18	0.23	1.34
OS-J5	297	1.08	3.00	1.00	0.76	1.07	0.24	1.19
OS-J6	274	1.02	3.00	1.00	0.75	1.05	0.27	0.98
OS-J7	219	0.93	3.00	1.67	0.90	1.18	0.32	1.02
OS-J8	311	1.01	2.00	1.04	0.63	0.98	0.16	1.13
OS-J10	196	1.01	2.00	1.00	0.71	1.16	0.20	0.99
OS-J11	232	0.83	2.00	0.76	0.59	1.27	0.14	1.09
KOA-J1	115	0.91	4.35	1.00	0.85	0.97	0.24	0.95

continued on next page

continued from previous page

	Obs_{mld}	$(\frac{Sim}{Obs})_{mld}$	Obs_{dmax}	$(\frac{Sim}{Obs})_{dmax}$	Obs_{sls}	$(\frac{Sim}{Obs})_{sls}$	Obs_{pr}	$(\frac{Sim}{Obs})_{pr}$
KOA-J6	82	0.96	2.18	1.00	0.68	1.11	0.24	1.04
KOA-C1	100	0.99	4.35	1.00	0.97	0.96	0.35	1.01
KOA-C3	98	1.05	4.35	1.00	0.98	0.48	0.36	0.95
PM-U1	129	1.16	4.18	1.50	0.90	1.14	NA	NA
PM-U2	140	0.94	4.18	2.00	0.69	1.64	NA	NA
EKOA-HC	127	1.03	4.35	1.00	0.96	0.96	0.30	1.15
EKOA-HLC	127	1.06	2.18	2.00	0.73	0.99	0.30	1.12
EKOA-LA1	160	1.06	4.08	1.00	0.82	0.72	0.21	0.97
EKOA-A1	150	1.08	4.08	1.00	0.87	0.85	0.23	0.95
HO-SD35Aa-4	25	0.93	1.18	1.00	NA	NA	NA	NA
HO-SD35Aa-7	25	1.06	1.18	1.00	NA	NA	NA	NA
HO-SD35Aa-8	25	1.38	2.35	1.50	NA	NA	NA	NA
HO-LSD35Aa-1	25	1.16	1.18	1.00	0.91	0.80	0.20	0.86
HO-LSD35Aa-2	24	1.41	2.35	1.00	NA	NA	NA	NA
HO-LSD35Ab-1	24	1.07	1.18	1.00	NA	NA	NA	NA
HO-LSD35Ab-2	23	1.46	2.35	1.05	NA	NA	NA	NA
B-U11	200	0.97	3.81	1.00	1.00	1.00	0.38	0.96
B-U12	205	0.99	3.81	1.00	1.00	1.00	0.37	1.21
W-PEER14	267	0.93	2.83	1.00	0.67	0.94	0.12	1.03
W-PEER22	360	0.99	1.89	1.00	0.62	0.81	0.12	1.03
A-PEER0850	209	0.98	2.83	1.00	0.96	1.05	0.17	1.15
A-PEER0995	416	0.86	2.53	1.13	0.75	1.00	0.17	1.31
A-PEER4150	561	0.74	1.69	0.75	0.60	1.01	0.14	0.98
Mean (C.O.V.)	All	1.03 (0.17)	1.12 (0.27)		1.04 (0.20)		1.04 (0.12)	
	JF	1.09 (0.23)	1.01 (0.26)		1.05 (0.20)		0.99 (0.14)	
	BYJF	1.00 (0.09)	1.21 (0.32)		1.03 (0.25)		1.03 (0.13)	
	BY	1.00 (0.08)	1.14 (0.20)		1.04 (0.16)		1.07 (0.10)	

where the explanation of each of these terms are provided in chapter 4. The term NA represents data not available.

Appendix C

MODELING OF CRACKS IN A CONTINUUM FRAMEWORK

The phenomena of crack formation is associated with tension along the direction perpendicular to that of the crack and compression parallel to the direction of crack. Within the context of numerical modeling, crack has been modeled by various means and can be classified into three different categories:

C.1 Discrete Crack models

This modeling technique was first proposed by Ngo and Scordelis (1967) who used a zero-thickness interface element between elastic solid elements at potential crack locations. The discrete crack model represents exactly strong displacement continuity that develops at the crack. However, in the most basic form the model suffers from two major disadvantage: the orientation and location of the crack must be known apriori and the cracks are constrained to occur along element edges. To mitigate these disadvantages, more recent research has resulted in

- advanced re-meshing techniques (Ingraffea and Saouma 1985, Cervenka 1994) and adaptive boundary/finite element methods for crack growth. (Carter et al. 1998, Spievak et al. 2001).
- techniques to permit discrete cracks through finite elements (Blaauwendraad and Grootenboer 1981, Blaauwendraad 1985).
- lattice methods (van Mier 1997, Bolander and Berton 2004).

C.2 Smeared Crack models

The concept of a smeared crack was first introduced by Rashid (1968). The primary concept is to smear the crack over a region of concrete and thereby apply continuum mechanics approach to solve the problem. Thus cracking is simulated using a fictitious constitutive

model that avoids the need for change in geometry and remeshing. Smearing out of cracks in a continua has been incorporated by a number of researchers utilizing various different techniques:

Empirical global models: These models typically consider the global effect of cracks on a reinforced concrete section. These models represent the effect of cracks by reduction of compressive strength envelope through empirical equations. Notable contribution in this category of modeling cracks at a global level for reinforced concrete sections are by Vecchio and Collins (1986), Shirai and Noguchi (1989), Hsu (1988), Stevens et al. (1991a), Belarbi and Hsu (1995), Pang and Hsu (1996), Kaufmann and Marti (1998), Vecchio (2000), Hsu and Zhu (2002), Palermo and Vecchio (2003). Even though these models are widely used to define the global behavior of reinforced cracked concrete, they are not derived from the underlying local physical phenomena governing cracks in concrete and hence cannot be classified as locally and physically sound models for crack. These models can also be classified as 'total strain models' in which the total strain in an gauss quadrature point is utilized to obtain the stress at that point.

Phenomenological models: The primary difference of these models with the previous set of model is that these consider a decomposition of concrete strain into concrete strain and crack strain. From a phenomenological perspective the concept of smeared cracking can be divided into three different categories (Rots and Blaauwendraad 1989): *Fixed crack model* in which the orientation of the major crack is kept constant once formed, *Coaxial rotating crack model* in which the orientation of the major crack is updated continuously as the crack progresses, *Multi-directional fixed crack* in which multiple cracks can originate once the cracking criterion is satisfied (i.e. user specified threshold angle is exceeded and also the maximum tensile strength is exceeded) (de Borst and Nauta 1986). Even though these models are physically and locally sound, they are not entirely devoid of some numerical problems. (Willam et al. 1987, Rots et al. 1985) have shown that fixed smeared crack models can lead to unreasonably high shear strength prediction in shear loading situations. The axes of orthotropy are fixed at their initial orientation. If the axes of principal stress shift away from the axes

of orthotropy due to non-proportional loading or a shift in the load resisting mechanism of the structure, the response of the fixed crack becomes dominated by its shear retention model. Since the shear retention model reduces only the shear stiffness, the material does not soften under continued loading. Fixed crack models also exhibit stiff behavior in post-peak regime as observed in Rots and Blaauwendraad (1989) in comparison to experimentally observed results. For the multi-directional fixed crack models, the disadvantage lies in the need to store information about many cracks, thereby alleviating the complexity in implementation considerably. Moreover, even though the excess in shear strength is reduced in multi-directional fixed crack model from the fixed crack models, the problem is not completely eliminated. The original rotating smeared crack model (Cope et al. 1980) forces the axes of orthotropy to coincide with the principle strain direction. The concept of rotating crack does not mean that the cracks would actually rotate. Rather it means that cracks of many orientation exists; in which cracks of some orientation close and some orientation open with the effect that the orientation of the dominant crack rotates. The major shortcoming of this approach is that since the crack is not aligned with the principle stress axes, the principle stress axes can deviate from the axes of orthotropy thereby resulting in excessive stiffness. Bažant (1983) laid the foundation for coaxial rotating crack model in which both the principle stress and strain direction are aligned with the axes of orthotropy. Later this was individually developed by Gupta and Akbar (1984), Willam et al. (1986), Crisfield and Wills (1989). Coaxial rotating smeared cracks also exhibit some drawbacks: the shear response of these crack models are governed by the response of the material under tension rather than by a mixed mode constitutive model (Spencer 2002). Since stresses and strains are forced to share the same principal direction, loading an existing crack in shear results in a rotation of the crack rather than in a sliding behavior.

Damage plasticity models: In order to obtain an unified and elegant concept, whose special cases would result in fixed and rotating smeared cracks, an anisotropic damage mechanics framework coupled with plasticity rules was evolved to explain the mechanism of cracks in concrete (de Borst 2002). Even though with classical plasticity it was

possible to model cracks at macroscopic level (Pramono and Willam 1989), but it was not possible to model stiffness degradation which is a result of micro-cracking process when a concrete sample is subjected to cyclic loading. Isotropic damage model with a scalar damage variable acting on the elastic stiffness were developed with different damage evolution rules (Simo and Ju 1987, Frantziskonis and Desai 1987, Mazars and Pijaudier-Cabot 1989, Lubliner et al. 1989, Yazdani and Schreyer 1990, Cervera and Oliver 1995, de Vree et al. 1995). The primary disadvantage of using these isotropic damage models is that the possibility of compressive strut action, which is a prevalent mechanism of load transfer for reinforced concrete members, is eliminated (de Borst 2002). To overcome this disadvantage, anisotropic damage models were proposed. Resende and Martin (1984) proposed an anisotropic model in which different damage rules were proposed to characterize damage in the deviatoric and volumetric modes of response. Such a model, which suggests that the orientation of damage is a function of load-history, is attractive given the effect of hydrostatic pressure on concrete response. Lee and Fenves (1998) proposed an anisotropic model as an extension to the model by Lubliner et al. (1989) in which two different damage variables were utilized to represent separate damage behavior in tension and compression. A fully generalized anisotropic (fourth order damage tensor) model was proposed by Govindjee et al. (1995) in which the orientation of the material damage is a function of the direction of loading. This model was implemented in FEAP software for applications to concrete with 3 defined surfaces by Lowes (1999). Even though these are fully generalized elegant models, the problem associated with these models is in calibrating the models, since input variables are not directly obtained from experimental results.

Microplane models: The background of the microplane modeling approach, described in more detail in Bažant et al. (1996), is primarily based upon the novel idea of Taylor (1938) and Batdorf and Budianski (1949). The first in the series of microplane models, termed as M1, was proposed by Bažant (1984) with successive refinements to M2 in Bažant and Prat (1988), Bažant and Ožbolt (1990), M3 in Bažant et al. (1996), M4 in Bažant et al. (2000) and finally M5 in Bažant and Caner (2005). A detailed review of the models (till M4) can be obtained in Bažant et al. (2000). The main concept

in the formulation of the microplane models is to define stress-strain relationship independently on planes of all possible orientations in the microstructure and then to constrain these microplane stresses or strains either kinematically or statically to the macroscopic stress or strain tensor. Even though mathematically these models can be derived from the general formulation of anisotropic damage plasticity but conceptually these models present a different perspective from the damage plastic models. Damage plasticity models are based upon the concept of continuum whereas these models consider a structure to be composed of several micro-structures and thereby the definition of a continuum is relaxed. Conceptually these models are much more appealing in defining the response of quasi-brittle materials like concrete. The microplane models are in a way similar to the multi-directional fixed crack models and this similarity has been explored in details in de Borst (2002).

A variety of smeared models exist in the literature, all of which are primarily based on changing the constitutive relation of the materials (at a global or local level) so as to capture the material response behavior. Most of the smeared crack models rely upon two variables: the fracture energy of the material G_f and also the characteristic length h over which the crack is assumed to be smeared. The fracture energy is described as a material parameter and will be discussed in details later in the chapter. The concept of characteristic length is important since without it would result in mesh-dependent results. Bažant and Oh (1983) introduced the concept of crack-band width which is a function of the element area and the direction of the crack advancement. Crisfield (1986) proposed the characteristic length to be the jacobian at an individual gauss point. Rots (1988) suggested the characteristic length to be dependent upon the element type, number of integration points in an element and orientation of crack in an element. Oliver (1989) calculated the element characteristic length as a function of element size and elastic stress state. Feenstra (1993) assumed that the characteristic length in an element is related to the area of the element. Lee and Willam (1997) proposed a crack density, h_c, that maps the area of the crack surface under compression failure into continuum volume. This crack density can also be considered as a element characteristic length and is defined on the basis of experimental

data as a function of the continuum element geometry. Even though various proposition was made as regards to the characteristic length in an element, the underlying idea is that in finite element calculations this length should correspond to a representative dimension of the mesh size. For our evaluation later the definition as suggested by Rots (1988) has been considered because of its simplicity.

C.3 Enriched Continua methods

The principle idea of the enriched continua methods is to model cracks utilizing a local enrichment of the stress and/or displacement and/or strain relations in a finite element formulation. Various set of enriched continua methods have emerged in the literature over the years.

Cosserat continuum: The primary concept behind the Cosserat continuum approach (Cosserat and Cosserat 1909) is the augmentation of three translational degrees of freedom in a continuum by three rotational degrees of freedom. Several variations of the original Cosserat theory led to the formulations of couple stress elasticity (Mindlin and Tiersten 1962, Toupin 1962; 1964), theory of elasticity with micro-structure (Mindlin 1964), micro-polar and micromorphic theories (Eringen 1964), multipolar theory (Green and Rivlin 1964a, Green 1965). Nonlinear extensions to the Cosserat theory was also proposed in Lippmann (1969), Besdo (1974). The first application of micro-polar continuum theories in non-linear computational solid-mechanics framework was done in Vardoulakis (1989), Mühlhaus (1989), de Borst (1991) who analyzed the potentials of the elastoplastic micro polar constitutive theory to regularize the predictions of post-peak response behaviors of structural systems within the theoretical framework of the smeared-crack approach. On a contemporary line, Willam and Dietsche (1992), Sluys (1992), Willam et al. (1995) analyzed the localization indicators and localization properties of nonlinear micro polar continua. Later a thermodynamically consistent micro-polar micro-plane constitutive law satisfying the classical Clausius-Duhem inequality for isothermal process was developed in Etse et al. (2003), Etse and Nieto (2004). Even though these models are quite elegant but the applica-

bility of the Cosserat theories are limited to cases where rotational degrees of freedom are activated upon deformation, thus it is a proper regularization method for shear dominated problems but fails for pure tension.

Higher order gradient methods: These type of enriched continua methods differ from the Cosserat theories in that they retain the displacement field as the only independent kinematic field but improves the resolution by incorporating gradients of strain (Green and Rivlin 1964b, Mindlin 1965). These first generation of higher order gradient methods were limited to elastic materials. Later gradient dependent plasticity models were developed (Zbib and Aifantis 1989, Vardoulakis and Aifantis 1991, Mühlhaus and Aifantis 1991, de Borst and Mühlhaus 1992) to develop a gradient approach to address various material instability problems such as metal fatigue, polycrystal/soil shear banding, failure in concrete and liquefaction. These later gradient models were not only limited in incorporation of gradients of strain (as the first generation models) but also incorporated gradients in the plasticity yield criteria (Bažant and Jirásek 2002). Computational issues of gradient theory for both damage and plasticity was discussed extensively in Pamin (1994), de Borst et al. (1995), Peerlings et al. (1996) in which a series of finite elements have been formulated considering higher order deformation gradients. Using consistent thermodynamics, Voyiadjis and Dorgan (2001) proposed gradient dependent theories of plasticity and damage over multiple scales that incorporated internal variables and corresponding gradients at both the macro and meso-scales in plasticity and damage potential function as well as the yield and damage criteria. Even though these models represent the physical continua but they are hard to implement and are computationally intensive. The robustness and ease of applicability of these methods are yet to be tested by other researchers.

Embedded discontinuity methods: These can also be referred to as solid finite elements with embedded displacement discontinuities. Discontinuous shape functions are used to describe an enhanced displacement field within a cracked finite element. This procedure allows discrete cracks to be introduced into the finite elements during the analysis without altering the mesh. There is no need to define the location of potential cracks

prior to the analysis since cracks can be introduced into the elements at any time. In a comprehensive review of various embedded crack models, Jirásek (2000) grouped the formulation in literature into three categories: kinematically optimal symmetric (KOS), statically optimal symmetric (SOS), and statically and kinematically optimal symmetric (SKON).

KOS formulation: The KOS approach uses strong kinematics in the representation of both the enhanced displacement field and the traction on the embedded surface. Even though the KOS elements can give an excellent kinematic representation of cracking, the interface traction can be very unrealistic. The models developed utilizing this approach are by Lotfi (1992), Lotfi and Shing (1995), Spencer (2002).

SOS formulation: The SOS approach uses statics to represent the displacement field and interface traction. Even though the SOS formulation can realistically model interface traction, but the weak kinematic representation of cracking leads to severe locking problems. The models developed utilizing this approach are by Belytschko et al. (1988), Larsson and Runesson (1996), Larsson et al. (1996), Sluys (1997), Sluys and Berends (1998).

SKON formulation: The SKON approach takes on the pros of the both the above two methods. The resulting element represents the crack displacement with strong kinematics and also provides a good representation of the interface traction. The problem associated with these models are that they are generally nonsymmetric and are sometimes difficult to solve using existing solution techniques. The models developed utilizing this approach are by Dvorkin et al. (1990), Klisinski et al. (1991), Olofsson et al. (1994), Simo and Oliver (1994), Armero and Garikipati (1995), Oliver (1996a;b), Ohlsson and Olofsson (1997), Oliver et al. (1998), Tano et al. (1998), Oliver and Pulido (1998), Spencer (2002).

Appendix D

SPECIMEN LOAD DEFLECTION PLOTS USING COMPONENT BASED MODEL

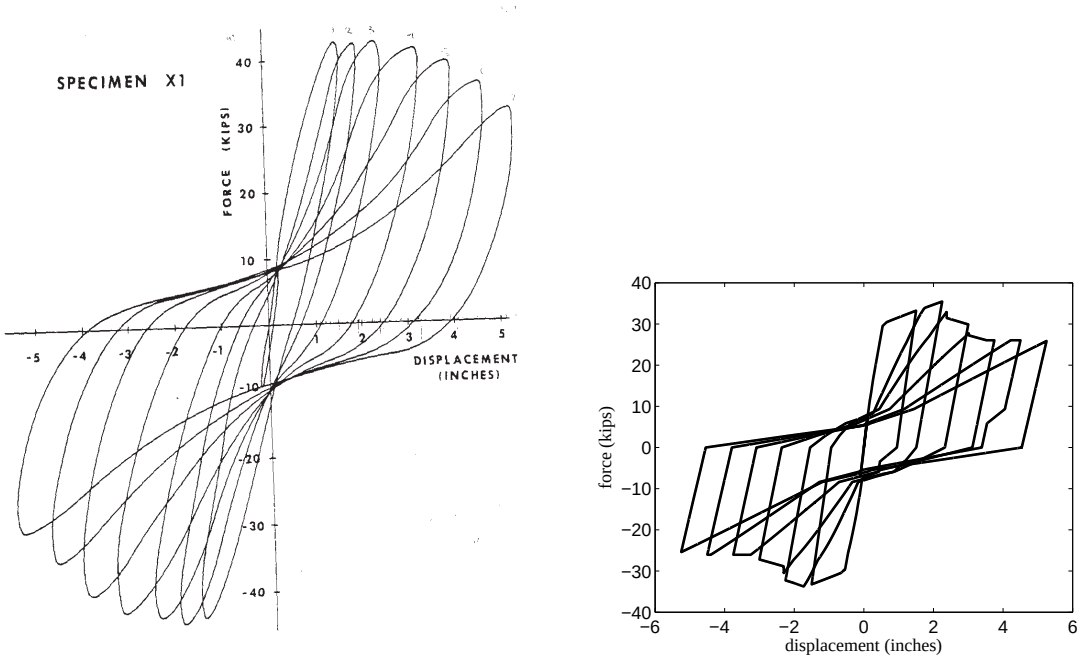

(a) Experimental (b) Simulated

Figure D.1: Load deformation response of DW_X1 specimen

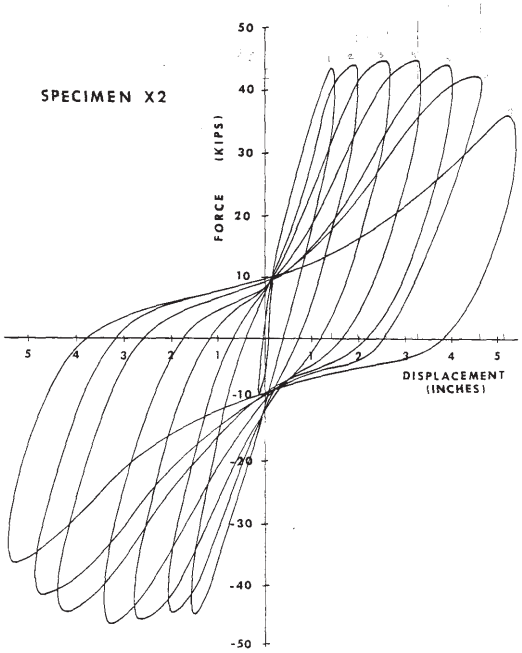

(a) Experimental

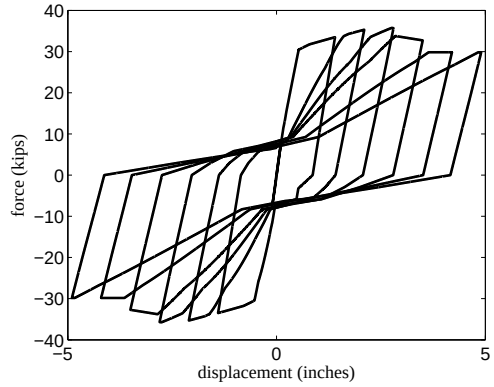

(b) Simulated

Figure D.2: Load deformation response of DW_X2 specimen

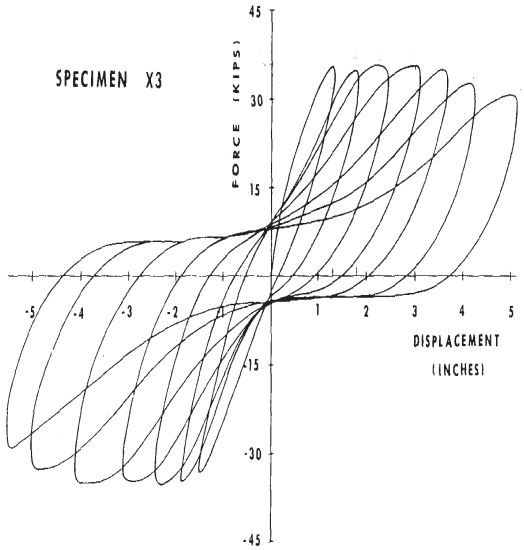

(a) Experimental

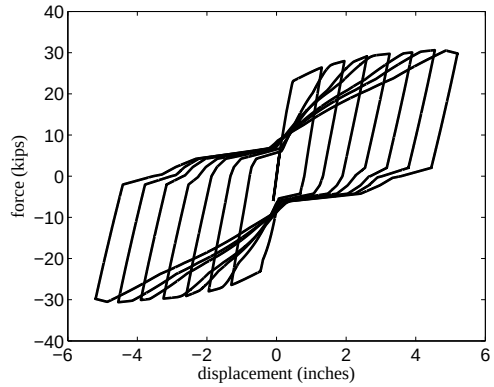

(b) Simulated

Figure D.3: Load deformation response of DW_X3 specimen

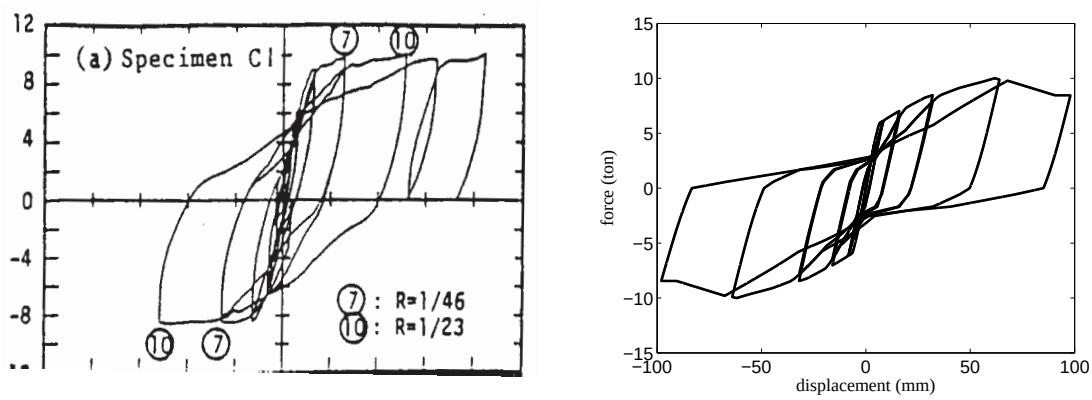

(a) Experimental (b) Simulated

Figure D.4: Load deformation response of KOA_C1 specimen

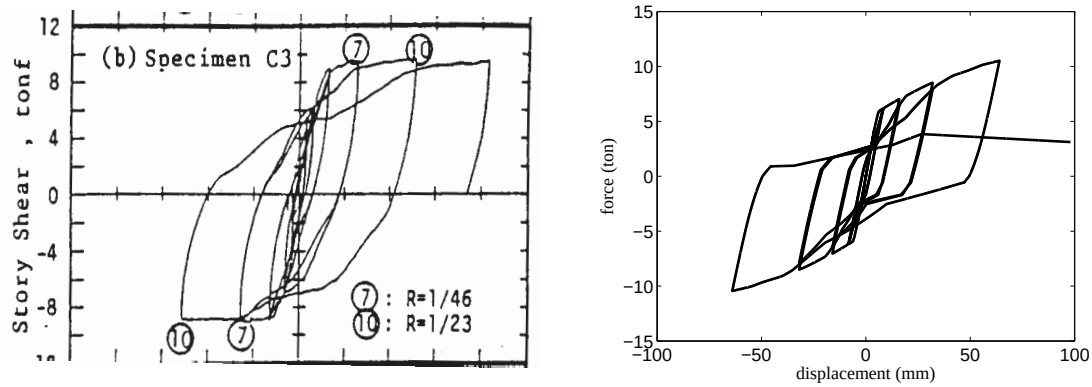

(a) Experimental (b) Simulated

Figure D.5: Load deformation response of KOA_C3 specimen

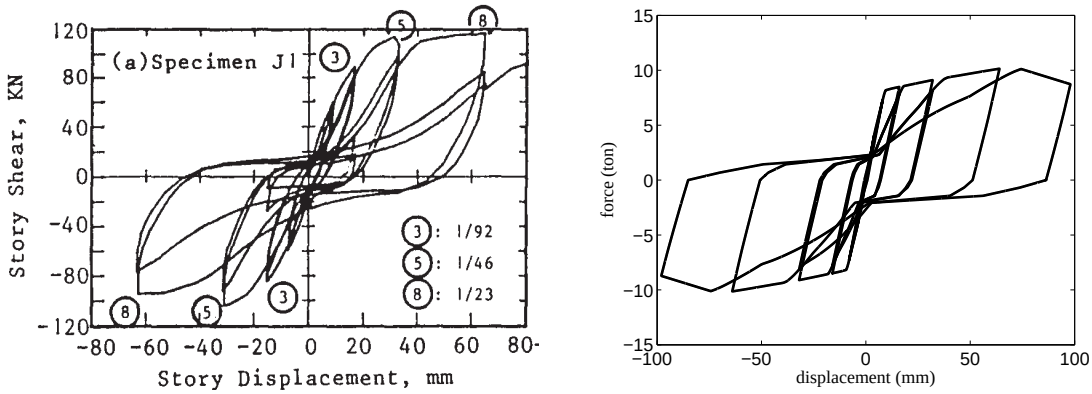

(a) Experimental (b) Simulated

Figure D.6: Load deformation response of KOA_J1 specimen

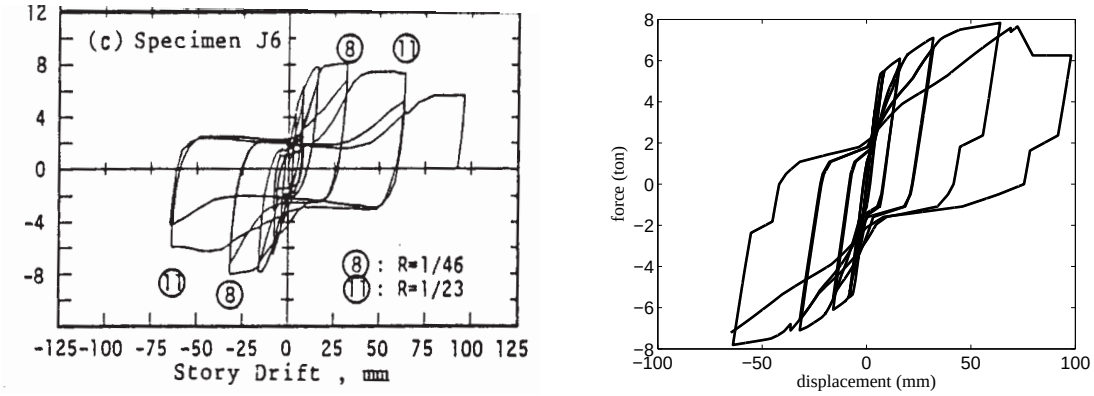

(a) Experimental (b) Simulated

Figure D.7: Load deformation response of KOA_J6 specimen

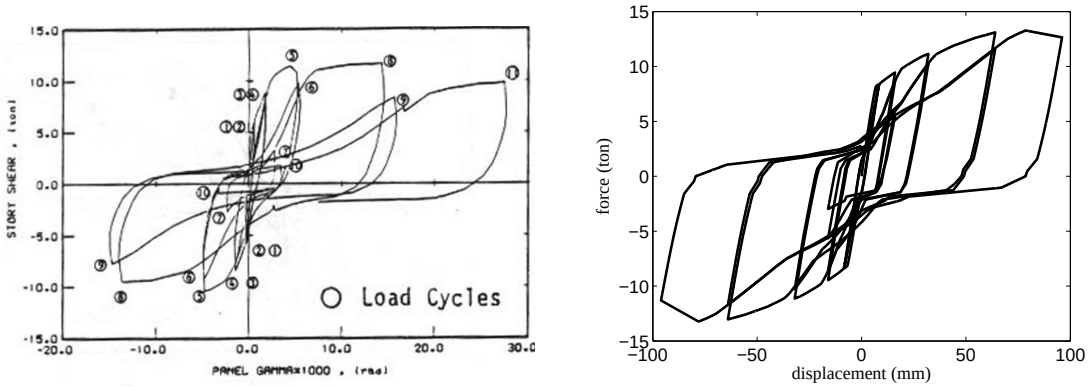

(a) Experimental (b) Simulated

Figure D.8: Load deformation response of OKA_J1 specimen

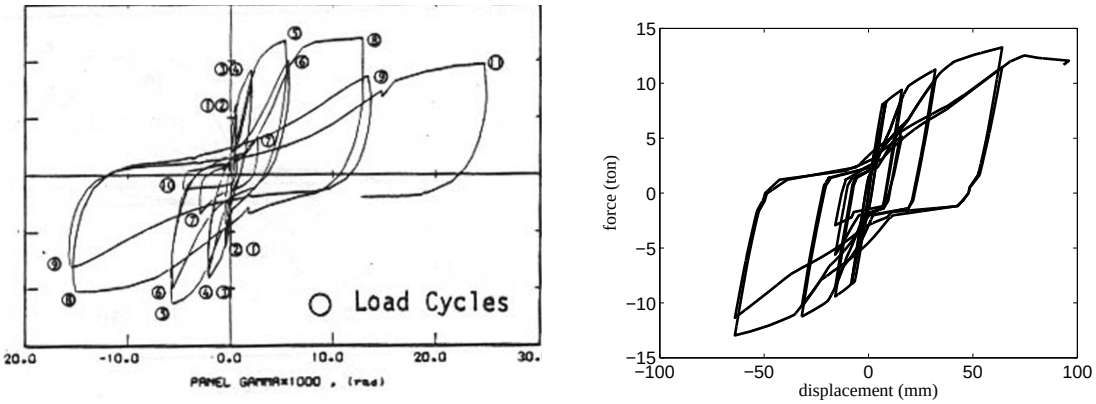

(a) Experimental (b) Simulated

Figure D.9: Load deformation response of OKA_J2 specimen

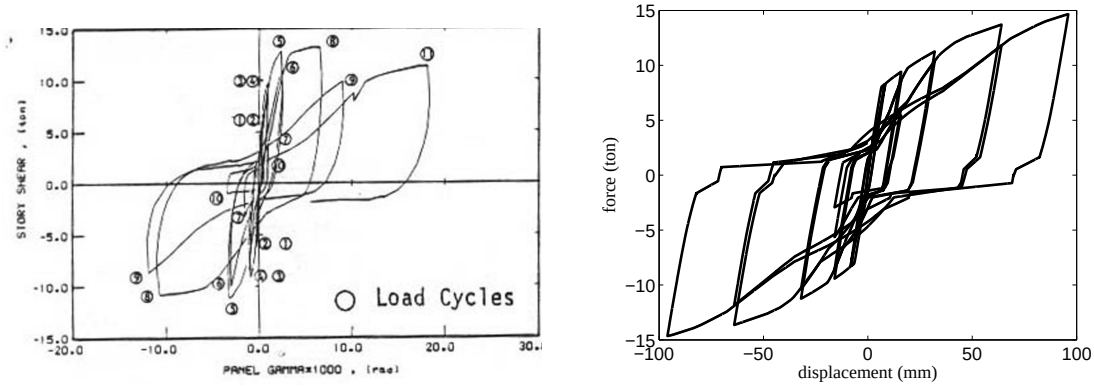

(a) Experimental (b) Simulated

Figure D.10: Load deformation response of OKA_J3 specimen

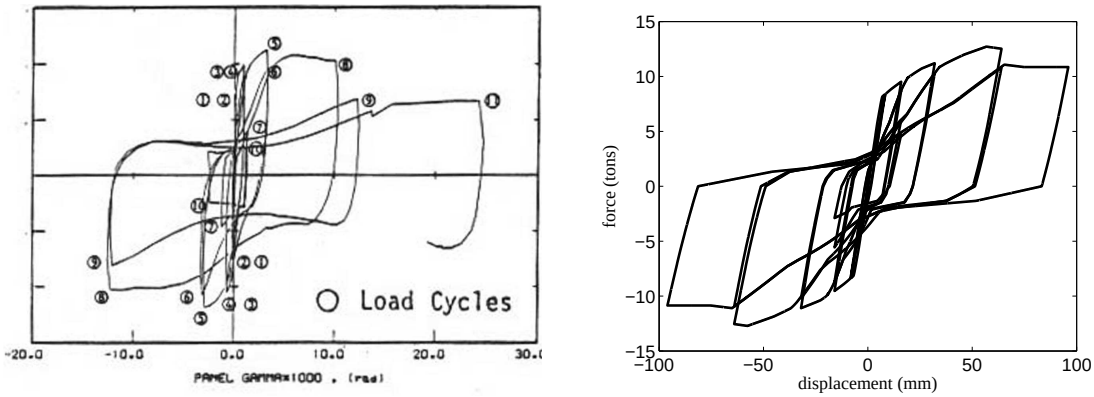

(a) Experimental (b) Simulated

Figure D.11: Load deformation response of OKA_J4 specimen

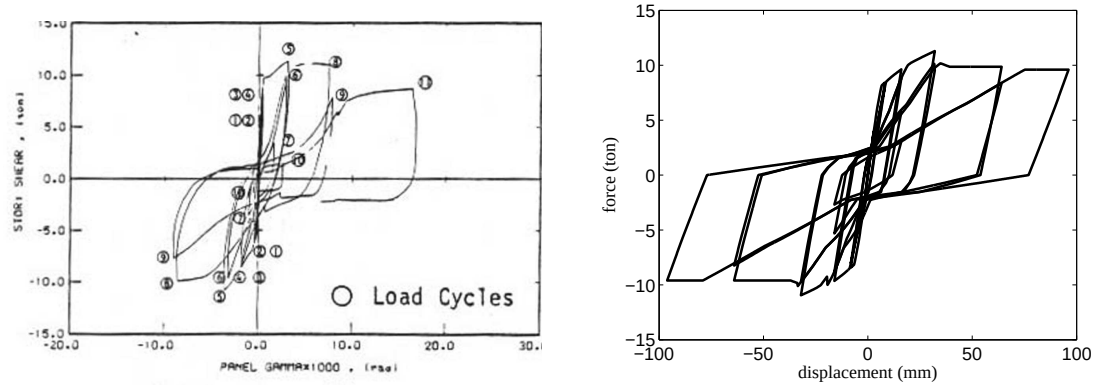

(a) Experimental (b) Simulated

Figure D.12: Load deformation response of OKA_J5 specimen

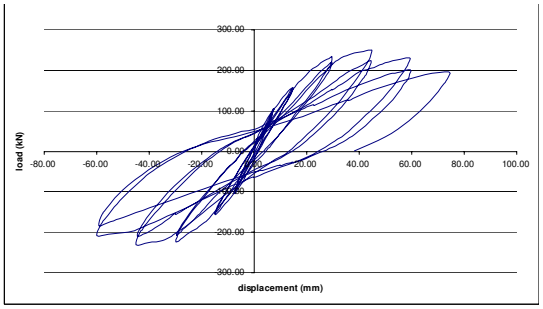

(a) Experimental

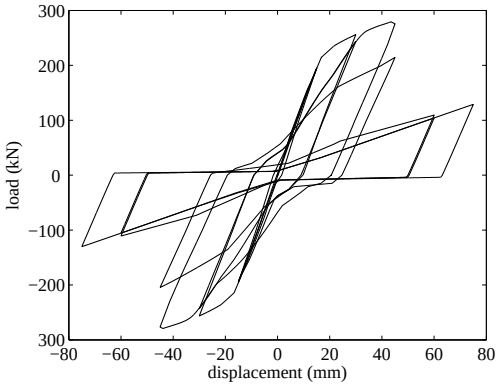

(b) Simulated

Figure D.13: Load deformation response of NK_OKJ4 specimen

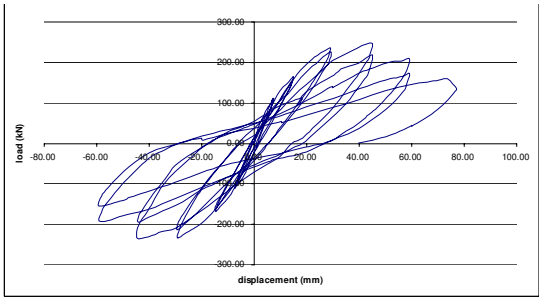

(a) Experimental

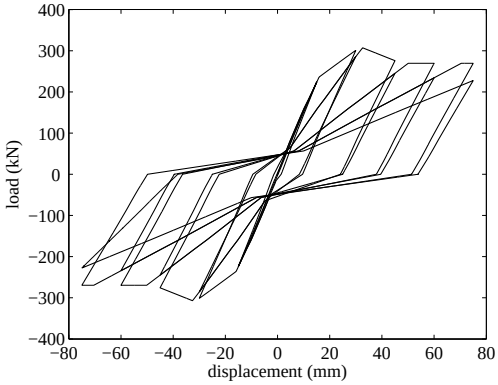

(b) Simulated

Figure D.14: Load deformation response of NK_OKJ5 specimen

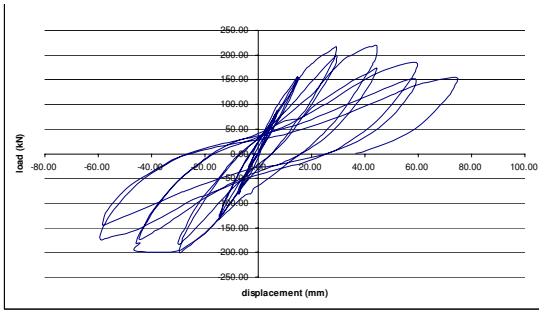

(a) Experimental

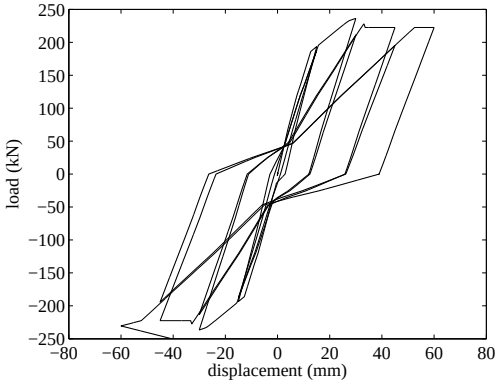

(b) Simulated

Figure D.15: Load deformation response of NK_OKJ6 specimen

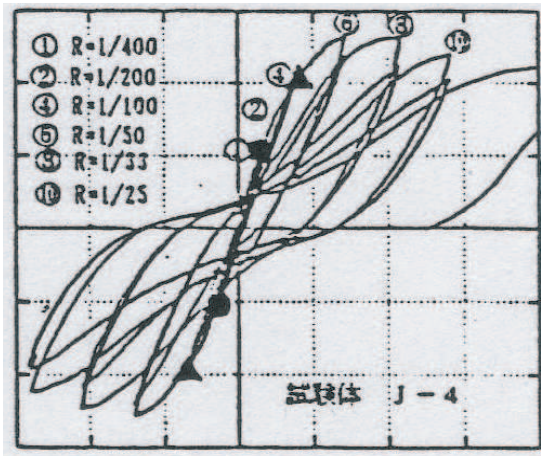

(a) Experimental

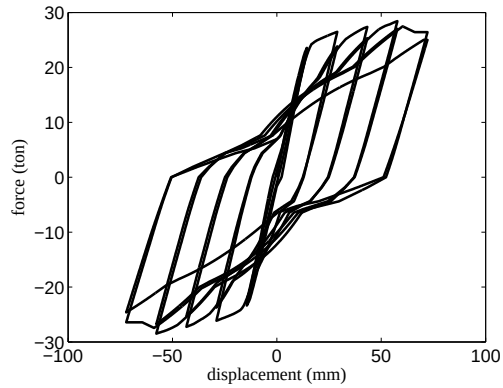

(b) Simulated

Figure D.16: Load deformation response of OS_J4 specimen

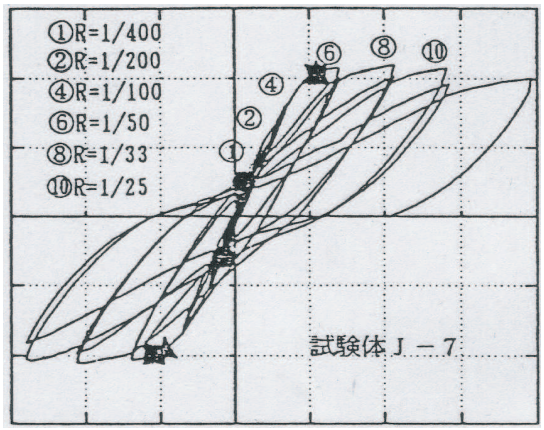

(a) Experimental

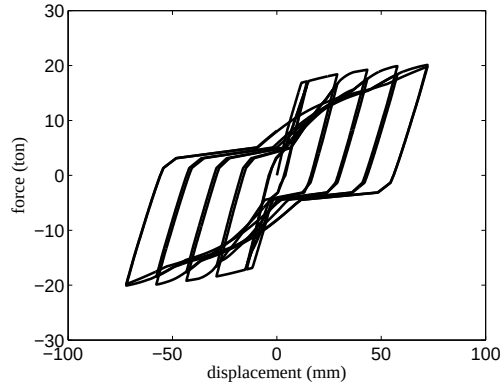

(b) Simulated

Figure D.17: Load deformation response of OS_J7 specimen

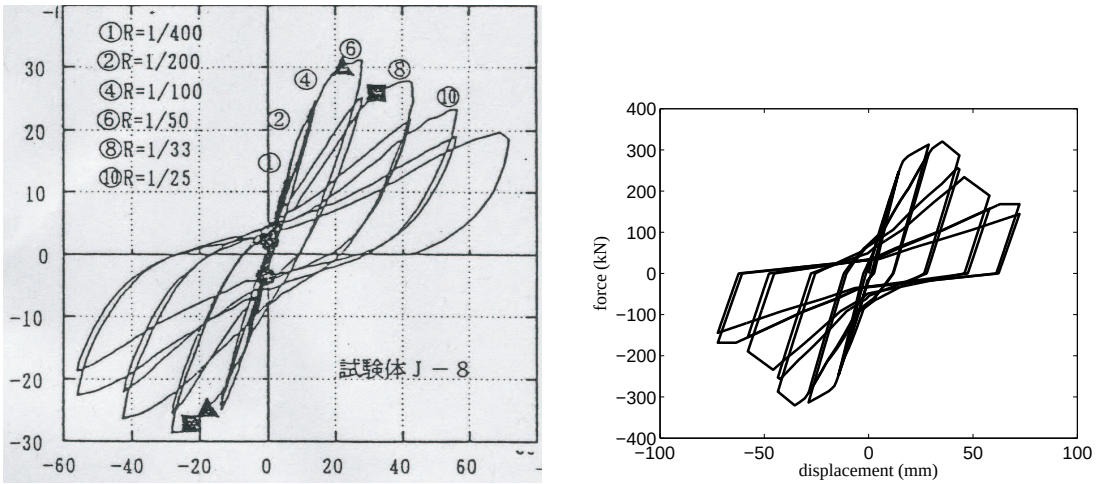

(a) Experimental (b) Simulated

Figure D.18: Load deformation response of OS_J8 specimen

Appendix E

SPECIMEN STRUT-AND-TIE MODELS

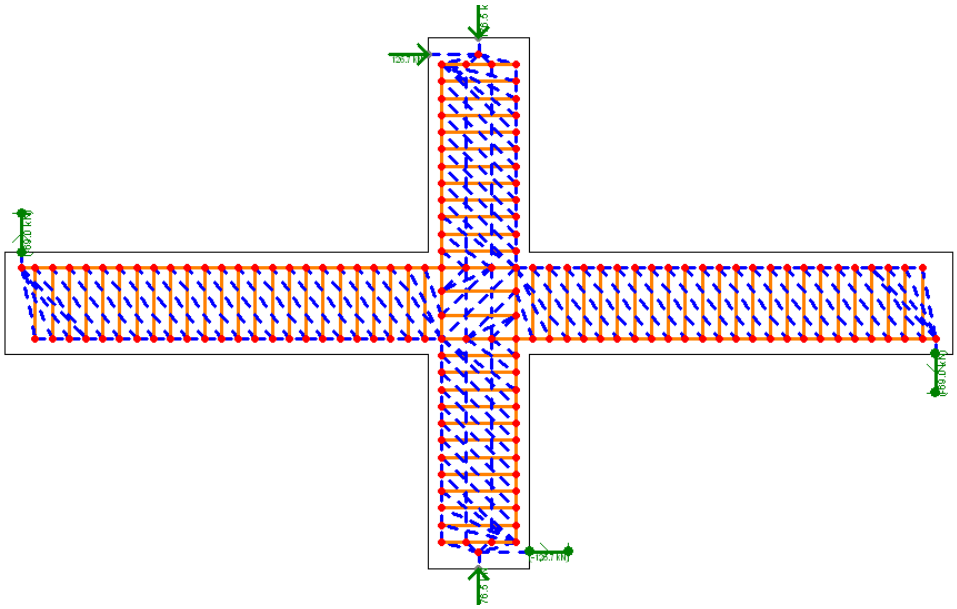

Figure E.1: Typical combined strut-truss model for Specimen *EKOA_HC*

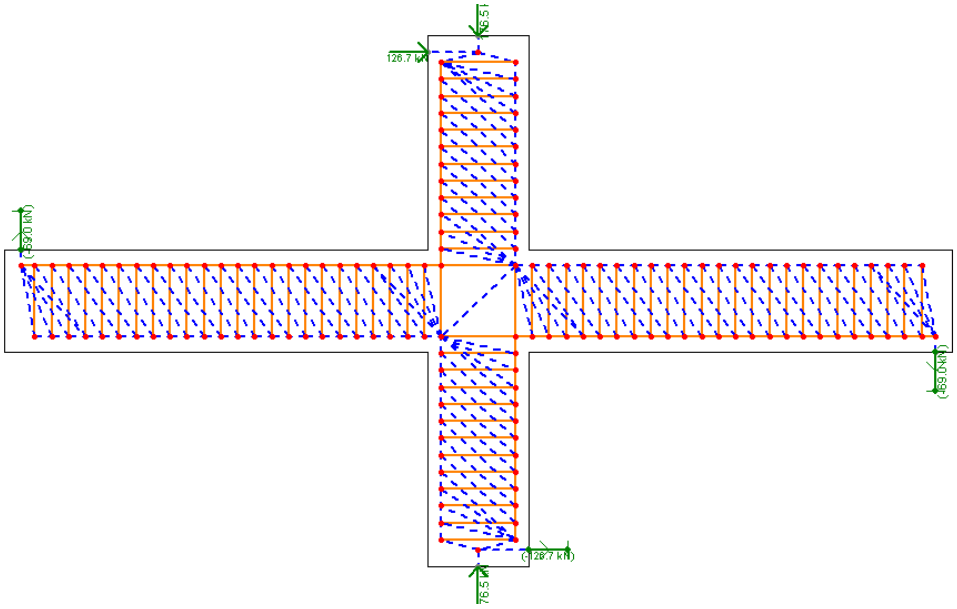

Figure E.2: Typical single strut model for Specimen $EKOA\_HC$

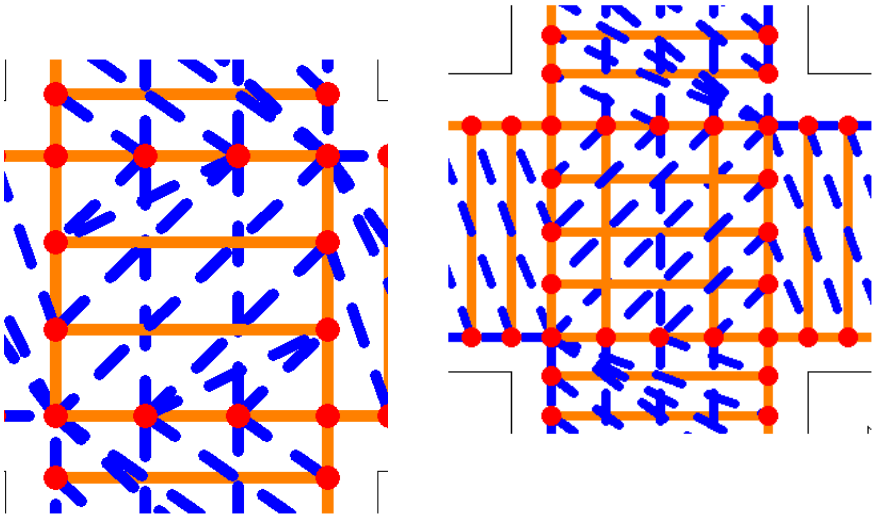

(a) Specimen $EKOA\_HLC$ (b) Specimen $EKOA\_LA1$

Figure E.3: Combined strut-truss model for EKOA specimens

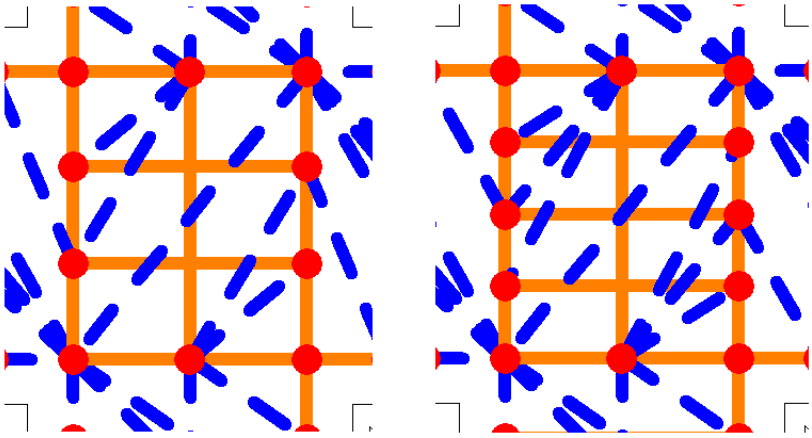

(a) Specimen DW_X1 and DW_X3 (b) Specimen DWX_X2

Figure E.4: Combined strut-truss model for DWX specimens

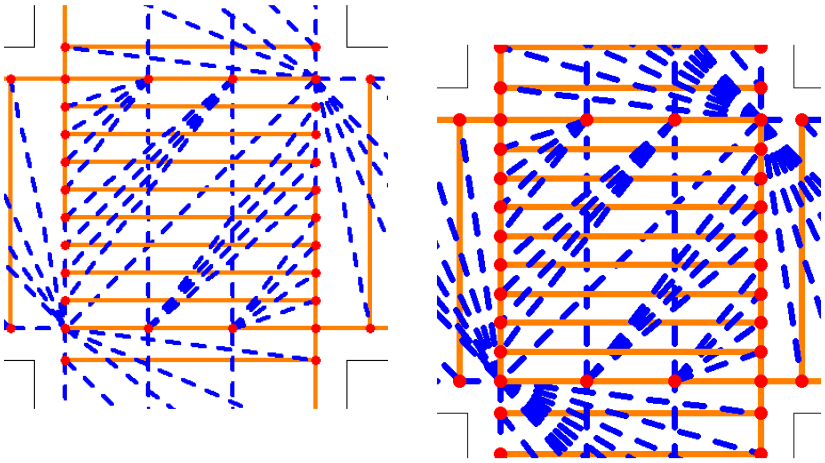

(a) Specimen $TKHS\_HJ1$ (b) Specimen $TKHS\_HJ12$

Figure E.5: Combined strut-truss model for TKHS specimens

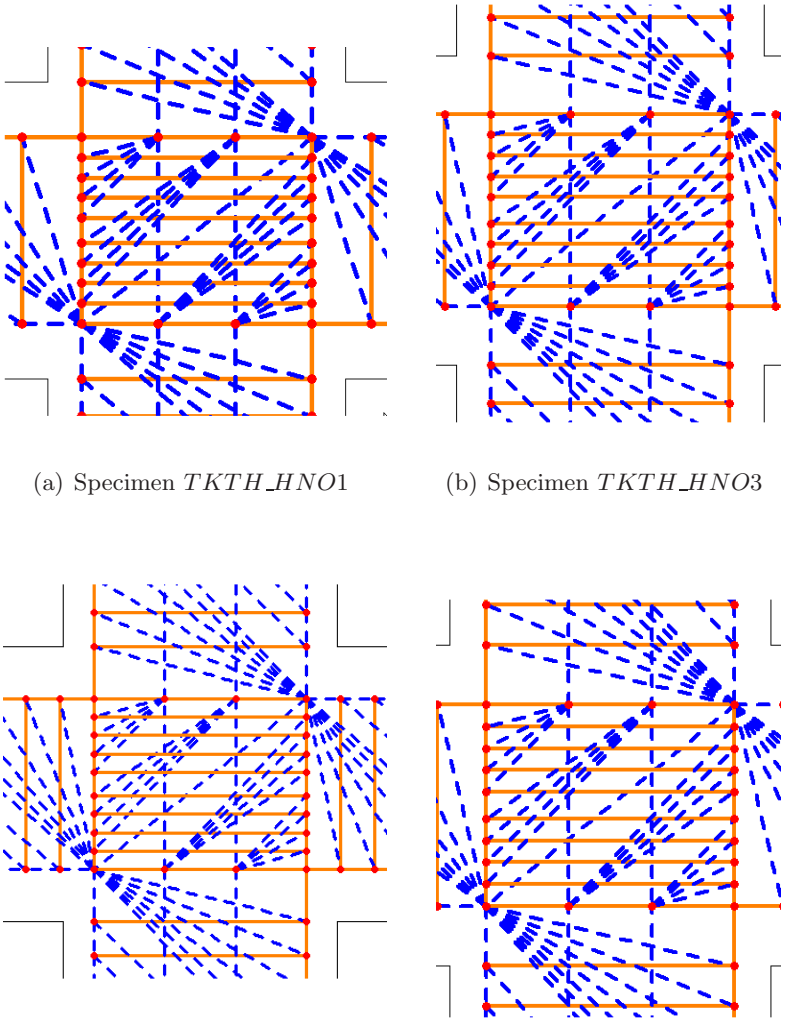

(a) Specimen $TKTH\_HNO1$ (b) Specimen $TKTH\_HNO3$

(c) Specimen $TKTH\_HNO4$ (d) Specimen $TKTH\_HNO5$

Figure E.6: Combined strut-truss model for TKTH specimens

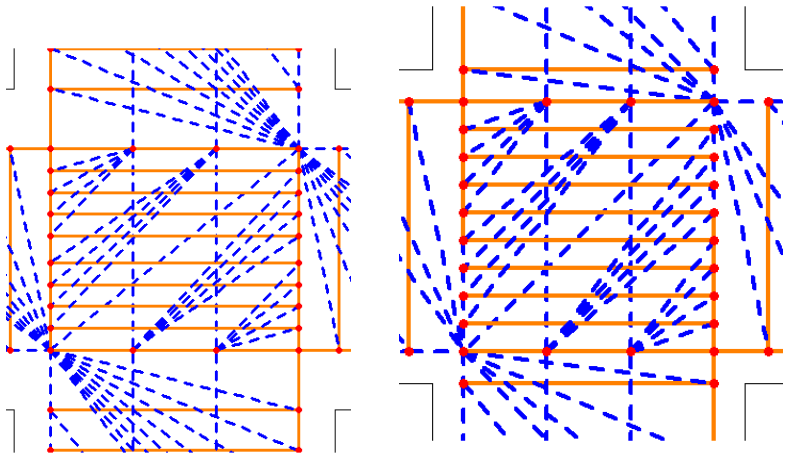

(a) Specimen $TKTH\_HNO6$ (b) Specimen $TKTH\_HNO8$

Figure E.7: Combined strut-truss model for more TKTH specimens

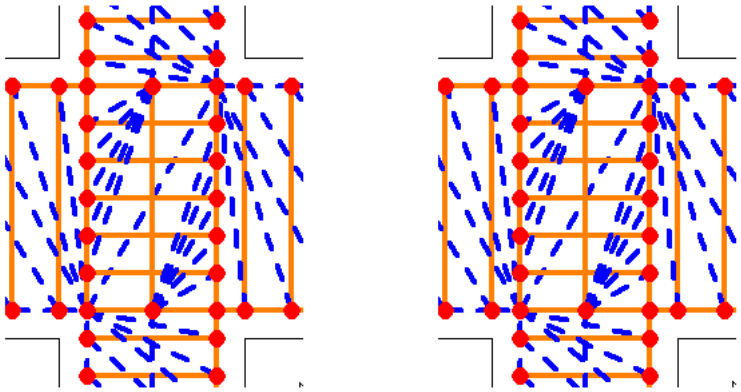

(a) Specimen $HO\_SD35Aa4$ (b) Specimen $HO\_LSD35Aa1$

Figure E.8: Combined strut-truss model for HO specimens

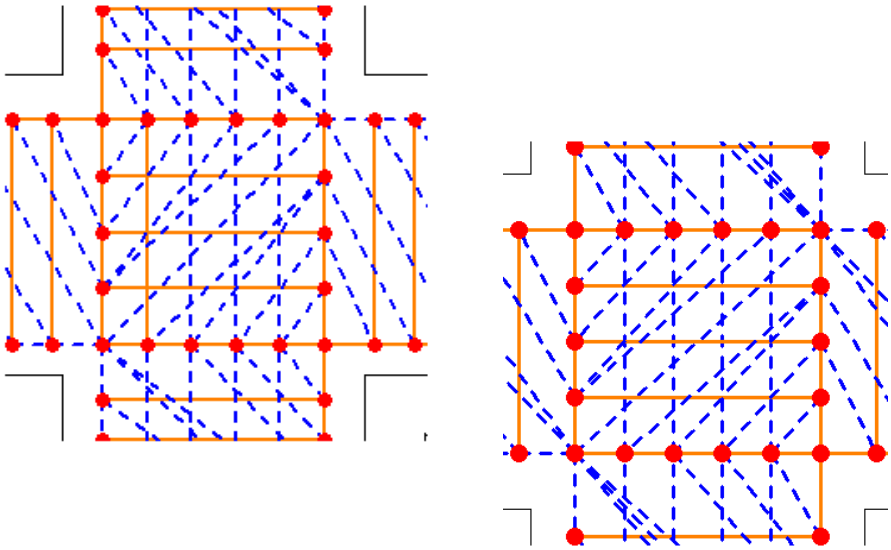

(a) Specimen NK_OKJ1 (b) Specimen NK_OKJ3

Figure E.9: Combined strut-truss model for NKOKJ specimens

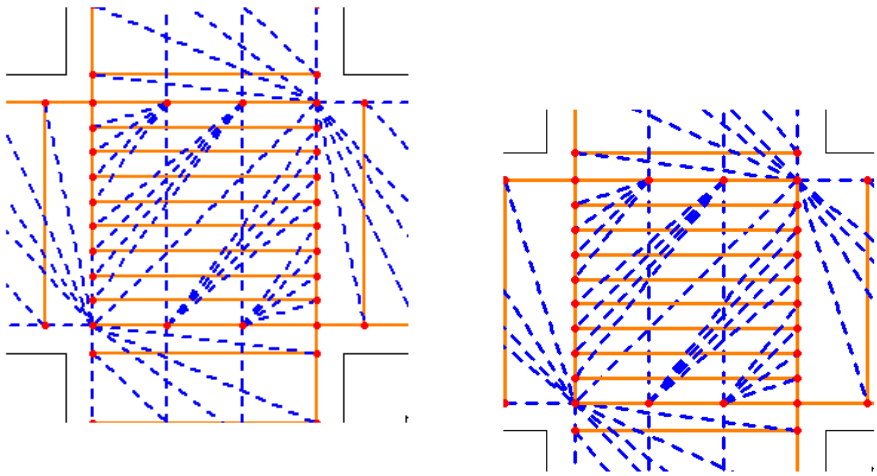

(a) Specimen $HTMK\_NO44$ (b) Specimen $HTMK\_NO49$

Figure E.10: Combined strut-truss model for HTMK specimens

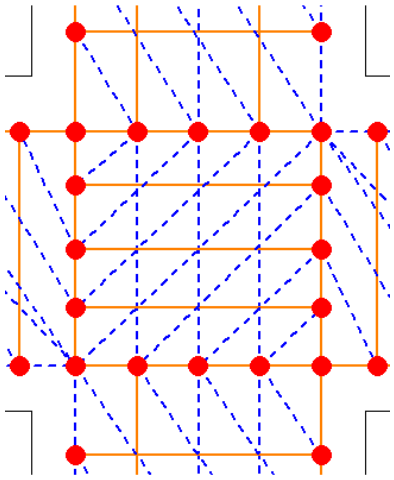

(a) Specimen OKA_J1

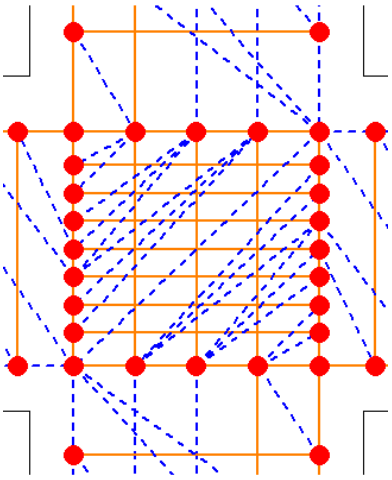

(b) Specimen OKA_J3

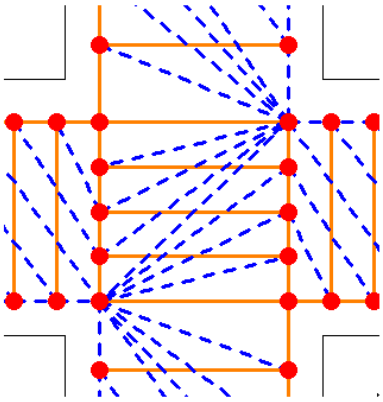

(c) Specimen OKA_J5

Figure E.11: Combined strut-truss model for OKA specimens

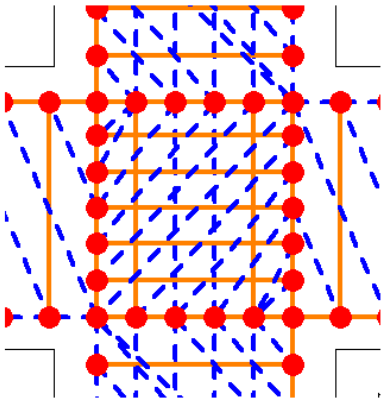

(a) Specimen OS_J1

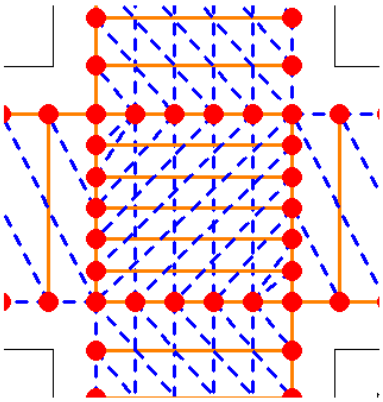

(b) Specimen OS_J4

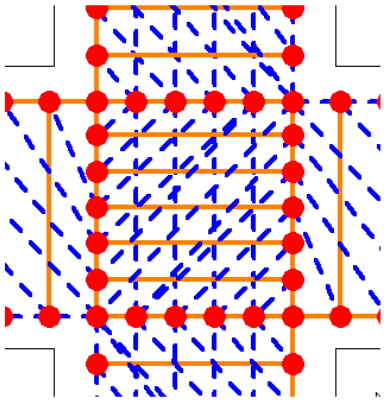

(c) Specimen OS_J8

Figure E.12: Combined strut-truss model for OS specimens

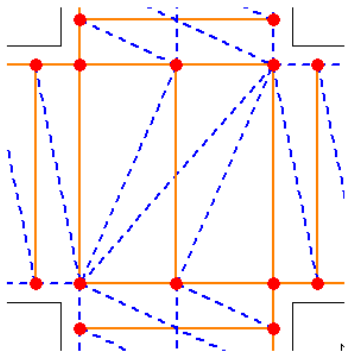

(a) Specimen $PEER14$

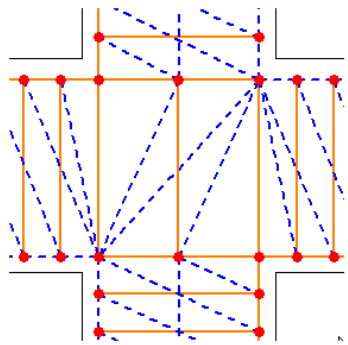

(b) Specimen $PEER22$

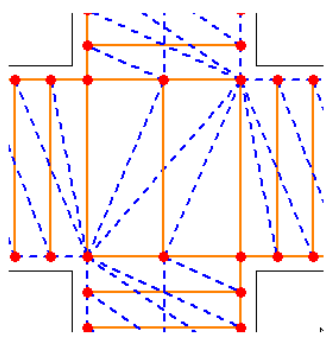

(c) Specimen $PEER4150$

Figure E.13: Combined strut-truss model for PEER specimens

VITA

Nilanjan Mitra completed his undergraduate in Civil Engineering from Bengal Engineering and Science University, Shibpur, India in 1998. Upon completion of his graduation, he joined a multi-national structural design firm, based in India to work as a structural design engineer. Gaining a year of industrial experience in the design of National Stock Exchange, India, Ltd. building, he decided to go in for higher education. To obtain a multi-disciplinary perspective in structural engineering, he joined Indian Institute of Technology, Kharagpur to do master's in Ocean Engineering in 1999. During this time he learnt about other types of structures, such as propellers, naval and offshore structures. During his MTech. in Ocean Engineering, based upon his excellent academic performance, he received the coveted DAAD scholarship to do research work in Germany. Thereby, he went to Technische Universität Darmstadt, Germany to do research on "Control of vortex excited vibration of bundled conductors in overhead transmission lines". After completing his Master's, to pursue a carrier in academia, he came to University of Washington, Seattle to do a Ph.D. on "Reinforced concrete beam-column joints subjected to seismic action" in 2001. Since then he has been working as a graduate student in UW, Seattle and will be finishing in Winter of 2007. In the meantime, since Fall 2006 he has been a lecturer in Civil Engineering Department at CalPoly San Luis Obispo.